AN EXPERIMENTAL AND ANALYTIC STUDY OF EARTH LOADS ON RIGID RETAINING WALLS

by

George Michael Filz

Dissertation submitted to the Faculty of the

Virginia Polytechnic Institute and State University

in partial fulfillment of the requirements for the degree of

DOCTOR OF PHILOSOPHY

in

Civil Engineering

APPROVED:

J. M. Duncan, Chairman

T. L. Brandon

G. W. Clough

T. Kuppusamy

J. N. Reddy

April, 1992

Blacksburg, Virginia

AN EXPERIMENTAL AND ANALYTIC STUDY OF EARTH LOADS ON RIGID RETAINING WALLS

by

George Michael Filz

Committee Chairman: J. M. Duncan

Civil Engineering

(ABSTRACT)

Experimental and analytic investigations were performed to examine the influences of wall height, backfill behavior, and compaction on the magnitudes of backfill loads on rigid retaining walls.

Measurements of lateral and vertical backfill loads were made during tests using the Virginia Tech instrumented retaining wall facility. The tests were performed with two soils, moist Yatesville silty sand and dry Light Castle sand. Two hand-operated compactors, a vibrating plate compactor and a rammer compactor, were used to compact the backfill. The backfill height was 6.5 feet in all of the tests.

Analyses of backfill loads were made using a compaction-induced lateral earth pressure theory and a vertical shear force theory. The compaction-induced lateral earth pressure theory was revised from a previous theory. The revisions improved the accuracy with which the theory models the hysteretic stress behavior of the backfill during compaction. The theory was also extended to include the pore pressure response of moist backfill in a rational manner.

A vertical shear force theory was also developed during this research. The theory is based on consideration of backfill compressibility and mobilization of interface shear strength at the contact between the backfill and the wall. The theory provides a useful basis for understanding how wall height, backfill compressibility, wall-backfill interface behavior, and compaction-induced lateral pressures affect the vertical shear forces on rigid walls.

Studies were also made to investigate the cause of erratic pressure cell readings. An important cause of drift in pressure cell readings was found to be moisture changes in the concrete in which the pressure cells were mounted. It was found that this problem could be mitigated by applying a water-seal treatment to the face of the wall.

Both the vibrating plate compactor and the rammer compactor were instrumented to measure dynamic forces and energy transfer during compaction. The force applied by the vibrating plate compactor was about one-quarter of the manufacturer's rated force. The force applied by the rammer compactor was about twice the manufacturer's rated force. The transferred energy measurements provided a basis for relating laboratory and field compaction procedures.

ACKNOWLEDGEMENTS

Professor J. M. Duncan made considerable contributions to every aspect of this research, including the experimental work, the analytic work, and the manuscript preparation. He provided support and encouragement, and was a continuous source of new ideas and solutions for difficulties encountered. Discussions about soil mechanics, finite element analyses, and the practical utility of research results were especially enjoyable.

Professors T. L. Brandon, G. W. Clough, T. Kuppusamy, and J. N. Reddy also contributed to the research. Professor Brandon helped with the instrumentation, data acquisition, and data reduction. Professors Clough, Kuppusamy, and Reddy contributed their knowledge of mechanics, finite element analyses, and soil behavior. The work of all the committee members in reviewing the manuscript is gratefully acknowledged.

Al Sehn, together with Professor Duncan, designed and constructed the Virginia Tech instrumented retaining wall facility. Ken Berry, Tony Brizendine, and Eric Zeimer helped with the instrumented retaining wall tests and performed the laboratory tests.

Reed Mosher offered many useful comments and suggestions.

Financial support for the work was provided by Nikken Sekkei Corporation of Japan, the US Army Corps of Engineers, and Virginia Polytechnic Institute and State University.

TABLE OF CONTENTS

LIST OF FIGURES

LIST OF TABLES

CHAPTER 1 - INTRODUCTION

Predicting the magnitude of loads applied by backfill to retaining walls is important for designing walls that are safe against instability, structural failure, and excessive deformation. For walls that are free to move away from or towards their backfills, earth loads have traditionally been calculated using the theories of Coulomb (1776), Rankine (1857), or Caquot and Kerisel (1948). For walls restrained from movement, earth loads are frequently calculated using an arbitrary value of the lateral earth pressure coefficient, or Jaky's (1948) empirical relationship for soil in the at-rest condition. None of these approaches represents the influence of soil-structure interaction effects on the earth loads, nor do they rationally consider the influence of compaction equipment on the loads.

Neglecting to consider these effects has led to excessively conservative design in some cases, and to inadequate performance in others. Ebeling et al. (1988) describe several earth retaining structures that do not satisfy conventional design criteria, but nevertheless perform satisfactorily. This suggests that the conventional criteria may be too conservative for certain types of structures. On the other hand, Mosher et al. (1991) describe retaining walls that cracked because of compaction-induced lateral earth pressures. The walls required extensive rehabilitation.

Recently, both analytic and experimental studies have been undertaken to gain a better understanding of soil-structure interaction

and the influence of compaction equipment on the earth loads that act on retaining walls. Analytic studies performed by Seed and Duncan (1983), Ebeling et al. (1988), Ebeling et al. (1989), and Regalado et al. (1992) included development of new methods to calculate compaction-induced lateral earth pressures and to account for soil-structure interaction effects during backfilling. Soil-structure interaction effects include the influence of wall movement, wall geometry, and settlement of backfill due to self-weight. Backfill compression produces vertical shear stresses that are favorable for stability, according to the analyses.

Experimental studies have been performed by Sehn and Duncan (1990). The experimental work included construction of a 7-foot high by 10-foot long instrumented retaining wall that can be used to measure earth loads from compacted backfill. Using the new facility, Sehn and Duncan performed preliminary tests that served to establish procedures for tests subsequently performed with the instrumented retaining wall as part of the research described herein.

These recent studies have shown that the magnitudes of earth loads on retaining walls depend on the compaction equipment used, the backfill behavior, the wall characteristics, and the foundation characteristics. The emphasis of the research described herein is on rigid walls with vertical back sides. For this class of walls, the most important factors that influence earth loads are the compactor, the soil behavior, and the wall height.

Accordingly, the purpose of this research was to use the instrumented retaining wall to measure the influences that compaction, soil type, and backfill height have on earth loads on walls, and to compare the measured loads with those expected based on the analytic studies. As the work progressed, it became clear that an improvement to the compaction-induced earth pressure theory was warranted, and that an extension of the theory to include partially saturated, fine-grained soils was possible. It also became clear that a simple vertical shear force theory would be useful to supplement the previous analytic studies, which used the finite element method. These theoretical developments constitute the analytic portion of this research.

This dissertation is divided into nine chapters and two appendices. A description of previous work on the subject is presented in Chapter 2, including a description of the Virginia Tech Instrumented Retaining Wall Facility developed by Sehn and Duncan (1990).

Chapter 3 presents an overview of the series of tests that were performed with the instrumented retaining wall as part of this research. The variables of the test program, the backfill soils used, the test procedures employed, and modifications made to the equipment are all described in Chapter 3.

During the course of the experimental work, the cause of drift in pressure cell readings obtained from the instrumented retaining wall was identified. This, and other findings related to instrumentation behavior, are presented in Chapter 4.

Measurements of dynamic compactor force and transferred energy are presented in Chapter 5. A method for calculating contact forces from compactor characteristics and soil properties is developed.

A personal communication received from Peck (1991) pointed out that unrealistic results are sometimes obtained from the compaction-induced earth pressure theory of Seed and Duncan (1983). Peck's observation led to development of a revised compaction-induced earth pressure theory, which is presented in Chapter 6. The revised theory was extended to include the effects of pore water pressure in partially saturated backfill soil.

Horizontal force and pressure measurements from the series of instrumented retaining wall tests performed as part of this research are presented and discussed in Chapter 7. The measured pressures are compared with calculations using the theory developed in Chapter 6. A case history of damage to two navigation lock walls caused by compaction-induced lateral pressures is also discussed and analyzed in Chapter 7.

A theory for calculating vertical shear forces on rigid walls with vertical back sides is developed in Chapter 8. The new theory provides insight into the influences of backfill compressibility, interface behavior, wall height, and compaction-induced lateral stresses on development of vertical shear loads. The parameter studies by Ebeling et al. (1988), Ebeling et al. (1989), and Regalado et al. (1992) were reviewed to assess the influence of other factors on vertical shear loads. Measured vertical shear forces from the instrumented retaining

wall tests are presented and discussed in light of the findings from the theory and the review of the parameter studies.

A summary, conclusions, and recommendations for further work are presented in Chapter 9.

The results of laboratory tests performed on specimens of the backfill soils used in the instrumented retaining wall tests are presented in Appendix A. The user's guide and program listing for EPCOMPAC, which calculates compaction-induced lateral earth pressures using the theory described in Chapter 6, are included in Appendix B.

CHAPTER 2 - PREVIOUS WORK

2.1 Introduction

This research is a continuation of work begun by Seed and Duncan (1983), Sehn and Duncan (1990), Ebeling et al. (1988), Ebeling et al. (1989), and Regalado et al. (1992) concerning the earth loads that act on retaining walls.

The particular emphasis of the work by Seed and Duncan (1983) was compaction-induced lateral earth pressures. Seed and Duncan reviewed previous theoretical developments, as well as the large scale model tests and field studies documented in the literature. They developed analytic methods for calculating compaction-induced lateral earth pressures on rigid walls. They also developed techniques to incorporate compaction-induced lateral earth pressures in finite element analyses so that the stresses in, and deflections of, flexible structures could be analyzed. They compared the results of analyses using the newly developed techniques with published data from model tests and field studies.

Sehn and Duncan (1990) updated the earlier literature review by Seed and Duncan (1983) and performed experimental studies of earth pressures due to compaction. They developed a new oedometer capable of measuring the horizontal stresses that occur in laterally restrained soil subject to vertical loads. They also developed an instrumented retaining wall test facility, which includes a 7-foot high by 10-foot long model wall that can be used to measure earth loads of backfill on

the wall. Sehn and Duncan (1990) performed four tests in the instrumented retaining wall facility.

The literature reviews performed by Seed and Duncan (1983) and Sehn and Duncan (1990) constitute a current, complete review of the lateral earth pressure literature. Consequently, no separate literature review is included here. However, many of these references are relevant to the current research. The relevant references are cited and discussed where appropriate in the following chapters.

The focus of the experimental portion of this research is on use of the instrumented retaining wall facility to measure vertical and lateral forces due to compacted backfill. So that the experimental work can be best understood, this chapter presents a description of the instrumented retaining wall and its operation. The principal findings from the four tests performed by Sehn and Duncan (1990) are also described.

Ebeling et al. (1988), Ebeling et al. (1989), and Regalado et al. (1992) performed parameter studies using the finite element method to assess the influence that several factors have on retaining wall stability. The principal findings of these studies are discussed in Chapter 8.

2.2 The Instrumented Retaining Wall Facility

The instrumented retaining wall facility was described in detail by Sehn and Duncan (1990) from whom the following summary has been adapted.

2.2.1 Configuration of the Instrumented Retaining Wall

The instrumented wall consists of four panels located within a very stiff reinforced concrete structure, as shown by the oblique view in Figure 2.1. Each panel is 2.5 feet long and 7 feet high, so the overall size of the wall is 10 feet long and 7 feet high. The backfill area is 6 feet wide, 10 feet long, and 7 feet high. Backfill is typically placed up to about 6.5 feet high against the wall. Backfill is also placed in the access ramp that leads down into the backfill area.

Lateral support for the instrumented wall is provided by the 15-inch thick concrete reaction wall shown in Figure 2.1. A cross-section through the reaction wall and the lateral support system for the instrumented wall is shown in Figure 2.2. The lateral support system includes load cells, a steel frame, and screw jacks. The instrumented wall is directly supported by load cells, which react against the steel frame. The steel frame is, in turn, supported by screw jacks, which bear on the 15-inch thick concrete wall. The reaction wall is part of the massive U-frame structure that contains the instrumented wall and the backfill area, as shown in Figure 2.2. The base of the U-frame structure is 21 inches thick. The U-frame structure is essentially non-deflecting under the loads applied by the backfill.

The screw jacks permit the instrumented wall to be moved towards or away from the backfill. The upper jacks can be moved independently of the lower jacks so that the instrumented wall can be rotated as well as translated. However, the panels cannot be moved independently; the

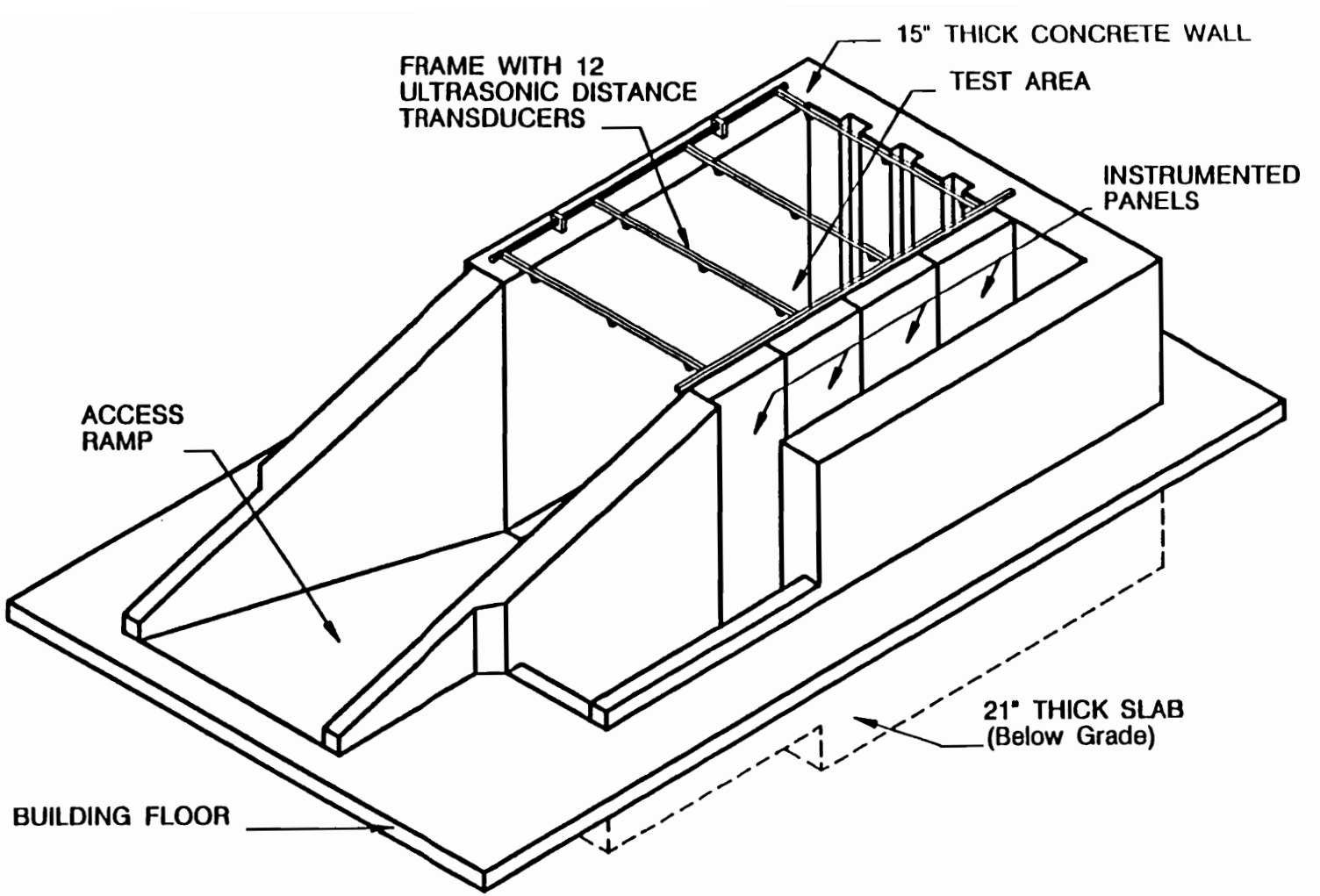

Figure 2.1:The Virginia Tech Instrumented Retaining Wall Test Facility (after Sehn and Duncan, 1990)

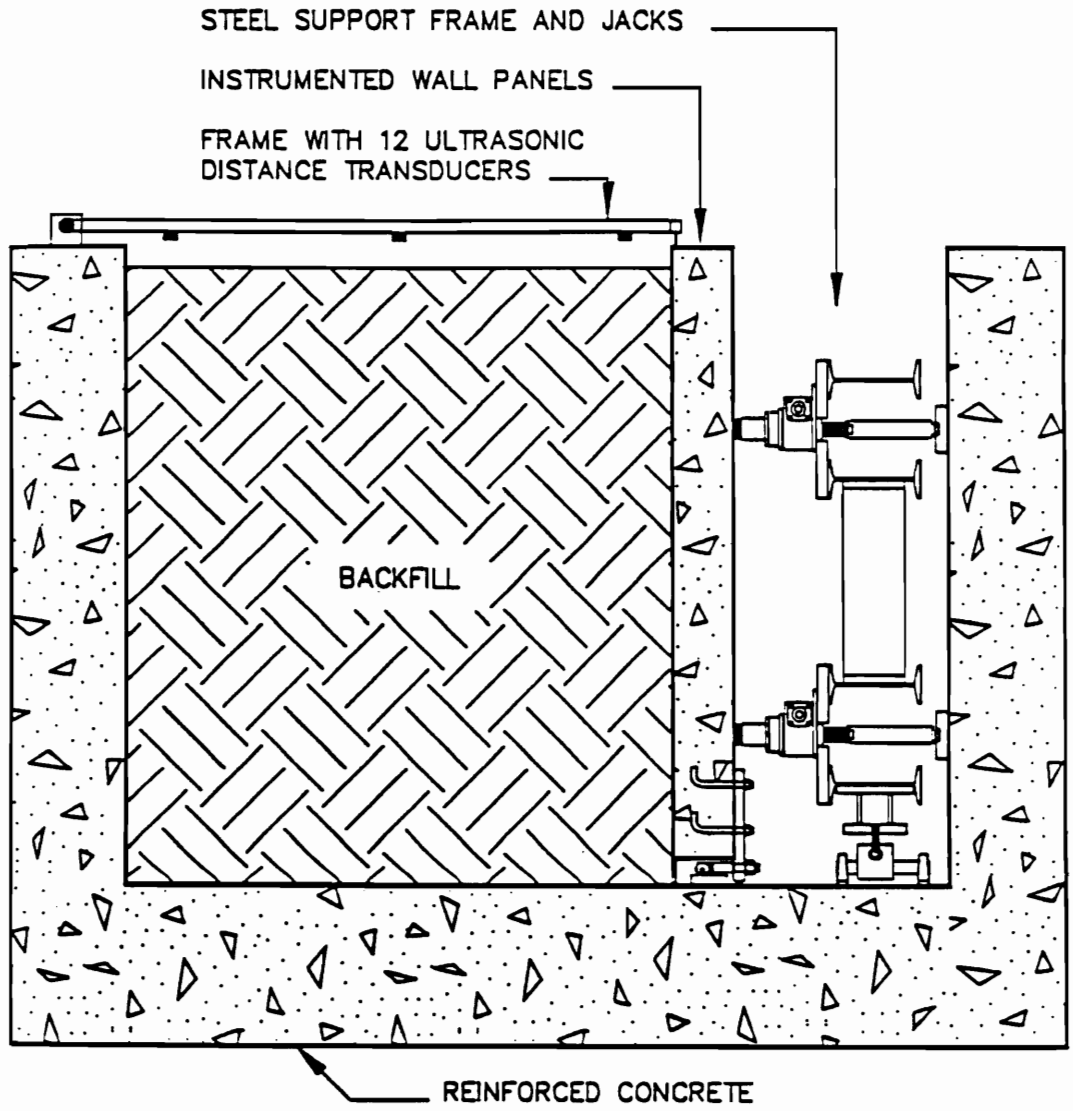

Figure 2.2: Cross-Section Through the Instrumented Retaining Wall Facility (after Sehn and Duncan, 1990)

steel frame moves all four panels the same distance, and in the same mode.

2.2.2 Transducers

The instrumented retaining wall includes 17 pressure cells, 20 load cells, 8 linear variable differential transducers (LVDTs), 13 ultrasonic distance measuring devices (UDMs), and 6 thermocouples. The locations of the pressure cells and the load cells with respect to the instrumented panels are shown on the instrumented wall elevation in Figure 2.3. The view in Figure 2.3 is of the instrumented wall from the backfill side. Thus, panel 1 is nearest the end wall of the facility, and panel 4 is nearest the access ramp.

The pressure cells are flush mounted in panels 2 and 3. There are 11 Gloetzl cells, 4 Carlson cells, and 2 Geonor cells. The Gloetzl cells are 14 cm long, 7 cm wide, and 0.45 cm thick. They are hydraulic, oil-filled cells. The oil in each Gloetzl cell is connected to an electrical pressure transducer through a thick-walled, small diameter steel tube. The Carlson cells are 7.4 inches in diameter and 1 inch thick. They are hydraulic, mercury-filled cells with thick outer faces. Pressure changes in the mercury cause deflections in a small diaphragm, and the deflections are read by a sensitive extensometer. The Geonor cells are 16.5 cm in diameter and 4.6 cm thick. They are diaphragm cells. Deformation of the diaphragm is measured by a vibrating wire transducer. The Gloetzl cells and the Carlson cells are functioning satisfactorily. One of the Geonor cells failed soon after installation

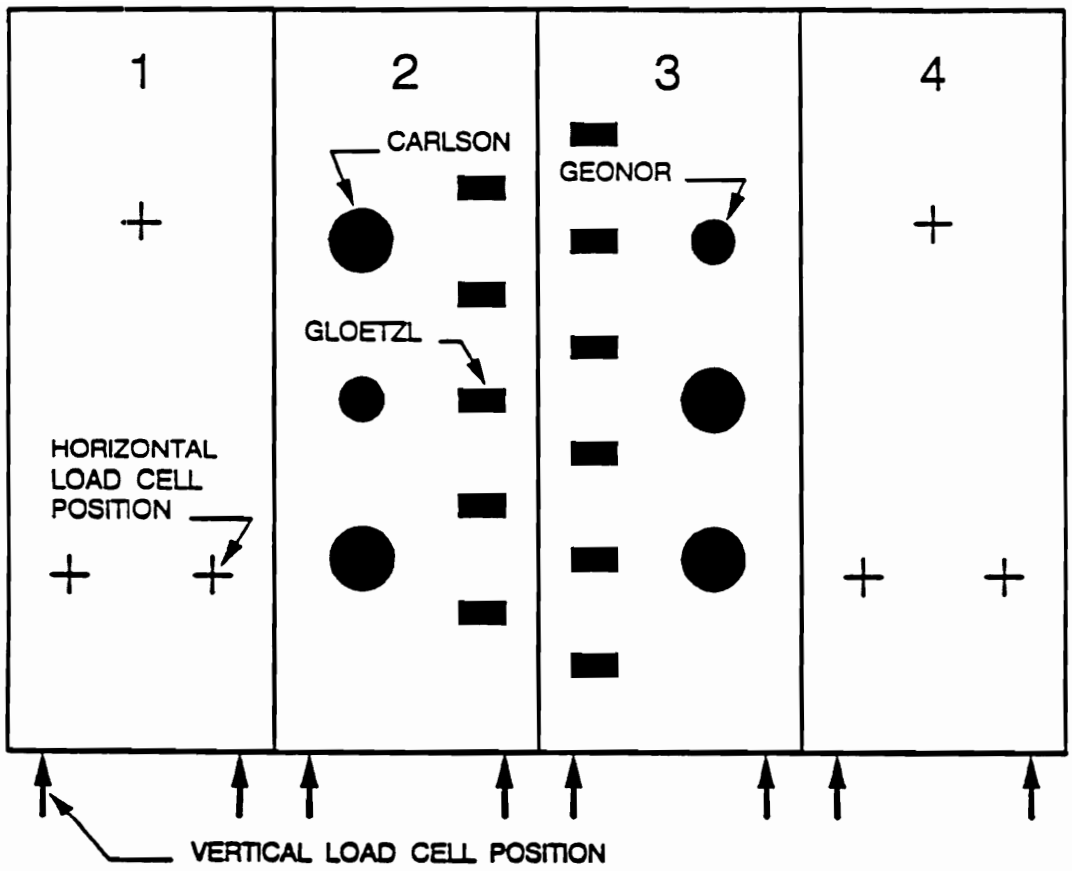

Figure 2.3: Instrumented Retaining Wall Panels (after Sehn and Duncan, 1990)

in the instrumented wall. The other Geonor cell continues to function but gives erratic, unreliable readings. Consequently, only readings from the 11 Gloetzl cells and 4 Carlson cells are discussed in subsequent chapters.

The load cells provide both vertical and lateral support for the instrumented panels. There are three horizontal load cells and two vertical load cells for each panel, as shown in Figure 2.3. Diagrams of the load cells are shown in Figure 2.4. The horizontal load cells are compression members instrumented with resistance strain gages. The vertical load cells must be able to accommodate movement of the instrumented wall without transferring shear forces. As shown in Figure 2.4, a cantilever beam instrumented with resistance strain gages was developed for the vertical load cells. The beam, which is mounted to the panel with a steel bracket, supports a hardened steel roller that travels on a hardened steel pad.

Movements of the instrumented wall are measured by 8 LVDTs, one at the top and one at the bottom of each wall panel. The LVDTs are located on the front of the instrumented wall, on the side opposite from the backfill.

The ultrasonic distance measuring devices (UDMs) are used to measure the total thickness of the backfill after each lift is placed. The UDMs are mounted on a movable frame, as shown in Figures 2.1 and 2.2. The UDMs emit a burst of high frequency sound that is reflected off the surface of the compacted backfill and returned to the UDM. The

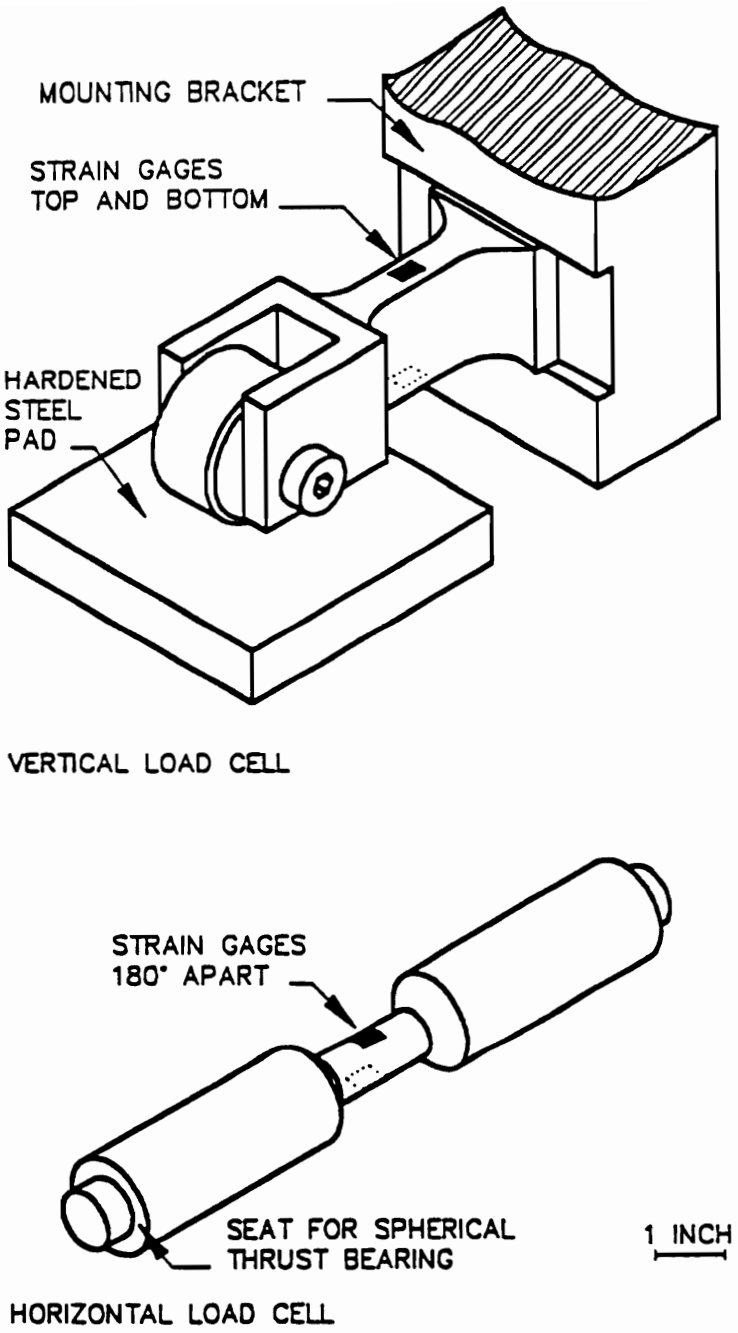

Figure 2.4: Horizontal and Vertical Load Cell Details (after Sehn and Duncan, 1990)

travel time of the sound is used to determine the distance between the UDM and the reflecting surface.

Six thermocouples are used to measure temperatures at several locations in the instrumented retaining wall system. Three thermocouples are located on the face of the instrumented retaining wall, near three of the Gloetzl cells, to determine the effect of temperature changes on the cell readings. Two thermocouples are located in the support system area between the instrumented wall and the reaction wall to determine the effect of temperature changes in this area on instrumentation response. One thermocouple is located in a cabinet that contains the multiplexing cards for the data acquisition system.

2.2.3 Data Acquisition

Data acquisition is automated. Software developed for an IBM XT microcomputer controls analog-to-digital converters and multiplexing cards to read each transducer. To make one set of readings, each transducer is read several times, the readings are averaged, the average reading is converted to engineering units, and the result is stored in a file on the hard disk drive in the microcomputer. A complete set of readings of all the transducers can be taken in less than three minutes.

2.3 Findings from Tests EP 1 through EP 4

Sehn and Duncan (1990) performed four tests, designated EP 1 through EP 4, using the instrumented retaining wall facility. Moist Yatesville silty sand, which is described in Chapter 3 and Appendix A,

was used as backfill. The silty sand was compacted with a Wacker BPU2440A vibrating plate compactor, in 4-inch thick lifts for tests EP 1 and EP 2, and in 6-inch thick lifts for tests EP 3 and EP 4. In all four tests, the backfill was transported to the backfill area with a small front-end loader, and the loader was operated on the surface of the compacted lifts during backfill placement.

These tests were preliminary in nature, and were used to develop consistent procedures for subsequent tests. The tests resulted in several important findings:

1) The instrumented retaining wall system is stiff. Deflections under the applied earth loads are very small, and the system is suitable for measuring compaction-induced lateral earth pressures.

2) The forces applied by the backfill to the instrumented wall were influenced by the wheel loads from the front-end loader. Panel 4, which is closest to the access ramp and which received the most nearby passes of the loader, was most strongly influenced.

3) The forces on panel 1 were influenced by the presence of the end wall of the facility.

4) The horizontal force on the wall was calculated two ways: 1) by integrating the pressure distribution measured with the pressure cells, and 2) by summing the horizontal load cell readings. During backfilling, agreement between the two methods was good. After backfilling, agreement between the two methods became worse with time.

5) Significant vertical shear forces were measured on the instrumented retaining wall. The vertical shear forces tended to increase with time after filling.

CHAPTER 3 - TEST PROGRAM

3.1 Introduction

The experimental part of this research includes instrumented retaining wall tests, dynamic compactor force measurements, and laboratory tests. This chapter presents an overview of the experimental work, including a summary of the variables in the instrumented retaining wall tests, a description of the soils used in the testing, a description of the backfill placement and compaction procedures, and a list of modifications to the instrumented retaining wall facility made during the course of the work. Additional details regarding these items are presented in the chapters where the information is most relevant.

3.2 Instrumented Retaining Wall Test Details

A total of 16 tests have been performed using the instrumented retaining wall facility. Tests EP 1 through EP 4 were performed by Sehn and Duncan (1990). Tests EP 5 through EP 16 were performed as part of this research. The conditions of all 16 tests are summarized in Table 3.1. Special instrumentation and procedures used during some of the tests are listed in Table 3.2.

3.3 Soil Descriptions

Two soil types were used as backfill in the instrumented retaining wall tests: Yatesville silty sand, and Light Castle sand. The results of laboratory tests performed on these materials are presented in Appendix A.

TABLE 3.1: Instrumented Retaining Wall Test Conditions

Test Number	Soil Type(1)	Water Content (%)	Dry Unit Weight (pcf)	Compactor Type(2)	Lift Thickness (in)	Lubricated Walls(3)	Bobcat Use(4)	Time to Fill (days)	Duration after Filling (days)
EP 1	YSS1	14.5	115.5	Vib	4	0	Y	1.2	1.0
EP 2	YSS1	14.2	115.4	Vib	4	0	Y	0.6	4.5
EP 3	YSS1	13.7	114.2	Vib	6	0	Y	0.4	5.6
EP 4	YSS1	10.1	102.5	Vib	6	0	Y	0.4	4.6
EP 5	YSS1	9.3	102.5	Vib	6	2	Y	0.4	4.1
EP 6	YSS1	9.7	101.9	Vib	6	2	N	0.4	4.1
EP 7	YSS1	11.1	107.6	Vib	6	0	N	0.4	7.7
EP 8	YSS1	12.1	109.9	Vib	6	2	N	0.4	6.9
EP 9	YSS1	12.5	112.7	Vib	6	2	N	0.4	6.7
EP 10	YSS1	11.8	109.8	Vib	6	3	N	0.6	6.5
EP 11	YSS1	13.5	110.3	Vib	6	0	N	0.4	6.6
EP 12	YSS1	12.3	110.3	Vib	6	2	N	2.7	7.3
EP 13	YSS2	12.7	119.5	Vib + Ram	6	2	N	1.3	5.6
EP 14	YSS2	10.1	118.6	Vib + Ram	6	2	N	1.2	13.7
EP 15	LCS	0.0	106.2	Ram	6	2	N	1.3	1.6
EP 16	LCS	0.0	104.7	Vib	6	2	N	1.3	4.6

Notes:
1) YSS1 indicates Yatesville silty sand No. 1. YSS2 indicates Yatesville silty sand No. 2. LCS indicates Light Castle sand.
2) Vib indicates the Wacker BPU2440A vibrating plate compactor. Ram indicates the Wacker BS60Y rammer compactor.
3) 2 indicates that the end wall and the wall opposite from the instrumented wall are lubricated. 3 indicates that the instrumented wall, the end wall, and the wall opposite from the instrumented wall are all lubricated.
4) The Bobcat loader was operated on the backfill during backfill placement for the tests indicated.

TABLE 3.2: Special Instrumentation and Test Procedures

Test Number	Buried Pressure Cells	Surface Settlement Gages	Interface Telltales	Compactor Force Measurements	Plate Load Test	Wall Movement Test
EP 1	N	N	N	N	N	N
EP 2	N	N	N	N	N	N
EP 3	N	N	N	N	N	N
EP 4	N	N	N	N	N	N
EP 5	N	Y	N	N	N	N
EP 6	N	Y	N	N	N	N
EP 7	N	Y	N	N	N	N
EP 8	N	Y	N	N	N	N
EP 9	N	Y	N	N	N	N
EP 10	N	Y	N	N	N	N
EP 11	N	Y	N	N	N	N
EP 12	Y	Y	Y	Y	N	Y
EP 13	Y	Y	Y	Y	N	Y
EP 14	Y	Y	Y	Y	Y	Y
EP 15	Y	Y	Y	Y	Y	Y
EP 16	Y	Y	Y	Y	Y	Y

Yatesville silty sand is an alluvial soil from the foundation of Yatesville Lake Dam on Blaine Creek in Lawrence County, Kentucky. About 47 percent of the Yatesville silty sand passes the No. 200 sieve. It is non-plastic and its Unified Classification is SM. The specific gravity of solids is about 2.67. Two batches of the Yatesville silty sand were used in the testing. They are designated Yatesville silty sand No. 1 (YSS1), which was used in tests EP 1 through EP 12, and Yatesville silty sand No. 2 (YSS2), which was used in tests EP 13 and EP 14. As indicated in Appendix A, it is not possible to distinguish between the batches based on index property test results or strength test results. However, there is a difference in the moisture-density relationships for the two batches. For the YSS1, the standard Proctor maximum dry unit weight is 120 lbs. per cu. ft. with an optimum water content of 12.5 percent, and the modified Proctor maximum dry unit weight is 128 lbs. per cu. ft. with an optimum water content of 9 percent. For the YSS2, the standard Proctor maximum dry unit weight is 125 lbs. per cu. ft. with an optimum water content of 11 percent, and the modified Proctor maximum dry unit weight is 132 lbs. per cu. ft. with an optimum water content of 8.5 percent.

Light Castle sand is a clean, fine sand consisting predominantly of subangular grains of quartz. The sand was obtained from a quarry in Craig County, Virginia. About 68 percent of the Light Castle sand passes the No. 40 sieve and less than 1 percent passes the No. 200 sieve. The coefficient of uniformity is 1.8, the coefficient of curvature is 0.9, and the Unified Classification is SP. The specific

gravity of solids is 2.65. The maximum and minimum densities determined according to ASTM D4253-83 and ASTM D4254-83 are 106 and 88.5 lbs. per cu. ft., respectively.

3.4 Backfill Placement and Compaction Procedures

Before it was used as backfill in the instrumented retaining wall test facility, the Yatesville silty sand was conditioned to a uniform moisture content and placed in the stockpile area, which is located in the same building as the instrumented wall. The soil was moved to the backfill area with a small front-end loader. In tests EP 1 through EP 5, the loader was driven onto the surface of the previously compacted lift in order to place the soil for the next lift. The data from these five tests indicated that the wheel loads from the front-end loader were influencing the earth loads on the instrumented wall. In the remaining tests with Yatesville silty sand backfill, EP 6 through EP 14, the soil was deposited at the entrance to the backfill area, and was moved by hand to cover the backfill area. The soil was spread by hand in loose lifts of sufficient thickness to provide the desired compacted lift thicknesses. For tests EP 1 and EP 2, the compacted lift thickness was 4 inches. For tests EP 3 through EP 14, the compacted lift thickness was 6 inches.

In tests EP 1 through EP 12, the backfill was compacted by 5 passes of a Wacker BPU2440A vibrating plate compactor. In tests EP 13 and EP 14, both the vibrating plate compactor and a Wacker BS60Y rammer compactor were used to compact the backfill. It was found that a much

more uniform lift surface was produced if each lift was covered with two passes of the vibrating plate compactor prior to using the rammer compactor. As discussed in Chapter 5, both compactors make significant contributions to the compactive effort applied to the backfill. However, the compaction-induced lateral pressures are controlled by the larger peak contact force from the rammer compactor, as discussed in Chapters 5 through 7. Two passes of the rammer compactor were applied to each lift in tests EP 13 and EP14.

The backfill placement and compaction procedures were slightly different for the Light Castle sand, which was used in tests EP 15 and EP 16. The sand was kept dry; hygroscopic moisture was less than 0.1 percent. The sand was moved from the stockpile area to the backfill area in a hopper lifted by an overhead crane. After depositing the sand in the backfill area, it was spread by hand in loose lifts of sufficient thickness to produce a compacted lift thickness of 6 inches.

In test EP 15, each lift of backfill was compacted by 2 passes of the rammer compactor. This produced a relatively flat compacted lift surface for the Light Castle sand backfill, without using the vibrating plate compactor. In test EP 16, each lift of backfill was compacted by 5 passes of the vibrating plate compactor.

3.5 Modifications to the Instrumented Retaining Wall

During the course of the research, the following modifications were made to the instrumented retaining wall:

1) The instrumentation area between the front of the instrumented wall (the side opposite the backfill) and the reaction wall was insulated with 4 inches of foam insulation board. This reduced

temperature fluctuations to about ±2°F during each test. The insulation was added between tests EP 5 and EP 6.

2) Six additional thermocouples (for a total of 12 thermocouples) were added to check the influence of temperature changes on the pressure cell readings. These thermocouples were added between tests EP 8 and EP 9. Two thermocouples were placed on each of three Gloetzl pressure cells, one on the steel tube that extends from the back of each cell and the other located beneath the surface of the concrete panel at the depth of the back of the Gloetzl cells. Readings from these thermocouples showed that the temperature fluctuations were small and not consistent with observed changes in pressure cell readings. Thus, it was concluded that temperature changes did not have a significant effect on the pressure cell readings, for the conditions of these tests.

3) Ball transfers were added between adjacent panels of the instrumented wall, and between the outmost panels and the fixed walls of the facility. The ball transfers prevent frictional interaction between the panels, as well as preventing friction between the entire instrumented wall and the adjacent fixed walls. After installing the ball transfers, the wall was moved without any backfill in place, using the chain drive described in the next item. Load cell measurements taken before and after moving the wall showed that the wall was free from frictional drag. The ball transfers were installed between tests EP 11 and EP 12.

4) A chain drive was added to permit moving the instrumented wall towards or away from the fill. The screw jacks for moving the wall were already in place, and only drive shafts, sprockets, and chain were required to be able to move the wall. The current movement capability is for translation of the wall. Other gearing would be required to permit rotating the wall.

5) An aliphatic petroleum distillate, Thompson's Water Seal, was applied to the center two panels, panels 2 and 3, to reduce drift in the pressure cell measurements. This treatment is discussed in more detail in Chapter 4. The Thompson's Water Seal treatment was applied between tests EP 12 and EP 13.

6) A laminated plastic covering was applied to the end wall of the facility and the wall opposite from the instrumented wall. The plastic covering made the process of lubricating these walls much easier. Wall lubrication is discussed in Chapter 7. The laminated plastic was applied between tests EP 11 and EP 12.

CHAPTER 4 - INSTRUMENTATION BEHAVIOR

4.1 Introduction

The instrumented retaining wall includes 20 load cells, 15 contact pressure cells, 9 LVDT's, 12 thermocouples, and 13 ultra-sonic distance measuring devices. Sehn and Duncan (1990) have described the characteristics, installation, and calibration of these instruments, as well as their performance during the first four instrumented retaining wall tests. Subsequent tests (EP 5 through EP 16) disclosed some new information about the performance of the load cells and pressure cells. That new information is the subject of this chapter.

The tests show that the load cell data are free from scatter and are stable over time. The pressure cell readings, however, exhibit scatter and drift over time. Scatter and drift in contact pressure cell readings have also been reported by Spangler and Mickle (1956), Corbett et al. (1971), Jones and Sims (1975), Coyle and Bartoskewitz (1976), Roth et al. (1979), Smoltczyk et al. (1979), Schulze et al. (1981), and Vogt et al. (1986), among others. Dunnicliff (1988) attributes scatter in pressure cell readings to calibration errors from cell to cell and to local variations in soil conditions which affect individual cells because of their small size. Pressure cell drift is often attributed to temperature changes. However, in some reported instances, the drift does not seem to be caused by temperature changes and has remained unexplained.

An unanticipated result of this research is the discovery that moisture migration from backfill to concrete is also a source of drift for contact pressure cells, at least for hydraulic cells which are cast in concrete walls. It appears as though a slight expansion of the concrete around a cell decreases the fluid pressure inside the cell and thereby causes negative drift of the cell readings. This source may account for at least part of the pressure cell drift that has been reported in the literature for contact pressure cell installations.

4.2 Some Previous Examples of Contact Pressure Cell Drift

Coyle and Bartoskewitz (1976) instrumented the back side of a precast panel retaining wall with nine Terra Tec contact pressure cells. These are hydraulic pressure cells with a pneumatic pressure sensing system. The concrete panel was laterally supported by four load cells. The force on the panel was computed both by summing the load cell readings and by integrating the pressure cell readings over the area of backfill. The results of the measurements are shown in Figure 4.1. Negative drift of the pressure cell readings compared to the load cell readings is clear, even though the last reading suggests a possible reversal of the trend at day 443. The relatively constant force from the load cells indicates that neither relaxation of compaction induced stresses nor reduction of lateral pressures due to creep movements of the wall away from the backfill could account for the negative pressure cell drift in this case. An attempt was made to correct the pressure cell readings for temperature changes, but the temperature correction

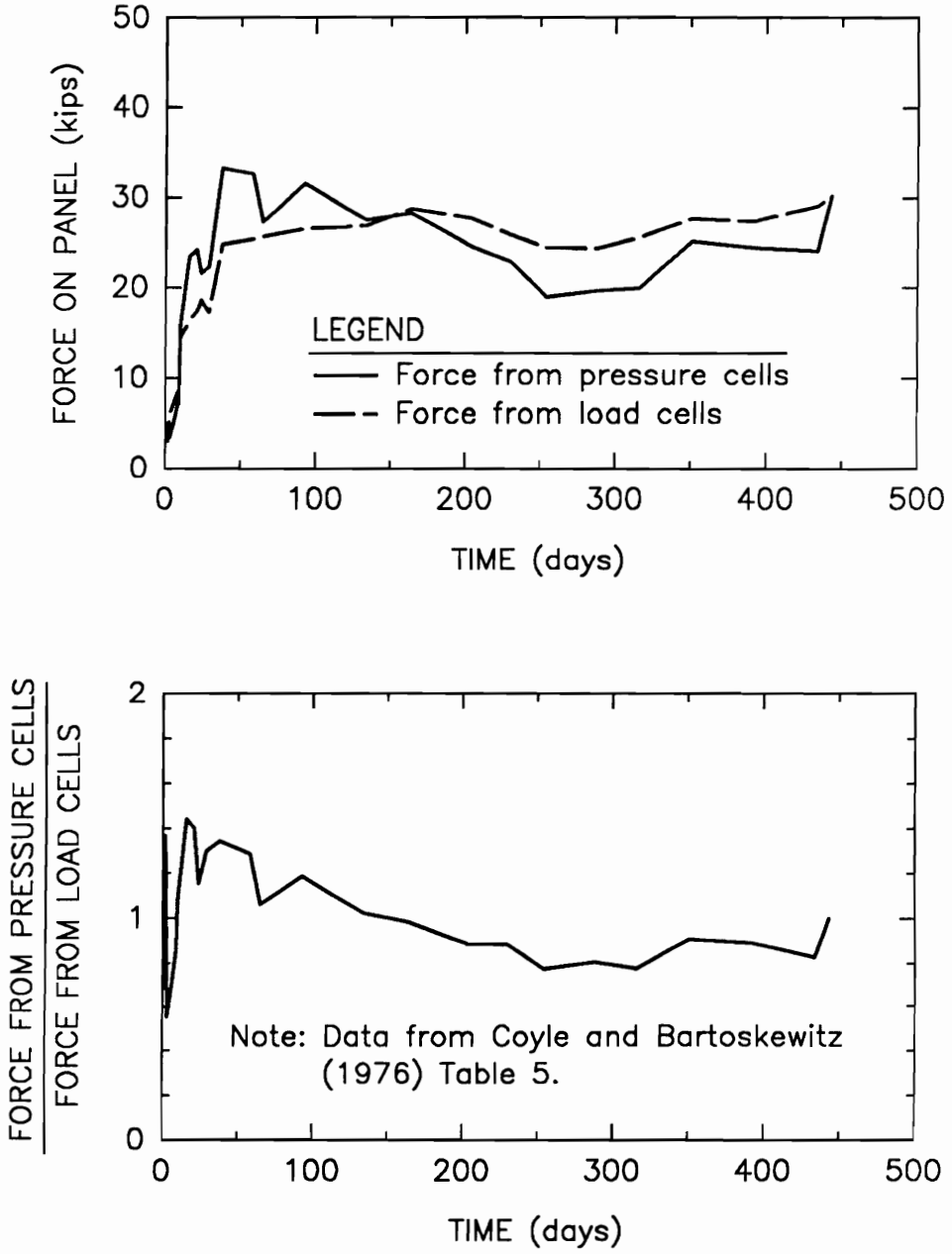

Figure 4.1: Contact Pressure Cell Drift for an Instrumented Precast Panel Retaining Wall (Coyle and Bartoskewitz, 1976)

was established with the cells exposed to air and probably understates the effect of temperature changes on buried pressure cells. Nevertheless, it seems unlikely that temperature decreases could have been the cause of the negative pressure cell drift, at least during the early part of the time history shown in Figure 4.1, since the summer season occurred from days 79 to 170, a period of negative pressure cell drift. Thus, the negative drift in this case is unexplained by the usual sources.

Roth et al. (1979) installed contact pressure cells on a deep basement wall and recorded pressures during and after backfilling. Decreasing pressure readings were recorded under constant, and even occasionally increasing, fill height. They believed that most of the decrease was due to relaxation of compaction-induced pressures.

Schulze et al. (1981) installed 12 contact pressure cells on a cantilevered, concrete retaining wall with a spread footing and key. The cells were Terra Tec cells and they were installed on the back of the stem, on the footing, and on the key of the retaining wall. All the pressure cells experienced negative drift and most drifted negative so far that they produced pressure readings less than zero. The drift was seasonal, with the pressures decreasing during the fall and winter and increasing during the spring and summer. This suggests that temperature changes could be a cause of the drift. A temperature correction was applied and it removed some, but not all, of the seasonal fluctuation. Pressure cell readings less than zero still occurred after applying the correction. Readings less than zero cannot result from either

relaxation of compaction induced pressures or from creep movements of the wall away from the backfill. The authors concluded that the negative pressure readings could not be explained.

4.3 Pressure Cell Calibrations

Two types of calibration are commonly performed for contact pressure cells: calibration by applying a fluid pressure and calibration by applying pressure through soil in contact with the cell. Dunnicliff (1988) recommends that both types of calibration be performed and that the soil calibration be performed using the same soil and placement conditions as will occur in service.

Both fluid and in-situ calibrations were accomplished for the pressure cells used in the instrumented retaining wall. After the cells were mounted in the wall, they were calibrated using a fluid (air) pressure applied through a rubber membrane. Details of the fluid calibration are presented by Sehn and Duncan (1990). The fluid calibrations are useful for evaluating the performance of the pressure cells and for comparing the pressure cell measurements to the load cell measurements.

The in-situ calibrations were accomplished by determining the average effect of the soil backfill in each test on the pressure cell response. It was not feasible to perform individual soil calibrations on each cell for each soil condition because there are 15 cells in the wall and the soil conditions change with every change of soil type, water content, and compactor type. Instead, readings from the

horizontal load cells, whose accuracy is unaffected by soil backfill characteristics, were used to adjust the pressures obtained using the fluid calibrations of the pressure cells. The adjustment factor is the ratio of the horizontal force obtained from the load cells to the horizontal force obtained by integrating the pressure cell readings over the backfill height. Thus, the best estimate of the pressure distribution on the wall is given by multiplying the individual pressure cell readings (reduced using the fluid calibrations) by the adjustment factor from the load cell data. This method was used by Carder, et. al. (1977) for their test wall. The values of the adjustment factors calculated at the end of backfilling using this technique are listed in Table 4.1.

The adjustment factors in Table 4.1 are all close to unity, indicating that the response of these pressure cells is not strongly dependent on the characteristics of the medium through which pressure is applied. As described in Chapter 2, both Gloetzl cells and Carlson cells are installed in the instrumented retaining wall. Both types of pressure cells are hydraulic cells with thin fluid layers behind active outer faces. In our specially modified Gloetzl cells, the fluid pressure is read by an electric pressure transducer. In the Carlson cells, the pressure is read by a sensitive extensometer connected to a small diaphragm located on the opposite side of the fluid layer from the active face. Because both types of pressure cell are very stiff, it is reasonable that calibration with an applied fluid pressure is not much different from in-situ calibration with pressure applied through a soil.

TABLE 4.1: Pressure Cell Adjustment Factors from In-Situ Calibration

Instrumented Retaining Wall Test Number	Backfill Type[1]	Backfill Water Content (percent)	Pressure Cell Adjustment Factors[2]
EP 5	YSS1	9.3	1.16
EP 6	YSS1	9.7	1.04
EP 7	YSS1	11.1	1.05
EP 8	YSS1	12.1	1.01
EP 9	YSS1	12.5	1.06
EP 10	YSS1	11.8	1.15
EP 11	YSS1	13.5	0.93
EP 12	YSS1	12.3	0.98
EP 13	YSS2	12.7	0.97
EP 14	YSS2	10.1	0.88
EP 15	LCS	<0.1	0.87
EP 16	LCS	<0.1	0.92

Notes: 1) YSS1 indicates Yatesville Silty Sand No. 1, YSS2 indicates Yatesville Silty Sand No. 2, and LCS indicates Light Castle Sand.

2) The Pressure Cell Adjustment Factor is the ratio of the horizontal force obtained from the load cells to the horizontal force obtained by integrating the pressure cell readings. The factors listed are calculated at the end of backfill placement.

4.4 Instrumented Retaining Wall Test Results

A set of typical test results is shown in Figures 4.2 through 4.6. These results are from test EP 8, in which the Wacker BPU2440A vibrating plate was used to compact Yatesville Silty Sand backfill. Characteristics of instrumentation behavior illustrated by these results are discussed in the following sections.

4.4.1 Pressure Cell Data Scatter

Figure 4.2 shows the pressure cell readings immediately after compaction of the last lift of backfill. There is significant scatter in the data, but, because there are so many cells (15 cells in the 6.5-foot fill height), the pressure distribution on the wall can still be discerned reasonably well. Similar scatter in contact pressure cell readings, and the need for a large number of cells to permit a confident interpretation of the data, have been noted by Vogt, et. al. (1986) and Dunnicliff (1988).

4.4.2 Load Cell Behavior

The significant scatter in the pressure cell data is not mirrored in the load cell data. Figure 4.3 shows the variation in horizontal force with fill height and time after backfilling for each of the four instrumented panels. The horizontal force shown is the sum of the readings from the three horizontal load cells behind each panel divided by the 2.5-foot panel width. Some averaging of individual load cell readings occurs because three load cell readings are added together to

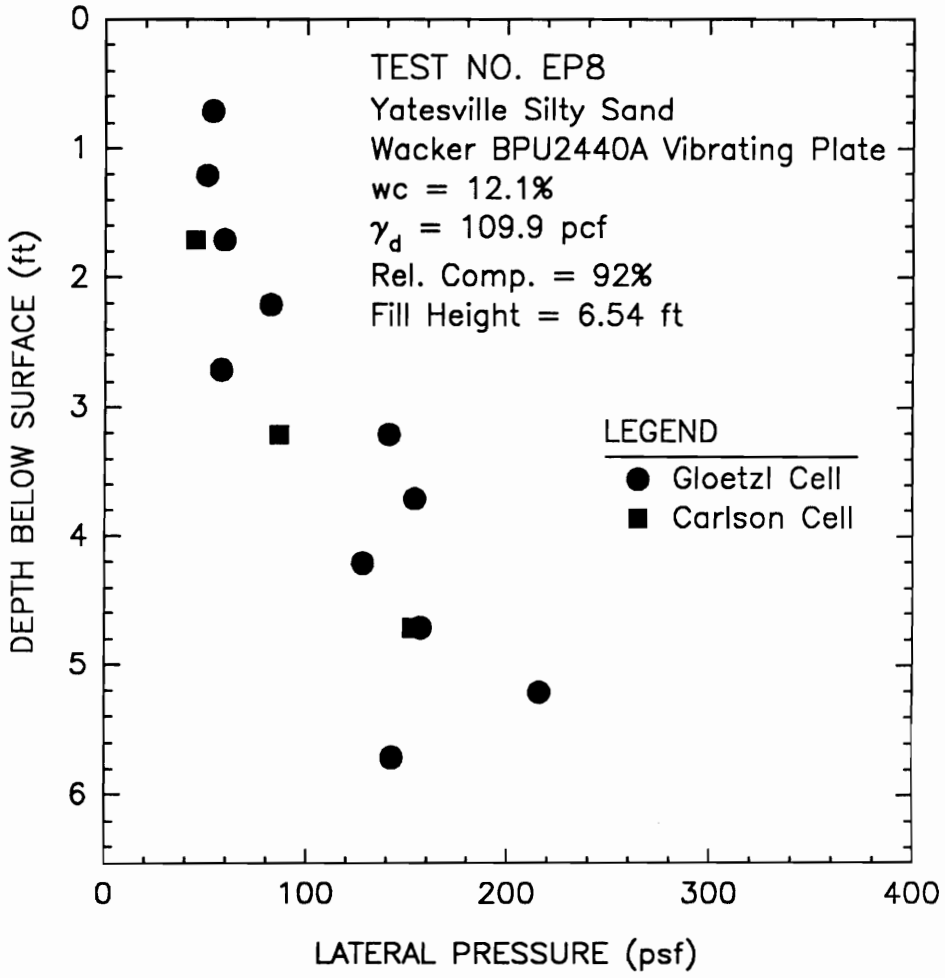

Figure 4.2: Contact Pressure Cell Readings at End of Backfilling for Test EP 8

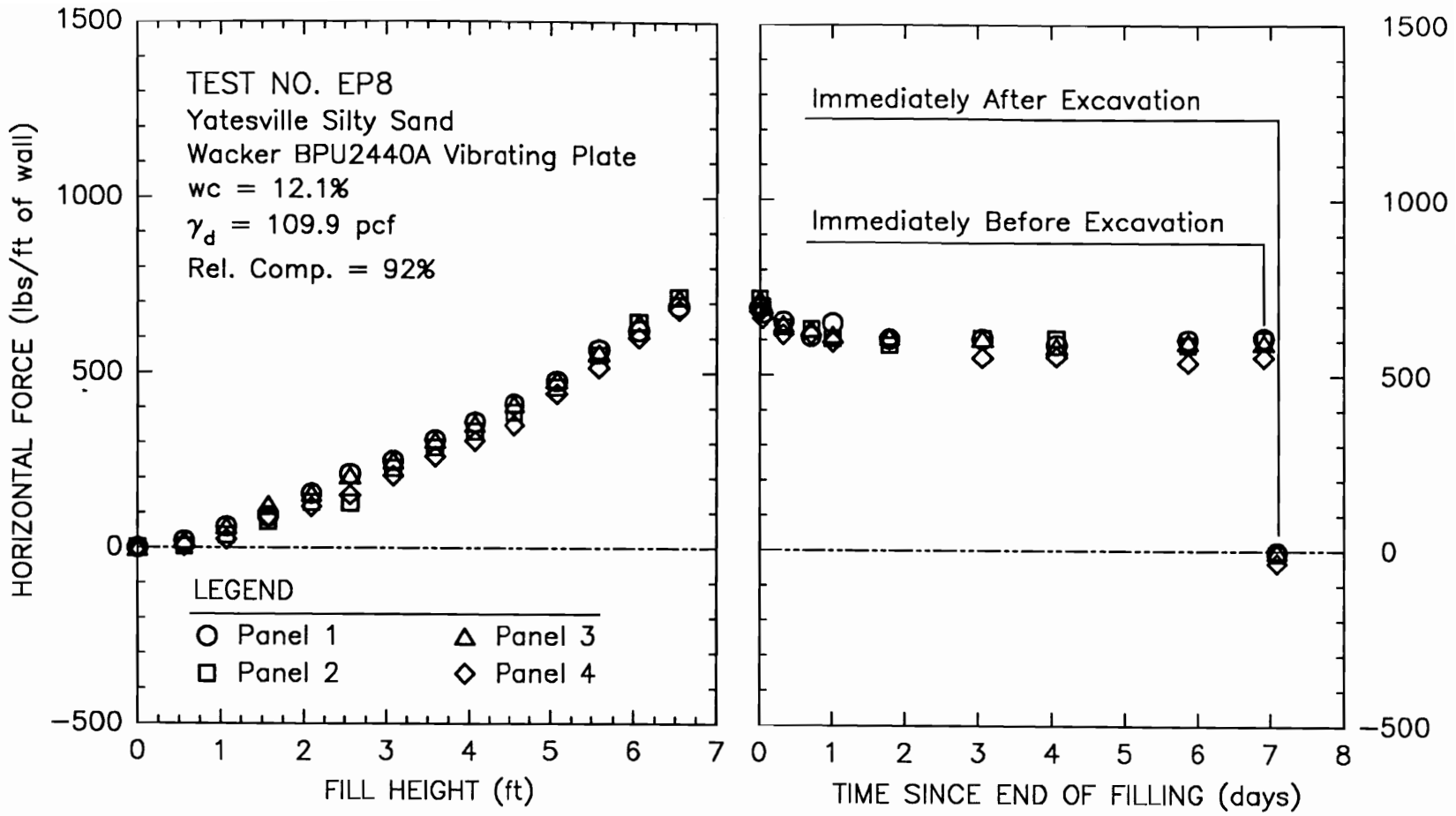

Figure 4.3: Horizontal Load on the Instrumented Retaining Wall from Load Cell Data during Test EP 8

obtain the horizontal force on each panel. Nevertheless, the very close agreement among the data for the four panels shown in Figure 4.3 indicates that the load cell data are not subject to the degree of scatter which affects the pressure cell data. The consistency in the data from panel to panel is undoubtedly due to the large contact areas for the panels, approximately 16.3 ft^2 per panel.

The horizontal forces shown in Figure 4.3 increase with increasing fill height during the backfilling period, as expected. Subsequent readings show a slight decrease in horizontal load during the first two days after completion of backfilling, and approximately constant horizontal load thereafter. The decrease in horizontal load could be due to relaxation of compaction-induced horizontal pressures and, possibly, due to a decrease in pore water pressures with time. Figure 4.3 also shows the measured horizontal loads immediately after the backfill was excavated. As shown, the loads return essentially to zero, indicating that the load cell response is stable over the test period.

Similar data for the vertical shear forces on each panel are shown in Figure 4.4. In this case, the forces are obtained from the two vertical load cells at the bottom of each panel. Again, there is very close agreement among the data for the four panels.

Figure 4.4 shows that the vertical shear load increases with increasing fill height during the backfilling period and then, for this test, continues to increase with time after completion of backfill placement. The increase in vertical shear load with time is due to settlement of the backfill and mobilization of additional shear stress

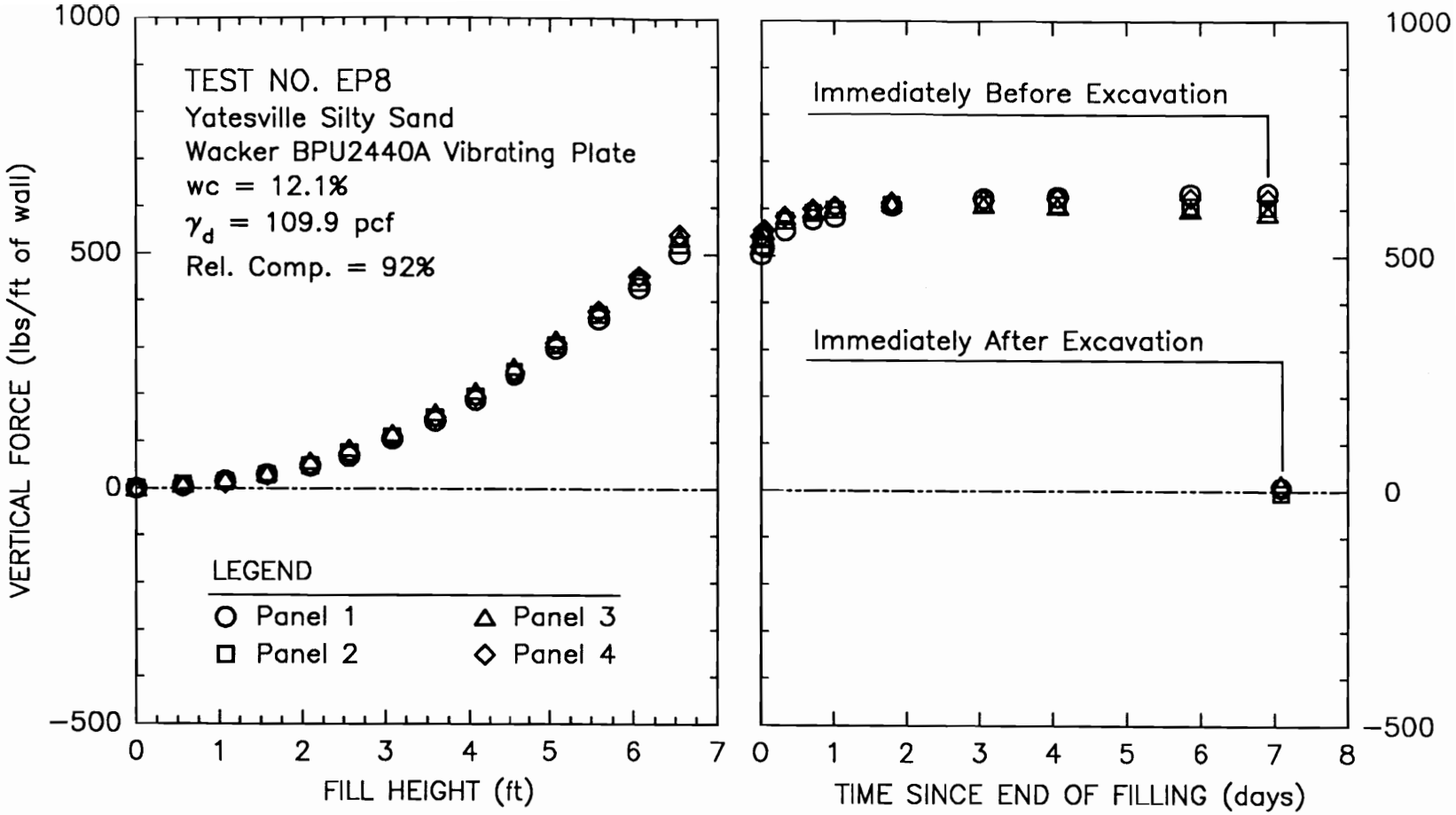

Figure 4.4: Vertical Load on the Instrumented Retaining Wall from Load Cell Data during Test EP 8

at the interface with the wall. After excavation, the vertical loads return essentially to zero, indicating that the load cell response is stable over the test period.

In test EP 8, the force data for all four panels are essentially the same. Consequently, studies of the forces applied by the backfill to the wall could be based on the average of the readings for all four panels in this case. In test EP 8, the end wall of the backfill placement area was lubricated so that the test would model two-dimensional conditions. End wall lubrication resulted in forces on panel 1 that matched those from the other panels. However, the end wall was not lubricated for all tests and, when it was not lubricated, the forces on panel 1 were different than the forces on the other panels. In order to adopt a standard procedure for all tests which eliminates the potential influence of end effects on panels 1 and 4, only averages of the forces measured on panels 2 and 3 have been used.

4.4.3 Comparison of Pressure Cell and Load Cell Data

As discussed previously, the performance of the pressure cells, when reduced with their fluid calibrations, can be compared to the performance of the load cells by integrating the pressure cell data over the depth of backfill and comparing the resultant horizontal force to the horizontal force from the load cell data. Figure 4.5 shows this type of comparison for test EP 8. The forces agree well during the backfilling period, but diverge with time after filling.

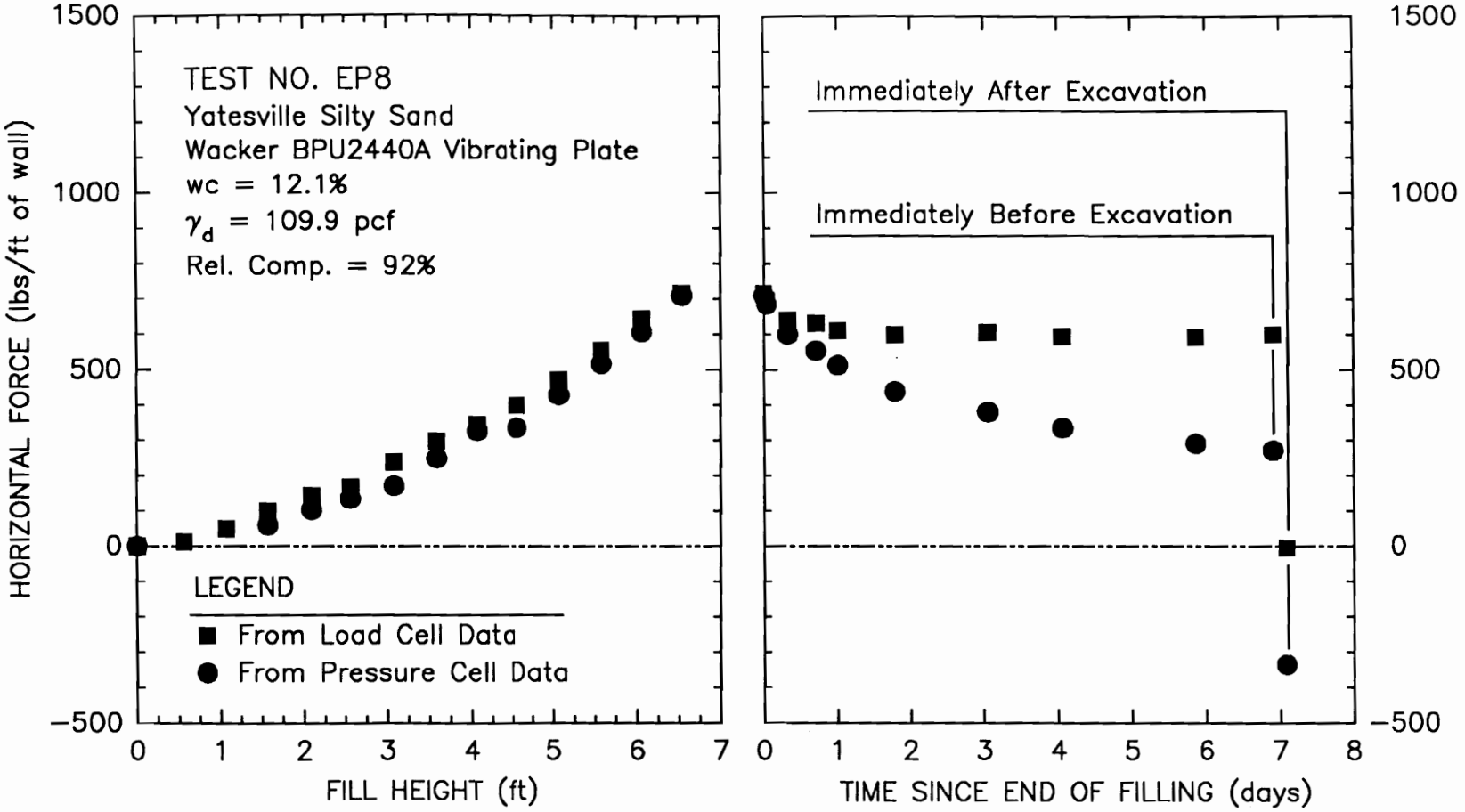

Figure 4.5: Comparison of Horizontal Force Magnitudes Computed from the Load Cell Data and from the Pressure Cell Data for Test EP 8

For all the instrumented retaining wall tests, the forces obtained by these two methods were in good agreement during backfilling. The closeness of agreement is indicated by the proximity to unity of the adjustment factors in Table 4.1. After backfilling, on the other hand, the forces diverged for some tests and not for others. The divergence was generally greatest for the tests with wet Yatesville Silty Sand backfill. When the forces diverged, the force from the pressure cell data always drifted below the force from the horizontal load cells.

In the case of test EP 8, Figure 4.5 shows that at 6.9 days after filling the force from the pressure cell data is 329 lbs. per ft. of wall less than the force from the load cell data. Excavation of the backfill was completed at 7.1 days after filling and, at that time, the force measured by the load cells is -5 lbs. per ft. while the force computed from the pressure cell data is -336 lbs. per ft. Since the load cells returned essentially to zero load after excavation, the data indicate that the pressure cell readings drifted negative. The average drift per cell for this test can be computed by dividing the total drift of about -330 lbs. per ft. by the backfill height, in this case 6.54 feet, to get an average drift of -50 psf for each pressure cell.

The average drift of the pressure cells relative to the load cell data was computed in this manner for all the instrumented retaining wall tests and the results are listed in Table 4.2. The pressure cell drift is negative for all the tests except for the two with the dry Light Castle Sand backfill. During these two tests, there was essentially no drift.

TABLE 4.2: Pressure Cell Drift

Instrumented Retaining Wall Test Number	Backfill Type[1]	Backfill Water Content (percent)	Retaining Wall Surface Treatment[2]	Pressure Cell Drift[3] (psf)
EP 5	YSS1	9.3	Untreated	-30.7
EP 6	YSS1	9.7	Untreated	-51.6
EP 7	YSS1	11.1	Untreated	-39.8
EP 8	YSS1	12.1	Untreated	-38.8
EP 9	YSS1	12.5	Untreated	-71.1
EP 10	YSS1	11.8	Lubricated	-5.8
EP 11	YSS1	13.5	Untreated	-56.1
EP 12	YSS1	12.3	Untreated	-58.1
EP 13	YSS2	12.7	Water Seal	-28.9
EP 14	YSS2	10.1	Water Seal	-13.8
EP 15	LCS	<0.1	Water Seal	+2.0
EP 16	LCS	<0.1	Water Seal	+0.1

Notes:
1) YSS1 indicates Yatesville Silty Sand No.1, YSS2 indicates Yatesville Silty Sand No. 2, and LCS indicates Light Castle Sand.
2) The Untreated wall surface is the screeded, unfinished concrete surface. The Lubricated wall condition was obtained by placing two sheets of 6-mil polyethylene, with a thin layer of grease between the sheets, against the instrumented wall surface. The Water Seal treatment was obtained by applying three coats of Thompson's Water Seal to the concrete surface.
3) The Pressure Cell Drift is the average drift of 11 Gloetzl cells and 4 Carlson cells occurring during a four day period following completion of backfill placement. The drift is computed relative to the horizontal load cell data, as explained in the text.

In addition to comparing horizontal force magnitudes from the pressure cell data to the load cell data, the location of the resultant force on the wall can be determined from each type of data by summing moments about the base of the wall. Figure 4.6 shows this comparison for test EP 8. Again, the results from the two types of data agree well during the backfill period but diverge with time after filling. For all the instrumented retaining wall tests, the resultant locations obtained from these two methods were in good agreement during backfilling, but, after backfilling, the resultant locations diverged for some tests and did not diverge for others. When the resultant locations diverged, the location from the pressure cell data was always below the location from the load cell data. This indicates that, when divergence occurred, the upper pressure cells drifted negative by a greater fraction of their end-of-filling readings than did the lower cells. This behavior is consistent with negative drift that is independent of the pressure registered at the end of filling.

4.5 Cause of Pressure Cell Drift

Two possible causes for the observed pressure cell drift are temperature effects and moisture effects on the concrete surrounding the pressure cells. Changes in temperature can cause changes in hydraulic pressure cell reading due to differences in thermal expansion coefficients of the fluid in the cell and the cell body, which is usually some type of metal container. Because of cell-soil interaction effects, the influence of temperature can be more pronounced when the

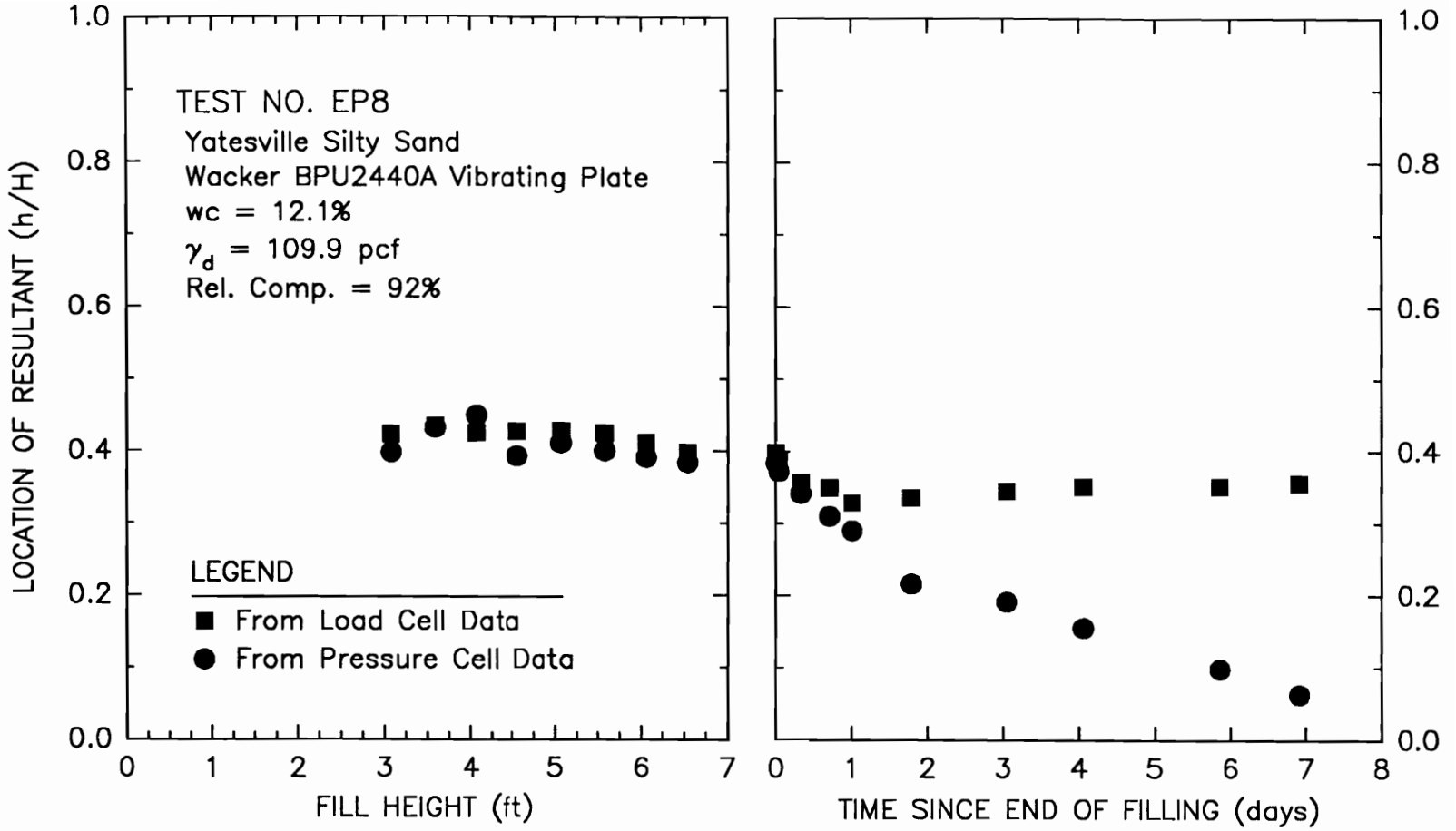

Figure 4.6: Comparison of the Resultant Force Locations Computed from the Load Cell Data and from the Pressure Cell Data for Test EP 8

cell is mounted in a wall and confined by soil than when it is only confined in a fluid such as air or water. According to Dunnicliff (1988), the best procedure to guard against temperature effects is to design the cell to have low temperature sensitivity by using a thin fluid layer in the cell. Both the Carlson and Gloetzl type cells used in these experiments have thin fluid layers and should not be very temperature sensitive. To further reduce temperature effects, the backfill was held at the same temperature as the wall by stockpiling the backfill between tests in the same room as the wall is located. In fact, the measured temperature changes at the pressure cell locations were always less than 2°F during the periods after backfilling when pressure cell drift occurred. Negative drift occurred whether the small temperature changes were positive or negative. For these reasons, temperature effects cannot account for the observed pressure cell drift in these experiments.

Another possible cause for contact pressure cell drift is the effect of moisture from the backfill moving into the concrete and causing a slight expansion of the concrete in the vicinity of the cell. Concrete expansion around the cell could cause a complex straining of the cell with the net effect being to reduce the pressure of the fluid inside the cell. Figure 4.7 shows a hypothesized zone of moist concrete around a contact pressure cell. Expansion of the concrete in such a zone could cause a fluid pressure reduction inside the cell due to bending of the cell body.

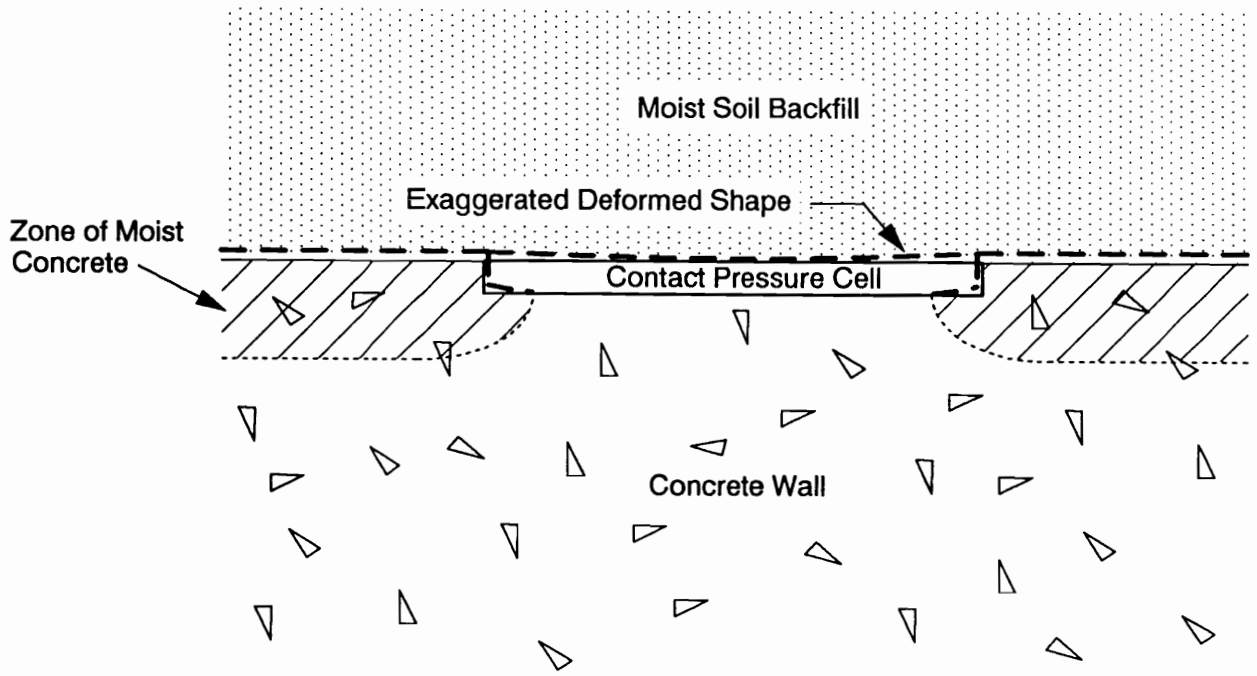

Figure 4.7: Hypothetical Mechanism for Negative Pressure Cell Drift Due to Moisture Migration from Backfill to Concrete

The first strong evidence in the instrumented retaining wall tests that moisture transfer from the backfill to the wall could be the cause of the pressure cell drift came from test EP 10. This test was performed to study the effect on normal pressures of reducing shear stresses at the instrumented wall surface. The reduction in shear stress was accomplished by placing a lubricating layer, which consisted of two 6-mil plastic sheets with a thin layer of grease between the sheets, against the instrumented wall. Unintentionally, this lubricating layer also prevented moisture transfer from the backfill to the wall. The pressure cell drift listed in Table 4.1 for test EP 10 is only -6 psf, which is much less than the drift for the previous tests, and this supports the idea that moisture transfer could be the cause of the drift. However, other effects of the lubricating layer could have influenced the tendency for pressure cell drift. For example, Carder and Krawczyk (1975) found that contact pressure cell readings appeared to be affected by shear stresses at the contact. Thus, changes in shear stresses on the wall with time after filling could, conceivably, be part of the reason for the observed pressure cell drift in tests other than EP 10.

In order to further investigate whether moisture moving into the concrete could cause pressure cell drift, small reservoirs were constructed at two Gloetzl cell locations and readings were taken over time after the cells were submerged. The water used for submergence was at the same temperature as the wall to eliminate temperature effects during the test. Negative drift in the pressure cell readings occurred

and the drift is shown by the data labeled "Untreated" in Figure 4.8. The reference reading for the data in Figure 4.8 was taken immediately after submergence in order to zero the small positive pressure reading caused by the hydrostatic pressure.

Next, the reservoirs were removed and the concrete surface was treated with three applications of Thompson's Water Seal in test patches around the two Gloetzl cells used for the untreated submergence test. Thompson's Water Seal is an aliphatic petroleum distillate which makes the concrete surface hydrophobic and penetrates into the pores in the concrete, but does not seal the pores. Thus, if moisture migration into the concrete is the cause of the pressure cell drift, then applying Thompson's Water Seal should reduce but not eliminate the drift since moisture could still move into the concrete by vapor movement into the pores. After the Thompson's Water Seal dried, the reservoirs were replaced, the cells submerged, and readings were again taken over time. Negative drift still occurred, as shown in Figure 4.8, but it was much smaller than the drift which occurred for the untreated, submerged cells.

An interesting feature of the data in Figure 4.8 is that, for both the treated and untreated tests, the drift is very small for the first day following submergence. This may be due to the time required for the moisture to penetrate the concrete sufficiently to cause significant straining of the cell, as suggested in Figure 4.7. In any case, the fortunate one-day delay in pressure cell drift seems to permit the close

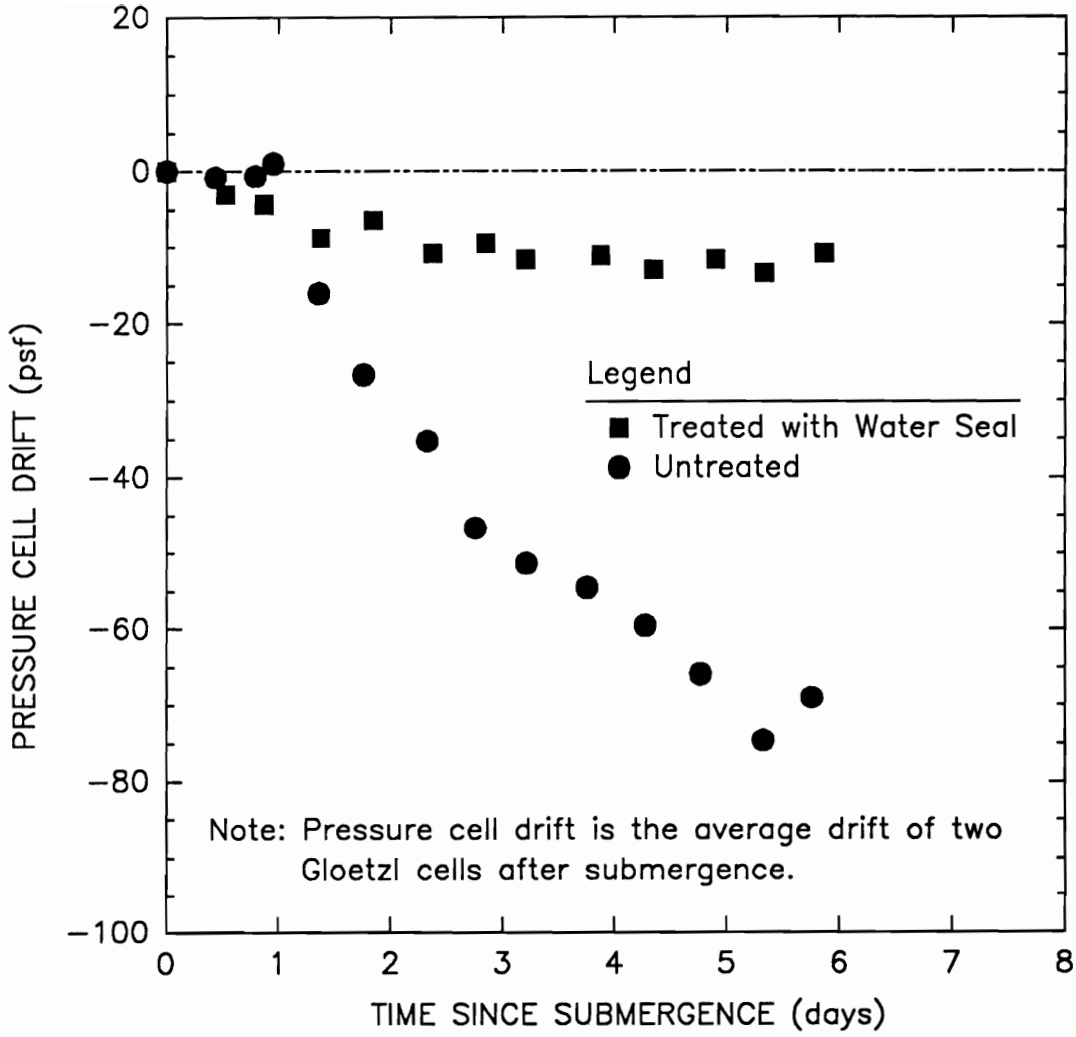

Figure 4.8: Gloetzl Cell Submergence Test Results

agreement between the pressure cell data and the load cell data shown in Figure 4.5 during the backfilling period.

The results of the submergence tests suggested that Thompson's Water Seal might reduce pressure cell drift during the instrumented retaining wall tests, so panels 2 and 3, which contain the pressure cells, were treated. The pressure cell drifts listed in Table 4.2 for tests EP 13 and 14, which were performed after treatment with Thompson's Water Seal, are smaller than the drifts for the untreated Yatesville Silty Sand tests, in agreement with the trend for the submergence tests.

The pressure cell drifts for all the Yatesville Silty Sand tests are shown in Figure 4.9. Though there is scatter in the data, the trend is for more negative drift in tests with higher backfill water contents. Figure 4.9 also shows the smaller drifts which occurred for the tests with Thompson's Water Seal treatment and the essentially zero drift for the lubricated wall condition. Finally, it is noted that the drift listed in Table 4.2 for tests EP 15 and 16, which were backfilled with dry (water content less than 0.1 percent) Light Castle Sand, were essentially zero. Together, this evidence leads to the conclusion that moisture moving from the backfill to the concrete wall was the cause of the observed negative pressure cell drift.

4.6 Summary and Conclusions

Both fluid and in-situ calibrations of the contact pressure cells were performed. The calibrations do not differ by more than 16 percent,

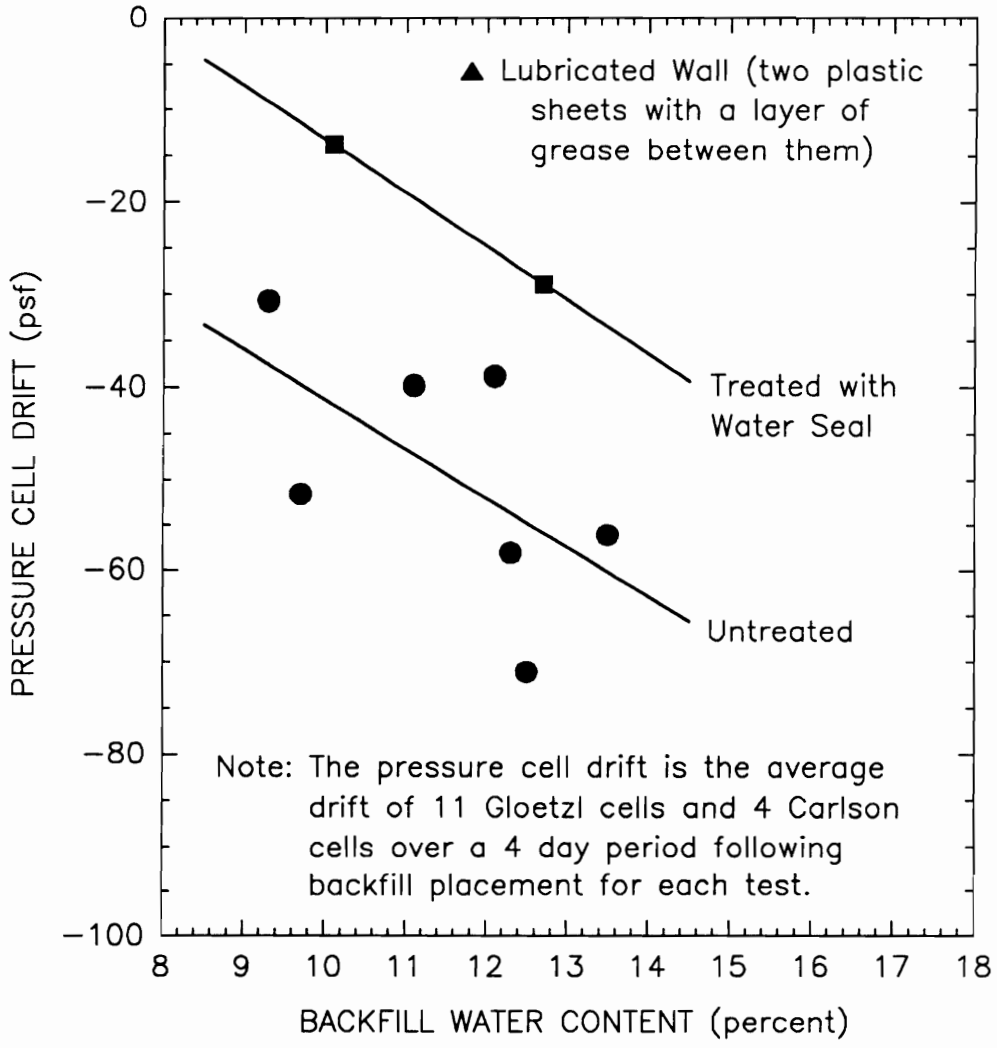

Figure 4.9: Summary of the Pressure Cell Drifts for the Yatesville Silty Sand Tests

probably because the pressure cells installed in the instrumented retaining wall are very stiff.

The contact pressure cell data exhibit significant scatter, which may be due to local variations in soil conditions. However, the pressure cells can still be used to determine pressure distributions on the instrumented retaining wall because of the great number of pressure cells in the wall (15 cells in the 6.5-foot fill height).

There is very little scatter in the load cell data, presumably because of the relatively large panel areas, about 16 ft^2 per panel. In addition, the load cell response is stable over the duration of the tests, returning to zero load readings after backfill excavation.

The pressure cell response can be compared with the load cell response by integrating the pressures over the depth of the backfill. These comparisons showed that the pressure cell data and the load cell data were in good agreement during the backfilling period, but that, for moist backfill, the pressure cell readings tended to drift negative over a several day period after completion of filling. It is well known that temperature changes can cause changes in pressure cell readings under constant externally applied pressure. However, temperature changes were not the cause of the observed pressure cell drift in these tests. Instead, a series of experiments showed that the drift was caused by moisture migrating from the backfill into the concrete retaining wall. The mechanism responsible for the drift is not known with certainty, but it is possible that a slight expansion of the concrete around the cells

could cause the cells to deform and decrease the fluid pressure inside the cells.

Applying Thompson's Water Seal to the retaining wall tended to reduce, but not eliminate, the pressure cell drift. An impervious coating, such as epoxy paint, would likely reduce the drift even further. It is also possible that an isolation system for the pressure cells could be employed to reduce drift. However, the isolation system would have to be carefully designed to provide rigid support for the cell while isolating the cell from expansion of the concrete.

In the instrumented retaining wall tests, the pressure cell drift over a four day period for moist backfill on untreated concrete ranged from -30 to -70 psf. That amount of drift is very significant when measuring lateral pressures on low walls. Where higher pressures are involved, drift from this source may be less important. However, the long-term influence of moisture on contact pressure cell drift is not known. The data in Figure 4.8 indicate that drift of the untreated, submerged cells had not stabilized at the end of the 6 day test period, suggesting that the drift may become large for long-term exposure to moisture.

It is clear that this potential source of drift should be considered when installing contact pressure cells and when interpreting contact pressure cell data.

CHAPTER 5 - HAND-OPERATED COMPACTOR PERFORMANCE

5.1 Introduction

Hand-operated equipment is commonly used to compact backfill in confined areas and adjacent to structures such as walls and culverts. The vertical force from the compactor tends to displace soil laterally and, after compaction, horizontal stresses in the backfill can exceed at-rest stresses. Compaction-induced horizontal stresses can cause structural damage and excessive deformations of walls and culverts. Theories for estimating the magnitude of compaction-induced lateral earth pressures have been proposed by Broms (1971) and Duncan and Seed (1986).

One very important factor in determining the magnitude of compaction-induced pressures is the vertical contact force between compactor and soil. In this research, the vertical contact force was measured for two hand-operated compactors: a 137-pound rammer compactor and a 275-pound vibrating plate compactor. Contact force measurements were made while operating the rammer compactor and the vibrating plate compactor on two soils: a moist, silty sand and a dry, clean fine sand.

In addition to their usefulness for the compaction-induced earth pressure problem, compactor force measurements may also provide insight into the effectiveness of different compactors for densifying soil (see, for example, Olsen, 1963, and Hilf, 1975).

5.2 Previous Compactor Force Measurements

Whiffen (1954), Toombs (1972), and D'Appolonia et al. (1969) have indirectly measured the force from vibratory roller compactors by using embedded earth pressure cells. The total dynamic compactor force, i.e., including the force from the static roller load, can be estimated by comparing pressure cell output during dynamic compactor loading to pressure cell output during static loading from the known roller load. According to Seed and Duncan's (1983) interpretation of these measurements, the total dynamic force from a vibratory roller is about 2 to 3 times the static roller load.

A different procedure for estimating the dynamic compactor force for a vibratory roller was employed by Yoo and Selig (1979) who proposed a two lumped mass model of the compactor with springs and dashpots to represent the compactor suspension and soil. They measured accelerations on a compactor during operation and selected values of the model parameters (stiffness and damping of the compactor suspension and stiffness and damping of the soil) to give the best fit to the measured accelerations. They then used the model to calculate the dynamic force during roller operation. For a self-propelled, 19,500-pound gross weight vibratory roller compactor operating in the 25 to 35 hz frequency range, Yoo and Selig calculated a total peak dynamic load of 1.4 times the static roller load.

To the writer's knowledge, there have not been any previous measurements of dynamic forces for hand-operated compactors. The Light Equipment Manufacturer's Bureau (LEMB) does provide procedures for

rating hand-operated compactor forces, but these ratings do not yield contact forces, as will be discussed below. The measurements described in this chapter are based on dynamic load cell measurements and on sums of masses times accelerations of compactor components. They do not rely on the dynamic response of embedded earth pressure cells or on an assumed model of soil response.

5.3 Compaction Equipment and Manufacturer's Ratings

5.3.1 Rammer Compactor

The rammer compactor used in this study is the hand-operated Wacker model BS 60Y. It is powered by a 4 horsepower, 2-cycle engine which drives a ramming shoe into contact with the soil at a percussion rate of about 10 blows per second. The ramming shoe is made of polyethylene with a steel bottom plate. A schematic diagram of the rammer compactor is shown in Figure 5.1. The operating weight of the entire compactor is 137 pounds.

The LEMB has developed a method for rating hand-operated, rammer compactors (LEMB, 1981a). In their method, a 3/4-inch diameter hardened steel ball is fastened to the bottom of the ramming shoe and the compactor is operated on a 1-inch thick steel plate. Indentations made by the steel ball on the plate are measured and compared to indentations produced during a calibration procedure in which a weight, with the steel ball attached, is dropped onto the metal plate from various heights. Thus, the LEMB procedure yields a measure of energy delivered to the steel plate per blow from the compactor. A rated force is also

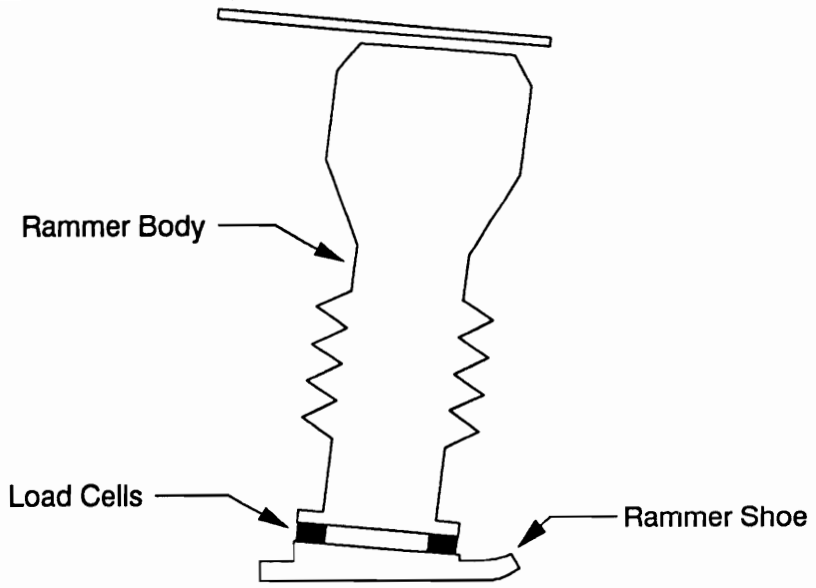

a) Rammer compactor

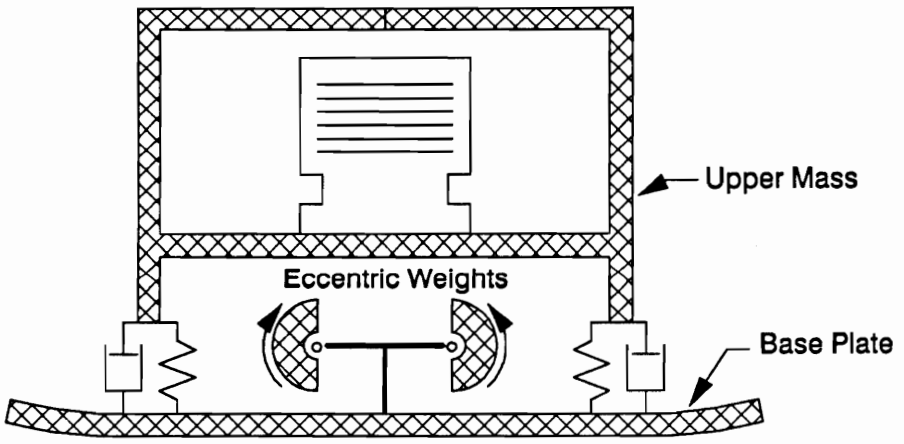

b) Vibrating plate compactor

FIGURE 5.1: Schematic diagrams of a) rammer compactor and b) vibrating plate compactor.

calculated in the LEMB procedure by dividing the rated energy by "the standard soil deflection" of 0.25 inches. For the rammer compactor model used in this study, the manufacturer's rated energy is 57.8 foot-pounds per blow and the rated force is 2775 pounds. The rated energy should be a fairly realistic measure of the energy the compactor will apply to soil, since energy is the basis of the rating method. On the other hand, the rated force is only a nominal value since it is based on an assumed soil deflection. Variations in soil stiffness between dry and wet soil, for example, will be accompanied by variations in deflection and contact forces, even if the energy per blow remains constant. Consequently, actual compactor forces are not expected to be the same for all soils, and they could be quite different from the rated force. Even if the deflection during impact on a particular soil is 0.25 inches, the rated force represents an average, and the peak force would be higher.

5.3.2 Vibrating Plate Compactor

The vibrating plate compactor used in this study is the hand-operated Wacker model BPU 2440A. It is powered by a 5 horsepower, 4-cycle engine which drives counter-rotating eccentric weights. The eccentric weights rotate at a frequency of about 100 hz on axles fixed to a steel base plate which contacts the soil. A schematic diagram of the vibrating plate compactor is shown in Figure 5.1. The operating weight of the compactor is 275 pounds.

Forward and reverse directional control is provided by shifting the eccentric weight on one shaft out of phase with the eccentric weight on the other shaft. This is accomplished by a hydraulic system actuated from a control on the operator's guide handle. In Figure 5.1, the eccentric weights are shown in their neutral position and the resultant centrifugal force is vertical. When the eccentric weights are held out of phase, a horizontal force component occurs. In addition to providing directional control, the phase shift also reduces the net eccentricity of the eccentric weights compared to the neutral position.

The LEMB (1981b) rated force for vibratory plate compactors is the peak centrifugal force calculated using the formula for eccentric weights rotating about a shaft fastened to a fixed support,

$$Q_0 = m_e e \omega^2 \tag{5.1}$$

where

Q_0 = the peak centrifugal force, lbs

m_e = the mass of the eccentric weights, $lb \cdot sec^2/in$

e = the distance from the center of rotation to the center of mass of the eccentric weights, inches

ω = the rotation rate of the eccentric weights, rad/sec

For the model BPU 2440A vibrating plate compactor, the manufacturer's rated centrifugal force is 5400 pounds. For the particular compactor used in this study, measurements of mass times eccentricity and rotation rate were made to calculate the centrifugal

force using Eq. 5.1. The mass times eccentricity was determined by static measurements of the shaft torque in the laboratory. These measurements were taken using both increasing and decreasing torque to cancel the effects of friction in the roller bearings supporting the shaft. As a check, one of the eccentric weights was removed, weighed, and the center of gravity determined. The mass times eccentricity from the direct check was within 0.3 percent of that determined by the shaft torque method. The measured values of mass times eccentricity from the shaft torque method are listed in Table 5.1. As listed in the table, the mass times eccentricity is higher with the eccentric weights held in the neutral position than in the forward position.

The eccentric weight rotation rate during compactor operation was measured using procedures described subsequently. The average measured frequency was 99 hz, and the manufacturer's rated frequency for the model BPU 2440A is 90 hz. Both frequencies were used to calculate the centrifugal force from Eq. 5.1, and the results are listed in Table 5.1. The values of centrifugal force in Table 5.1 are lower than the manufacturer's rating of 5400 pounds. For the neutral eccentric weight position, the value of mass times eccentricity for the compactor used in this study is evidently less than the value used for the manufacturer's rating. For the forward position, the centrifugal force is further reduced because the counter-rotating eccentric weights are shifted out of phase, and are thus less effective.

The centrifugal force calculated from Eq. 5.1 is different from the contact force between the base plate and the soil. There are two

TABLE 5.1: Calculated Centrifugal Force for the Vibrating Plate Compactor

Eccentric Weight Position	Measured Mass Times Eccentricity ($lb \cdot sec^2$)	Calculated Centrifugal Force (pounds)	
		At 90 hz	At 99 hz
Neutral	0.0130	4150	5020
Forward	0.00914	2920	3540

reasons for the difference: 1) the soil provides flexible support instead of the rigid support implicit in the centrifugal force calculation and 2) the weight of the compactor applies force to the soil that is not included in the centrifugal force calculation. The first effect results in contact force magnitudes which are generally below centrifugal force magnitudes. The second effect serves to increase contact forces. Since the compactor only weighs 275 pounds, however, it is expected that the first effect will dominate and that actual contact forces will generally be less than the centrifugal force. Exceptions could occur if the compactor is operating near resonant frequency or if it is operating on a hard material so that the base plate loses contact during part of each cycle. High contact forces could be generated at impact in the latter situation.

5.4 Instrumentation Systems

5.4.1 Rammer Compactor

In this study, the contact force between the bottom of the rammer shoe and the soil was determined by measuring the force on top of the shoe and adding the mass times acceleration of the shoe. The connection between the shoe and the main body of the rammer compactor provided a convenient location for installing load cells to measure the force on top of the shoe. The location of the load cells is shown on the schematic diagram of the rammer compactor in Figure 5.1. The acceleration of the shoe was measured by mounting accelerometers on the shoe.

Both the load cells and the accelerometers are commercially available instruments designed for dynamic applications. The load cells are Kistler 9031A load washers. They are piezoelectric force transducers in which the applied force compresses a quartz crystal and a charge proportional to the magnitude of the force develops across the crystal faces. The charge is converted to a voltage which can be easily measured and recorded. The load cell stiffness is 34,300 kips per inch per cell and, in this application, four cells were used in parallel so the combined stiffness was about 140,000 kips per inch. As a consequence of their high stiffness, the load cells did not appreciably alter the dynamic response of the compactor.

These load cells are not suitable for long term static measurements, because the charge across the quartz crystal in the transducer can dissipate with time. However, the internal resistance of the cells is high and accurate readings can be made for load durations of up to several minutes. This capability was used to calibrate the mounted cells by loading the instrumented compactor in an MTS loading frame in series with a calibrated reference cell.

Two Kistler 8602A500 accelerometers were mounted on the rammer shoe and the average measured acceleration was used to compute the force component from the shoe acceleration. The accelerometers work on the same principle as the load cells except that the force is provided by acceleration of a small reference mass attached to one side of the crystal. The factory calibrations were used for the accelerometers.

High speed data acquisition was necessary to record the short duration impact loads from the rammer compactor. The charge output of the piezoelectric transducers was first converted to an analog voltage signal and amplified. A high speed analog to digital converter installed in a personal computer was used to read data at the rate of 50,000 readings per second. At this rate, data could not be stored using software control so, instead, the data were written directly to memory during the sampling period. Following sampling, the data were read from memory and stored in a file on the hard disk.

A bench test of the instrumentation system was performed by operating the instrumented rammer compactor in a test stand which rigidly held the main body of the compactor and permitted the rammer shoe to move freely in air. The bench test provided an opportunity to check the manufacturer's calibration of the accelerometers against the calibration of the mounted load cells described above. When the rammer shoe moves freely in air, the force on top of the shoe from the load cells should be equal to the mass times acceleration of the shoe. This comparison using data from the bench test is shown in Figure 5.2, and it can be seen that the agreement is good.

5.4.2 Vibrating Plate Compactor

The contact force on the bottom of the vibrating plate compactor was determined by summing masses times accelerations of the compactor components. The compactor was modelled using three lumped masses to represent the components shown in the schematic diagram in Figure 5.1:

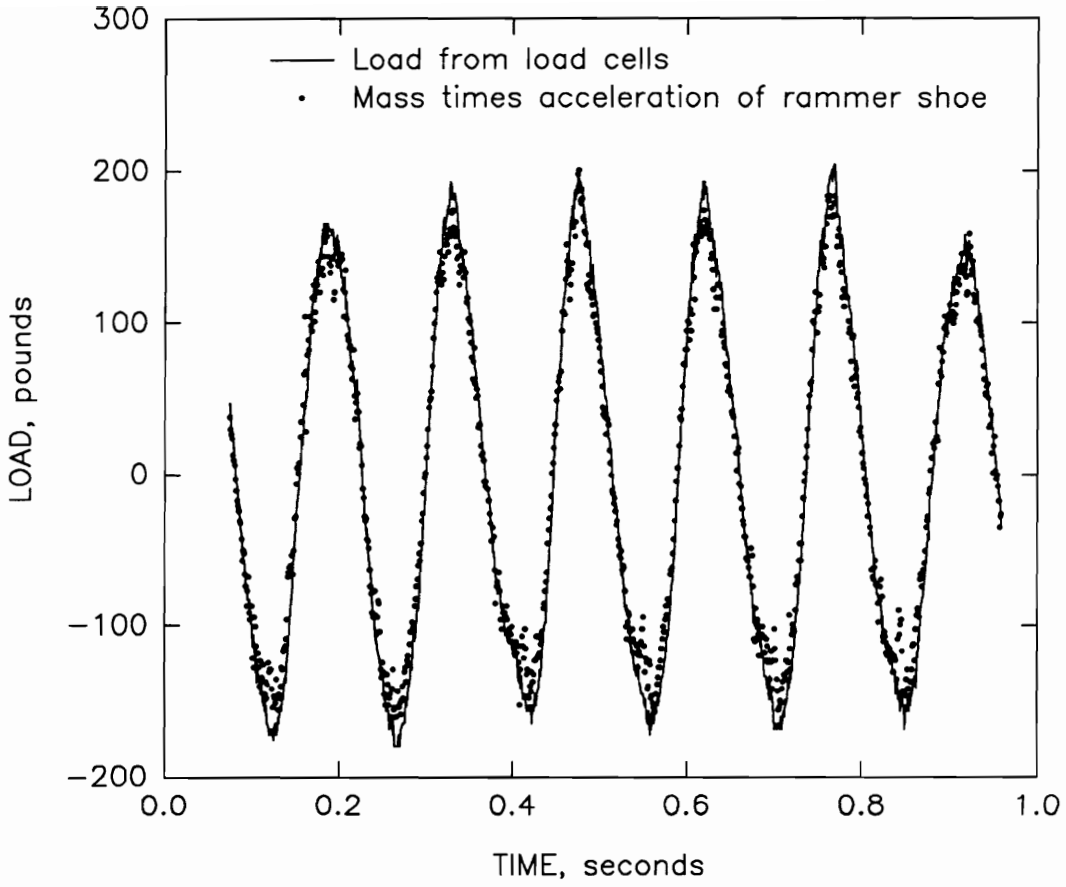

FIGURE 5.2: Rammer compactor bench test.

the base plate, the eccentric weights, and the upper mass. Accelerations of the base plate and the upper mass were measured using the same accelerometers used on the rammer compactor shoe. The vertical acceleration of the eccentric weights, a_e, is given by

$$a_e = a_b + e\omega^2 \sin(\omega t + \phi_0) \tag{5.2}$$

where

a_b = the acceleration of the base plate

t = time

ϕ_0 = the phase angle which indicates the position of the eccentric weights at time zero

In order to add the force component from the eccentric weights to the other two force components, the shaft position must be recorded at the same time as the accelerations of the upper mass and base plate are being recorded, so that the rotation rate and phase angle in Eq. 5.2 are known. To mark the shaft position, a Hall effect device (HED) was mounted on the eccentric weight enclosure and a magnet was mounted on the eccentric weight shaft. HEDs are semiconductor devices which can be configured to change state in the presence of a magnetic field. In this application, output from the HED indicated the shaft rotation rate and initiated data acquisition at the same shaft position for each data set.

The acceleration records for the vibrating plate compactor include noise from local high frequency vibrations at the points of accelerometer mounting. Since the three lumped mass model of this

compactor requires the average acceleration of each lumped mass, it is appropriate to filter the records to remove the noise. Filtering was accomplished by 1) obtaining four immediately sequential data records, each record triggered by the HED, 2) averaging the data from the four records, and 3) using a Fast Fourier Transform (FFT) with a low pass filter to smooth the raw data. The low pass filter passed all energy associated with frequencies below three times the eccentric weight rotation frequency. An example of this filtering process for the base plate acceleration is shown in the upper panel of Figure 5.3. Similar filtering was applied to the raw acceleration data for the upper mass.

The filtered accelerations were multiplied by the appropriate masses to obtain the force components from the upper mass and base plate. The contribution from the eccentric weights was computed using the shaft position and rotation rate from the HED to compute the acceleration with Eq. 5.2, and then multiplying the acceleration by the known mass of the eccentric weights. The three force components from a typical data set are shown in the middle panel of Figure 5.3. The sum of the force components gives the contact force versus time trace in the bottom panel of Figure 5.3.

In order to verify that the instrumentation system and data reduction procedures described above yield the correct force on the base of the compactor, a test was performed using a supplemental base plate with load cells between the original base plate and the supplemental base plate. The supplemental base plate was fabricated of 0.5-inch

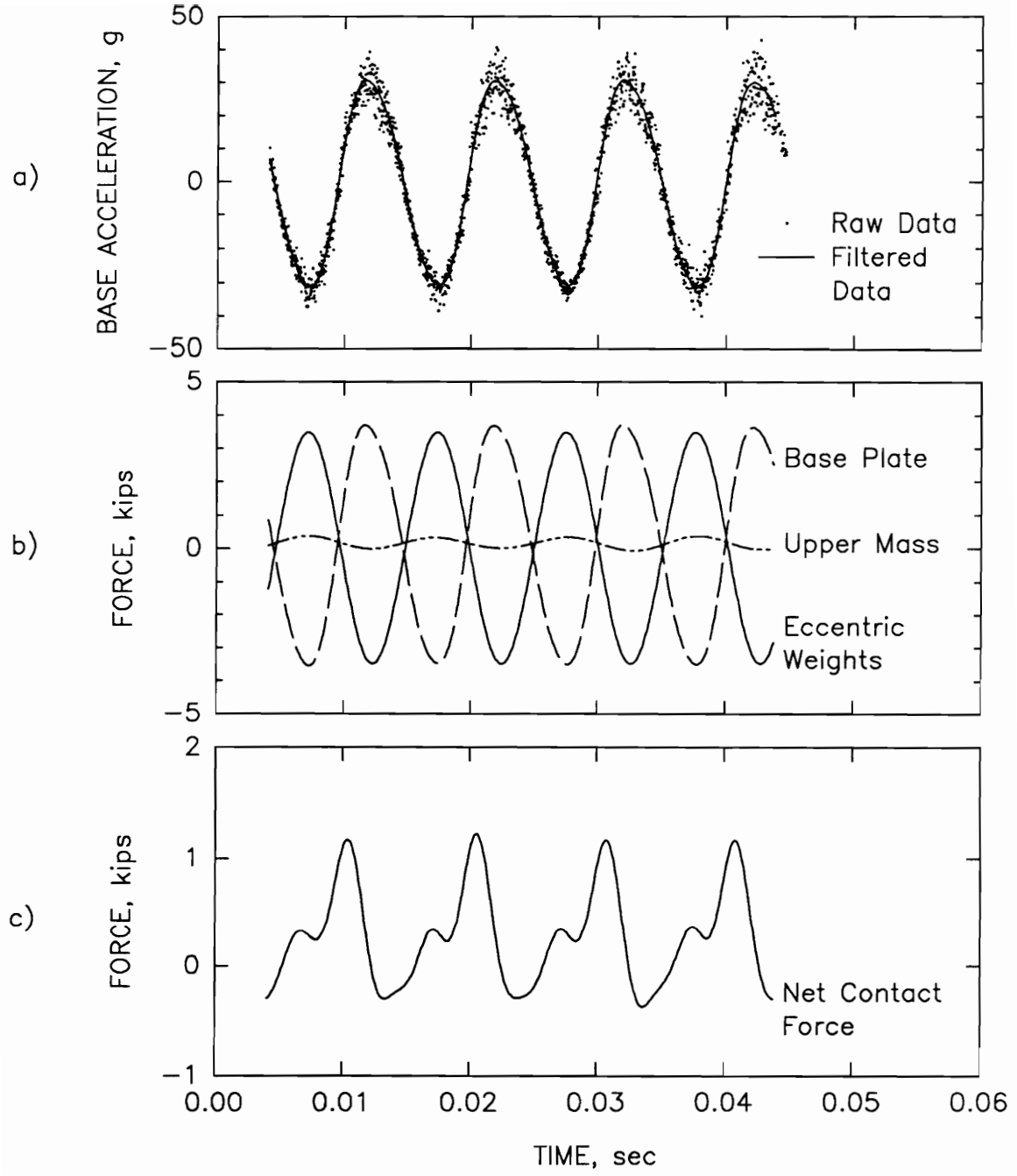

FIGURE 5.3: Vibrating plate compactor data reduction.

thick aluminum plate and was shaped to match the curvature and footprint of the original base plate. With this modification, the compactor was operated on soil and the force on the bottom of the original base plate was determined by both the sum of masses times accelerations method and by the dynamic load cell measurements. The comparison shown in Figure 5.4 indicates that the instrumentation system and data reduction procedure for the sum of the masses times accelerations method provides an accurate means of measuring the force on the base of the compactor. After the procedure was verified, the supplemental base plate and dynamic load cells were removed and subsequent contact force measurements were made for the unmodified compactor using the sum of the masses times accelerations method.

5.5 Force and Energy Measurements

Table 5.2 lists the compactor type and compaction time for the instrumented retaining wall tests in which backfill was compacted in 6-inch thick lifts. Compactor force measurements were made during tests EP 12 through EP 16, as indicated in Table 5.2.

A statistical summary of all the compactor force measurements made during this study is presented in Table 5.3. For each force measurement, the vertical position of the rammer shoe or vibrating plate base was determined by double integrating the shoe or base acceleration. Using the force and position traces, the energy imparted to the soil per cycle by the compactor can be computed. The energy values are listed in Table 5.3 along with the forces.

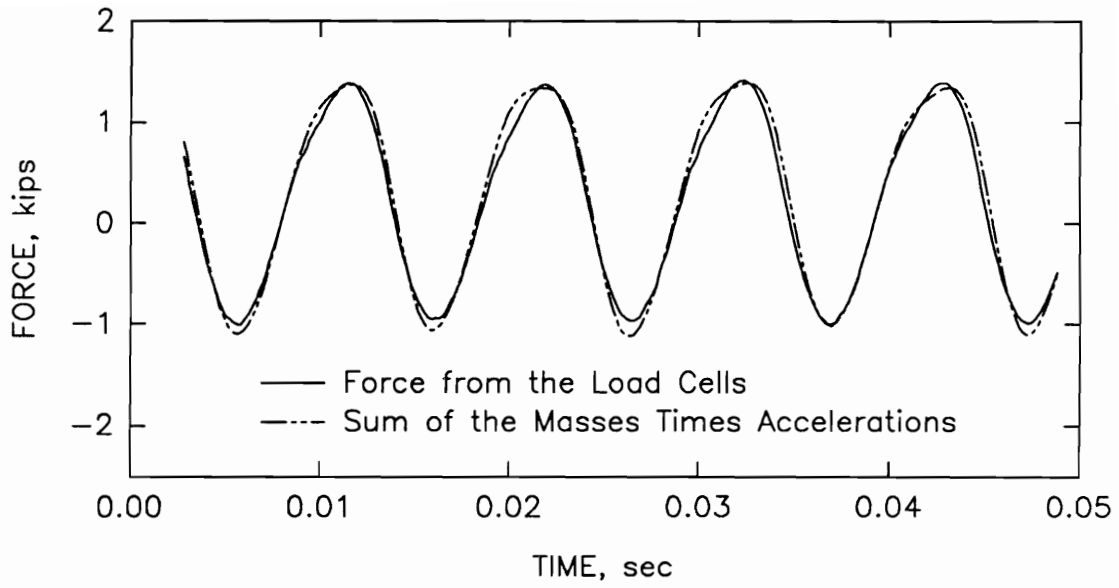

FIGURE 5.4: Vibrating plate compactor instrumentation verification test.

TABLE 5.2: Compactor Use in the Instrumented Retaining Wall Tests

Instrumented Retaining Wall Test Number	Soil Type(1)	Water Content (percent)	Compactor	Compaction Time (sec/cu ft)	Compactor Force Measurements
EP 3	YSS1	13.7	Vib. Plate	10.7	No
EP 4	YSS1	10.1	Vib. Plate	8.6	No
EP 5	YSS1	9.3	Vib. Plate	9.7	No
EP 6	YSS1	9.7	Vib. Plate	9.4	No
EP 7	YSS1	11.1	Vib. Plate	9.7	No
EP 8	YSS1	12.1	Vib. Plate	10.2	No
EP 9	YSS1	12.5	Vib. Plate	11.0	No
EP 10	YSS1	11.8	Vib. Plate	10.2	No
EP 11	YSS1	13.5	Vib. Plate	12.1	No
EP 12	YSS1	12.3	Vib. Plate	10.8	Yes
EP 13	YSS2	12.7	Rammer	12.9	Yes
			Vib. Plate	6.4	No
EP 14	YSS2	10.1	Rammer	8.7	Yes
			Vib. Plate	4.6	No
EP 15	LCS	<0.1	Rammer	8.6	Yes
EP 16	LCS	<0.1	Vib. Plate	8.2	Yes

Notes: 1) YSS1 indicates Yatesville silty sand No. 1.
YSS2 indicates Yatesville silty sand No. 2.
LCS indicates Light Castle sand.

TABLE 5.3: Summary of Compactor Force and Energy Measurements

Instrumented Retaining Wall Test Number	Soil Type(1)	Water Content (percent)	Compactor	Peak Force (pounds)			Energy (ft-lbs per cycle)		
				Average	Standard Deviation	Number of Readings	Average	Standard Deviation	Number of Readings
12	YSS1	12.3	Vib. Plate	1215	150	12	4.16	1.37	12
13	YSS2	12.7	Rammer	5040	460	10	55.7	3.2	10
14	YSS2	10.1	Rammer	7330	970	9	49.0	4.5	9
15	LCS	< 0.1	Rammer	4780	1120	15	52.2	4.2	15
16	LCS	< 0.1	Vib. Plate	1310	280	16	4.01	1.31	16

Notes: 1) YSS1 indicates Yatesville silty sand No. 1.
YSS2 indicates Yatesville silty sand No. 2.
LCS indicates Light Castle sand.

5.5.1 Rammer Compactor

A typical set of force, rammer shoe position, and energy traces versus time from the rammer compactor are shown in Figure 5.5. The peak force in Figure 5.5 is about 5500 pounds and the impact duration is short, less than 0.005 seconds for contact force greater than a few hundred pounds. The operating frequency is about 10.6 hertz. Between impacts the instrumentation system returns a measurement of zero force on the base of the rammer shoe, which is correct for the shoe not being in contact with the soil. The position trace shows that the rammer shoe moved through a vertical distance of about 2.5 inches during each cycle. The location of the zero position is arbitrary, and in Figure 5.5 it is set at the approximate point of rammer shoe contact with the soil, as indicated by the beginning of the force pulse. The energy applied by the compactor to the soil accumulates as a step function, increasing at a rate of about 55 foot-pounds per impact.

The first impact in Figure 5.5 is shown in Figure 5.6 with an expanded time scale. The approximate points of rammer shoe contact and departure from the soil are also shown. Figure 5.6 indicates that the soil in this test deformed about 0.3 inches during rammer impact.

The average measured energy per cycle for the rammer compactor for all the tests summarized in Table 5.3 is 52.4 foot-pounds, which is close to the manufacturer's rated energy of 57.8 foot-pounds. However, the measured peak contact forces ranged from 3520 pounds to 8550 pounds and averaged 5500 pounds. The substantial variation in peak force

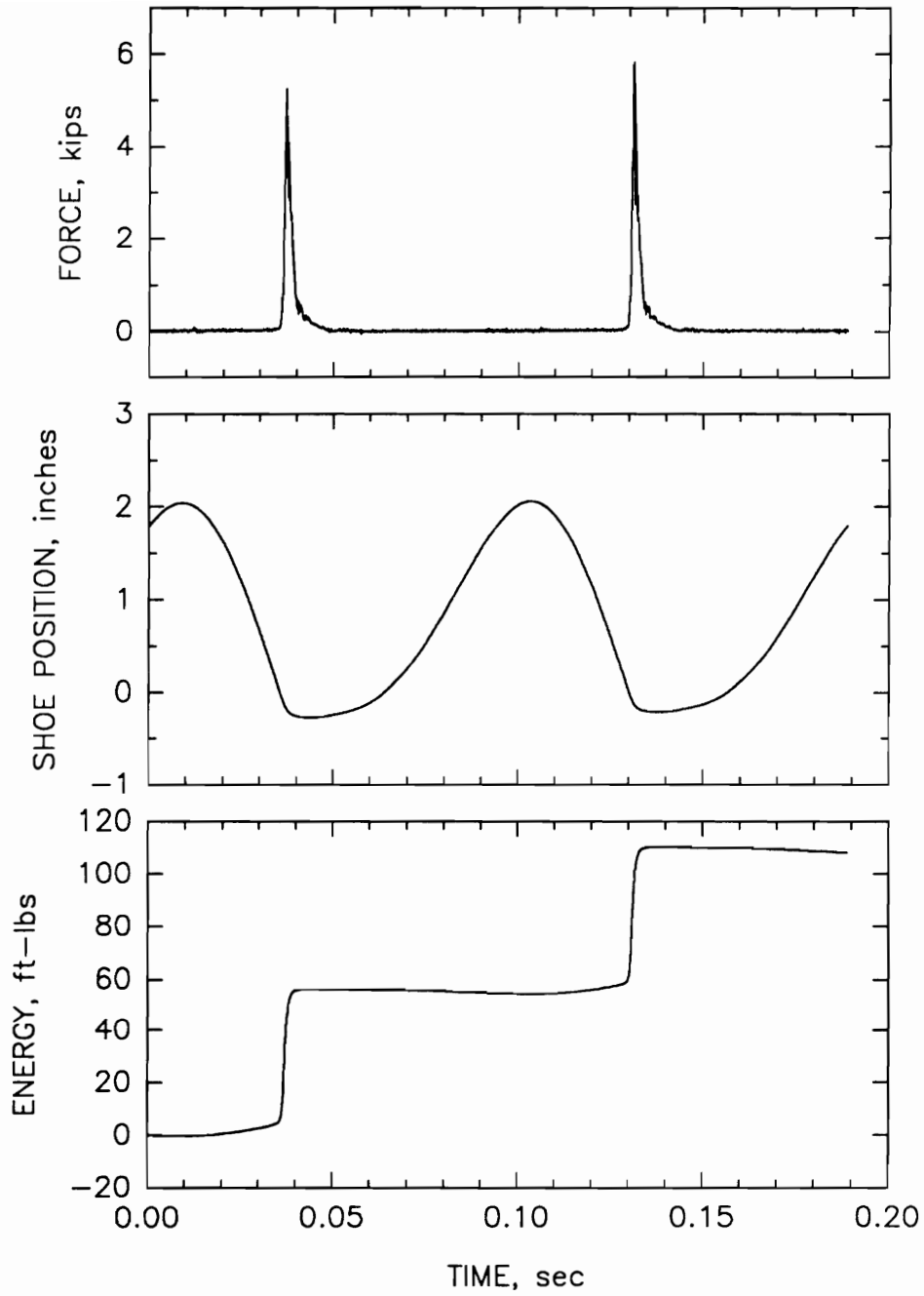

FIGURE 5.5: Typical rammer compactor force, position, and energy traces.

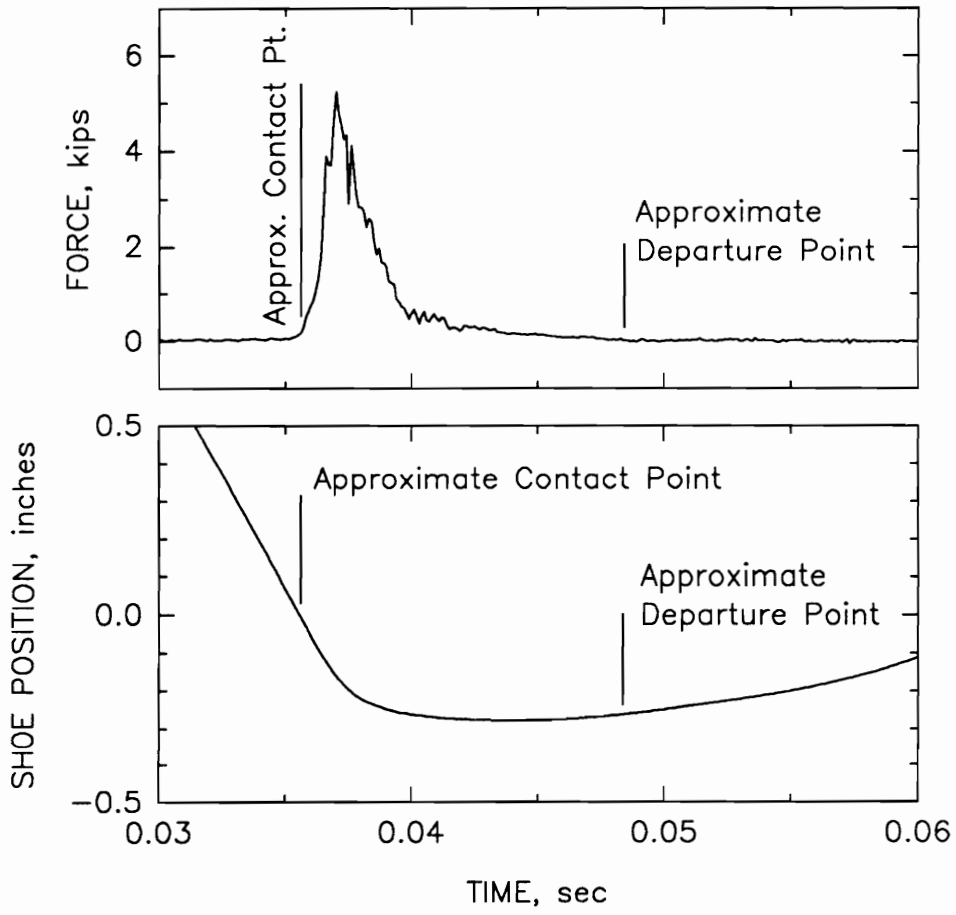

FIGURE 5.6: Rammer compactor force and position traces with an expanded time scale.

is due primarily to variations in soil stiffness as soil type and moisture condition changed from test to test. For example, the average of the peak force measurements for test EP 13, in which the backfill was soft because it was compacted wet of optimum, is 5040 pounds. On the other hand, the average of the peak force measurements for test EP 14, in which the backfill was stiff because it was compacted dry of optimum, is 7330 pounds. For all cases, the measured peak forces are greater than the manufacturer's rated force of 2775 pounds. As mentioned previously, the manufacturer's rated force represents an average force corresponding to "the standard soil deformation" of 0.25 inches during impact. Peak forces are expected to be higher. Interestingly, if soil deformation were proportional to contact force and no rebound occurred, the manufacturer's rated (average) force of 2775 pounds would correspond to a peak force of 5550 pounds, which is close to the average of the peak forces measured in this study. Such agreement is dependent, of course, on the stiffness of the soil on which the compactor operates.

5.5.2 Vibrating Plate Compactor

A typical set of force, base position, and energy traces versus time for the vibrating plate compactor during forward compactor travel are shown in Figure 5.7. The peak compressive forces are about 1200 pounds and peak tensile forces are about 300 pounds. The operating frequency is about 98 hz. The base position trace in Figure 5.7 shows a peak to peak displacement amplitude of about 0.06 inches. The location

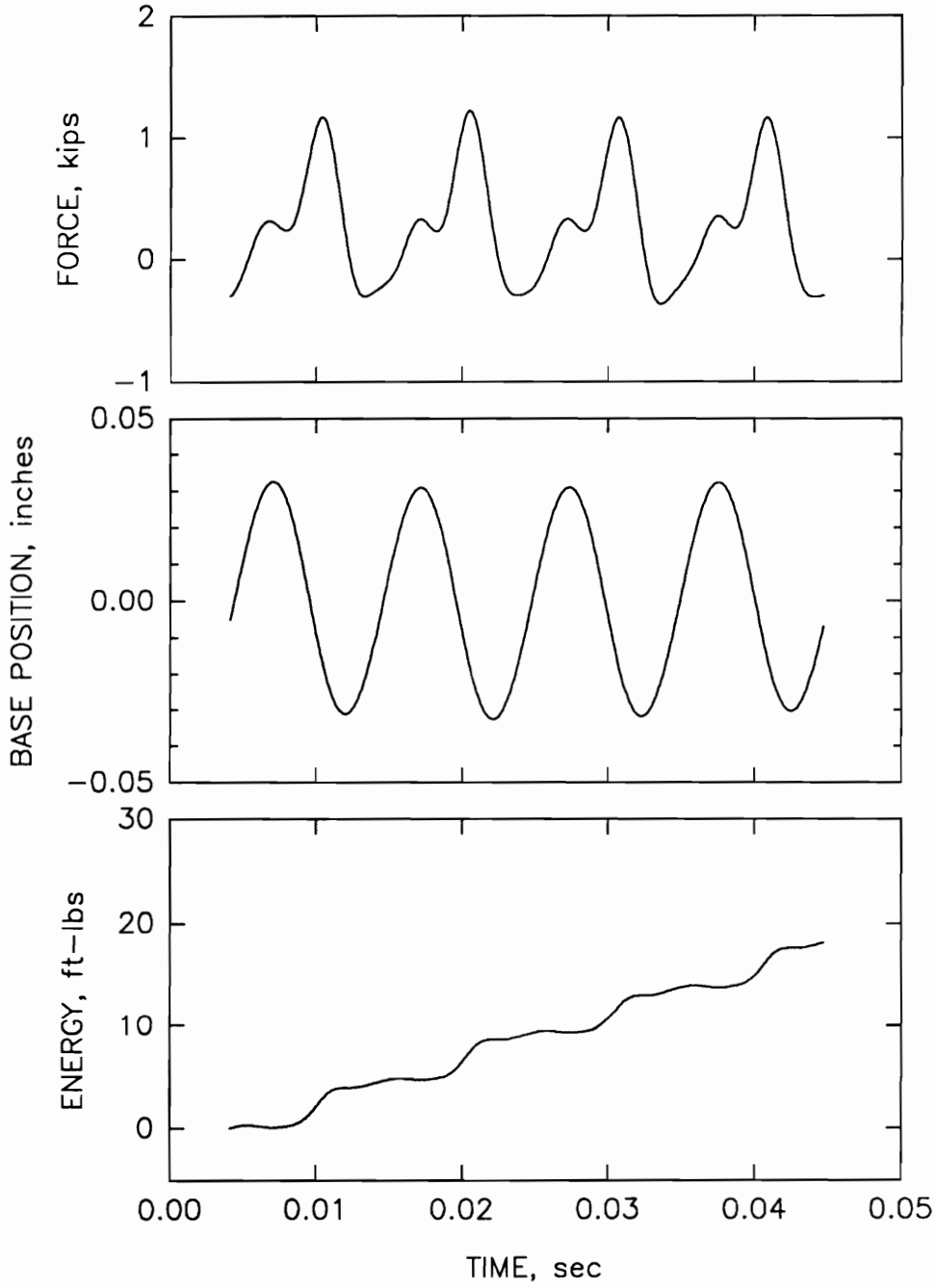

FIGURE 5.7: Typical vibrating plate compactor force, position, and energy traces.

of the zero position is arbitrarily set at the midpoint of the position range.

Peak tensile forces for all the measurements on the Yatesville silty sand average 410 pounds and peak tensile forces for all the measurements on the Light Castle sand average 250 pounds. The possibility of developing a small tensile stress, or "suction," between the surface of the moist Yatesville silty sand and the smooth base plate of the vibratory compactor during rapid loading could account for the tensile forces measured on the Yatesville silty sand. For the Light Castle sand, a short term air pressure reduction of 1 psi in the sand beneath the compactor base plate as it rapidly pulls up from the sand would account for the tensile force measured in this case.

The measured peak compressive force from the vibrating plate compactor for all the tests summarized in Table 5.3 ranged from 1030 to 1680 pounds and averaged 1270 pounds. These forces are much less than the manufacturer's rated centrifugal force of 5400 pounds. The reasons for the discrepancy are that 1) the manufacturer's rating seems to be based on a higher mass times eccentricity than exists for the compactor used in this study, as was shown in Table 5.1, and 2) the rating calculation is for eccentric weights rotating about a shaft fastened to a fixed support, whereas soil provides flexible support.

The measured energy per cycle for all the vibrating plate compactor measurements summarized in Table 5.3 ranged from 3.26 to 6.18 ft-lbs per cycle and averaged 4.81 ft-lbs per cycle. These energies are about one order of magnitude smaller than those for the rammer

compactor, but the operating frequency is about one order of magnitude higher so that the total energy transfer per unit time is about the same for the two compactors. The LEMB does not provide a method for rating the energy for vibrating plate compactors.

5.6 Compactive Effort

For the instrumented retaining wall tests in which compactor force measurements were made, the compactive effort (transferred energy per unit volume of compacted soil) can be computed because the energy per cycle, compactor period, compaction time, and compacted volume are known. The calculated compactive efforts for tests EP 12 through EP 16 are shown in Table 5.4.

Estimates of the compactive efforts for the instrumented retaining wall tests without compactor force measurements can be made by noting that the average values of transferred energy per cycle listed in Table 5.4 are not strongly dependent on the properties of the soil being compacted. In particular, the transferred energy per cycle for the vibrating plate compactor was 4.16 ft-lbs on moist Yatesville silty sand No. 1 (test EP 12), and 4.01 ft-lbs on dry Light Castle sand (test EP 16). The transferred energy per cycle for the rammer compactor was 55.7 ft-lbs on wet Yatesville silty sand No.2 (test EP 13), 49.0 ft-lbs on dry Yatesville silty sand No. 2 (test EP 14), and 52.2 ft-lbs on dry Light Castle sand (test EP 15). The peak force, on the other hand, is dependent on the properties of the soil being compacted, as discussed previously.

TABLE 5.4: Compactive Efforts in the Instrumented Retaining Wall Tests

Instrumented Retaining Wall Test Number	Soil Type(1)	Water Content (percent)	Compactor(2)	Compaction Time (sec/cu ft)	Transferred Energy per Cycle (ft-lbs)	Compactor Period (sec)	Compactive Effort (ft-lbs/cu ft)
EP 12	YSS1	12.3	Vib. Plate	10.8	4.16	0.0102	4,420
EP 13	YSS2	12.7	Rammer	12.9	55.7	0.0946	7,590
			Vib. Plate	6.4	4.08(3)	0.0101(3)	2,600
			Total	19.3			10,190
EP 14	YSS2	10.1	Rammer	8.7	49.0	0.0881	4,840
			Vib. Plate	4.6	4.08(3)	0.0101(3)	1,870
			Total	13.3			6,710
EP 15	LCS	< 0.1	Rammer	8.6	52.2	0.0888	5,030
EP 16	LCS	< 0.1	Vib. Plate	8.2	4.01	0.0100	3,300

Notes:
1) YSS1 indicates Yatesville silty sand No. 1.
YSS2 indicates Yatesville silty sand No. 2.
LCS indicates Light Castle sand.
2) Both the vibrating plate compactor and the rammer compactor were used during tests EP 13 and EP 14.
3) The energy per cycle and the compactor period for the vibrating plate compactor were not measured during tests EP 13 and EP 14. For these calculations, the values are assumed to be the average of those measured during tests EP 12 and EP 16.

The compactive efforts for the tests during which compactor force measurements were not made, i.e., tests EP 3 through EP 11, can be estimated using the compaction times listed in Table 5.2 and the approximately constant transferred energy per cycle measured for the vibrating plate compactor in tests EP 12 and EP 16. This results in compactive efforts ranging from 3,500 to 4,900 ft-lbs/cu ft for tests EP 3 through EP 12, which are all the tests backfilled with 6-inch thick lifts of Yatesville silty sand No. 1. The dry unit weights resulting from this level of compactive effort are compared with the dry unit weights resulting from the Standard Proctor and Modified Proctor compactive efforts in Figure 5.8. The figure shows that, because the compactive effort is lower for the instrumented retaining wall tests than for the Standard Proctor test, the maximum dry unit weight is lower and the optimum water content is higher.

A similar comparison was made for Yatesville silty sand No. 2. In this case, two non-standard, low-energy laboratory compaction curves were obtained in addition to the Standard Proctor and Modified Proctor curves. All four curves are shown on Figure 5.9, along with the results from tests EP 13 and EP 14. The compaction curve shown for the instrumented retaining wall tests in Figure 5.9 is for the compactive effort of test EP 14 only, since test EP 13 was compacted wet of optimum and, consequently, does not serve to define the maximum dry unit weight.

The maximum dry unit weights from Figures 5.8 and 5.9 are plotted versus compactive effort in Figure 5.10. The trend is for increasing maximum dry unit weight with increasing compactive effort. The maximum

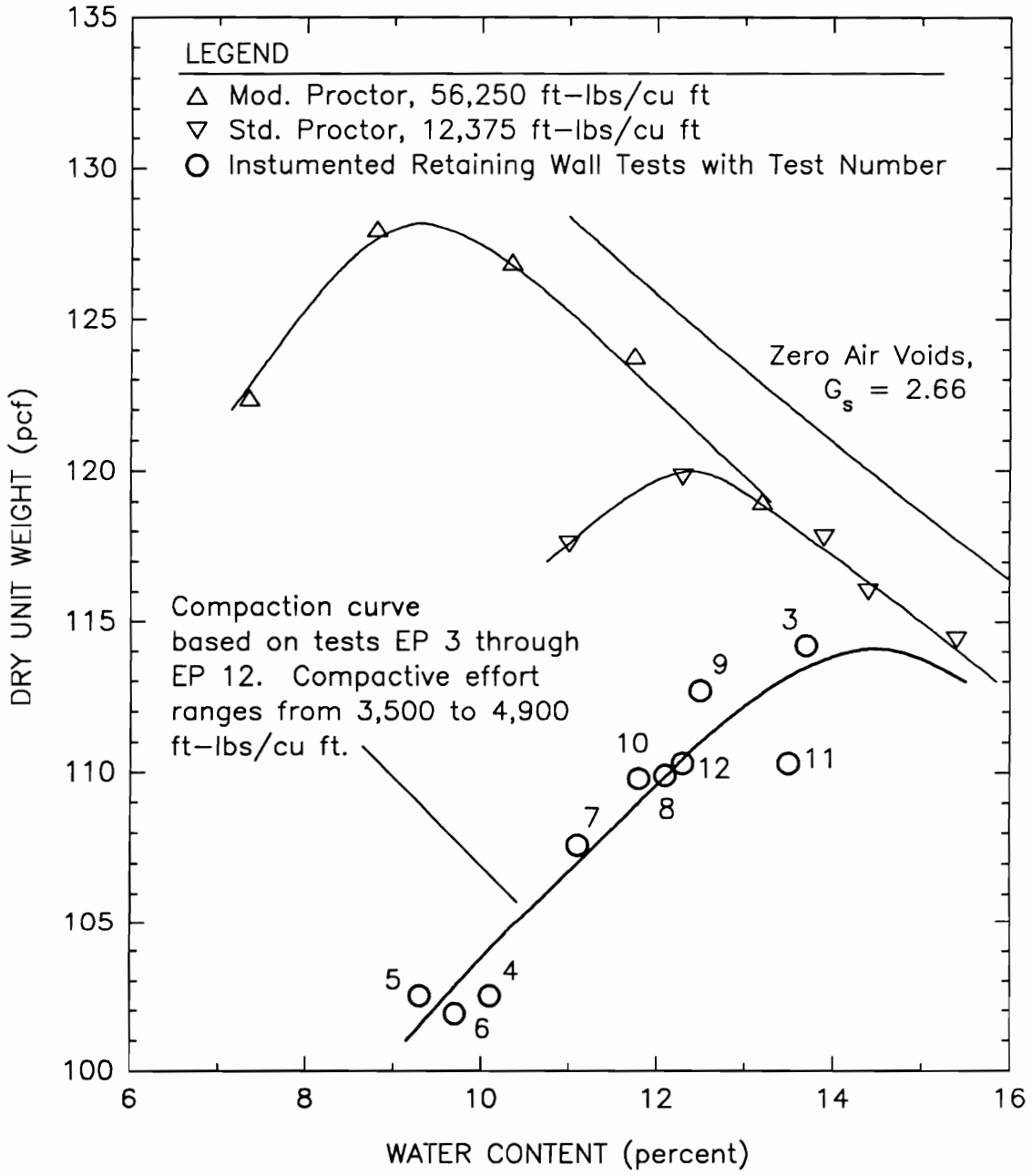

FIGURE 5.8: Compaction curves for Yatesville Silty Sand No. 1.

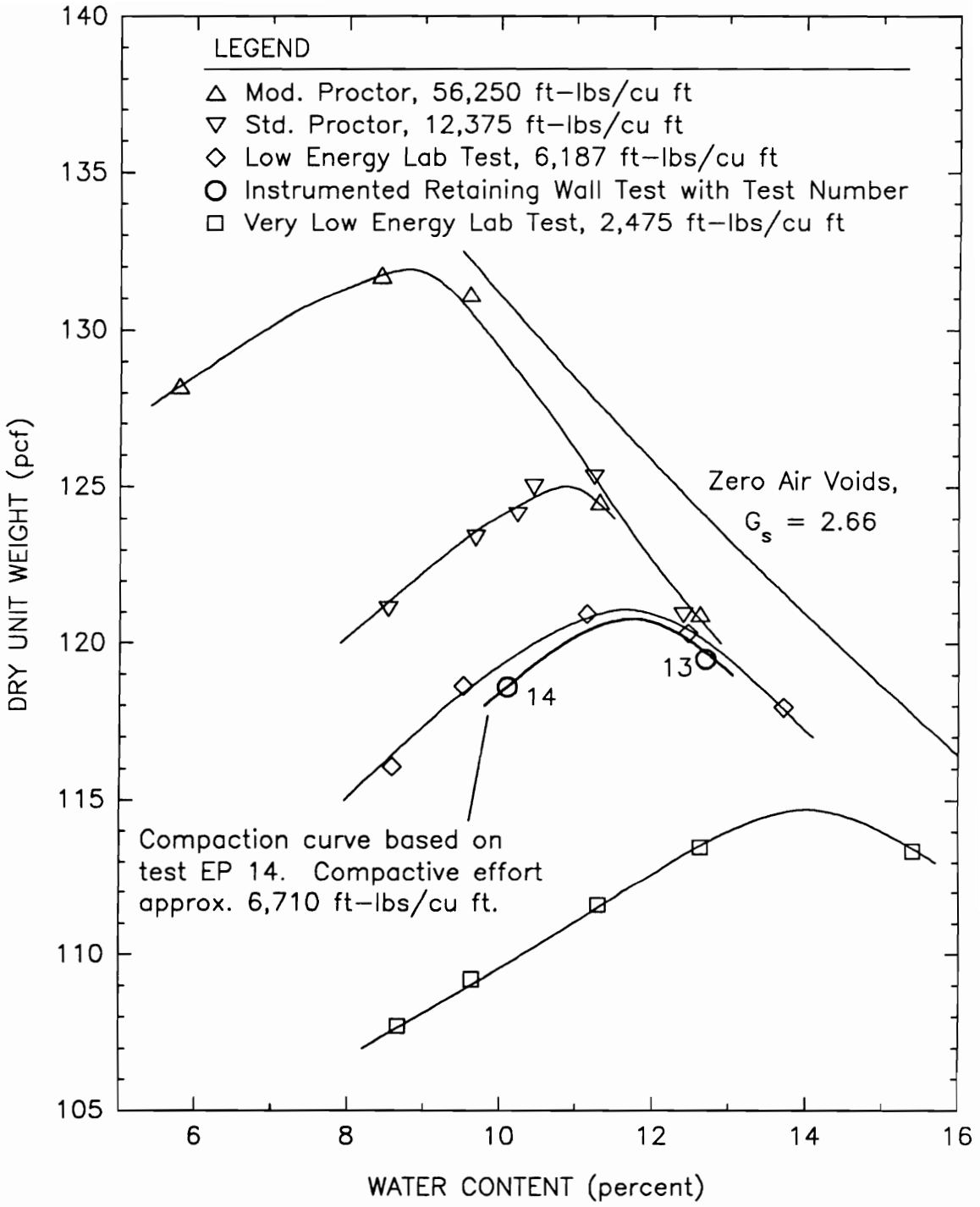

FIGURE 5.9: Compaction curves for Yatesville Silty Sand No. 2.

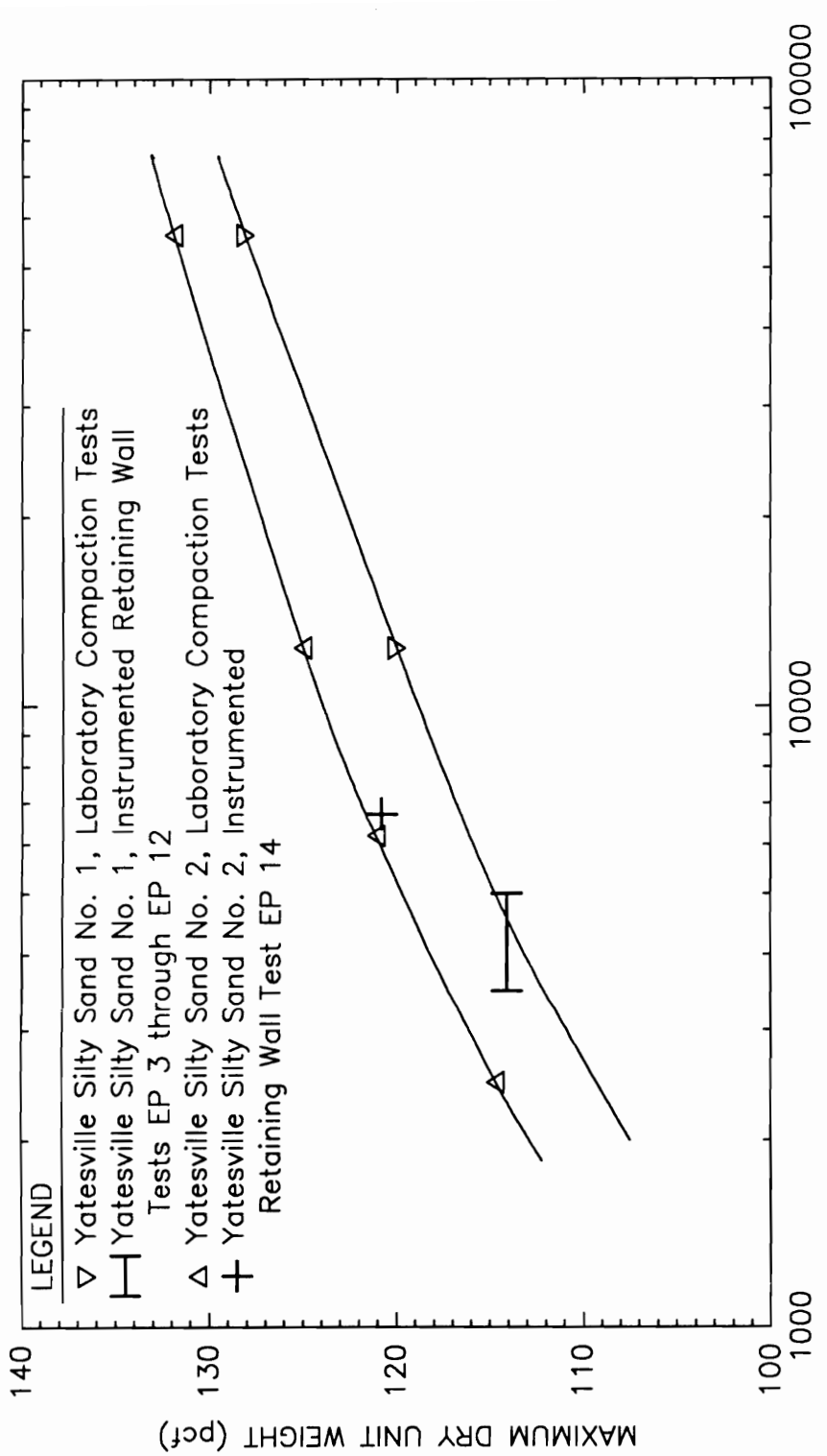

FIGURE 5.10: Maximum dry unit weight versus compactive effort.

dry unit weights for Yatesville silty sand No. 2 are greater than those for Yatesville silty sand No. 1. In both cases, the results from the instrumented retaining wall tests are in good agreement with the laboratory test data. The agreement indicates that the measured energies for these hand-operated compactors have the same effect on dry unit weights as equal energies applied in compaction tests in the laboratory.

As mentioned previously, it appears as though the transferred energy is not strongly dependent on the characteristics of the soil being compacted. Consequently, the data in Table 5.4 can be used to compute the average energy transfer rate (in units of foot-pounds per second) for each compactor. The rates are listed in Table 5.5, along with the time required to develop the standard Proctor energy in one cubic foot of compacted soil.

5.7 Compactor Performance Models

In order to gain further insight into the factors which influence the peak contact forces imposed by hand-operated compactors, compactor-soil interaction models were developed using the spring and dashpot analog of a dynamically loaded footing proposed by Lysmer and Richart (1966).

In previous sections of this chapter, the rammer compactor was discussed before the vibrating plate compactor because the rammer was simpler with respect to instrumentation and data reduction. Now the

TABLE 5.5: Compactor Energy Transfer Rates

Compactor Type	Energy Transfer Rate (ft-lbs/sec)	Compaction Time Required for Standard Proctor Energy (sec/cu ft)
Wacker BPU2440A Vibrating Plate	400	31
Wacker BS60Y Rammer	580	21

sequence is reversed because Lysmer and Richart's analog more closely matches the vibrating plate compactor operation.

5.7.1 Vibrating Plate Compactor

In Lysmer and Richart's analog, a machine is represented by a lumped mass with an oscillating force such as that provided by a rotating eccentric weight. The soil is replaced by a parallel spring and dashpot combination. The stiffness and damping constants are computed from soil properties and the equipment contact radius according to

$$k = \frac{4Gr}{1 - \nu} \tag{5.3}$$

where

k = the spring stiffness constant, lbs/in

G = the soil shear modulus, psi

$= \frac{E}{2(1 + \nu)}$

E = the Young's modulus of the soil, psi

r = the contact radius, inches

ν = the soil Poisson's ratio

and

$$c = \frac{3.4r^2}{1 - \nu}\sqrt{\rho G} \tag{5.4}$$

where

c = the damping constant, lbs/in/sec

ρ = the soil density, lbs·sec^2/in^4

The governing differential equation of the base plate motion is

$$m_b\ddot{y}_b + c\dot{y}_b + ky_b = Q_0 \cdot \sin(\omega t + \phi_0) \tag{5.5}$$

where

m_b = the mass of the compactor base plate, lb·sec^2/in

$y_b(t)$ = the vertical position of the base plate at time t, inches

In applying Eq. 5.5 to the vibrating plate compactor, the mass, m_b, represents the masses of the compactor base plate, the eccentric weights, and the eccentric weight housing. The upper mass of the compactor is not included because it is, for the most part, isolated from the motion of the base plate, as indicated by the data shown in Figure 5.7.

The solution of Eq. 5.5 is the contact position, y_b, a function of time. Once operating conditions have been established, y_b is given by

$$y_b(t) = A_b \cdot \sin(\omega t + \phi_0 - \phi_e) \tag{5.6a}$$

$$A_b = \frac{Q_0}{\sqrt{(k - m_b\omega^2)^2 + c^2\omega^2}} \tag{5.6b}$$

$$\tan \phi_e = \frac{c\omega}{k - m_b\omega^2} \tag{5.6c}$$

where

A_b = the half-amplitude of the base plate displacement

ϕ_e = the phase angle between the eccentric weight driving force, i.e., the right hand side of Eq. 5.5, and the base plate displacement

With the contact position known, the contact force, F(t), is given by

$$F(t) = ky_b + c\dot{y}_b \tag{5.7}$$

The soil modulus is necessary to compute the spring and dashpot constants in Eqs. 5.3 and 5.4. As described in Appendix A, samples of the compacted backfill from test EP 9, whose backfill was compacted to approximately the same moisture-density conditions as that of test EP 12, were tested in unconsolidated-undrained triaxial compression over a range of confining pressures. A representative value of initial Young's modulus of 350 psi was measured. Assuming a value of Poisson's ratio of 0.3, the stiffness and damping constants were calculated using Eqs. 5.3 and 5.4. The driving centrifugal force in the right hand side of Eq. 5.5 was computed using the value of mass times eccentricity listed in Table 5.1 for forward compactor travel and the rotation rate of 98 hz measured during compactor operation at the time of the measurements shown in Figure 5.7. A summary of the parameter values used for the

calculations is given in Table 5.6. The resulting performance of the compactor according to the analog is shown in Figure 5.11.

The correspondence between the analog performance in Figure 5.11 and the measured compactor performance in Figure 5.7 is close, with the peak force being about 1200 pounds and the peak to peak displacement being about 0.06 inches in both cases. Energy accumulation and maximum tensile force in the analog are greater than the measured quantities shown in Figure 5.7. Differences between the plots in Figures 5.7 and 5.11 are probably due to 1) non-linear behavior of the actual soil response versus the assumed linear behavior in the analog (nonlinearity may be particularly significant during the tensile portion of the compactor cycle), 2) the effect of the upper mass accelerations, which are not included in the analog, and 3) the effect of horizontal accelerations, which are not included in the analog, on the compactor-soil interaction.

The close correspondence between the analog and the measured compactor performance suggests that the analog can be used to assess the influences of changes in soil modulus, centrifugal force, rotation rate, base plate weight, and base plate size on peak contact force. The results of such an assessment are shown in Figure 5.12, which indicates that peak contact forces increase with increasing soil modulus, centrifugal force, and base plate size. Peak contact forces also increase with decreasing base plate weight and eccentric weight rotation frequency. The reason that decreases in base plate weight and eccentric weight rotation rate cause increases in peak contact forces is that the

TABLE 5.6: Parameter Values Used for Modelling the Vibrating Plate Compactor in Test EP 12

Parameter	Value
Young's Modulus of Soil, E	350 psi
Poisson's Ratio of Soil, ν	0.3
Moist Unit Weight of Soil, γ	125 pcf
Base Plate Contact Radius, r	8 in
Centrifugal Force, Q_0	3470 lbs
Base Plate Mass, m_b	0.303 lb sec^2/in
Eccentric Weight Rotation Rate, ω	616 rad/sec

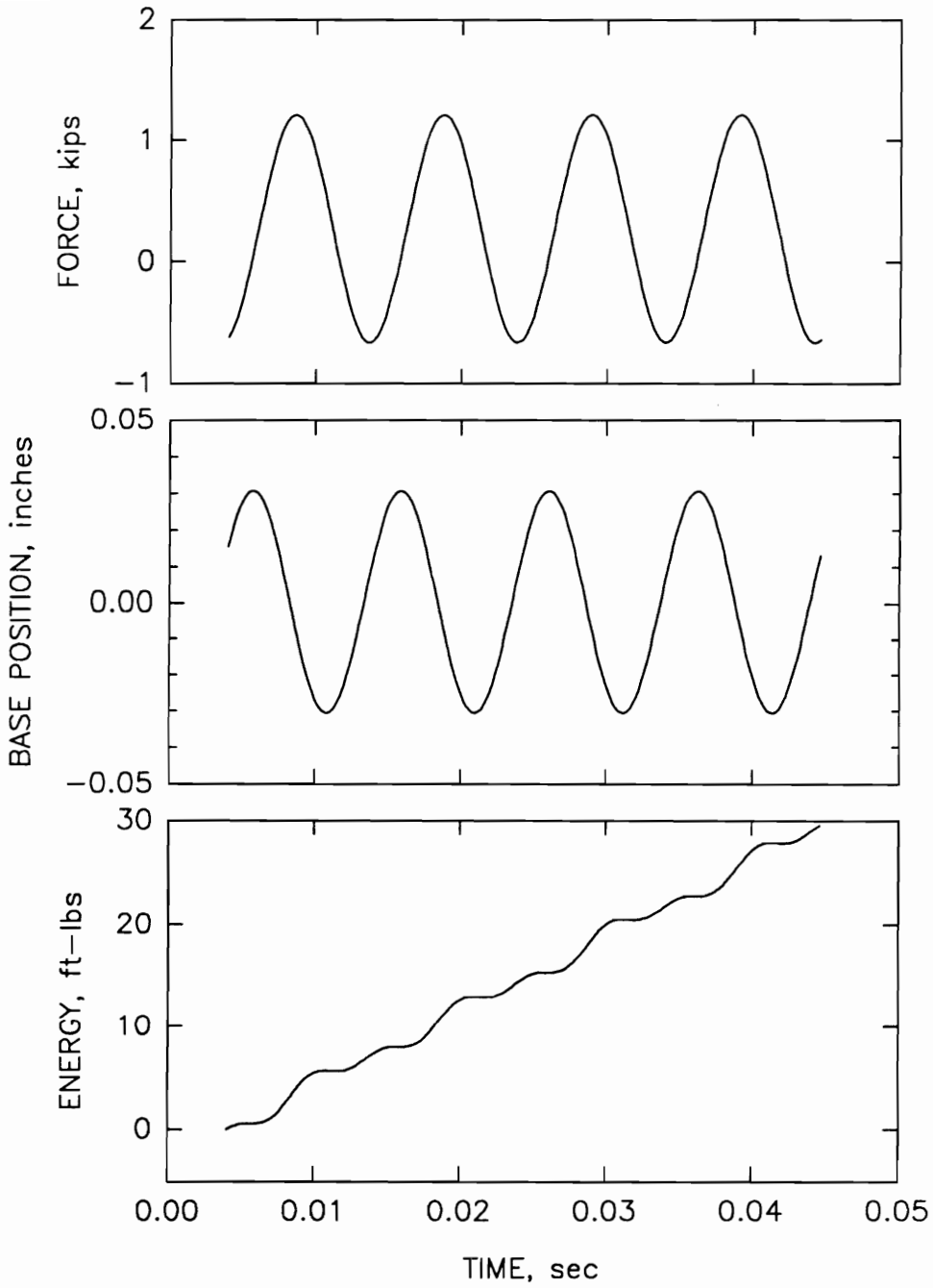

FIGURE 5.11: Vibrating plate compactor model performance.

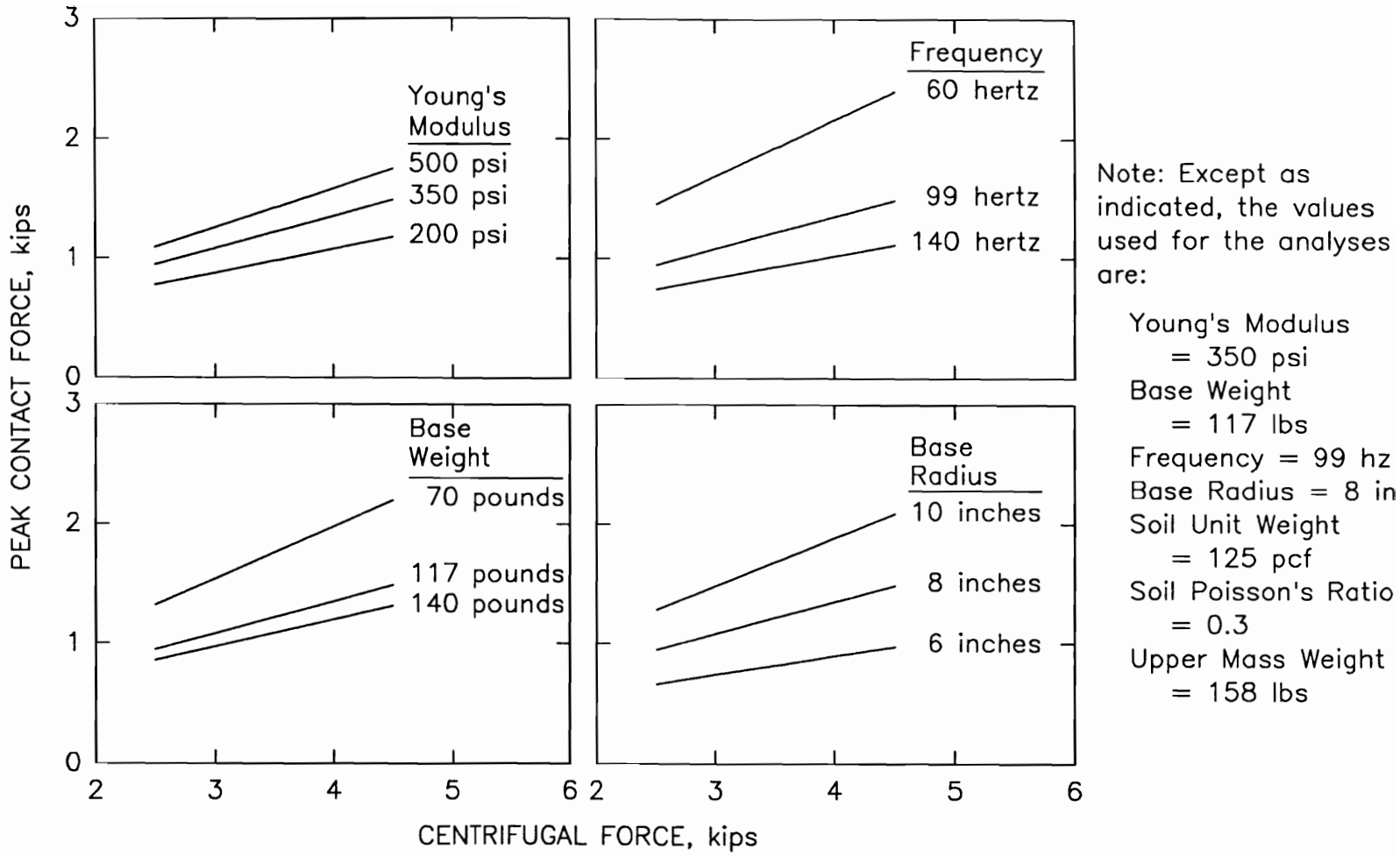

FIGURE 5.12: Influence of variation in model parameters on the peak contact force for the vibrating plate compactor.

compactor is operating above the system natural frequency for the range of conditions analyzed in Figure 5.12. The natural frequency for the system at the reference values listed in Figure 5.12 is 23 hertz. Decreases in either base plate weight or frequency bring the system closer to resonance and increase peak contact forces.

For all the cases shown in Figure 5.12, the peak contact force is much lower than the centrifugal force. Thus, the analog clearly shows that the centrifugal force from the eccentric weights is not a good measure of peak contact force. Several other factors have important influences on the contact force.

5.7.2 Rammer Compactor

Lysmer and Richart's analog, being based on elastic theory, is for small displacements of a footing which remains in contact with the soil. The vibratory plate compactor satisfies these conditions fairly well during the final compaction passes, provided that the soil is not too hard. On the other hand, the rammer compactor leaves the soil surface between each impact and causes permanent deformation for most soils even during the final pass. Nevertheless, it will be shown that the expressions for k and c in Eqs. 5.3 and 5.4 can be used with Eq. 5.7 to model the contact force for the rammer compactor, provided that an appropriate displacement function can be found.

Inspection of the force and displacement traces in Figure 5.6 indicates that the rammer shoe travels down into the soil at an approximately constant velocity until the peak contact force develops.

The rammer shoe decelerates rapidly after this point. An appropriate displacement function would begin with the soil at rest, and the soil velocity would increase from zero at the time of rammer shoe contact to a maximum velocity as the representative soil mass beneath the shoe accelerates downwards. A simple assumption for the model is that the maximum representative soil velocity equals the rammer shoe velocity as the shoe begins moving down into the soil. This velocity is about 135 inches per second for the data shown in Figure 5.6, and it did not vary by more than a few percent from this value for all the measurements made in this study. Apparently, this velocity is dependent primarily on the internal mechanics of the compactor and is not strongly dependent on the stiffness of the soil being compacted.

Another condition which the displacement function should satisfy is that the energy computed using the displacement function and the contact force from Eq. 5.7 should equal the measured energy per blow from the compactor. These conditions do not uniquely determine the displacement function but a simple candidate displacement function, which can be made to satisfy the conditions, is given by

$$y_r(t) = 4A_r\left[\frac{t}{t_p}\right]^3 \qquad \text{for } \frac{t}{t_p} < 0.5 \qquad (5.8a)$$

$$y_r(t) = A_r\left[1 - 4\left|1 - \frac{t}{t_p}\right|^3\right] \qquad \text{for } 0.5 < \frac{t}{t_p} < 1.5 \qquad (5.8b)$$

where

$y_r(t)$ = the representative soil displacement beneath the rammer shoe during impact

A_r = the maximum representative soil displacement during rammer shoe impact

t_p = the time at which the maximum soil displacement occurs

The constants A_r and t_p in Eq. 5.8 can be determined by requiring that

$$\dot{y}_r(0.5t_p) = v_{contact} \tag{5.9}$$

where

$v_{contact}$ = the rammer shoe velocity as it contacts the soil

and

$$\int_0^{t_p} F \cdot dy_r = E_1 \tag{5.10}$$

where

E_1 = the energy imparted by the compactor to the soil during one impact

The energy condition in Eq. 5.10 is approximate because the integration extends only to the point of peak deformation rather than to the point of loss of contact between the rammer shoe and soil. This approximation simplifies the calculations and introduces very little

error since the forces and changes in position during the time from peak deformation to loss of contact are small.

The model was applied to the conditions of tests EP 13 and EP 14, using the parameter values summarized in Table 5.7. The values of initial Young's moduli of 460 and 910 psi for tests EP 13 and EP 14 were obtained from unconsolidated-undrained triaxial compression tests described in Appendix A. A value of Poisson's ratio equal to 0.5 was used in the calculations since the load from the rammer compactor was high, the deformations were large, and the soil beneath the compactor was apparently in, or close to, a failure condition during compaction. After the spring and dashpot constants were evaluated using Eqs. 5.3 and 5.4, Eqs. 5.9 and 5.10 were solved to obtain the values of A_r and t_p. Finally, Eqs. 5.7 and 5.8 were evaluated to give the force and position traces versus time. The results for test EP 13 are shown in Figure 5.13. The agreement between the model in Figure 5.13 and the measured compactor performance in Figure 5.6 is reasonably good. The peak force in the model is 4710 pounds, which is about 7 percent less than the average measured peak force of 5040 pounds, as listed in Table 5.3 for test EP 13. The calculations for test EP 14 resulted in a peak force of 6430 pounds for the model, which is about 12 percent less than the average measured peak force of 7330 pounds, as listed in Table 5.3. Thus, the model appears to slightly underestimate the measured contact forces.

The reasonably good agreement between the model and the measurements suggests that the model can be used to assess the

TABLE 5.7: Parameter Values Used for Modelling the Rammer Compactor in Tests EP 13 and EP 14

Parameter	Value	
	Test EP 13	Test EP 14
Young's Modulus of Soil, E	460 psi	910 psi
Poisson's Ratio of Soil, ν	0.5	0.5
Moist Unit Weight of Soil, γ	135 pcf	130 pcf
Shoe Contact Radius, r	5 in	5 in
Transferred Energy, E_1	55.7 lbs	49.0 lbs
Shoe Velocity, $v_{contact}$	135 in/sec	135 in/sec

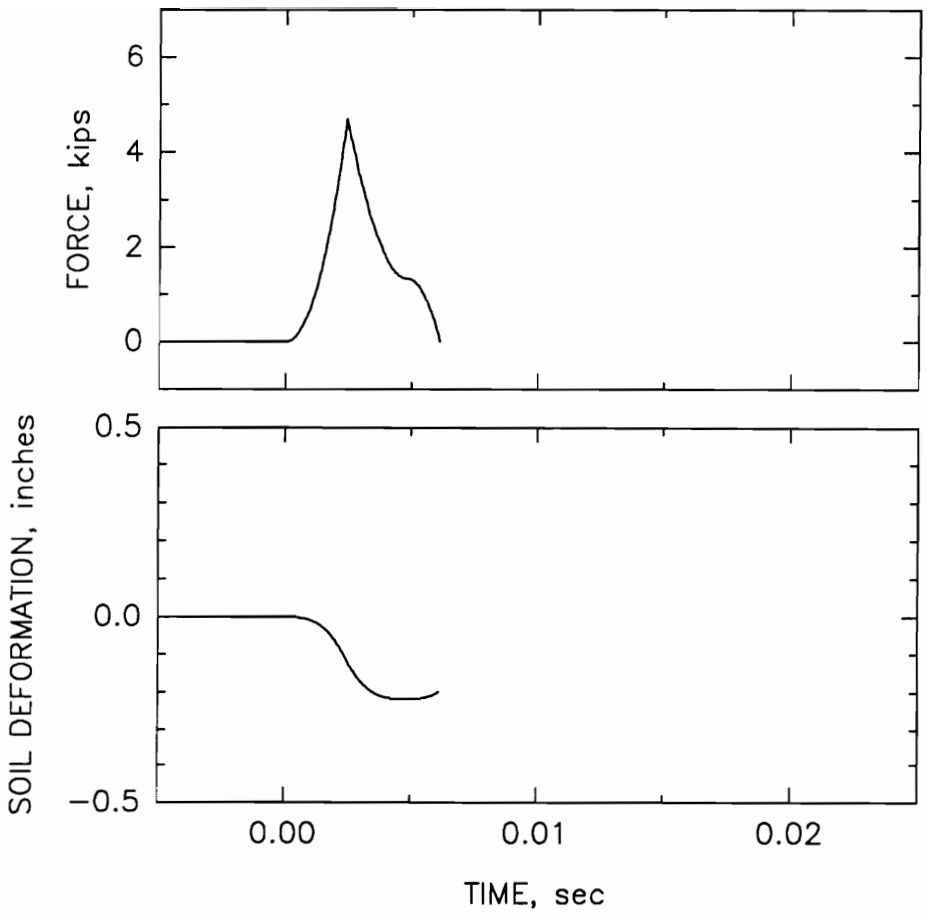

FIGURE 5.13: Rammer compactor model performance.

influences of changes in soil modulus, impact velocity, energy per blow, and shoe size on peak contact forces for rammer compactors. The results of the assessment are shown in Figure 5.14, which indicates that peak contact forces increase with increasing soil modulus, impact velocity, energy per blow, and shoe size. The influence of energy per blow on peak contact forces is shown to be small compared to the influences of the other factors.

5.8 Conclusions

Two hand-operated compactors were successfully instrumented to measure contact forces between compactor and soil during compactor operation. A combination of dynamic load cells and accelerometers were used to measure the contact force for a rammer compactor. The measurement scheme for the rammer compactor consisted of measuring the force on top of the rammer shoe and adding the mass times acceleration of the shoe to obtain the force on the bottom of the shoe. A combination of accelerometers and a Hall effect device were used to measure the contact force for a vibrating plate compactor. The measurement scheme for the vibrating plate compactor consisted of summing the masses times accelerations of the compactor components.

For the rammer compactor, peak contact forces ranged from 3520 to 8550 pounds and averaged 5500 pounds. The peak contact force increased with increasing soil stiffness. The average measured energy transfer was 52.4 foot-pounds per blow, and this value is close to the manufacturer's rated energy of 57.8 foot-pounds per blow. However, the

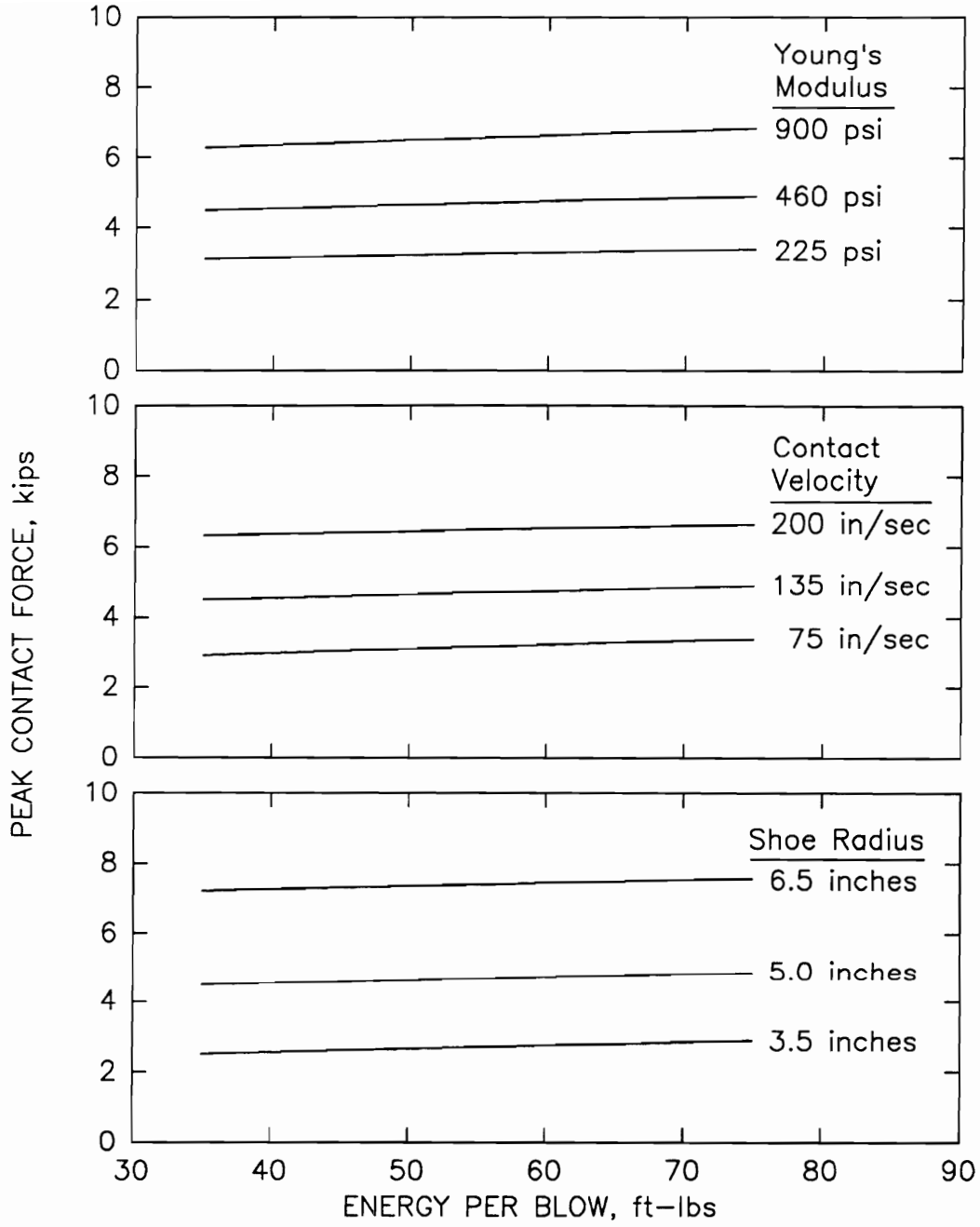

Note: Except as indicated, the values used for these analyses are: Young's Modulus = 460 psi, Contact Velocity = 135 in/sec, Shoe Radius = 5.0 inches, Soil Unit Weight = 135 pcf, and Soil Poisson's Ratio = 0.5

FIGURE 5.14: Influence of variation in model parameters on the peak contact force for the rammer compactor.

manufacturer's rated force of 2775 pounds is much lower than the measured peak forces. The LEMB rating procedure seems to give a reasonable estimate of the energy delivered per blow from a rammer compactor, but the LEMB rated force yields only a nominal value which can be quite different from the actual peak contact force, depending on the soil being compacted.

For the vibrating plate compactor, peak forces ranged from 1030 to 1680 pounds and averaged 1270 pounds. Measured peak forces were much less than the manufacturer's rated centrifugal force of 5400 pounds because 1) the manufacturer's rating seems to be based on an overestimate of mass times eccentricity and 2) the rating calculation is for eccentric weights rotating about a shaft fastened to a fixed support, instead of the flexible support which soil provides. The LEMB rating procedure for vibrating plate compactors is a relatively simple procedure that provides a means of comparing different models. However, the rated centrifugal force is not a good measure of the contact force because many more factors than the centrifugal force affect the contact force.

Models based on Lysmer and Richart's (1966) analog successfully imitate the performance of the hand-operated compactors studied in this research. The models can be used to assess the influence of the most important factors affecting peak contact forces. For the rammer compactor, the peak contact force increases with increasing soil stiffness, rammer shoe contact velocity, and rammer shoe size. For the vibrating plate compactor, the peak contact force increases with

increasing soil stiffness, centrifugal force, and base plate size, and the peak force decreases with increasing base plate weight and eccentric weight rotation rate.

The two hand-operated compactors used in this study are commonly employed to compact backfill in confined areas and adjacent to structures such as walls and culverts. The compactors are different in their frequency of operation, energy per cycle, and peak contact force. The consequences of these differences include:

1) Higher compaction-induced lateral earth pressures are expected in backfill compacted with the rammer compactor than in backfill compacted with the vibrating plate compactor. High compaction-induced lateral earth pressures can cause cracking or excessive deformation of structures.

2) It is generally recognized that rammer compactors are better than vibrating plate compactors at compacting cemented or cohesive soils. This difference may be due to the ability of the high rammer contact force to overcome interparticle forces and break the soil down into a more compact arrangement.

3) In instances where the two compactors achieve the same relative density or compaction, settlements of backfill compacted with the rammer compactor will probably be lower because the higher compaction-induced lateral stresses render the backfill less compressible.

CHAPTER 6 - COMPACTION-INDUCED LATERAL EARTH PRESSURE THEORY

6.1 Introduction

As initially envisioned, the purpose of this research with regard to compaction-induced lateral earth pressures was to obtain experimental measurements of compaction-induced pressures acting on the instrumented retaining wall and to compare the measured pressures with those predicted by the theory of Duncan and Seed (1986). However, during the coarse of the work, a personal communication from Peck (1991) pointed out that the results from the theory seemed unreasonable in certain instances. Motivated by Peck's observations, the reasons for the unreasonable results have been identified and revisions have been made to improve the theory. The theory has also been extended to include materials with significant non-zero pore pressures, e.g., compacted silty and clayey soils. This chapter describes the revisions and extensions that were made to the theory. Comparisons between measured pressures and values calculated using the new theory are presented in Chapter 7.

6.2 Predictions Using the 1986 Theory

Duncan et al. (1991) present calculated pressures using the compaction-induced earth pressure theory of Duncan and Seed (1986) for compactors operating adjacent to an unyielding wall. The calculated pressures depend, in part, on the closest distance of approach between the edge of the roller and the wall. Calculated pressures for

conditions where the roller is immediately adjacent to the wall (x = 0.0 ft) and for conditions where the edge of the roller is one foot from the wall (x = 1.0 ft) are shown in Figure 6.1. Peck (1991) suggested that the calculated pressures seemed unreasonably high for the x = 0.0 ft condition.

The reason that such high stresses were calculated for x = 0.0 ft using the 1986 theory is due to the very high stresses induced in the backfill during compaction when the roller operates immediately adjacent to the wall. The consequences of these high stresses are shown in Figures 6.2 and 6.3. An important part of the compaction-induced earth pressure theory is that the stress path for an element of soil next to the wall is modelled as if the soil were in k_0 compression. The control points for the k_0 stress path in the 1986 theory are shown in Figure 6.2. When a lift of backfill is placed, the stress path is assumed to follow the normally consolidated k_0 line to point A. Next the compactor is operated on the new lift, the stress in the lift moves up the k_0 line from A to B. When the compactor moves away, the stress path follows the non-linear unloading path from B to C. The horizontal stresses on this unloading path are higher than the horizontal stresses on the k_0 line. Unloading continues until the vertical stress is again equal to the overburden stress at point A. If the stress at point B is high enough, as shown in the example in Figure 6.2, the unloading stress path will intersect the passive pressure line, which is labelled k_{lim} in the figure, at point C and will move along this line to point D, where the vertical stress is the same as at A. The next cycle of loading, from

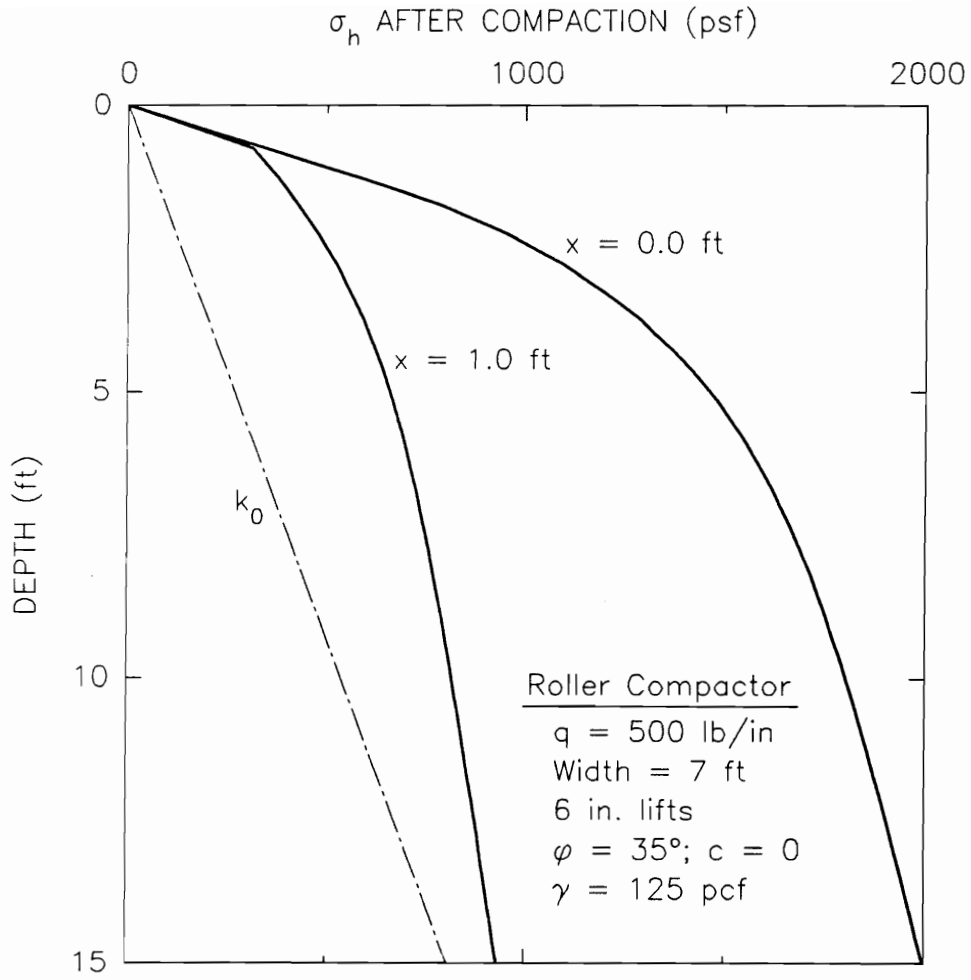

Figure 6.1: Compaction-Induced Lateral Earth Pressures Using the 1986 Theory

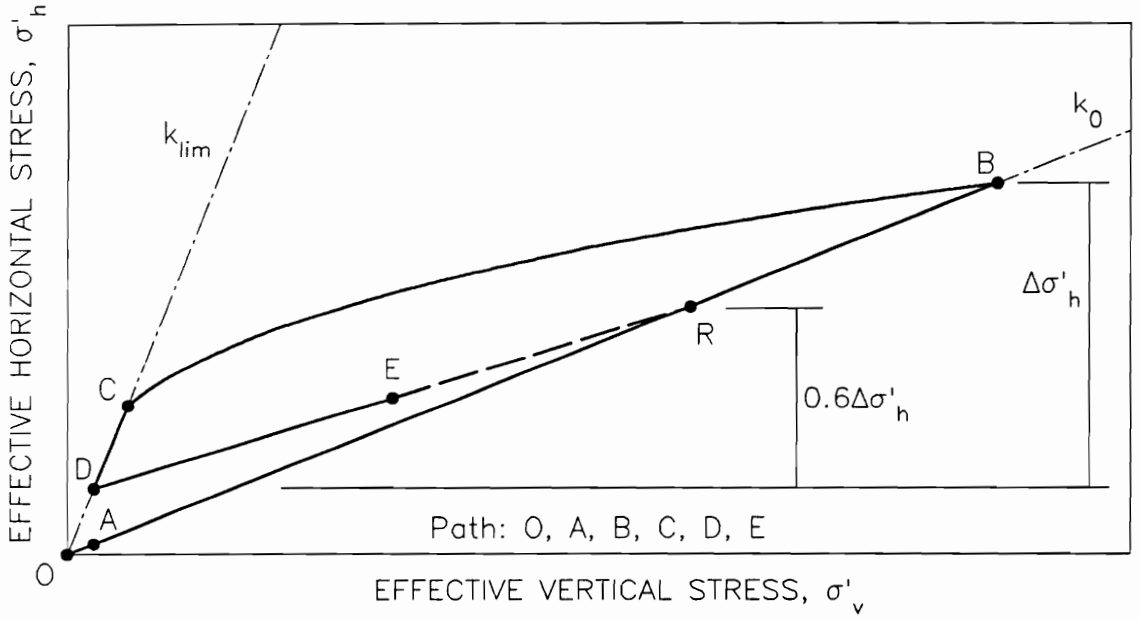

Figure 6.2: Control Points for the k_0 Model in the 1986 Theory

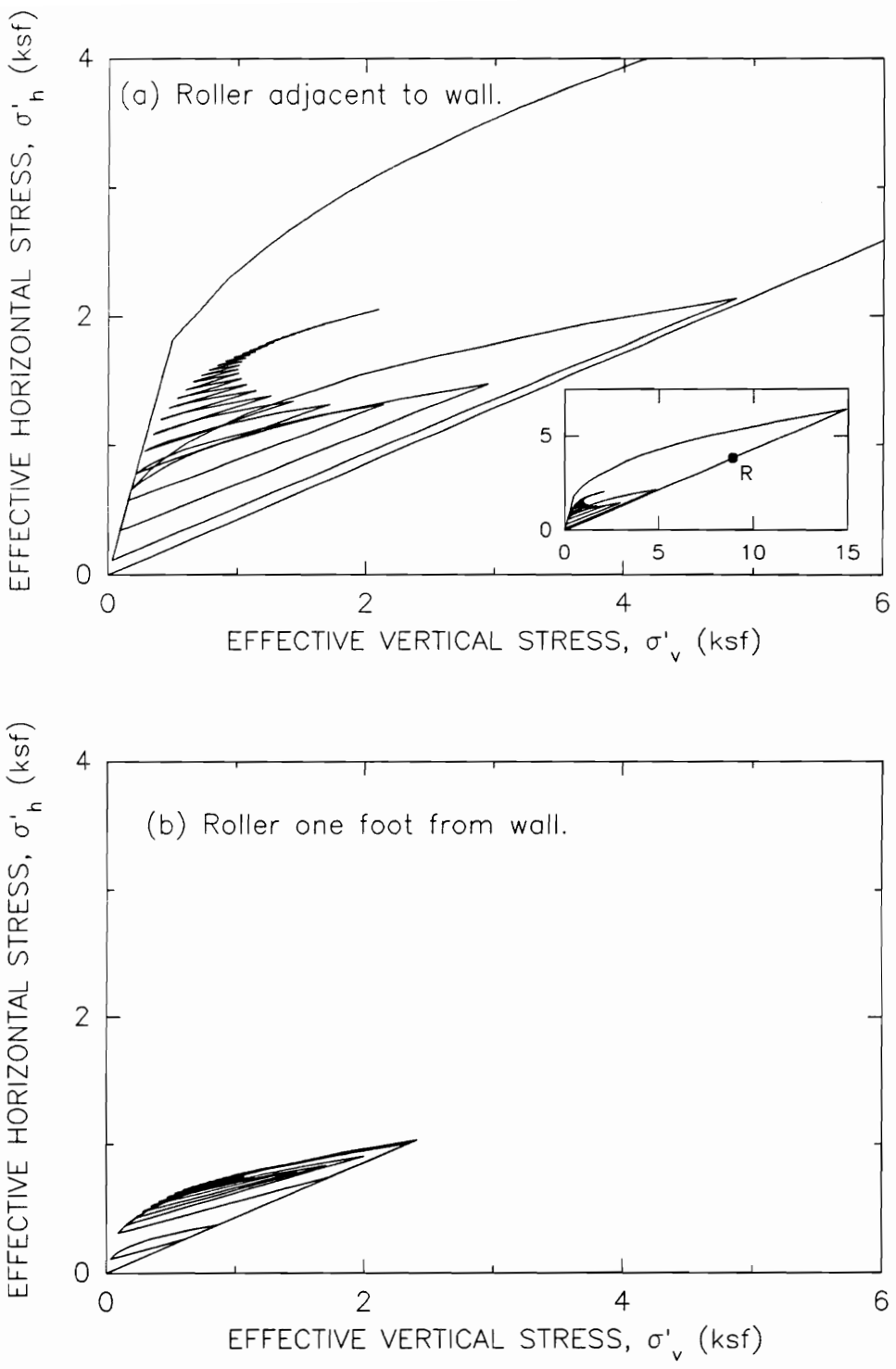

Figure 6.3: k_0 Stress Paths Using the 1986 Theory

another lift of fill and from the compactor operating on the surface of the new lift, causes the stress in the backfill to follow a reloading stress path from point D towards a reloading target point, labelled R in Figure 6.2, on the k_0 line. In the 1986 theory, the location of point R was determined in relation to points B and D according to the proportions shown in Figure 6.2. As a result, if the stresses from the compactor operating on the first lift were very high, as would occur when the compactor passed very close to the wall, point B would be located very far up the k_0 line. This caused point R to be located far up the k_0 line also. In this case, the stress path for subsequent loading moved up the relatively steep reloading path from point D to R. On the other hand, if the compactor did not approach so closely to the wall, the peak stresses from the compactor would not be so high, point B would be lower, and the reloading would follow a shallower stress path towards a lower point R.

The complete stress paths for the conditions analyzed in Figure 6.1 are shown in Figure 6.3. It can be seen that the peak value of stress calculated for compaction of the first lift is much higher when the compactor operates immediately adjacent to the wall than it is when the compactor operates one foot away, and that part of the analysis seems reasonable. However, the 1986 theory modelled the behavior in such a way that a permanent memory of the high stress event was retained in the form of a high position for the reloading target point, towards which all subsequent stress path excursions were directed. The reloading target point, at a vertical stress of about 9 ksf, is labelled

R in the small inset graph in Figure 6.3(a). Subsequent stress path excursions pivoted about point R. The 1986 model retained memory of the high stress event even when the stress path intersected and moved down the passive pressure failure line. The net effect was that the model was not truly hysteretic. This is shown in Figure 6.3(a), where the stress path for subsequent lifts works its way up above the stress path for the second lift. On the other hand, when the roller's closest approach was one foot from the wall, a very high stress event did not occur at the wall, and a high reloading target point was not locked in. This is shown by the stress path in Figure 6.3(b).

It does not seem reasonable that the soil response should be so strongly influenced by the maximum past loading when backfill experiences passive failure during unloading. Instead, it seems more reasonable that the subsequent soil response could be modelled as if the soil had experienced a smaller maximum past loading, one from which the non-linear unloading path would intersect the passive failure line at the unloading stress point (point D in Figure 6.2). This idea was the basis for the revisions to the 1986 model that are described in the following section.

6.3 Revised Hysteretic k_0 Model

Several important components of the revised hysteretic model are unchanged from the 1986 theory. These components are the virgin loading, virgin unloading, and virgin reloading stress paths for the case where the passive failure line is not encountered during unloading. As shown in Figure 6.4, a soil element follows the normally consolidated

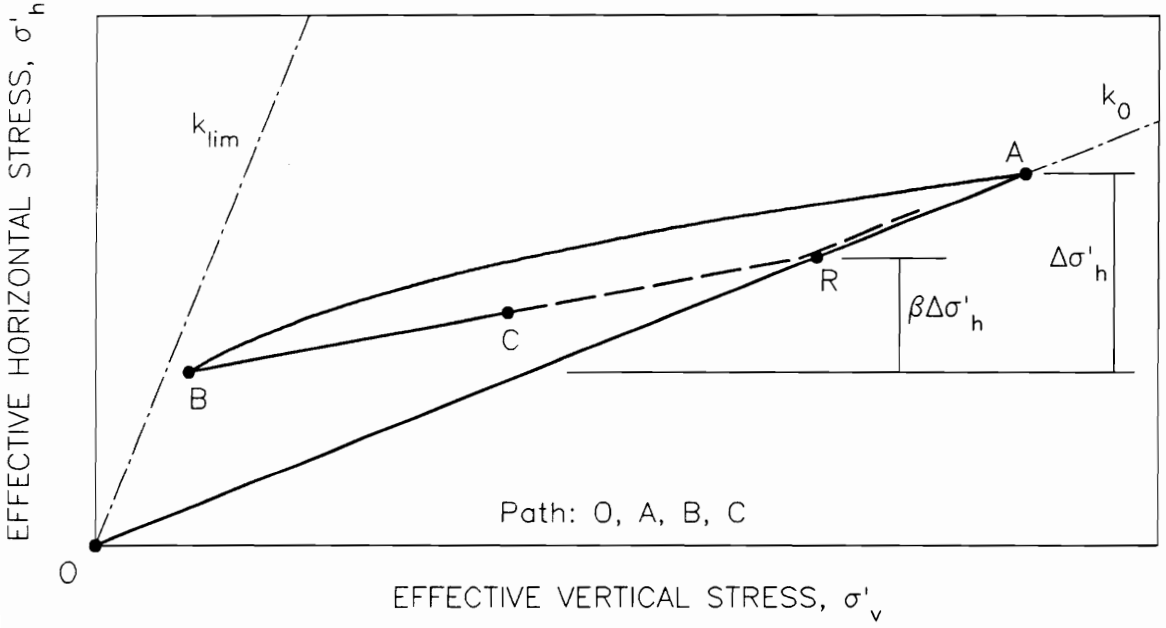

Figure 6.4: Virgin Loading, Unloading, and Reloading in the k_0 Stress Path Model

k_0 loading path from the origin to point A during primary loading. This portion of the stress path is defined by

$$\sigma'_h = k_0 \sigma'_v \tag{6.1}$$

where

σ'_h = the effective horizontal stress,

σ'_v = the effective vertical stress, and

k_0 = the normally consolidated at-rest pressure coefficient, a model parameter.

Virgin unloading from the peak stress state follows a non-linear unloading path from point A to point B. This stress path is defined by

$$\sigma'_{h,b} = k_0 \, OCR^{\alpha} \, \sigma'_{v,b} \tag{6.2}$$

where

OCR = the overconsolidation ratio, $\frac{\sigma'_{v,a}}{\sigma'_{v,b}}$, and

α = the unloading exponent, a model parameter.

Virgin reloading from point B on the virgin unloading path follows a linear reloading path towards the target reloading point R on the k_0 line. The location of point R is determined in proportion to the locations of points A and B according to

$$\sigma'_{h,r} = \sigma'_{h,b} + \beta \, (\sigma'_{h,a} - \sigma'_{h,b}) \tag{6.3a}$$

$$\sigma'_{v,r} = \frac{\sigma'_{h,r}}{k_0} \qquad (6.3b)$$

where

β = the virgin reloading slope factor, a model parameter.

If reloading is of sufficient magnitude that the virgin loading line is encountered, then the stress path follows the virgin loading line, as shown by the dashed line parallel to the k_0 line in Figure 6.4.

When test data is not available, the values of α and β are based on correlations with ϕ'. Duncan and Seed (1986) proposed the variation of α with ϕ' shown in Figure 6.5. They recommended that a reasonable value of β is 0.6.

The remaining details of the hysteretic model described in this section constitute revisions made to address the unreasonable result from the 1986 theory that was pointed out by Peck, and described earlier in this chapter.

Figure 6.6 shows the way that non-virgin unloading is represented in the revised hysteretic model. Non-virgin unloading follows an alpha-type unloading path from point C to point D, which is on the path towards point B, the end of the previous unloading path. A case where C is on the k_0 line is shown in Fig 6.6(a), and a case where C is above the k_0 line is shown in Figure 6.6(b). In either case, the unloading path is defined as follows:

$$\sigma'_{h,d} = k_1 \, OCR1^{\alpha 1} \, \sigma'_{v,d} \qquad (6.4)$$

where

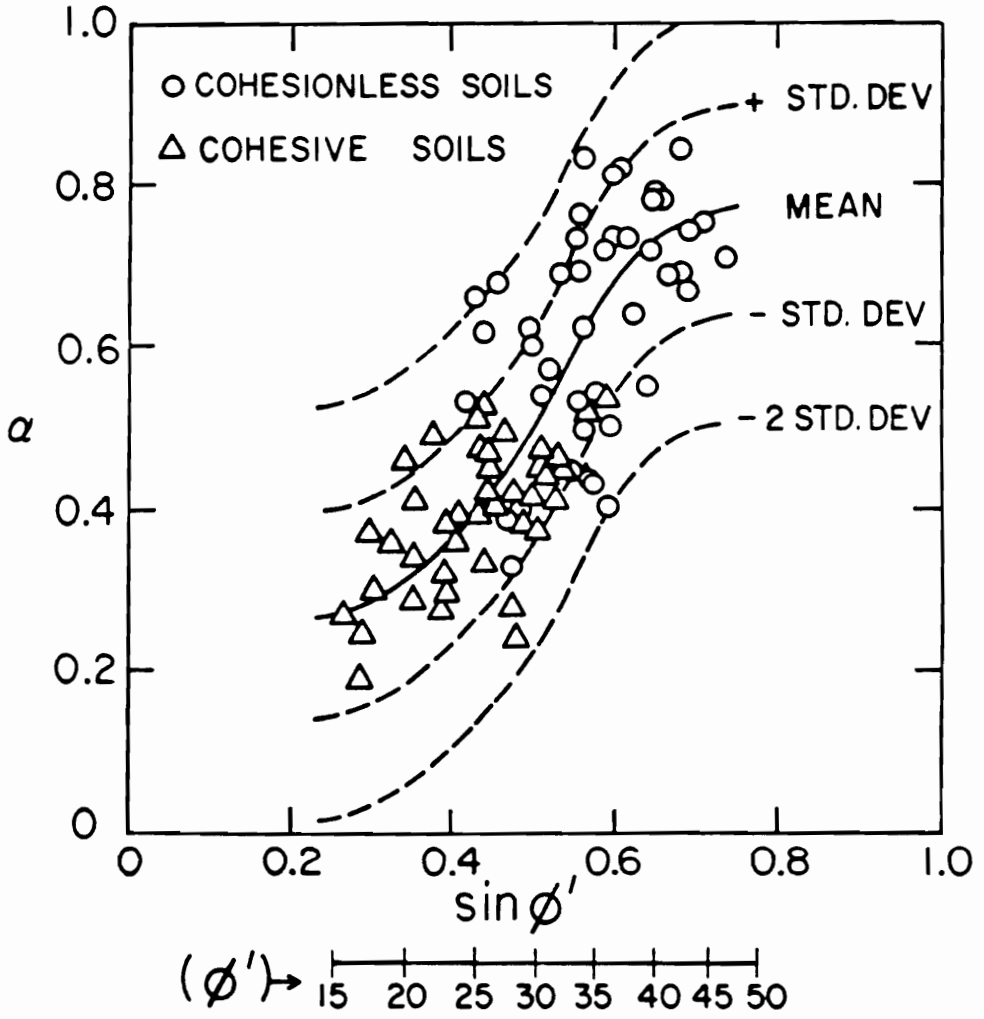

Figure 6.5: Recommended Values of α (after Duncan and Seed, 1986)

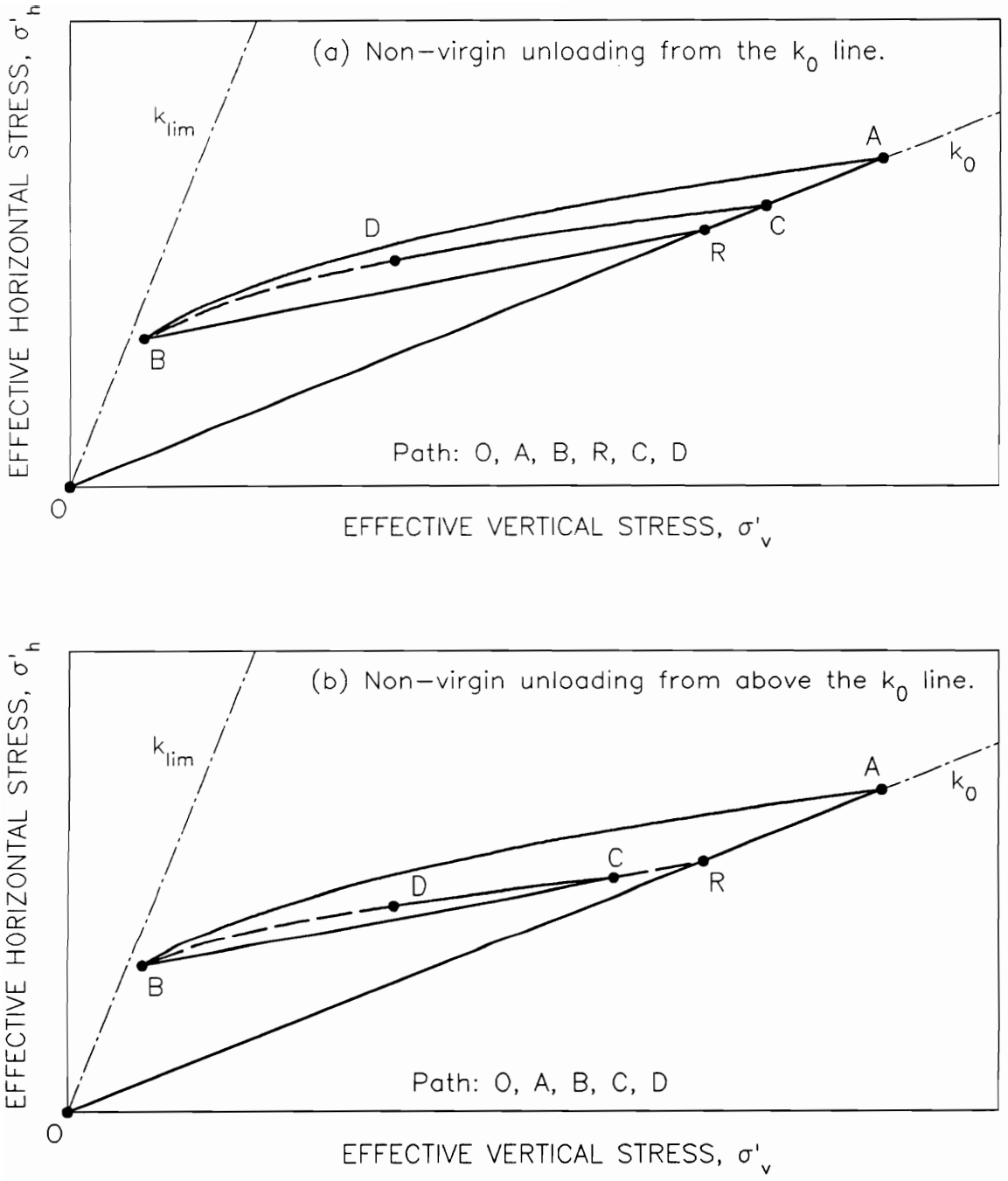

Figure 6.6: Non-virgin Unloading in the k_0 Model

$$k_1 = \frac{\sigma'_{h,c}}{\sigma'_{v,c}} ,$$

$$OCR1 = \frac{\sigma'_{v,c}}{\sigma'_{v,d}} , \text{ and}$$

$\alpha 1$ = the non-virgin unloading exponent.

$$= \frac{\log \left[\frac{\sigma'_{h,b}}{\sigma'_{v,b}} \cdot \frac{\sigma'_{v,c}}{\sigma'_{h,c}} \right]}{\log \left[\frac{\sigma'_{v,c}}{\sigma'_{v,b}} \right]}$$

As point C approaches the k_0 line in Figure 6.6(b), the value of k_1 approaches the value of k_0. As point C approaches point A in Figure 6.6(a), the value of $\alpha 1$ approaches the value of α. Thus, the formulation provides a smooth transition between virgin and non-virgin unloading.

Figure 6.7 shows the way linear reloading from non-virgin unloading is modelled by the revised theory. Two cases are shown: a) reloading from non-virgin unloading that originated on the k_0 line and b) reloading from non-virgin unloading that originated at a point above the k_0 line. For the first case, reloading follows a linear path from point D toward the reloading target point R_d on the k_0 line. The slope that establishes the location of point R_d is determined from the previous stress history. The relationships are as follows:

$$\sigma'_{h,rd} = \sigma'_{h,d} + \beta 1 \ (\sigma'_{h,c} - \sigma'_{h,d}) \qquad (6.5a)$$

$$\sigma'_{v,rd} = \frac{\sigma'_{h,rd}}{k_0} \qquad (6.5b)$$

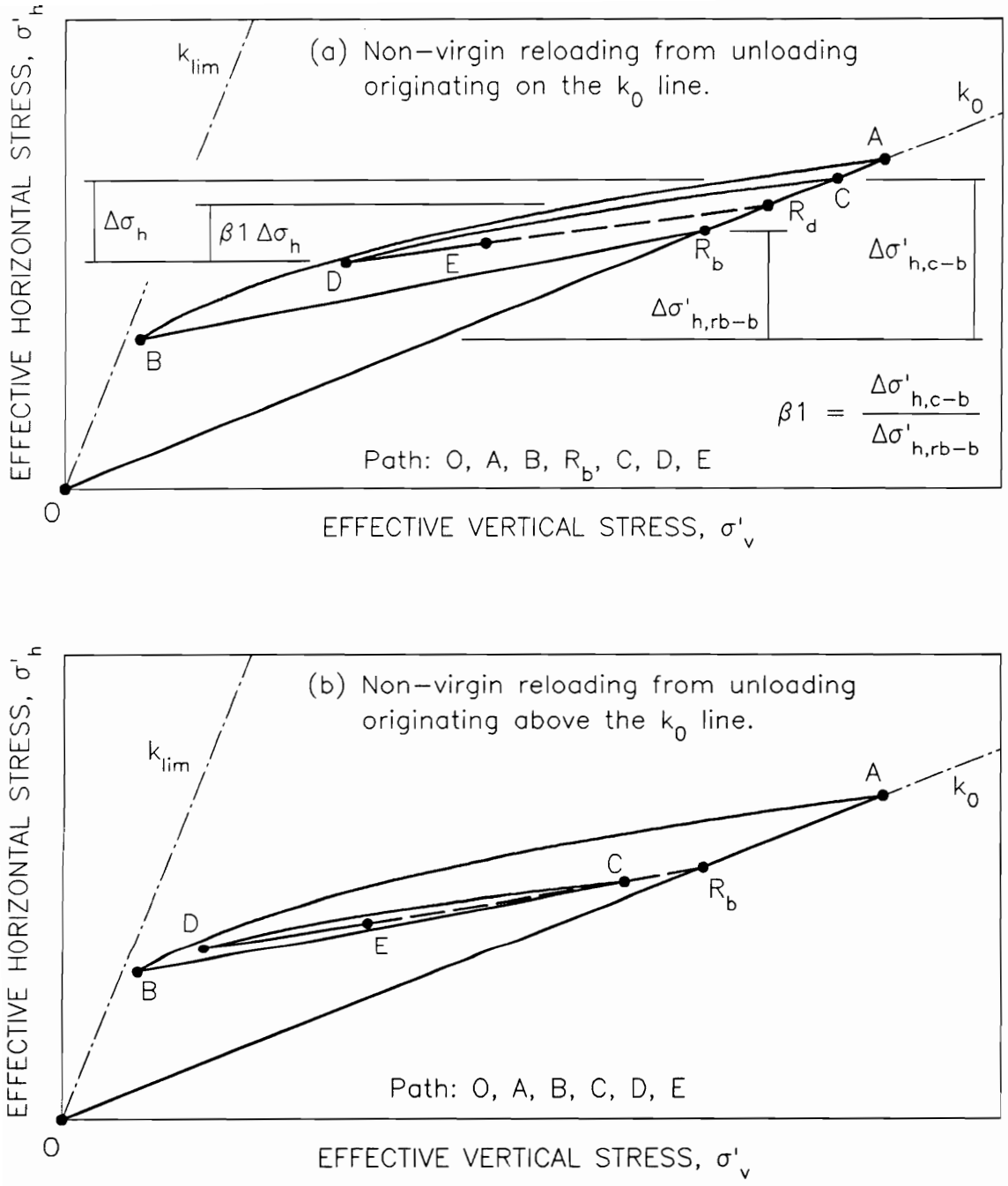

Figure 6.7: Non-virgin Reloading in the k_0 Model

where

$\beta 1$ = the slope factor for reloading after non-virgin unloading from the k_0 line

$$= \frac{\sigma'_{h,rb} - \sigma'_{h,b}}{\sigma'_{h,c} - \sigma'_{h,b}}$$

In Figure 6.7(a), it can be noted that, as point C approaches point R_b, the value of $\beta 1$ approaches unity. As point C approaches point A, the value of $\beta 1$ approaches the value of β. Thus, the formulation provides a smooth transition between virgin reloading and reloading after non-virgin unloading.

Figure 6.7(b) illustrates the case of reloading from non-virgin unloading that originated at a point above the k_0 line. In this situation, the reloading is linear from the unloading point, D, towards the previous loading point, C. Additional reloading beyond point C would follow the linear reloading path from points C to R_b, and would then progress up the k_0 line.

In this revised hysteretic model, the soil stress path consists of a set of nested loops created by a series of loading and unloading steps. If, at some stage, the applied stresses should take the stress path outside some of the interior loops, the exceeded interior loops are removed from the model memory. The process for unloading is shown in Figure 6.8. In Figure 6.8(a), the end point of a stress path that has created a series of nested loops is marked as point F. If further unloading occurs, the stress path will follow the unloading path shown by the dashed line from F to G. In this process, the interior loops

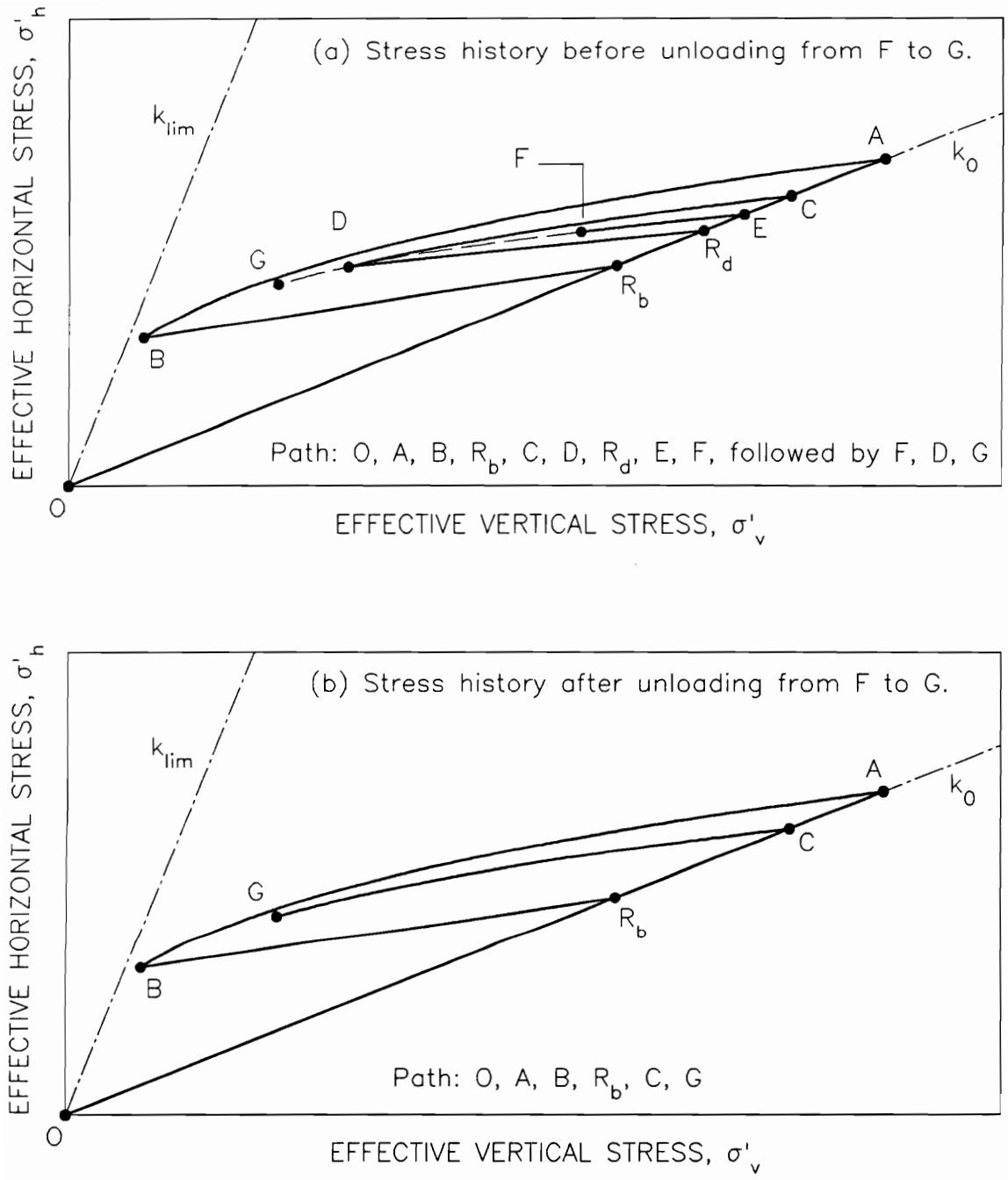

Figure 6.8: Erasure of Interior Loops During Unloading in the k_0 Model

whose limits are exceeded are removed from the model memory. The final stress state with its retained stress history is shown in Figure 6.8(b).

The process for loading is shown in Figure 6.9. In this case, the stress path follows the dashed line from D to E, as shown in Figure 6.9(a). As interior loops are exceeded they are removed from the model memory. The final stress state with its retained stress history is shown in Figure 6.9(b).

When the unloading path intersects the passive failure line, additional unloading follows the k_{lim} line, as shown by the segment from B to C in Figure 6.10. The passive failure line is defined by a slope, k_{lim}, and an intercept on the horizontal stress axis, $\sigma'_{h,0,lim}$. Assuming that the passive failure line has the same origin in normal stress space as the Mohr-Coulomb failure envelope, the slope, k_{lim}, and the intercept, $\sigma'_{h,0,lim}$, are related by

$$\sigma'_{h,0,lim} = \frac{c'}{\tan \phi'} (k_{lim} - 1) \qquad (6.6a)$$

where

c' = the effective stress cohesion intercept, and

ϕ' = the effective stress friction angle.

If k_{lim} is taken to be the Rankine passive pressure coefficient, k_p, then

$$\sigma'_{h,0,lim} = \frac{2c'\cos \phi'}{1 - \sin \phi'} \qquad (6.6b)$$

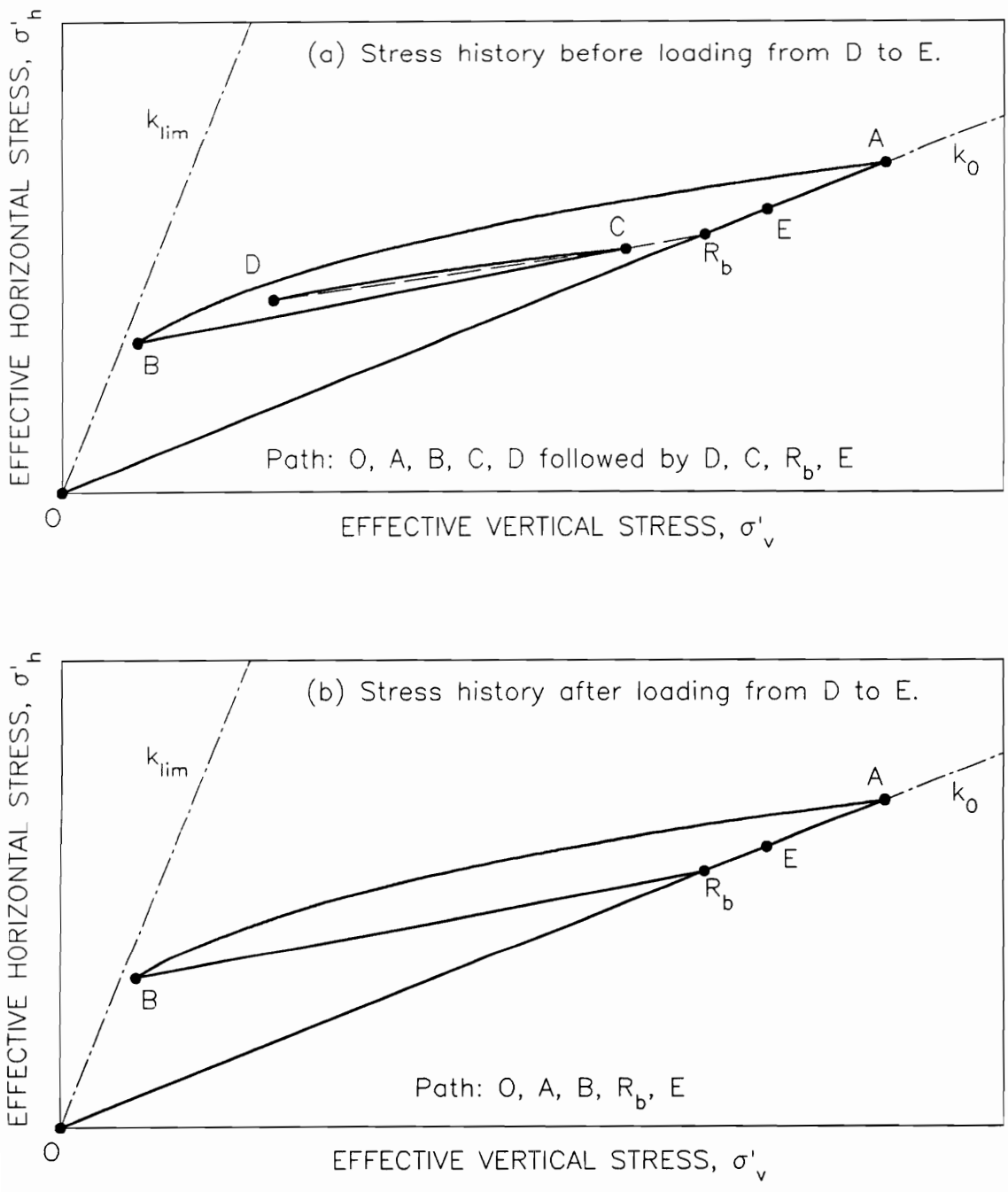

Figure 6.9: Erasure of Interior Loops During Reloading in the k_0 Model

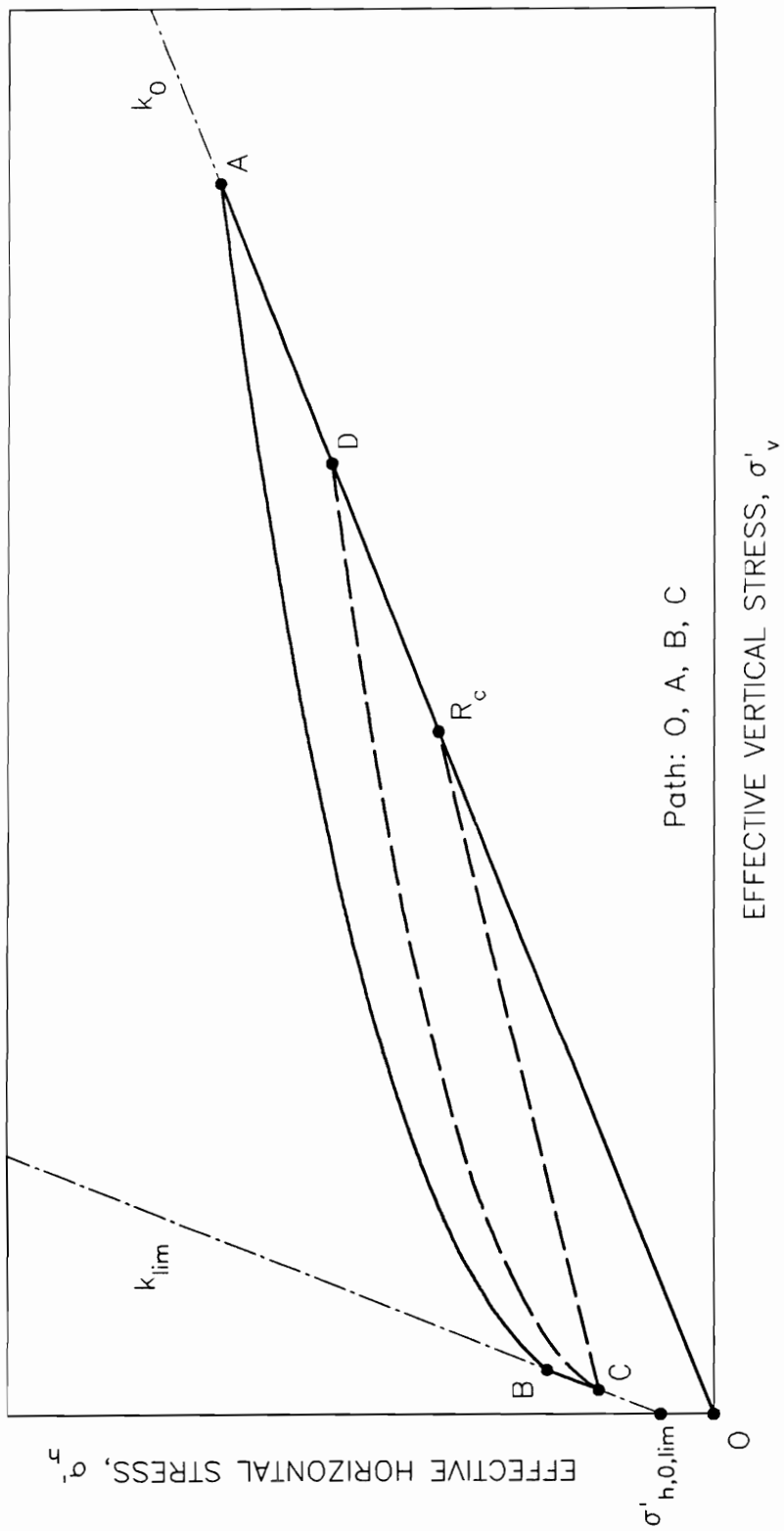

Figure 6.10: Resetting the Maximum Past Loading Point for Movement Down the Passive Failure Line

There is some evidence, which will be discussed in Chapter 7, that k_{lim} should be set equal to $1/k_0$ for compaction-induced earth pressure problems. In this case,

$$\sigma'_{h,0,lim} = \frac{c'}{\tan \phi'} \left(\frac{1}{k_0} - 1 \right) \tag{6.6c}$$

As mentioned previously, the reloading target point in the 1986 theory was established based on the maximum past loading, point A in Figure 6.10, and the current stress state, point C on the passive failure line. In the revised hysteretic model, the maximum past loading point is reset to point D, from which a virgin unloading path would intersect the passive failure line at the current stress state, point C. The location of point D is given by

$$\sigma'_{v,d} = \left[\frac{\sigma'_{h,0,lim} + k_{lim} \sigma'_{v,c}}{k_0 \sigma'_{v,c}} \right]^{1/\alpha} \sigma'_{v,c} \tag{6.7a}$$

$$\sigma'_{h,d} = k_0 \sigma'_{v,d} \tag{6.7b}$$

The location of the reloading target, point R_c in Figure 6.10, is based on the reset maximum past loading point, D, and the current stress point, C. The relationships are the same as those in equations 6.3, with the subscripts changed to match the point labels in Figure 6.10:

$$\sigma'_{h,rc} = \sigma'_{h,c} + \beta \, (\sigma'_{h,d} - \sigma'_{h,c}) \tag{6.8a}$$

$$\sigma'_{v,rc} = \frac{\sigma'_{h,rc}}{k_0} \qquad (6.8b)$$

Equations 6.7 and 6.8 accomplish an erasure of the memory of previous very high stress events when unloading progresses down the passive failure line.

In order to verify that the revised effective stress k_0 model described in the preceding paragraphs can track the stress paths for soils loaded in k_0 compression, the model was applied to published laboratory test results for two soils. The comparisons between model and data in Figures 6.11 and 6.12 show that the model closely simulates the hysteretic behavior of Haney Clay (Campanella and Vaid, 1972) and Monterey Sand (Wright, 1969) subjected to k_0 laboratory tests.

6.4 Incorporating the Revised Hysteretic k_0 Model in Compaction-induced Earth Pressure Theory

In order to incorporate the revised hysteretic k_0 model in a compaction-induced earth pressure theory, it is necessary to decide what vertical stress increments should be applied to drive the k_0 model. The k_0 model would then yield horizontal pressures, which are the compaction-induced lateral pressures. In this research, the methods of Duncan and Seed (1986) were used to determine the vertical stress increments which should be applied to the k_0 model. Their methods are reviewed in this section.

For backfill free from other applied loads, there are two sources of vertical stress increments when the backfill is compacted behind a rigid wall: 1) the self weight from the backfill lifts and 2) the load

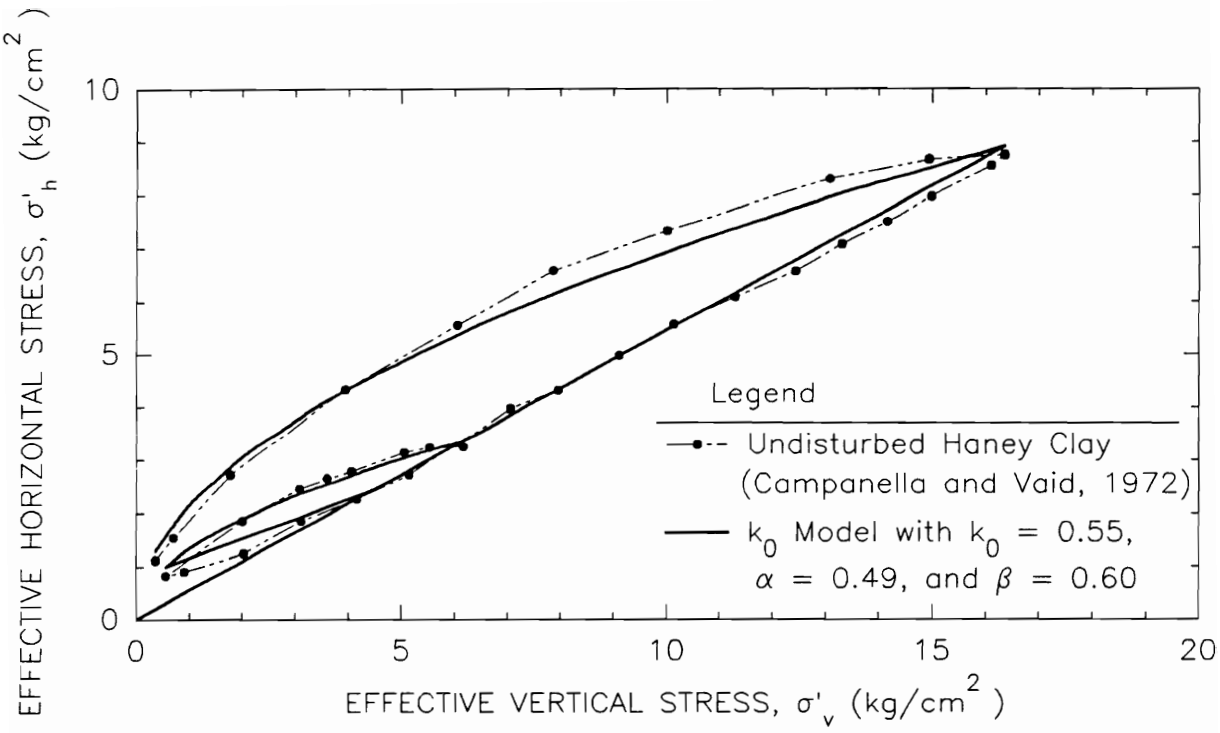

Figure 6.11: Comparison Between k_0 Model and Laboratory Data for Haney Clay

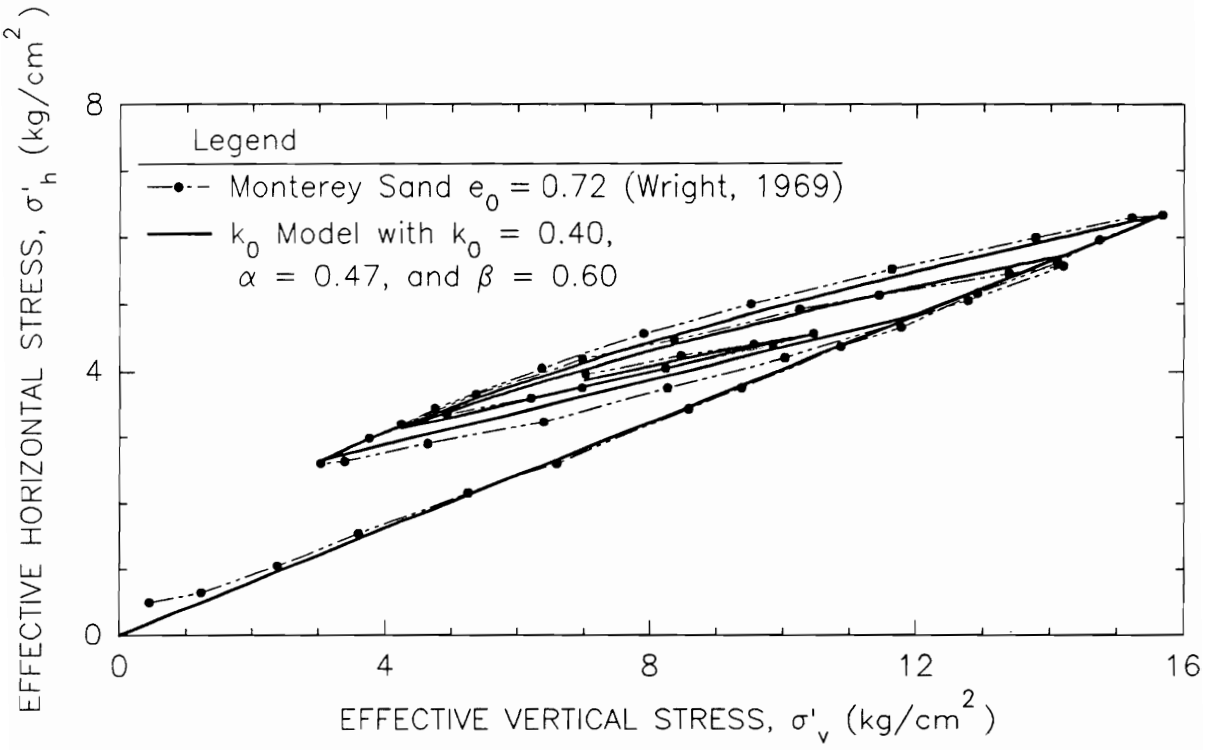

Figure 6.12: Comparison Between k_0 Model and Laboratory Data for Monterey Sand

from the compactor operating on the surface of each lift. Since the backfill lifts are of broad lateral extent, the vertical stress increment due to a lift of backfill can be simply calculated from

$$\Delta\sigma_v = \gamma \Delta z \tag{6.9}$$

where

$\Delta\sigma_v$ = the vertical stress increment,

γ = the moist unit weight of the backfill, and

Δz = the lift thickness.

The load from the compactor is applied over an area of limited lateral extent, resulting in three dimensional load distribution effects. To account for these effects, Duncan and Seed (1986) recommend the following two-step procedure:

1. The horizontal stress increase adjacent to the wall induced by the compactor load at the surface is calculated at the depth of interest using the integrated Boussinesq solution. The horizontal stress calculated from the Boussinesq solution is doubled to account for the presence of the rigid wall. In performing the Boussinesq calculation, Poisson's ratio (ν) is estimated using the following empirically based equation:

$$\nu = \frac{1}{2} (0.5 + \nu_0) \tag{6.10a}$$

where

$$\nu_0 = \frac{k_0}{1 + k_0} \text{ , and} \tag{6.10b}$$

$$k_0 = 1 - \sin\phi' \tag{6.10c}$$

Thus,

$$\nu = \frac{4 - 3\sin\phi'}{8 - 4\sin\phi'} \tag{6.11}$$

2. The horizontal stress increase, $\Delta\sigma_h$, calculated in step 1 is converted to an equivalent vertical stress increment by

$$\Delta\sigma_v = \frac{\Delta\sigma_h}{k_0} \tag{6.12}$$

This two step procedure results in an equivalent vertical stress increment which, when applied to the uncompacted soil in k_0 compression, produces a horizontal stress increment equal to that calculated from the Boussinesq solution. In the compaction-induced earth pressure theory, this equivalent vertical stress increment is applied to the hysteretic k_0 model, whether the soil has been previously compacted or not. When the soil has been previously compacted, and consequently has a horizontal stress higher than the k_0 at-rest stress, then the equivalent vertical effective stress calculated using Eqn 6.12 produces a smaller change in horizontal stress in the k_0 model than that computed using the Boussinesq solution. As shown in Figure 6.13, the difference occurs because the previously compacted soil follows a reloading stress path for at least part of the vertical stress increment application. This

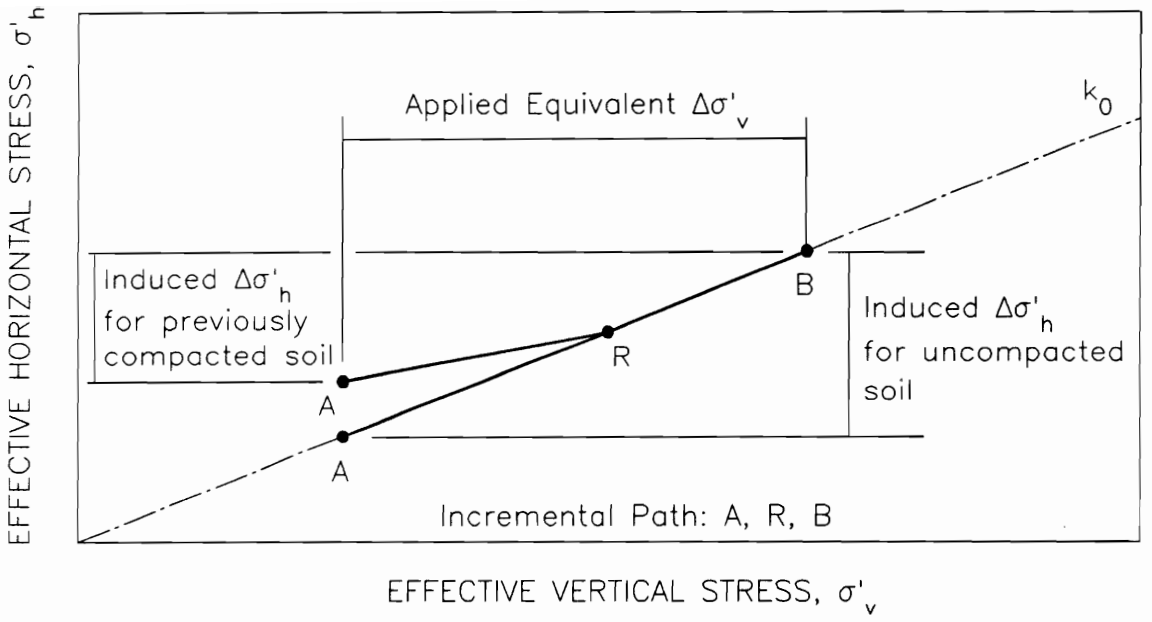

Figure 6.13: Effect of the Applied Equivalent Vertical Stress Increment in the k_0 Model

approach for calculating the equivalent vertical stress increment seems logical, and Duncan and Seed (1986) have shown that the method produces results in reasonable agreement with field data.

In order to compute compaction-induced earth pressures using these procedures, three calculations must be performed for each lift of backfill: first, the stress increase due to the weight of the fill lift is applied to the hysteretic k_0 model; second, the equivalent vertical stress from the compactor on the surface of the current lift is applied; and third, a stress equal in magnitude and opposite in sign to the equivalent vertical stress from the compactor is applied, since compaction is assumed to be a temporary load that causes no net change in vertical stress. Due to the large number of calculations required, a computer program, EPCOMPAC, was developed to track the stress paths at the center of each lift of backfill behind a rigid wall using the methods described in this chapter. A user's manual for EPCOMPAC is contained in Appendix B.

EPCOMPAC was used to analyze the conditions shown in Figure 6.1, which were previously analyzed using the 1986 theory. The pressure versus depth results calculated using EPCOMPAC with k_{lim} equal to k_p are shown in Figure 6.14. The pressures calculated with the revised theory are much smaller for x = 0 ft than those calculated using the 1986 theory. The reason for the difference is shown by the hysteretic stress paths in Figure 6.15. These stress paths are for the analyses of Figure 6.14, and they show that with the revised theory the stress paths do not

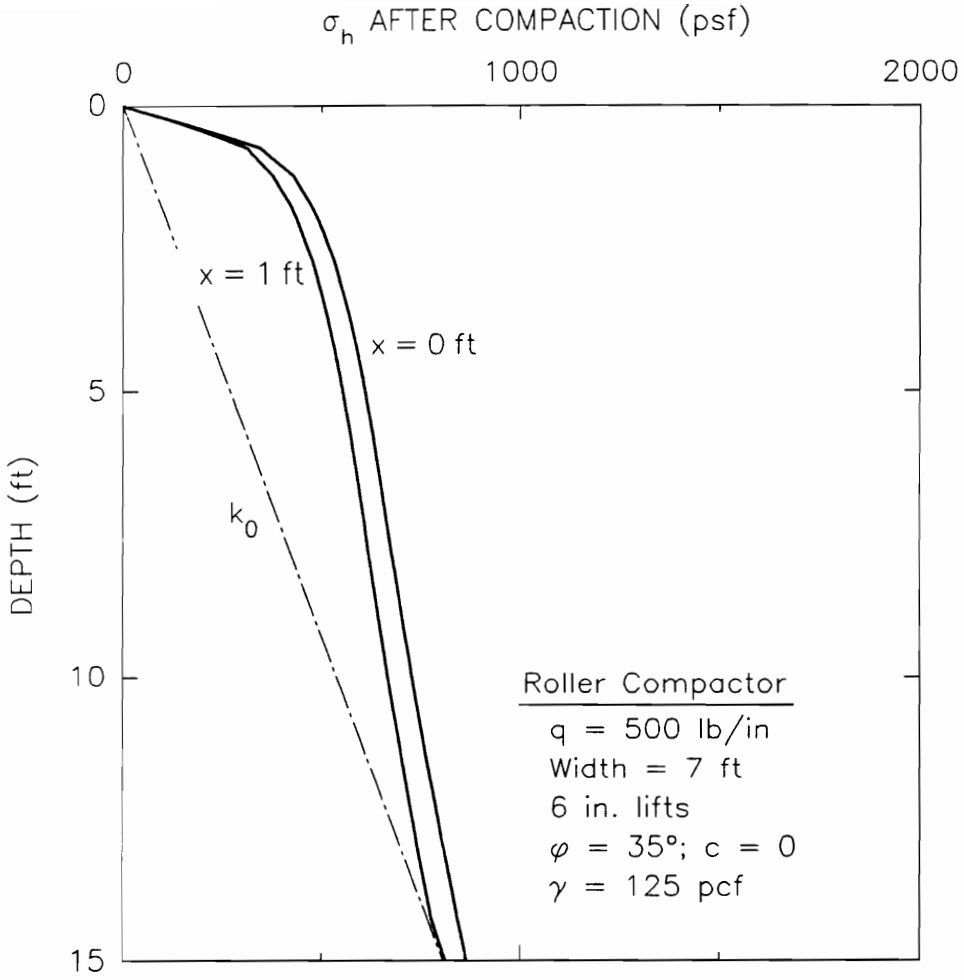

Figure 6.14: Compaction-Induced Lateral Earth Pressures Using the Revised Theory with $k_{lim} = k_p$

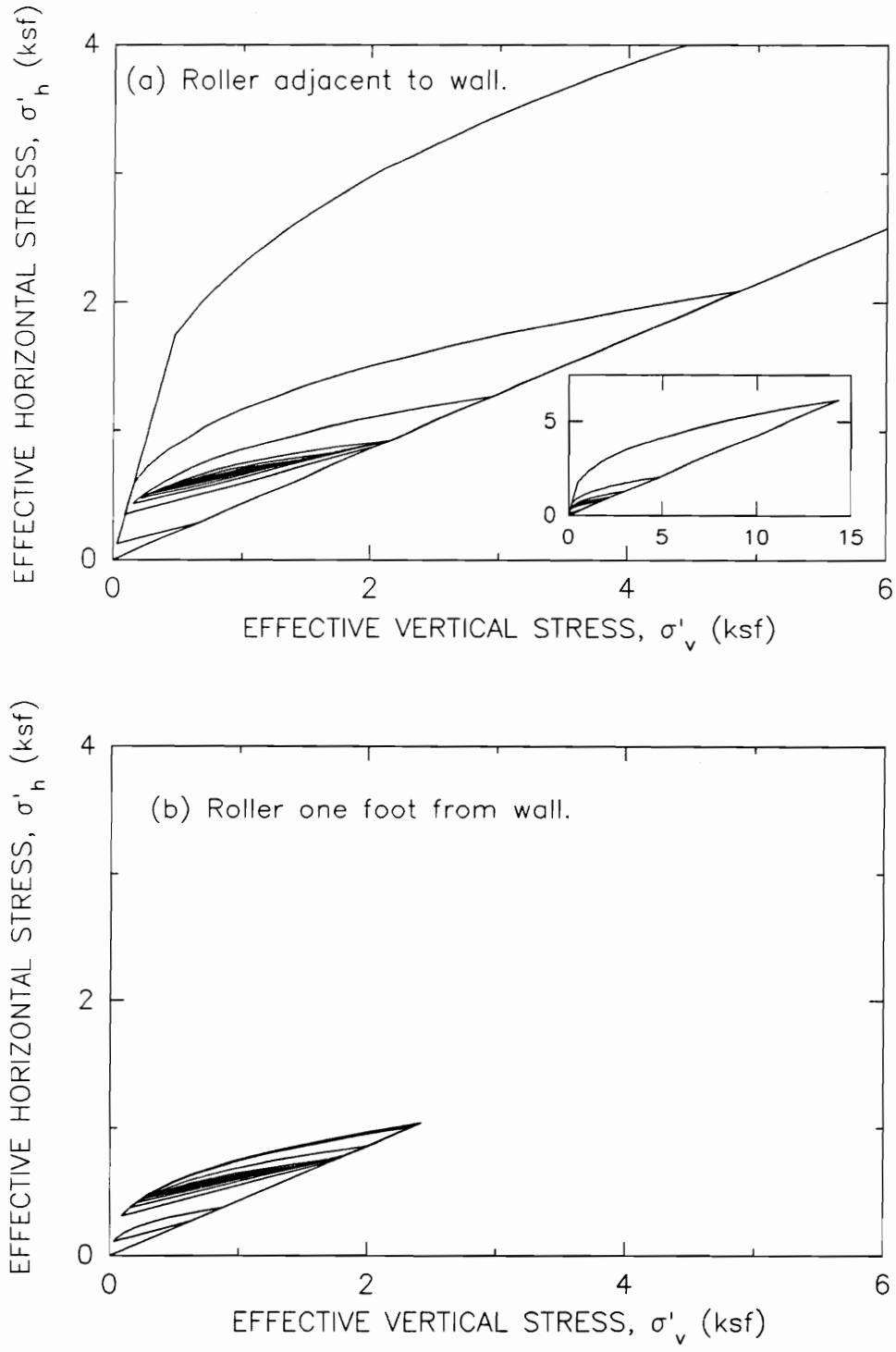

Figure 6.15: Hysteretic Stress Paths Using the Revised Theory with $k_{lim} = k_p$

pivot about an unrealistically high reloading target point, as they did in Figure 6.3 for the 1986 theory.

Calculations for the same roller compactor were also made using EPCOMPAC with k_{lim} equal to $1/k_0$, and the results are shown in Figure 6.16. In Figure 6.15, $k_{lim} = k_p = 3.7$, whereas in Figure 6.16, $k_{lim} = 1/k_0 = 2.35$. The lower value of k_{lim} in Figure 6.16 controls the maximum possible horizontal stress to a greater depth than does the higher value of k_{lim} in Figure 6.15. At the depth in Figure 6.16 at which k_{lim} ceases to control the horizontal stresses, the applied stress from the compactor is approximately the same whether the roller passes adjacent to the wall or approaches no closer than one foot from the wall. Consequently, the calculated compaction-induced lateral pressures are almost exactly the same for both roller positions, as shown in Figure 6.16.

6.5 An Extended Compaction-induced Earth Pressure Theory for Moist Soils with Significant Fines Content

The compaction-induced earth pressure theory described in previous sections of this chapter is an effective stress theory. It strictly applies only to dry cohesionless soils. However, it probably also can be applied with reasonable accuracy to moist sands and gravels that do not develop significant pore pressures. This section describes an extension of the compaction-induced earth pressure theory to include moist soils with significant fines content. Such soils represent an important group of backfill materials, which do develop significant pore pressures during compaction.

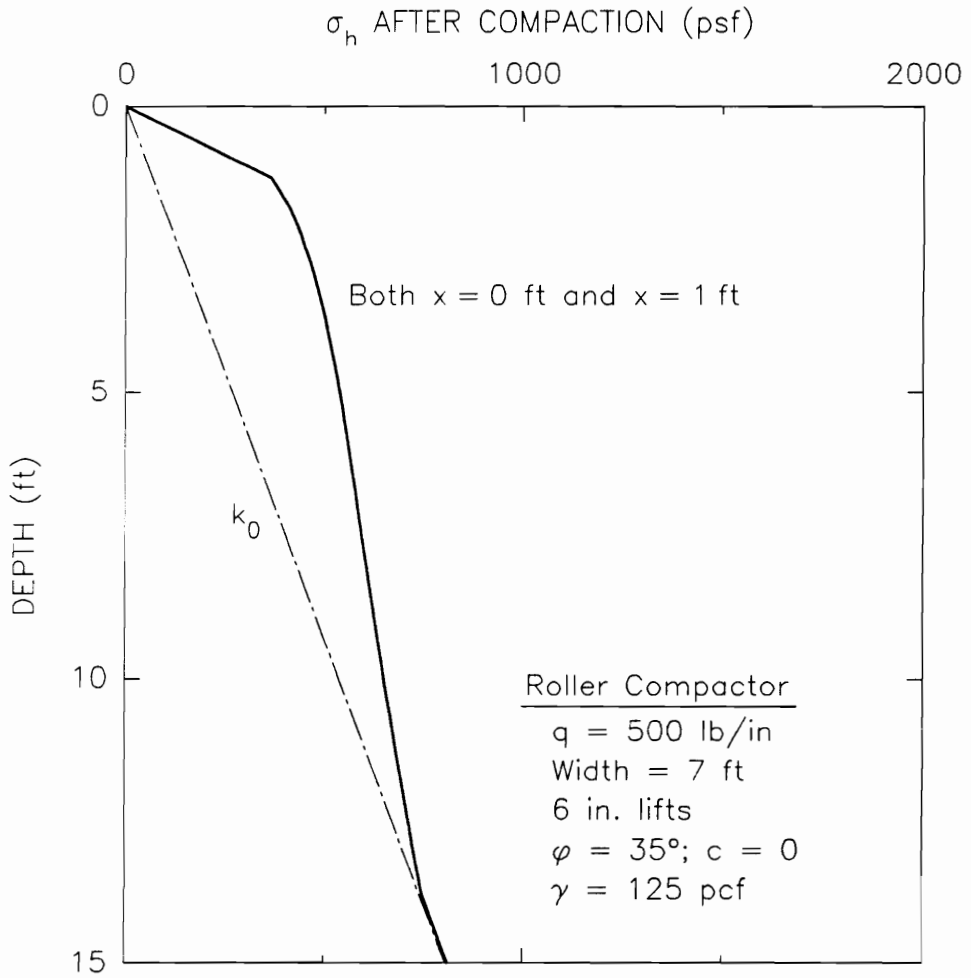

Figure 6.16: Compaction-Induced Lateral Earth Pressures Using the Revised Theory with $k_{lim} = 1/k_0$

The loads applied by the fill lifts and the compaction equipment are total stress loads. The hysteretic k_0 model described in section 6.3 is an effective stress model that requires effective vertical stress increments as input. Two possibilities for developing a compaction-induced earth pressure theory for backfill with significant pore pressures are: 1) to express the pore pressure as a function of the total stress state of the soil and use the effective stress k_0 model to track the compaction-induced effective stresses, or 2) to develop a new total stress compaction-induced earth pressure theory that computes total horizontal stress increments directly from total vertical stress increments. In this research, the first approach was followed because of the success of the effective stress k_0 model and because the laboratory total stress k_0 data for moist compacted soils that would be necessary as a basis for the second approach were not available.

Bishop et al. (1960) extended Terzaghi's effective stress concept to include unsaturated soils by introducing the following equation:

$$\sigma' = \sigma - \chi u_w - (1-\chi)u_a \qquad (6.13)$$

where

σ' = the effective normal stress,

σ = the total normal stress,

u_w = the pore water pressure,

u_a = the pore air pressure, and

χ = a parameter related to the degree of saturation. Its value is zero for a dry soil and one for a saturated soil.

The parameter χ is normally determined by performing shear tests on unsaturated specimens and solving Eqn 6.13 for χ using the value of effective stress which would give the same response in otherwise similar saturated specimens. Other approaches have been proposed for unsaturated soils (notably, Fredlund, 1979); however, the effective stress concept embodied in Eqn 6.13 will be used here because it is readily adaptable to compaction-induced earth pressure analyses. If the pore air pressure is zero (gage), then an apparent pore pressure, u, may be defined as

$$u = \chi u_w \tag{6.14}$$

Eqn 6.13 then reduces to the form of the familiar effective stress equation for saturated soils

$$\sigma' = \sigma - u \tag{6.15}$$

Now it is necessary to express the apparent pore pressure as a function of the total stress. This will be done by defining the initial apparent pore pressure, u_0, to be the apparent pore water pressure in an element of soil free from external stress, and then adding the change in apparent pore pressure that occurs due to application of total stress to the element, using Skempton's (1954) pore pressure parameters to calculate the change in apparent pore pressure. Skempton proposed that

changes in pore pressure, Δu, can be related to changes in total stress, $\Delta\sigma_3$ and $\Delta\sigma_1$, by the pore pressure coefficients A and B:

$$\Delta u = B\,(\Delta\sigma_3 + A\,(\Delta\sigma_1 - \Delta\sigma_3)) \tag{6.16a}$$

$$= B\,\Delta\sigma_3 + \bar{A}\,(\Delta\sigma_1 - \Delta\sigma_3) \tag{6.16b}$$

$$= \bar{B}\,\Delta\sigma_3 + \bar{A}\,\Delta\sigma_1 \tag{6.16c}$$

where

$\bar{A} = BA$, and

$\bar{B} = B(1 - A)$ [This definition of $\bar{B}$ is different from Skempton's, but it is more convenient for the derivations that follow.]

The coefficient B represents the effect of increasing degree of saturation on the pore pressure response to applied loads. As the soil approaches complete saturation, the value of B approaches unity for soils whose grain structure is much more compressible than water. The coefficient A represents the contribution of the deviatoric stress increment to the pore pressure response. For saturated normally consolidated clays, the value of A is frequently close to one. For saturated overconsolidated clays, the value of A can be small or negative. If the value of A is one-half, then $\bar{A}$ equals $\bar{B}$, and the contributions of $\Delta\sigma_3$ and $\Delta\sigma_1$ to pore pressure response are the same.

The coefficients A and B are not constants for a given soil, even at a given density. Their values depend on the stress history, the magnitudes of the total stresses, and on the size of the total stress increments. The traditional approach is to evaluate A and B over a

specific range of stresses relevant to the problem of interest, and then treat the coefficients as constants over that stress range. In this development, the coefficients are treated as constants, even though the stresses during compaction cover a large range, from low stresses due to self weight of the backfill at shallow depths to high stresses from large compactors or from the fill weight at great depths. The limitations associated with treating the coefficients A and B as constants are discussed in more detail in Chapter 7.

With the assumption that the pore pressure parameters are constant, and because $u = u_0$ at $\sigma_3 = \sigma_1 = 0$, the apparent pore water pressure can be expressed as a function of the total stress state by applying Eqn 6.16,

$$u = u_0 + \Delta u \tag{6.17a}$$

$$= u_0 + \bar{B}\,\sigma_3 + \bar{A}\,\sigma_1 \tag{6.17b}$$

In this development, it is assumed that the moist soil obeys the effective stress and total stress Mohr-Coulomb failure laws:

$$\sigma'_1 - \sigma'_3 = (\sigma'_1 + \sigma'_3)\sin\phi' + 2c'\cos\phi' \tag{6.18}$$

$$\sigma_1 - \sigma_3 = (\sigma_1 + \sigma_3)\sin\phi + 2c\cos\phi \tag{6.19}$$

Based on these considerations, several important relationships can be derived. Eqns 6.15 through 6.19 can be solved to yield the following expression for u_0:

$$u_0 = - \frac{[1 + (2A - 1) \sin \phi'] \cos \phi}{[1 + (2A - 1) \sin \phi] \sin \phi'} c + \frac{c'}{\tan \phi'} \quad (6.20)$$

Eqns 6.15 through 6.19 can also be solved to yield the following relationship among A, B, ϕ, and ϕ':

$$\sin \phi = \frac{(1-B) \sin \phi'}{1 + B (2A-1) \sin \phi'} \quad (6.21)$$

According to Eqn 6.21, if the value of B is zero, then the total stress friction angle equals the effective stress friction angle. If the value of B is unity, then the total stress friction angle is zero.

Another important total stress relationship for these analyses of compaction-induced earth pressures is evaluation of the incremental, total stress at-rest lateral earth pressure coefficient, Δk_0^T, which may be defined as:

$$\Delta k_0^T = \frac{\Delta \sigma_h}{\Delta \sigma_v} \quad (6.22)$$

where $\Delta \sigma_h$ and $\Delta \sigma_v$ are the vertical and horizontal total stress increments occurring during k_0 compression of an element of soil. The effective stress at-rest lateral earth pressure coefficient, k_0, is constant over a large stress range, and is defined as

$$k_0 = \frac{\Delta \sigma'_h}{\Delta \sigma'_v} \quad (6.23)$$

The values of $\Delta\sigma'_h$ and $\Delta\sigma'_v$ in Eqn 6.23 are related to $\Delta\sigma_h$ and $\Delta\sigma_v$ in Eqn 6.22 by the apparent pore pressure increment, Δu:

$$\Delta\sigma'_h = \Delta\sigma_h - \Delta u \tag{6.24a}$$

$$\Delta\sigma'_v = \Delta\sigma_v - \Delta u \tag{6.24b}$$

Because the horizontal and vertical stresses in k_0 compression are principal stresses, Eqns 6.16 and 6.22 through 6.24 yield the following expression for Δk_0^T:

$$\Delta k_0^T = \frac{k_0 + BA\,(1 - k_0)}{1 - B\,(1 - A)\,(1 - k_0)} \tag{6.25}$$

According to Eqn 6.25, when the value of B is zero, Δk_0^T is equal to k_0. When the value of B is one, the value of Δk_0^T is also one. Thus, Eqn 6.25 indicates that as the degree of saturation increases, the incremental increase in total horizontal stress approaches equality with the incremental increase in total vertical stress, for a soil loaded in k_0 compression.

To incorporate pore pressure response for a moist soil in the compaction-induced earth pressure theory, it is necessary first to establish a reasonable equivalent initial stress history for a soil element that is free from external total stress, and with horizontal and vertical effective stresses equal to $-u_0$. In Figure 6.17, the relationship between the total and effective stress states for the unstressed soil element, at point B, are shown. It is simple and reasonable to assume that the soil arrived at point B by following the

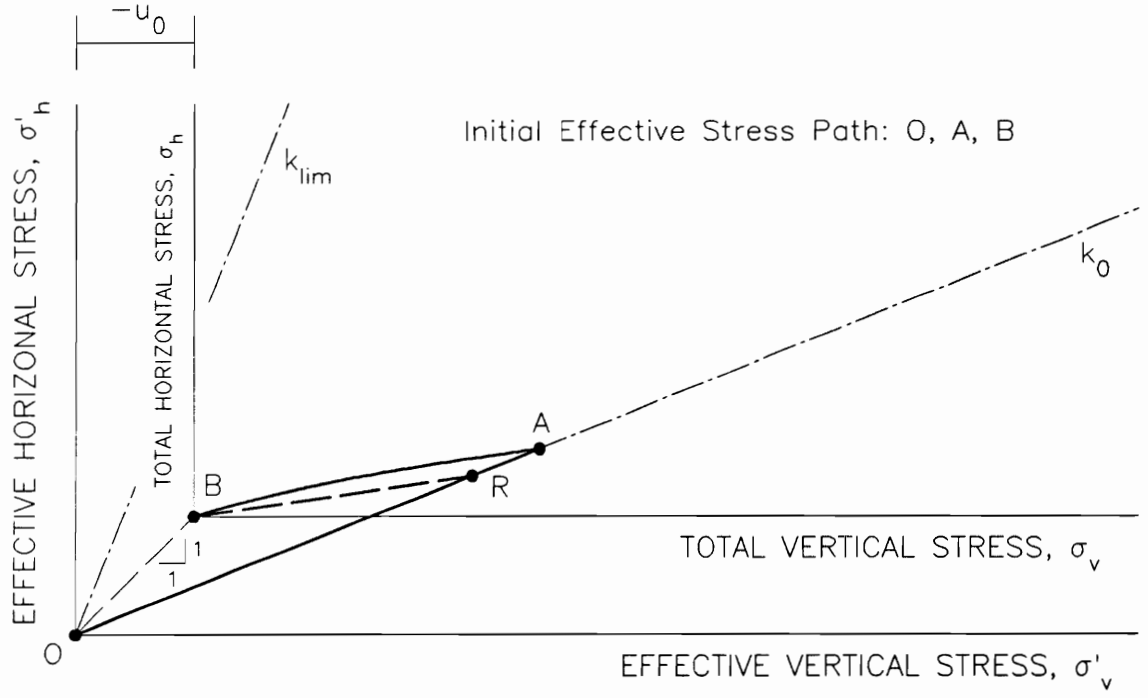

Figure 6.17: Initial Stress History for a Moist Soil Considering the Effect of Pore Pressures

minimum possible effective stress k_0 loading, which is shown by the path O, A, B in Figure 6.17. This approach gives the soil an initial stress history, reflecting the fact that the initial stress state is above the effective stress k_0 line. The location of point A is given by

$$\sigma'_{v,a} = \left[\frac{1}{k_0}\right]^{1/\alpha} (-u_0) \tag{6.26a}$$

$$\sigma'_{h,a} = k_0 \, \sigma'_{v,a} \tag{6.26b}$$

Loading from the initial stress state follows the effective stress path from points B to R and then up the k_0 line shown in Figure 6.17. If the coefficient B in Eqn 6.16 is positive, a positive change in pore pressure will develop in response to the loading, and the total stress axes will shift towards the effective stress axes. This will cause the slope from B to R to be steeper in total stress space than it is in effective stress space. This shift also causes the value of Δk_0^T to be greater than the effective stress k_0 value.

The slope from B to R in effective stress space, k_i, is given by

$$k_i = \frac{\beta\left[k_0^2\left[\frac{1}{k_0}\right]^{1/\alpha} - 1\right] + 1}{\beta\left[k_0\left[\frac{1}{k_0}\right]^{1/\alpha} - 1\right] + 1 - k_0} \tag{6.27}$$

The slope from B to R in total stress space, k_i^T, is given by

$$k_i^T = \frac{k_i + BA\,(1 - k_i)}{1 - B\,(1 - A)\,(1 - k_i)} \tag{6.28}$$

Analysis of the effects of placing and compacting successive lifts of backfill proceeds in an iterative, incremental fashion. The analysis is incremental to account for the placement and compaction of the backfill in lifts. The analysis is iterative in each incremental loading step because the magnitude of the change in pore pressure, which must be known before the change in effective vertical stress can be computed, cannot be evaluated until after the horizontal stress increment has been calculated. The iterative procedure for each incremental loading step is as follows:

1) The change in total vertical stress, $\Delta\sigma_v$, is calculated in one of two ways, depending on the type of load being applied:
   a) For a fill lift, the change in vertical stress is computed using Eqn 6.9.
   b) For the load from the compactor, the same two-step procedure described previously for the effective stress theory is applied, except that Δk_0^T from Eqn 6.25 is used in place of k_0 in Eqns 6.10(b) and 6.12.
2) A trial value of the change in apparent pore pressure, Δu, is assumed. Experience with these calculations has shown that if the trial value of Δu is computed using Eqn 6.16, with the value of $\Delta\sigma_h$ taken as one-half the value of the applied $\Delta\sigma_v$ from (1), then the iteration closes without difficulty.
3) The effective vertical stress increment, $\Delta\sigma'_v$, is computed from Eqn 6.24(b) and applied to the effective stress k_0 model. This

yields the effective horizontal stress increment, $\Delta\sigma'_h$, and the corresponding total horizontal stress increment, $\Delta\sigma_h = \Delta\sigma'_h + \Delta u$.

4) A new value of Δu is computed from Eqn 6.16 using the applied $\Delta\sigma_v$ and the value of $\Delta\sigma_h$ from (3).

5) The new value of Δu is compared with the previous value of Δu. Steps (3) through (5) are repeated until convergence occurs.

This procedure is incorporated in the program EPCOMPAC. To illustrate the method, the same roller compactor and soil analyzed previously in this chapter is analyzed again, but this time with the soil behaving as a moist soil with a total stress friction angle, ϕ, of 25 degrees and a total stress cohesion intercept, c, of 500 psf. The effective stress strength parameters of ϕ' = 35 degrees and c' = 0 are unchanged from the previous analyses. The value of the pore pressure coefficient A was taken to be 0.5, and the corresponding value of the coefficient B is 0.26, according to the relationship among A, B, ϕ, and ϕ' expressed by Eqn 6.21. The value of u_0 from Eqn 6.20 is -790 psf. The results of the analysis for the moist soil are shown in Figure 6.18. For reference, the corresponding effective stress analysis, which would be applicable for a dry sand with the same unit weight and effective stress strength properties, is also shown. According to the analyses, the compaction-induced horizontal stresses for the moist soil are larger than those for the dry soil. There are two reasons for the difference. One reason is that the total stress cohesion intercept for the moist soil permits development of higher compaction-induced lateral pressures near the fill surface. The other reason is that, for the moist soil,

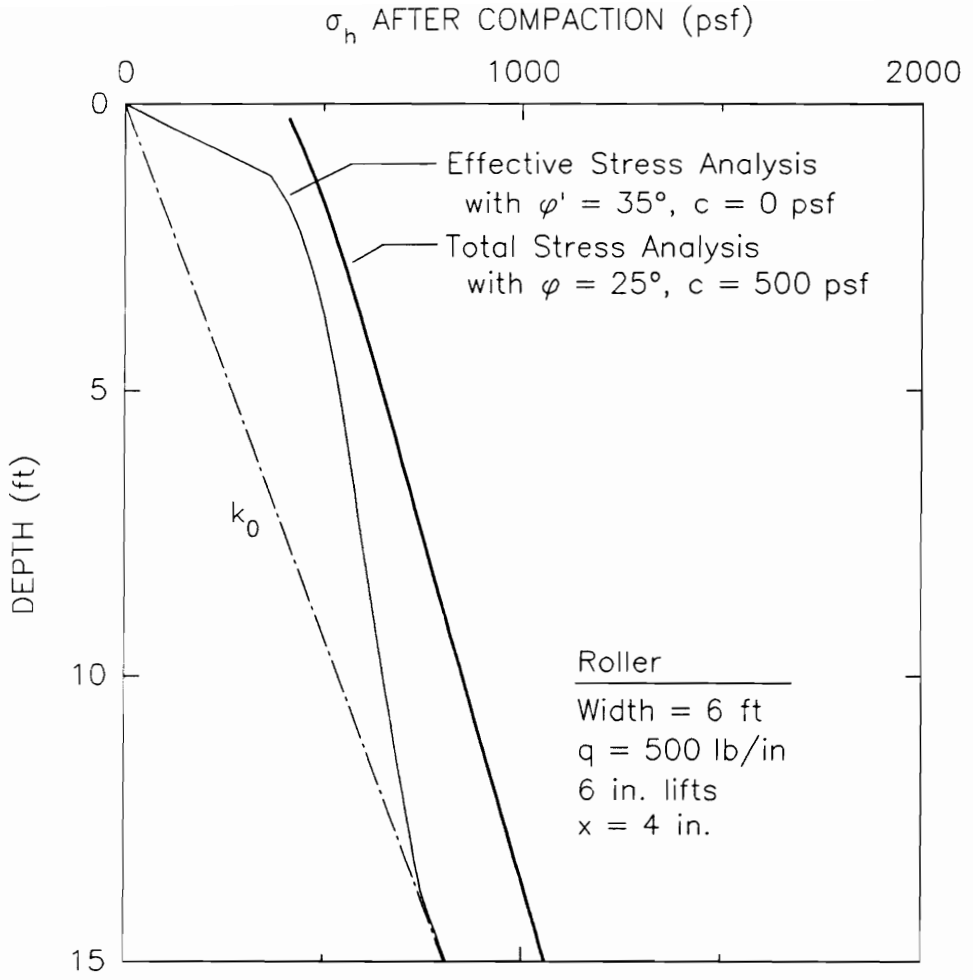

Figure 6.18: Compaction-Induced Earth Pressures for a Moist Soil Considering the Effect of Pore Pressures

the pore pressure increases in response to the applied vertical loads. The pore pressure acts equally in both vertical and horizontal directions, and this means that the changes in horizontal stress induced by vertical loads are greater for the moist soil than for the dry soil.

Both effective and total stress paths for the moist soil analysis are shown in Figure 6.19. Placement and compaction of the first lift follows the path A, B, C, D. Placement and compaction of the second lift follows the path from D to E, and then returns along the path shown, to a point very near D. The initial offset between the effective and total stress axes due to the initial apparent pore pressure, u_0, is shown by the relative positions of the point A in Figures 6.19(a) and (b). The loading path from A to B is steeper in the total stress plot than in the effective stress plot because of the increase in pore pressure that occurs during loading. The value of Δk_0^T is greater than the value of k_0 for the same reason. Removal of the compactor load is described by the unloading path from C to D. In the effective stress path plot, it is clear that the unloading path does not intersect the passive failure line. This situation exists because of the effective stresses induced by u_0. If, instead, the pore pressures were always zero, then point A would have been at the origin of the effective stress path plot, and the unloading path would have intersected the passive failure line. Thus, near the ground surface, the moist soil is able to sustain higher compaction-induced lateral earth pressures than the dry soil.

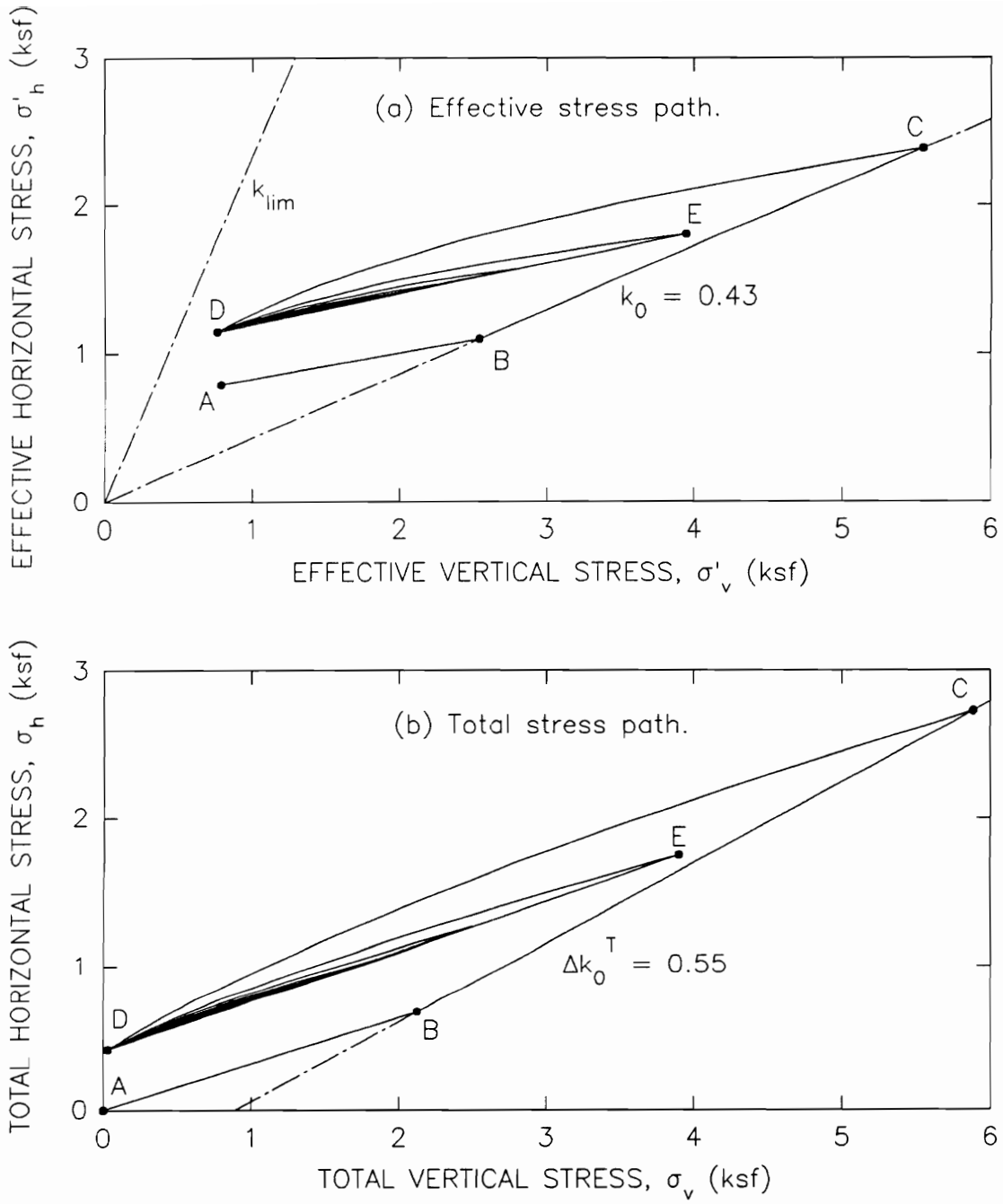

Figure 6.19: Total and Effective Stress Paths for Compaction of a Moist Soil

6.6 Summary

This chapter presents a revised effective stress k_0 model and an extension of the compaction-induced earth pressure theory to include moist soils that develop significant non-zero pore pressures.

The revisions to the effective stress k_0 model were motivated by an observation by Peck (1991) that the original compaction-induced earth pressure theory (Duncan and Seed, 1986) yields unrealistically high lateral earth pressures in some instances. The reason for the unrealistic result is that the 1986 theory incorporates a permanent memory of the maximum past loading event in the form of a high level reloading target point, located on the k_0 line, about which all subsequent stress path excursions pivot. The consequences of this memory characteristic are that the model is not truly hysteretic, and that relatively large horizontal stresses can develop from repeated small loading cycles as the stress path pivots about the high reloading target point.

In the revised effective stress k_0 model presented in this chapter, the basic framework and model parameter definitions from the 1986 theory were retained, but the model was made truly hysteretic. In the revised model, the stress history of a soil element consists of a set of nested stress path loops corresponding to repeated cycles of loading and partial unloading. When the applied stresses take the stress path outside the limits of some interior loops, either by loading or unloading, the exceeded interior loops are removed from the model memory. When the unloading path travels down the passive failure line,

the maximum past loading point is reset to a point from which a virgin unloading path would just intersect the passive failure line at the current unloading point.

The revised effective stress k_0 model was incorporated in compaction-induced earth pressure theory using the procedures of Duncan and Seed (1986) to calculate the vertical stress increments that drive the k_0 model. A computer program, EPCOMPAC, is used to make the calculations. An example problem demonstrated that the revised theory is not subject to the pivoting action which occurs in the 1986 theory. As a consequence, the unrealistically high compaction-induced pressures from the 1986 theory that were noted by Peck are not developed in the revised model.

The compaction-induced earth pressure theory was extended to include moist soils. The extension was made by expressing changes in apparent pore water pressure using Skempton's A and B parameters and applying the revised effective stress theory. The extension for moist soils is included in the program EPCOMPAC. An example problem analyzed by EPCOMPAC illustrates the effect of pore pressures on compaction-induced earth pressures. For the conditions of the example problem, the pore pressure effects result in higher compaction-induced lateral earth pressures than in the same problem without pore pressure effects included. A limitation of the approach taken is that the parameters A and B were approximated as constants.

CHAPTER 7 - MEASURED AND CALCULATED COMPACTION-INDUCED LATERAL EARTH PRESSURES

7.1 Introduction

The results of tests to measure compaction-induced earth pressures in the Virginia Tech instrumented retaining wall facility, and in the British Transportation and Road Research Laboratory facility, are discussed in this chapter. The effects of backfill type, water content, compactor force, and wall lubrication are examined, and the measured earth pressures are compared with values calculated using the theories discussed in the previous chapter.

Damage to Eisenhower and Snell Locks, which resulted from high compaction-induced lateral earth pressures, is also discussed. Earth pressures measured in the field are compared to values calculated using the theories discussed previously.

7.2 Test Wall Data

As discussed in Chapter 4, it is difficult to obtain reliable measurements of earth pressures on walls from contact pressure cell readings alone. More reliable measurements are obtained when load cells and pressure cells are used together. When load cells are used to support a wall panel, they provide a means of determining the magnitude and location of the resultant earth forces on the panel. These can be used to check or adjust the earth pressures measured using earth pressure cells mounted on the backfill side of the panel. Sehn and Duncan (1990) reviewed lateral earth pressure measurements reported in

the literature and found that, prior to development of the Virginia Tech instrumented retaining wall, the test wall used by Carder et al. (1977) and Carder et al. (1980) appeared to be the best facility available because it used both load cells and pressure cells. The Virginia Tech instrumented retaining wall also uses both load cells and pressure cells. Consequently, it yields verifiably reliable earth pressure measurements. Both the earth pressure measurements of Carder and the measurements made as part of this research are presented in this chapter.

7.2.1 Virginia Tech Instrumented Retaining Wall Tests

The measured lateral earth pressure distributions for instrumented retaining wall tests EP 6 through EP 16 are presented in Figures 7.1A, 7.1B, and 7.1C. In these tests, the backfill was spread by hand so that the wheel load from the Bobcat would not influence lateral earth pressures. The procedural details for these tests have been summarized earlier in Table 3.1. For all these tests, the backfill was placed in 6-inch thick compacted lifts. Notes on the figures indicate the material type (Yatesville silty sand or Light Castle sand), the water content, the compacted dry density, the compactor type, and the use of lubricated walls in the test facility.

In tests EP 6 through EP 12, the wall was backfilled with Yatesville silty sand that was compacted with the Wacker BPU2440A vibrating plate compactor. In the EP 6 through EP 12 test series, the backfill water content and wall lubrication boundary conditions were

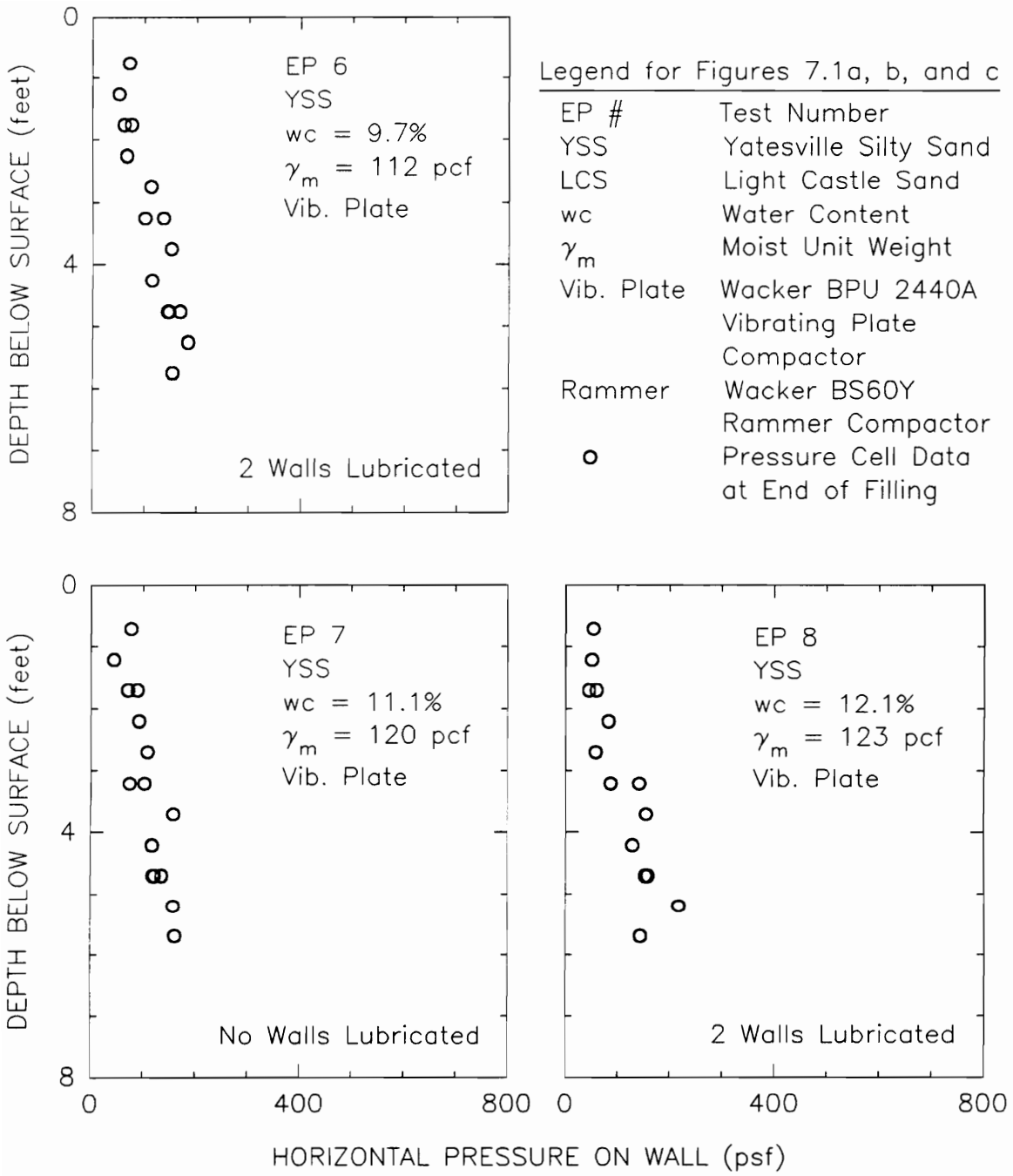

Figure 7.1A: Lateral Pressure Measurements in the Instrumented Retaining Wall Tests

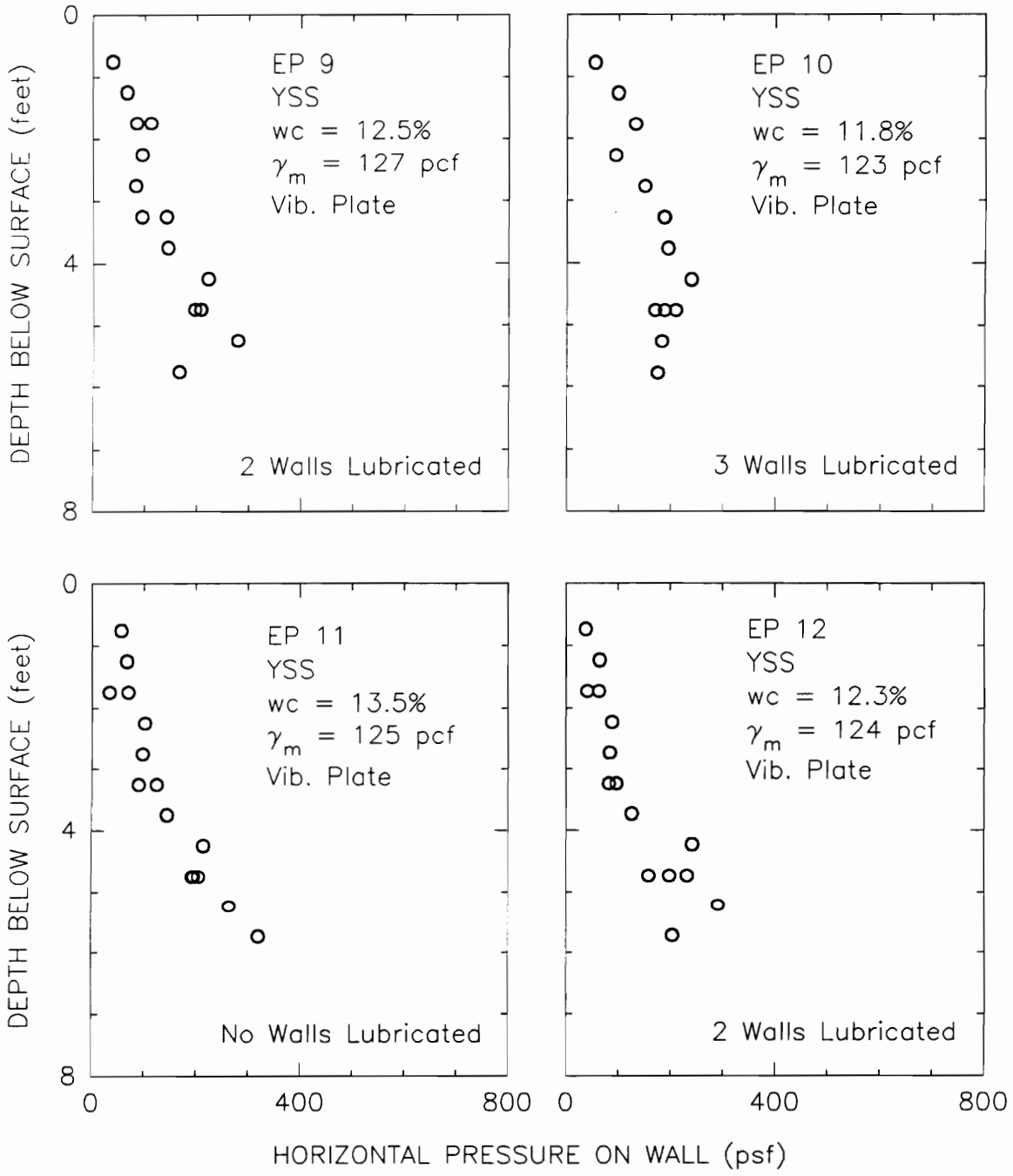

Figure 7.1B: Lateral Pressure Measurements in the Instrumented Retaining Wall Tests

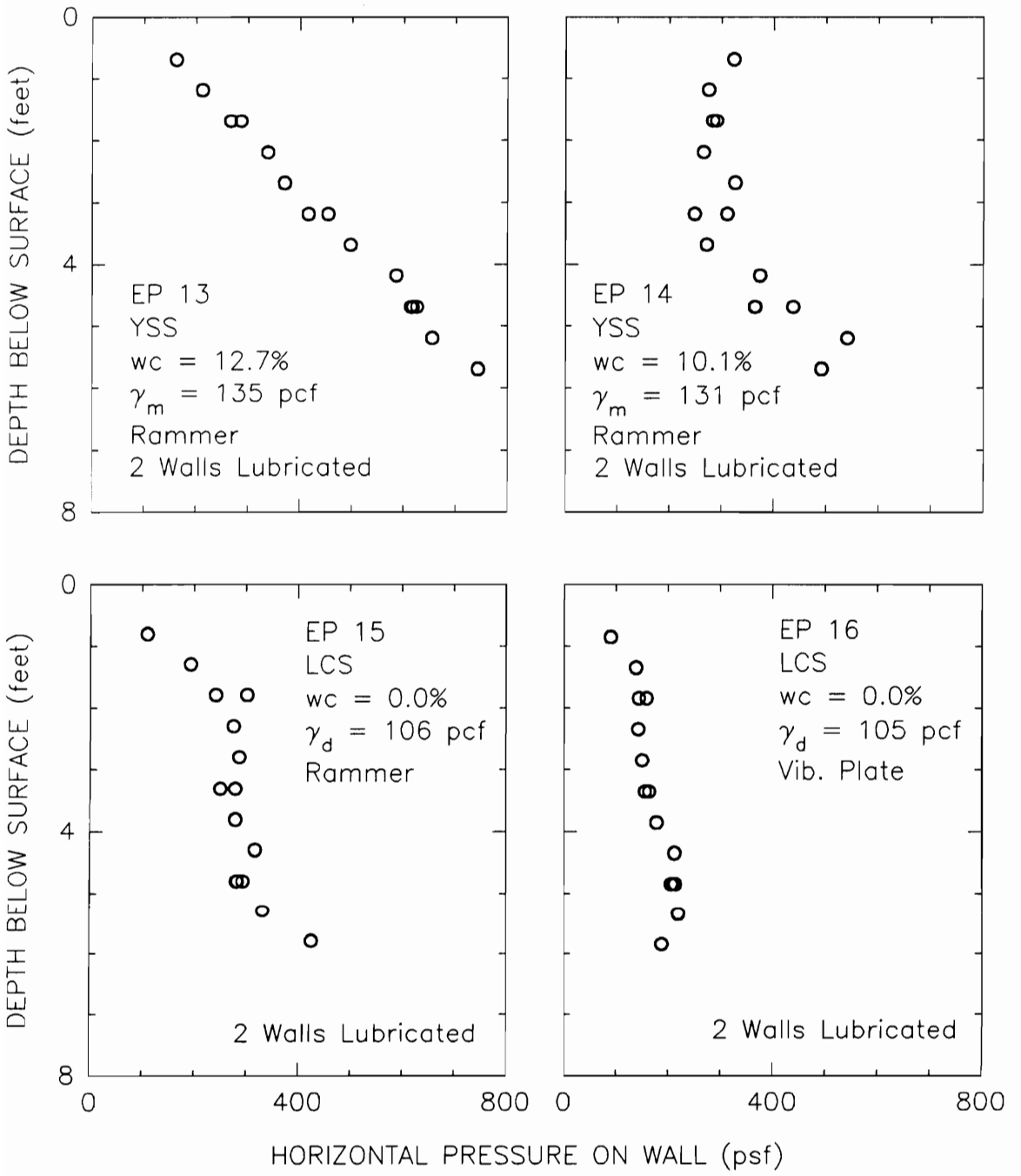

Figure 7.1C: Lateral Pressure Measurements in the Instrumented Retaining Wall Tests

varied. The measurements indicate that horizontal pressures increase slightly as the compaction water content increases. The results of these tests are discussed in more detail in Section 7.3.

In tests EP 13 and EP 14, the wall was backfilled with Yatesville silty sand that was compacted with the Wacker BS60Y rammer compactor. The measured pressures in Figures 7.1A, 7.1B, and 7.1C show that the lateral pressures for backfill compacted with the rammer compactor are much higher than those for backfill compacted with the vibrating plate. This result is reasonable since, as discussed in Chapter 5, the dynamic contact forces for the rammer compactor are much higher than those for the vibrating plate compactor.

In tests EP 15 and EP 16, the wall was backfilled with Light Castle sand. The backfill for test EP 15 was compacted with the Wacker BS60Y rammer compactor, and the backfill for test EP 16 was compacted with the Wacker BPU2440A vibrating plate compactor. Again, the lateral pressures for backfill compacted with the rammer compactor are higher than for backfill compacted with the vibrating plate. The comparison between the results for tests EP 15 and EP 16 is especially interesting since the unit weights of the compacted backfill for these two tests are almost identical. The difference in lateral pressures cannot be attributed to a difference in unit weights.

Compactor contact force measurements were made during the backfilling operation for tests EP 12 through EP 16. The earth pressure measurements from these tests, together with Carder's measurements, are used for the comparisons with theory discussed in Sections 7.4 and 7.5.

7.2.2 TRRL Model Retaining Wall Tests

Carder et al. (1977) described a model retaining wall facility built at the Transport and Road Research Laboratory (TRRL) in Crowthorne, England. The facility consisted of a massive concrete trough with a movable metal wall installed inside the trough, near one of the trough walls. Backfill was placed between the metal wall and the opposite concrete wall of the trough. The trough was 3.0 meters deep, the metal wall was 2.0 meters high, and the distance between the metal wall and the opposite concrete wall was 5.2 meters.

The metal wall was supported laterally by load cells. Both the metal wall and the far concrete wall were instrumented with contact pressure cells. The system was designed so that both the metal wall and the concrete wall would be very rigid. Nevertheless, the concrete wall was considered to be the more rigid wall, and slightly higher lateral pressures were measured on the concrete wall. The load cells supporting the metal wall were used to perform in-situ calibrations of the pressure cells in the metal wall. The calibration factors developed for the pressure cells in the metal wall were also applied to the earth pressures measured using the pressure cells in the concrete wall.

In the tests described by Carder et al. (1977), moist sand was compacted in the model wall facility in 6-inch lifts using a Bomag BW90S walk-behind vibrating roller. The sand backfill was a washed, uniform, medium sand. The compaction water content was 12.5 percent and the compacted moist unit weight was 125 pcf. The minimum distance from the edge of the compactor to the wall was 6 inches. Three pressure cells

were located at each of six instrumentation elevations on the concrete wall. The readings from these cells at the end of backfilling are shown in Figure 7.2(a).

In a second series of tests, described by Carder et al. (1980), silty clay was compacted in the model wall facility in 5-inch lifts using a static, smooth steel-wheeled roller. The liquid and plastic limits of the silty clay backfill were reported to be 42.5 and 17.0 percent, respectively. The compaction water content was 18.5 percent and the compacted moist unit weight was 125 pcf. The static roller used for compaction was a three-wheeled, self-propelled roller. The wheel approaching closest to the wall had a wheel load of 2,475 pounds and was 16 inches wide. The distance from the edge of the wheel to the wall was 4 inches. The pressures on the concrete wall measured in these tests are shown in Figure 7.2(b). The average of readings from three pressure cells located at each of six instrumentation elevations are shown in Figure 7.2(b).

There is some scatter in the data in Figure 7.2, but the average pressure is slightly higher for the silty clay than for the sand.

The pressure measurements shown in Figure 7.2 exhibit more scatter than the pressure measurements made with the Virginia Tech instrumented retaining wall. The reason for the difference is not known.

7.3 Boundary Conditions in the Instrumented Retaining Wall Tests

Because both the TRRL and the Virginia Tech test facilities are of limited extend, it is recognized that the boundary conditions at the

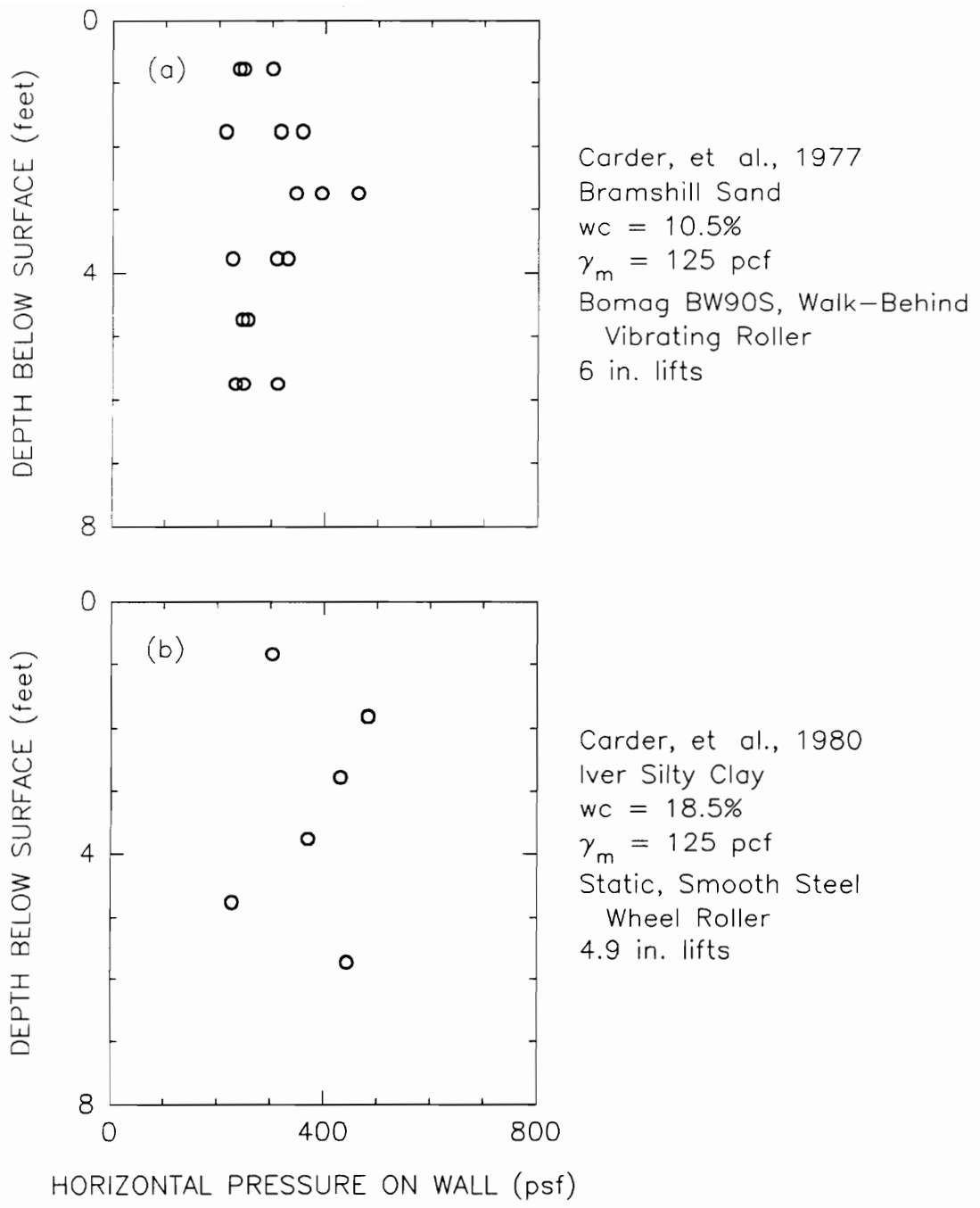

Figure 7.2: Lateral Pressure Measurements in the TRRL Tests

walls may influence the test results. As the backfill compresses due to self-weight, shear stresses are mobilized at the contact between the backfill and the vertical walls that contain the backfill.

If shear stresses in the Virginia Tech test facility could be eliminated on the end wall and the wall opposite the instrumented wall, then the facility would model the 2-D case of an infinitely long retaining wall with an infinitely wide backfill. If shear stresses were eliminated on the instrumented wall, the end wall, and the far wall, then the facility would model a 1-D case. Both experimental and analytic studies were performed to assess the significance of changes in the boundary conditions on the measured pressures and forces.

7.3.1 Experimental Study of Boundary Conditions

To study the influence of boundary conditions on the test results, some of the walls were lubricated in some of the instrumented retaining wall tests, as listed in Table 3.1. To lubricate the walls, a sheet of 6-mil polyethylene was taped in placed on the wall to be lubricated. A thin layer of wheel bearing grease was applied to the polyethylene sheet, which was then covered with a second polyethylene sheet. This method was used for the tests with lubricated walls prior to test EP 12. For test EP 12 and subsequent tests, the end wall and the far wall were always lubricated, and the first sheet of polyethylene was replaced by a sheet of formica glued to the concrete, to facilitated the lubricating procedure.

Tests EP 6 through EP 12 were performed to study the influence of both changes in water content of the Yatesville silty sand and changes in boundary conditions of the test facility on the forces measured by the instrumented wall panels. The results are shown in Figure 7.3. The forces were measured at the end of backfilling on panels 2 and 3, which are the center two panels of the instrumented wall. The results show that both horizontal and vertical forces tend to increase with increasing backfill water content. The measurements for the test in which three walls were lubricated (EP 10) show that the lubricating procedure reduced the vertical shear force to a value near zero.

The data in Figure 7.3 also shows that there is very little difference between the forces on the instrumented wall for tests in which no walls were lubricated and tests in which the end wall and far wall were lubricated. This indicates that the end wall and far wall are far enough from the center two panels of the instrumented wall that the existence of shear forces at these locations does not significantly influence the measurements. On the other hand, the measured horizontal force on the instrumented wall for the test in which all three walls were lubricated is about 26 percent higher than the force on the trend line at the same water content for the tests with zero and two walls lubricated.

7.3.2 Finite Element Study of Boundary Conditions

An analytic study of the effect of the boundary conditions on the forces applied by the backfill to the instrumented wall was made using a

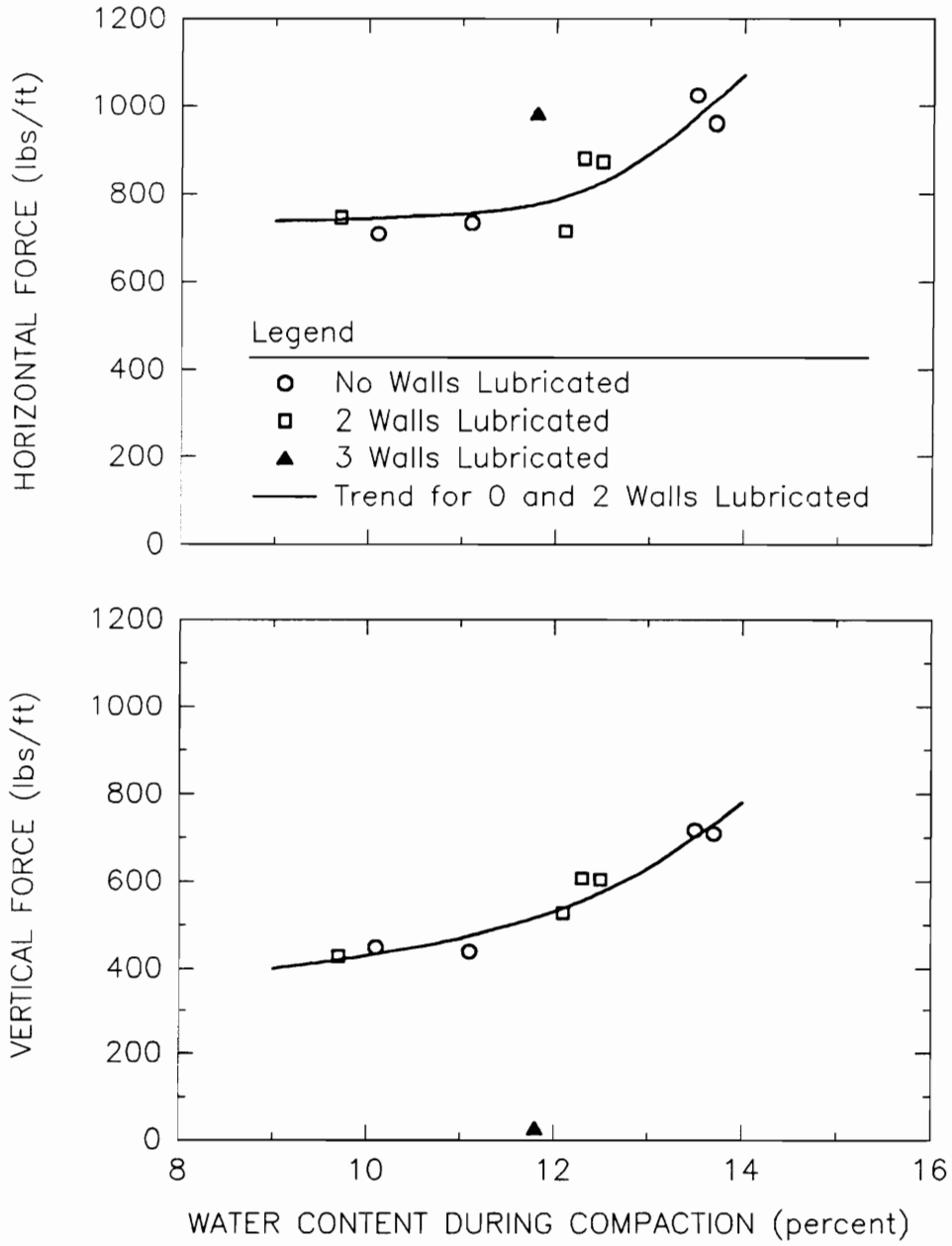

Figure 7.3: Influence of Water Content and Boundary Conditions on the Instrumented Retaining Wall Test Results

2-D, plane strain finite element representation of the backfill and wall.

The analysis was performed to model the average conditions of instrumented retaining wall tests EP 8, EP 9, and EP 12. As indicated in Table 3.1, these tests have the following characteristics in common: Yatesville silty sand was used as backfill, the water content during compaction was about 12.3 percent, the backfill was compacted in 6-inch lifts with the vibrating plate compactor, the compacted dry unit weight was about 111 pcf, and the end wall and the far wall were both lubricated.

The properties used to model the backfill soil were determined from the laboratory tests described in Appendix A. The unconsolidated-undrained triaxial compression test results indicate that the stress-strain relationship for the compacted Yatesville silty sand is approximately linear for strains up to 6 to 8 percent. This suggests that, for the case of backfilling without wall movement, a simple elastic analysis could be used. Interpolating from the results in Table A.3, the average value of Young's modulus for the density and water content conditions of tests EP 8, EP 9, and EP 12 is about 350 psi.

The value of Poisson's ratio, ν, was determined from

$$\nu = \frac{k_i^T}{1 + k_i^T} \tag{7.1}$$

where the total stress initial reloading slope, k_i^T, is determined from Eqn 6.28, with the value of the parameter A assumed to be one half. In

order to evaluate the other parameters in Eqn 6.28, it is necessary to know the value of the effective stress friction angle, and this was determined from Figure A.9 to be 35 degrees. The value of Poisson's ratio determined in this manner was 0.21.

Bi-linear interface elements (Goodman et al. 1968) were used to model the contact between the backfill and concrete surfaces. The backfill-concrete interface properties were evaluated from the interface shear test results described in Appendix A. For analyses in which lubricated walls were to be modelled, the interface shear stiffnesses of the appropriate elements were set to a very low value.

The mesh used for the analyses is shown in Figure 7.4. The instrumented wall is shown on the right side. The mesh in the backfill area is refined near the boundaries, and interface elements are provided at all contacts between backfill and concrete. The concrete floor and far wall were modelled as non-deflecting. The instrumented wall in the real facility is supported by load cells, and these were modelled as linear elastic springs in the finite element analyses. The spring stiffnesses were calculated using the measured loads and deflections of the instrumented wall during the tests. In the finite element analyses, the lateral and vertical forces applied by the backfill to the instrumented wall are equal to the forces in the springs.

The analyses were made using the program SOILSTRUCT (Clough and Duncan, 1969, and Filz et al. 1990). The analyses proceeded in a series of loading steps, with a single step being used to model each backfill lift. The loads from backfill placement during each step were

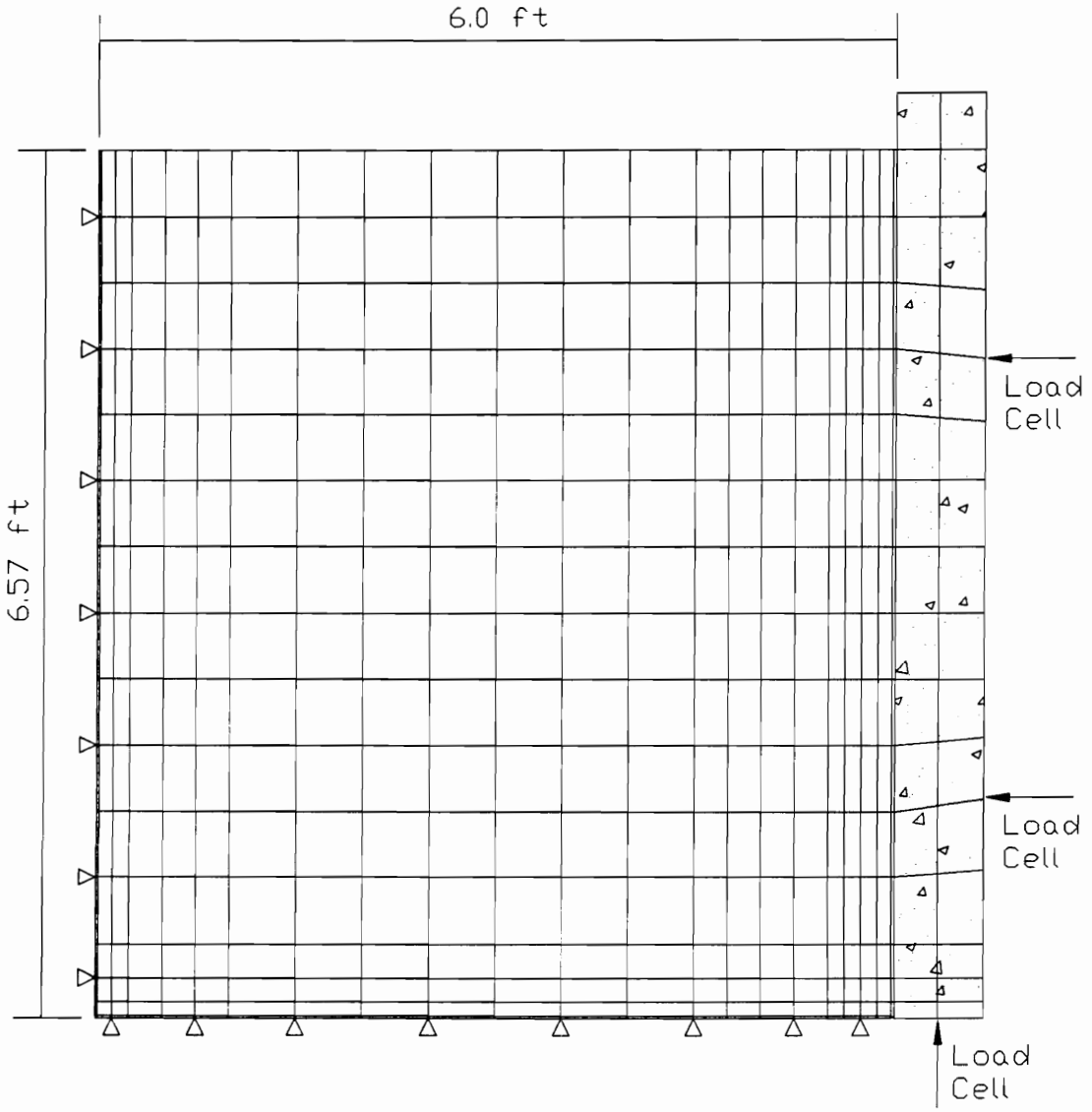

Figure 7.4: Finite Element Mesh for Analytic Boundary Condition Study

divided into eight substeps. These procedures effectively prevented overshoot in the bi-linear interface elements.

Because the vibrating plate compactor was used to compact the backfill in tests EP 8, EP 9, and EP 12, compaction-induced lateral earth pressures are not a very important factor in the results. Nevertheless, a simple approach was taken to include consideration of the compaction-induced pressures in the analyses. The program EPCOMPAC, described in Chapter 6, was used to compute the compaction-induced lateral pressures for the average conditions of tests EP 8, EP 9, and EP 12. The computed lateral pressures adjacent to the wall were 1.22 times the overburden pressure at the center of the first lift. The compaction-induced earth pressures for deeper lifts were negligible. In the finite element analyses, the effect of compaction-induced pressures was modelled by using a k_0 value of 1.22 to compute the initial horizontal stress in each lift of backfill as it was being placed. The corresponding lateral force (i.e., the product 1.22 times the overburden stress at the center of the lift times the lift thickness) was applied to the instrumented wall as part of the load step. The increase in horizontal stress due to placement of overlying lifts occurs due to the Poisson effect, and this was calculated in the usual way as part of the finite element method.

To study the influence of changes in boundary conditions, three finite element analyses were performed. First, an analysis was performed using a lubricated far wall condition. This matches the boundary conditions for tests EP 8, EP 9, and EP 12. Thus, the results

from the first analysis could be compared with the experimental data to determine if the analysis procedures and material properties were reasonable. Next, analyses were performed with a) both the far wall and the instrumented wall lubricated and b) with no walls lubricated. The results of these analyses could be compared on a percentage basis with the results of the first analysis to see if the finite element results show the same trends as the experimental data in Figure 7.3.

The computed horizontal and vertical forces on the instrumented wall from the first analysis are shown as a function of backfill height in Figure 7.5. The experimental data from tests EP 8, EP 9, and EP 12 are also shown on the figure. It can be seen that the analysis results are in good agreement with the measured forces. There is some scatter in the measured values, and the forces from the finite element analyses seem to be in best agreement with the results from test EP 8. The overall closeness of agreement suggests that the methods and material properties used in the analyses provide a reasonable model of the actual conditions. It should be noted that the material properties were obtained from laboratory tests and the theory developed in Chapter 6, not from back-analyses.

Using the results of the first analysis as a base, the percentage change in the horizontal and vertical forces due to changes in boundary conditions can be calculated using the other two finite element analyses. The results are listed in Table 7.1. A similar evaluation using the experiments can be made from the data in Figure 7.3, and these results are also listed in Table 7.1.

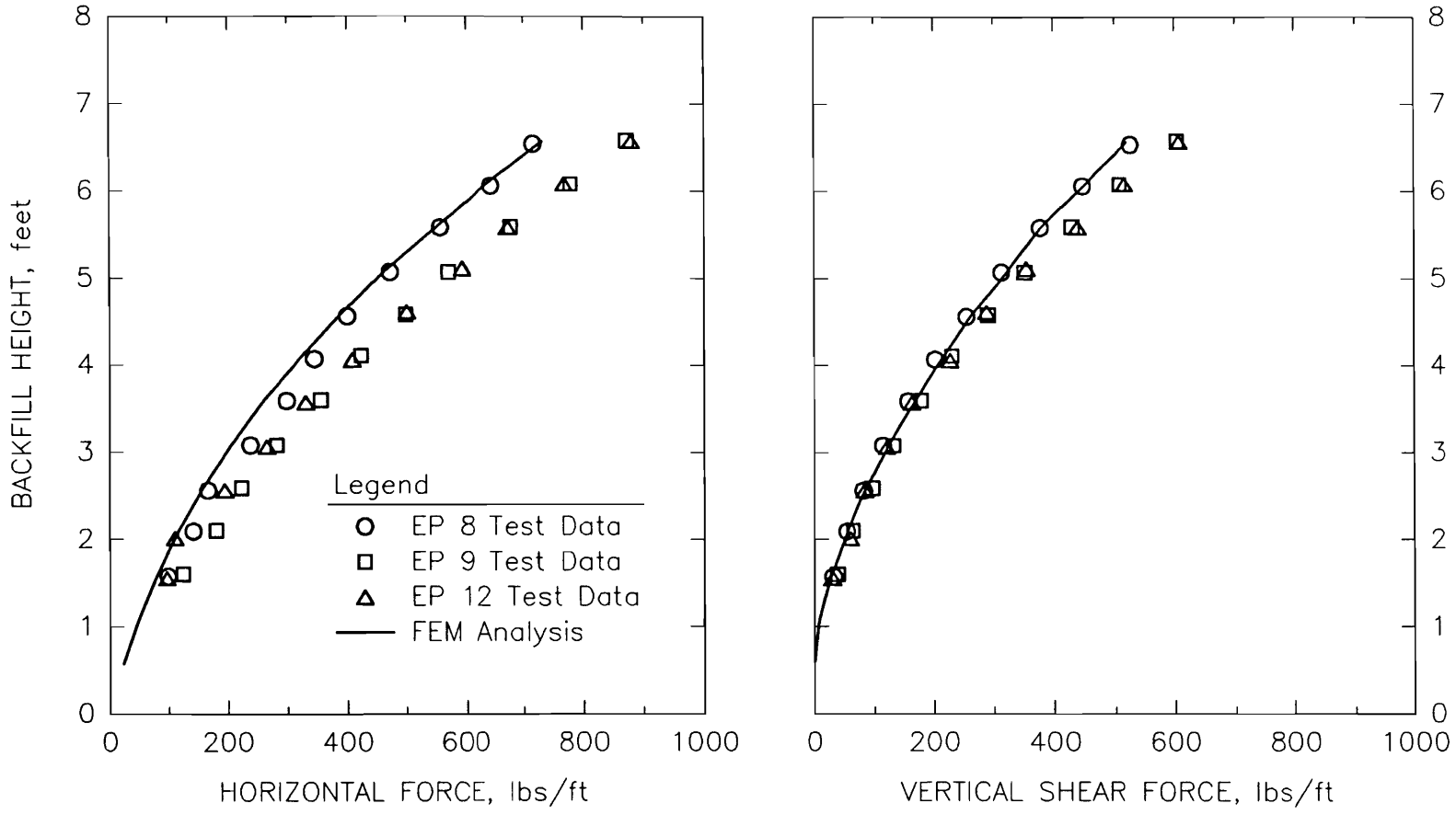

Figure 7.5: Comparison Between Finite Element Analysis Results and Force Measurements from Instrumented Retaining Wall Tests EP 8, EP 9, and EP 12

TABLE 7.1: Effect of Wall Lubrication on Measured Forces

Lubricated Walls	Horizontal Force (percent)[1]		Vertical Shear Force (percent)[1]	
	Experiments[2]	FEA[3]	Experiments[2]	FEA[3]
None	100	99	100	98
Far Wall[4]	100	100	100	100
Instrumented and Far Walls[4]	126	115	5	0

Notes: 1) In each instance, the forces are expressed as a percentage of the force for the corresponding case of the far wall being lubricated.

2) The experimental forces are obtained from the data in Figure 7.3, evaluated at a water content of 11.8 percent. The force for the cases of no walls and the far wall being lubricated are obtained from the trend line shown on the figure.

3) FEA = Finite Element Analyses.

4) For the experimental results, the end wall is also lubricated in these cases. For the finite element calculations, the representation is 2-D and there is no end wall.

Both the analyses and the experiments show that there is very little change in the forces on the instrumented wall due to lubrication of the far wall. This indicates that the results of tests performed without far wall lubrication can be interpreted without consideration of the shear forces that develop on the far wall. On the other hand, when the instrumented wall, the far wall, and the end wall are all lubricated, the horizontal forces increase, as determined by both the analyses and the experiments. The finite element results showed an increase of 15 percent, and the experiments showed an increase of 26 percent. The experimental increase of 26 percent is based on just one test, EP 10. Since some scatter is expected in experimental data, and since the water content of test EP 10 is near an abrupt change in slope of the horizontal force curve in Figure 7.3, the experimental values may not be accurate enough to determine the effect of wall lubrication with high precision. An increase of 15 percent, as determined from the finite element analyses, may be a reasonable estimate of the effect of instrumented wall lubrication on horizontal forces. This amount of change in earth pressures due to wall lubrication probably only applies to conditions of very light compaction, like that achieved with the vibrating plate compactor. For compactors with larger contact forces and higher associated compaction-induced lateral pressures, a smaller percentage increase in horizontal forces due to instrumented wall lubrication would be expected.

7.4 Comparison Between Measurements and Theory for Sands

Sand backfill was used for instrumented retaining wall tests EP 15 and EP 16 and for the model wall test of Carder et al. (1977). The measurements from these three tests comprise the best data available for evaluating compaction-induced earth pressure theories for sands.

The backfill placement and compaction conditions for these tests are summarized in Table 7.2. The Light Castle sand used in tests EP 15 and EP 16 was compacted dry. The Bramshill sand used in Carder's test was compacted moist. Since the Bramshill sand is a clean, medium-grained sand, the apparent negative pore pressures in the moist compacted sand probably do not significantly influence lateral earth pressures. Consequently, all three tests can be analyzed using the effective stress theory developed in Chapter 6 without taking pore pressures into account.

The dynamic compactor forces listed in Table 7.2 for tests EP 15 and EP 16 were obtained from the force measurements described in Chapter 5. The total compactor force listed in Table 7.2 for the walk-behind vibratory roller compactor used by Carder, et. al. (1977) is the sum of the compactor weight and the dynamic force, both as provided by the compactor manufacturer. The ratio between the total vibratory roller compactor force and the compactor weight is 3.2. This is in the range of force ratios recommended by Seed and Duncan (1983) for estimating the total contact force for vibratory rollers. Consequently, the force listed for Carder's compactor is probably a reasonable estimate. How-

TABLE 7.2: Data for Calculating Compaction Induced Earth Pressures - Sandy Soil Test Cases

	EP 15(1)	EP 16(1)	Carder, et al., 1977
Soil Type	Light Castle sand	Light Castle sand	Bramshill sand
Soil Moist Unit Weight	106 pcf	105 pcf	125 pcf
Compaction Water Content	0.0%	0.0%	10.5%
Effective Stress Friction Angle	42°	42°	38.7°
Effective Stress Cohesion Intercept	0	0	0
Compactor Type	Wacker BS60Y, Rammer	Wacker BPU2440A, Vibrating Plate	Bomag BW90S, Walk-Behind Vibratory Roller
Compactor Width	10.6 in	15 in	36 in
Compactor Length	7 in	15 in	0 in
Distance from Edge of Compactor to Wall	1 in	1 in	6 in
Total Compactor Force	4780 lbs(2)	1310 lbs(2)	4530 lbs(3)
Lift Thickness	6 in	6 in	6 in

Notes: 1) Soil property values for these instrumented retaining wall tests are obtained from the laboratory test results described in Appendix A.

2) This is the total dynamic contact force from the measurements described in Chapter 5.

3) This is the sum of the static plus the dynamic load on a single wheel, both as reported by the compactor manufacturer.

ever, it is only an estimate, and should not be considered as reliable as the measured contact forces for tests EP 15 and EP 16.

The compaction-induced earth pressure theory described in Chapter 6 was used to calculate lateral pressures for tests EP 15 and EP 16 using the parameter values in Table 7.2. The calculated pressures are shown on Figure 7.6 along with the measured pressures. Two calculated pressure distributions are shown for each test: one in which the slope of the passive failure line, k_{lim}, in the compaction-induced earth pressure theory equals the Rankine passive pressure coefficient, k_p, and another in which the slope of the passive failure line equals the reciprocal of the at-rest pressure coefficient, $1/k_0$. Carder et al. (1977) suggested that k_{lim} should be equal to $1/k_0$ for unloading, and, when this value is used, the calculated lateral pressures from the compaction-induced earth pressure theory are in good agreement with the measured pressures.

7.5 Comparison Between Measurements and Theory for Silty and Clayey Soils

Yatesville silty sand was used as backfill for most of the instrumented retaining wall tests. Compactor force measurements were made during compaction of the Yatesville silty sand in tests EP 12 through EP 14. Since the compactor force is known for these three tests, they were selected for the comparisons between measurements and theory described in this section. In addition, the results from the test of Carder et al. (1980) are analyzed. Carder's 1980 test used Iver silty clay backfill compacted with a static roller. The

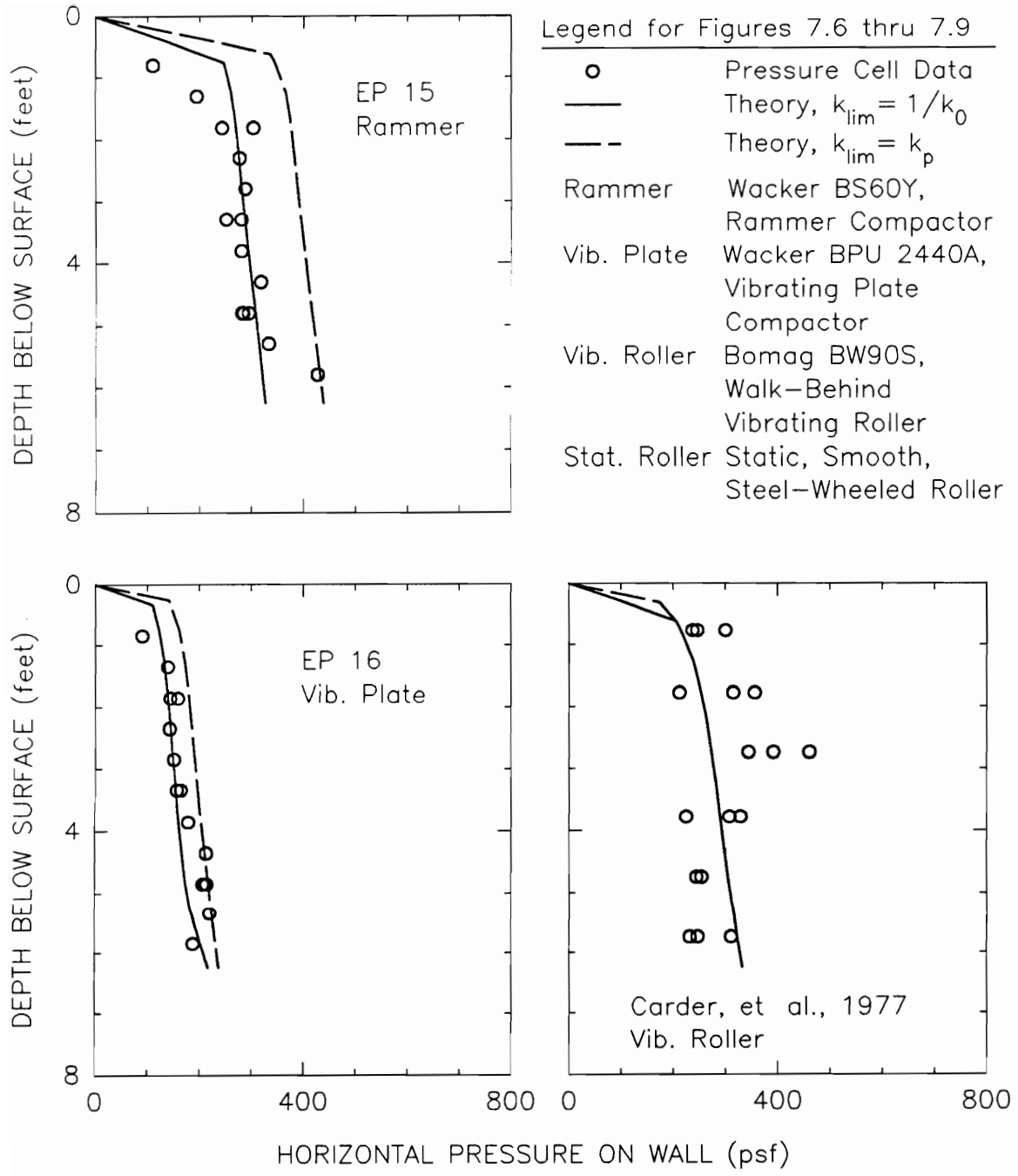

Figure 7.6: Comparison Between Compaction-Induced Earth Pressure Measurements and Theory for Sands

measurements from these four tests comprise the best data available for evaluating compaction-induced earth pressure theories for silty and clayey soils.

The backfill placement and compaction conditions for these four tests are summarized in Table 7.3. The backfill was in a moist condition for all four tests. The final degree of saturation after compaction was about 65 percent for tests EP 12 and EP 14 and about 85 percent for test EP 13 and Carder's test. The Yatesville silty sand contains about 47 percent non-plastic fines, and the Iver silty clay contains about 80 percent plastic fines. Both materials are moisture sensitive, and significant positive or negative pore water pressures may be expected under the conditions involved in these tests.

One way to assess the impact of the pore pressures on compaction-induced lateral earth pressures is to analyze these four tests using the compaction-induced earth pressure theory without accounting for pore water pressures, i.e., $u_0 = 0$ and $B = 0$, and to compare the calculated pressures with the measured pressures. The results of such a comparison are shown in Figure 7.7. It can be seen that the pressures calculated in this way are in fair agreement with the measured pressures for tests EP 12 and EP 14, in which the degree of saturation of the backfill was about 65 percent. The agreement is not as good for test EP 13 and Carder's test, in which the degree of saturation of the backfill was about 85 percent. This suggests that relatively dry backfill behaves as if the pore water pressures are not very important with regard to

TABLE 7.3: Data for Calculating Compaction Induced Earth Pressures - Silty and Clayey Soil Test Cases

	EP 12(1)	EP 13(1)	EP 14(1)	Carder, et al., 1980
Soil Type	Yatesville silty sand	Yatesville silty sand	Yatesville silty sand	Iver silty clay
Soil Moist Unit Weight	124 pcf	135 pcf	131 pcf	125 pcf
Compaction Water Content	12.3%	12.7%	10.1%	18.5%
Degree of Saturation	65%	87%	67%	85%
Effective Stress Friction Angle	34.5°	37.3°	37.0°	37°
Effective Stress Cohesion Intercept	0	0	0	0
Total Stress Friction Angle	27.7°	28.4°	32.9°	13°
Total Stress Cohesion Intercept	150 psf	315 psf	390 psf	520 psf
Compactor Type	Wacker BPU2440A, Vibrating Plate	Wacker BS60Y, Rammer	Wacker BS60Y, Rammer	Static Roller
Compactor Width	15 in	10.6 in	10.6 in	16 in
Compactor Length	15 in	7 in	7 in	0 in
Distance from Edge of Compactor to Wall	1 in	1 in	1 in	4 in
Total Compactor Force	1210 lbs(2)	5040 lbs(2)	7330 lbs(2)	2475 lbs(3)
Lift Thickness	6 in	6 in	6 in	5 in

Notes: 1) Soil property values for these instrumented retaining wall tests are obtained from the laboratory test results described in Appendix A.

2) This is the total dynamic contact force from the measurements described in Chapter 5.

3) This is the static load on the wheel that operated closest to the wall.

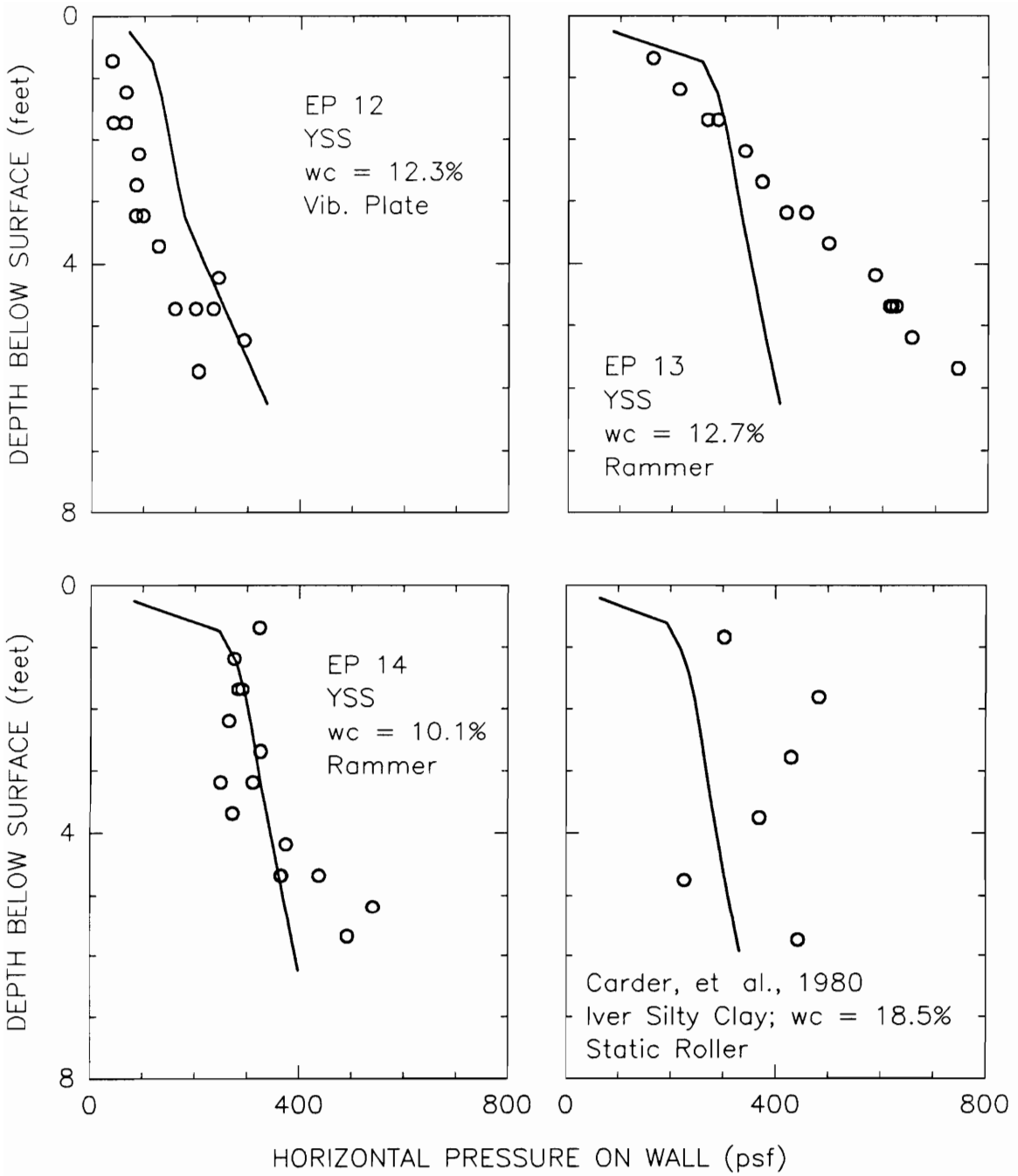

Figure 7.7: Comparison Between Compaction-Induced Earth Pressure Measurements and Theory without Pore Pressure Effects for Silty and Clayey Soils

compaction-induced lateral stresses; however, more tests on other materials would be needed to confirm this.

For the wetter materials, pressures calculated using the compaction-induced earth pressure theory without pore pressures tend to underestimate the measured pressures. This is particularly noticeable for the deepest portions of the fill in test EP 13. Thus, the comparisons shown in Figure 7.7 indicate that, at least for relatively wet materials, pore pressures appear to influence compaction-induced lateral earth pressures.

In Chapter 6, the compaction-induced earth pressure theory was extended to include materials with significant pore water pressures. It is known that the pore pressure parameters A and B are not constant, but instead depend on the state of stress and stress history of a soil, as well as its density and water content. Nevertheless, the extended theory was based on the simplifying assumption that these parameters are constant for all stress levels and stress paths. Using this assumption, Eqns 6.20 and 6.21 can be used to express u_0 and B in terms of the total and effective stress strength parameters, ϕ, c, ϕ', and c′, and the pore pressure parameter A.

As discussed in Chapter 6, if the value of the pore pressure parameter A is one-half, then the contributions of changes in major and minor principal stress to changes in pore pressure are the same. Without any test data to determine the value of A, it was taken to be one-half for the calculations that follow.

Values of u_0 and B were computed using Eqns 6.20 and 6.21, together with the strength parameter values listed in Table 7.3, and the assumption that A equals one-half. The total stress strength parameter values in Table 7.3 are from unconsolidated-undrained compression tests performed at confining pressures of 0, 2, and 4 psi. These confining pressures are representative of those that existed in the backfill after compaction, but, for backfill compacted with the rammer compactor, higher pressures existed during compaction.

Values of u_0 and B determined in this way were used in the extended compaction-induced earth pressure theory to calculate the lateral pressures shown in Figure 7.8. Except for test EP 12, it can be seen that the agreement between measured and calculated pressures is not good. These results suggest that including non-linearity of pore pressure response is important and should not be neglected for calculating compaction-induced earth pressures.

Two possibilities present themselves for accommodating non-linearity of pore pressure response. One is to develop a non-linear theory and a corresponding method to measure parameters that would represent the non-linear response. The other possibility is to approximate the non-linear response as being linear over limited stress ranges.

To determine whether there is any chance of success for the second possibility, an attempt was made to find values of u_0 and B that, when used with the extended compaction-induced earth pressure theory, would yield pressures in good agreement with the measure pressures for the

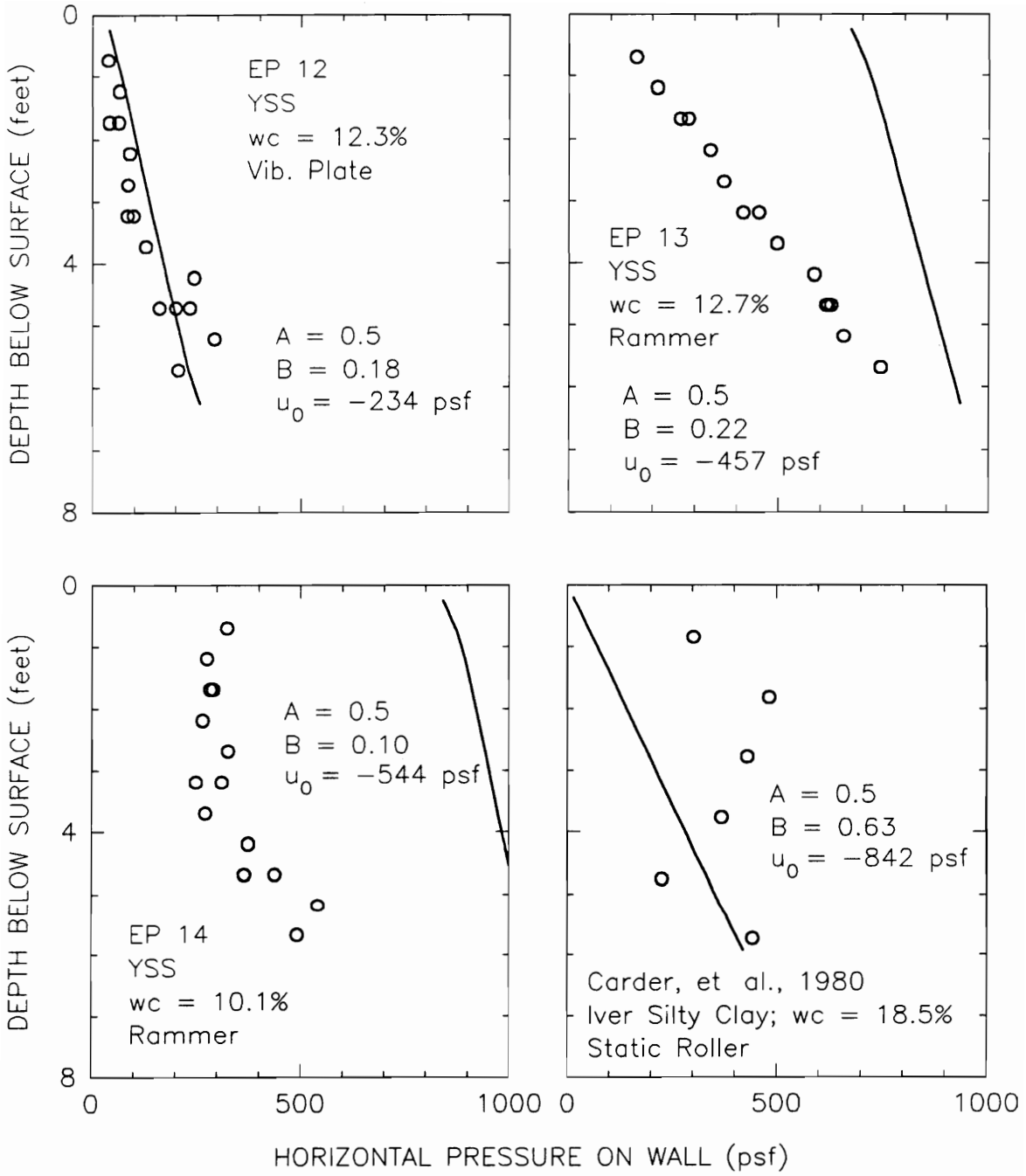

Figure 7.8: Comparison Between Compaction-Induced Earth Pressure Measurements and Theory, with Pore Pressure Parameters Computed from Laboratory Test Results

four tests analyzed in this section. The results of the attempt are shown in Figure 7.9. The figure shows that values of u_0 and B can be found to give good agreement between calculated and measured pressures.

The values of u_0 and B that were used to obtain the calculated compaction-induced lateral earth pressures shown in Figures 7.8 and 7.9 are listed in Table 7.4. A comparison of the values indicates that agreement between measured and calculated pressures is generally achieved when higher values of u_0 and B are used than those determined from undrained strength tests performed using low confining pressures. This trend is most evident for tests EP 13 and EP 14, which were compacted with the rammer compactor. An exception is that a better fit was achieved for Carder's data when a lower value of B was used. The values of confining pressure applied in Carder's laboratory tests are not reported.

One possible reason that higher values of u_0 and B gave a better fit for tests EP 13 and EP 14 is that the pore pressure of a soil, and its B value, both tend to increase with increasing confining pressure. The laboratory specimens were tested at low confining pressures, which were not representative of the pressures in the rammer compacted backfill, especially during compaction.

The results in Figure 7.9 suggest that it may be possible to use constant values of the pore pressure parameters A and B to analyze compaction-induced lateral pressures. The difficulty is to find a suitable means to determine the appropriate values of A and B for a particular backfill type, water content, and compactor. One possibility

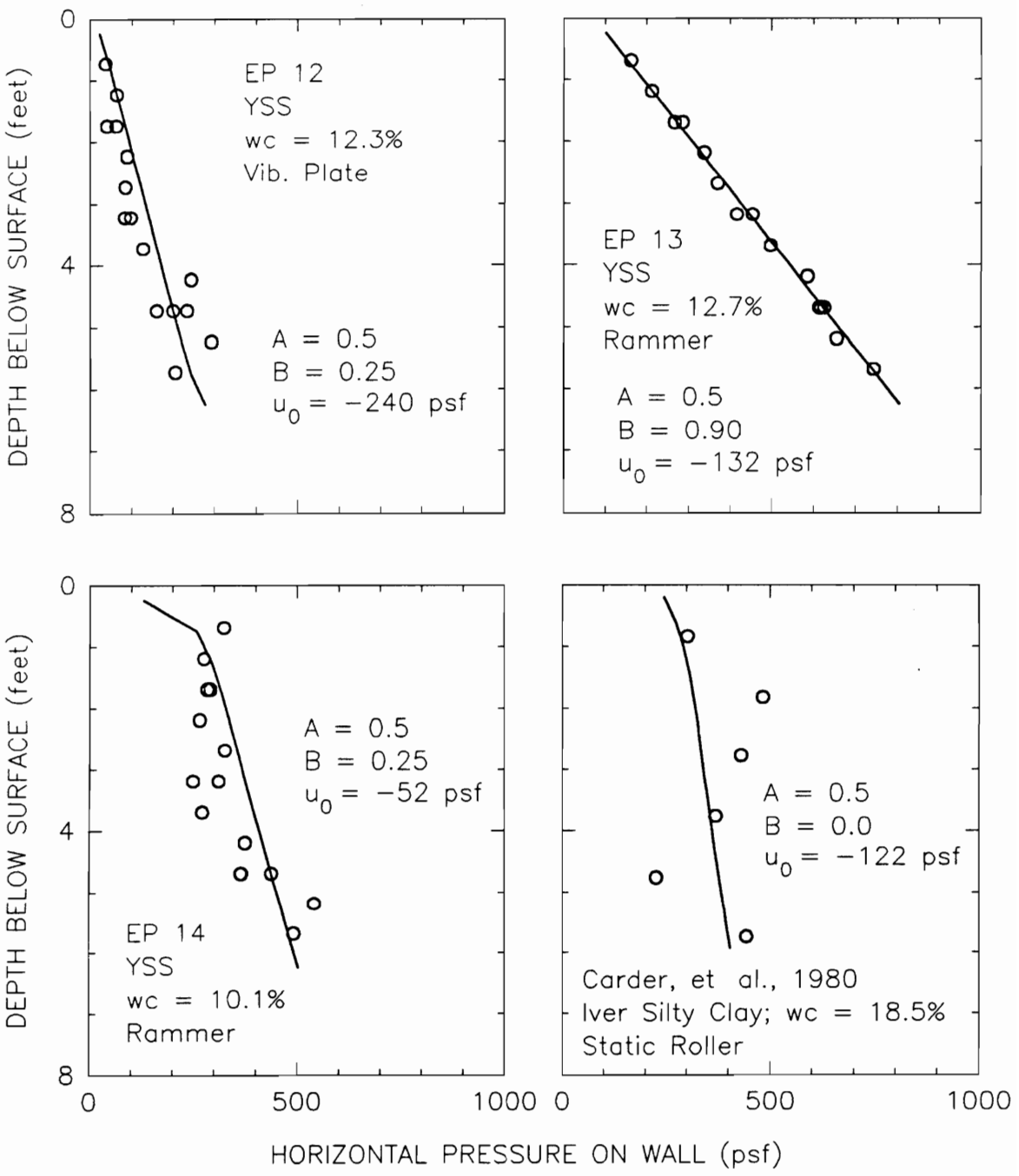

Figure 7.9: **Comparison Between Compaction-Induced Earth Pressure Measurements and Theory, with Pore Pressure Parameters Selected to Give a Good Agreement**

TABLE 7.4: Values of u_0 and B for Compaction-Induced Earth Pressure Calculations - Silty and Clayey Soil Test Cases

Test	Degree of Saturation	Compactor Type	Values from Laboratory Tests Performed at Low Confining Pressures		Values Selected to Give Good Agreement Between Measurements and Theory	
			B	u_0 (psf)	B	u_0 (psf)
EP 12	65%	Vib. Plate	0.18	-230	0.25	-240
EP 13	87%	Rammer	0.22	-460	0.90	-130
EP 14	67%	Rammer	0.10	-540	0.25	-52
Carder, et al., 1980	84%	Static Roller	0.63	-842	0.00	-122

would be to use the extended compaction-induced earth pressure theory developed in Chapter 6 in combination with k_0 oedometer testing to find the appropriate values. This could be done by testing an undisturbed specimen of the compacted backfill, or a specimen compacted in the laboratory to field density and water content, in a k_0 oedometer. The extended compaction-induced earth pressure theory predicts that the initial loading stress path would be as shown in Figure 7.10. If the value of k_0 is known (from laboratory tests or correlations) and the value of A can be estimated, then the value of B can be computed from the slope Δk_0^T in Figure 7.10 using Eqn 6.25. Similarly, the value of u_0 can be computed from the following equation:

$$u_0 = \frac{k_0 + BA(1 - k_0)}{k_0 - 1} \sigma_{v,0} \qquad (7.2)$$

where $\sigma_{v,0}$ = the intersection of the Δk_0^T line with the vertical total stress axis, as shown in Figure 7.10.

Evaluating u_0 and B for moist soils using this method may be a fruitful area for further research.

7.6 A Case History: Eisenhower and Snell Locks

The Eisenhower and Snell Locks are located on the Saint Lawrence Seaway near Massena, NY. The locks were constructed between 1955 and 1958 to provide passage around the Saint Lawrence Power Project. The lock chambers are 80 feet wide and 860 feet long. The lock walls are unreinforced concrete monoliths founded on the dolomite rock that is also the floor of the lock chambers. The locks are about 110 feet high

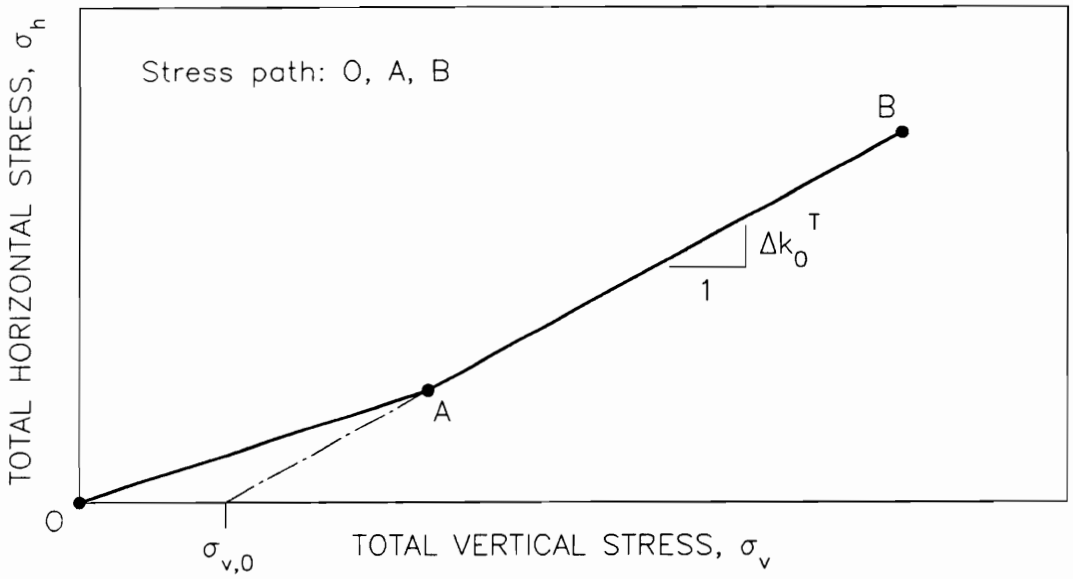

Figure 7.10: Proposed Method to Evaluate u_0 and B for Compaction-Induced Earth Pressure Calculations

and 63 feet wide at the base. A typical lock wall cross-section is shown in Figure 7.11. The backfill behind the lock walls is compacted glacial till.

As shown in Figure 7.11, the lock walls contain interior culverts for filling and emptying the chambers and for supplying the lower pool. During a 1967 inspection of the locks, continuous cracks were observed at the landward-ceiling corner of the filling and emptying culverts in both walls of both locks. It was subsequently determined that the cracks extended through the monoliths to the back faces of the walls. To assure continued ability to operate the locks, the lock walls were rehabilitated by installing post-tensioned anchors across the cracks of all four walls during the period from 1967 to 1969. A typical anchor is shown in Figure 7.11.

A recent study by the US Army Corps of Engineers (Mosher et al. 1991) was undertaken to assess the current structural integrity of the lock walls. As part of the work, the cause of the cracks in the lock walls was studied. It was concluded that the cracks occurred because the walls had been subjected to higher lateral loads than were anticipated during design. One unanticipated source of load was that the actual groundwater level in the backfill was about 20 feet higher than had been assumed during design. However, the Corps' study demonstrated that this factor alone could not have been responsible for the cracks. The other contributing factor was that higher than anticipated lateral earth loads were developed during compaction of the backfill with a large rubber-tired roller.

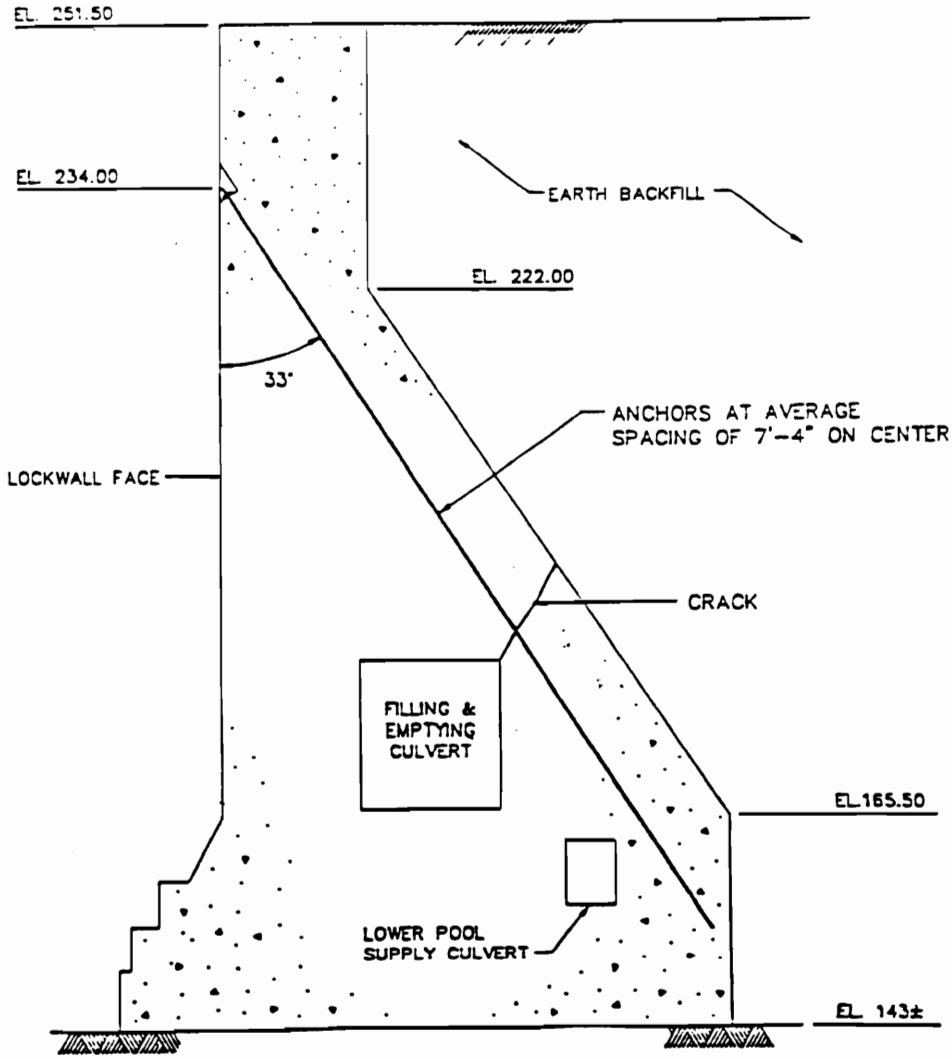

Figure 7.11: Typical Lock Wall Section for Eisenhower and Snell Locks

To investigate the magnitude of the lateral stresses in the backfill, a series of pressuremeter tests and hydrofracture tests were performed at both locks (Schmertmann, 1986). The tests were performed to depths as great as 60 feet, in boreholes located in the backfill directly over the heel of the wall. Schmertmann's interpretations of the test results for Snell Lock are shown on Figure 7.12. The tests at Snell lock were performed after the tests at Eisenhower Lock, and Schmertmann concluded that the tests at Snell Lock were of better quality. For reference, the at-rest pressure distribution computed using a k_0 value of 0.37 (determined from drained triaxial k_0 tests by Christiansen, 1985) is also shown. The groundwater level in the backfill at the time of the testing was about 30 feet below the ground surface. It can be seen that the measured in-situ lateral stresses are much higher than at-rest k_0 stresses.

The compaction-induced earth pressure theory developed in Chapter 6 was used to calculate in-situ lateral pressures in the lock wall backfill. The parameter values necessary for the analyses are listed in Table 7.5. Only effective stress parameters are available for the backfill, and the calculations were made using the effective stress theory without consideration of pore pressure effects. The results presented previously in Figure 7.8 demonstrated that this approach can yield reasonable pressures for silty soils with degrees of saturation in the neighborhood of 65 percent. Records of the water content during compaction of the backfill for Eisenhower and Snell Locks are not available, but information from an investigation of the backfill

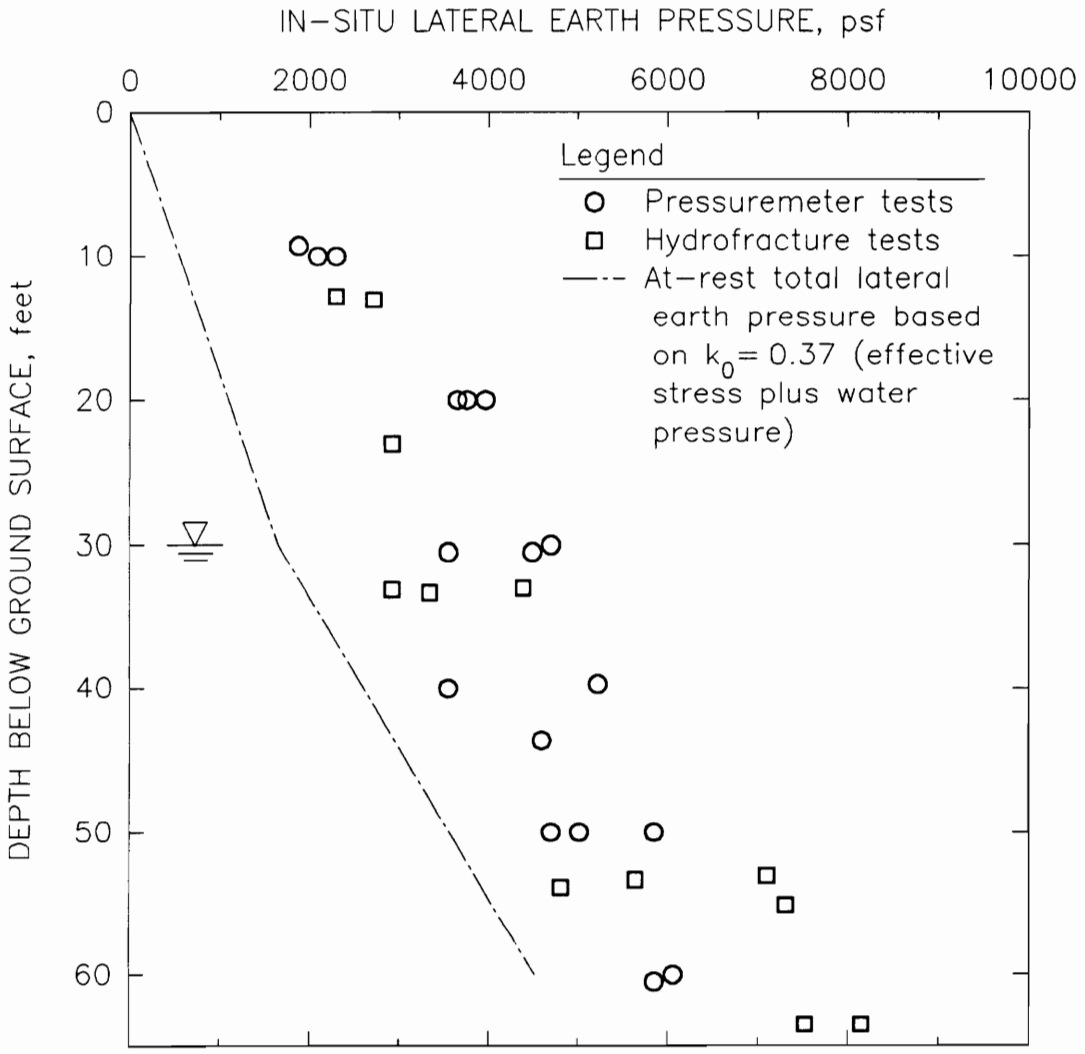

Figure 7.12: In-Situ Lateral Earth Pressure Measurements at Snell Locks

TABLE 7.5: Data for Calculating Compaction Induced Earth Pressures at Eisenhower and Snell Locks

Soil Type	Glacial till consisting of sand, gravel, cobbles, and boulders with some silt and clay. The 3-inch minus portion typically classifies as SM.(1)
Soil Moist Unit Weight	149 pcf(1)
Effective Stress Friction Angle	40 degrees(1)
Effective Stress Cohesion Intercept	1500 psf(1)
Effective Stress Coefficient of Lateral Earth Pressure at-Rest	0.37(1)
Compactor Type	Rubber-tired roller with four closely spaced wheels on a single axle.(2)
Total Compactor Load	Minimum load 25,000 pounds per wheel. Maximum load 50,000 pounds per wheel.(2)
Compactor Tire Pressure	80 to 100 psi for 25,000 pound wheel load. 100 to 150 psi for 50,000 pound wheel load.(2)
Lift Thickness	15-inch maximum loose lift thickness.(2) For the analyses, an average compacted lift thickness of 12 inches is assumed.

Notes: 1) These values are from tests performed by Empire Soils Investigations, Inc., (Christiansen, 1985).

2) These values are from the construction specifications for Eisenhower and Snell Locks.

(Christiansen, 1985) suggests that the degree of saturation was about 75 percent in 1985. It may have been lower during compaction.

Stresses were calculated beneath the center of the roller to determine the free-field stresses due to compaction, rather than the stresses against the wall. The lock wall was far enough from the locations at which the pressuremeter tests and hydrofracture tests were made that the wall did not significantly influence the compaction-induced lateral earth pressures at the test locations. After computing the compaction-induced lateral stresses with EPCOMPAC, the stresses below depth 30 feet were adjusted to account for a rise in the ground water level to depth 30 feet. This adjustment resulted in reduced effective lateral stresses and increased total lateral stresses below the water table.

The total lateral stresses computed in this way are shown in Figure 7.13, together with the measured values. Calculated pressure distributions are shown for both the lightest and the heaviest compactors specified for the job. The calculated pressures for the lightest compactor underestimate the measured pressures. The calculated pressures for the heaviest compactor are in reasonable agreement with the measured pressures. It should be noted that Schmertmann's (1986) interpretations of the pressuremeter test results were made to yield the highest in-situ lateral pressures consistent with the data. This was done to achieve agreement between the pressuremeter test results and the hydrofracture test results. Another interpretation of the pressuremeter

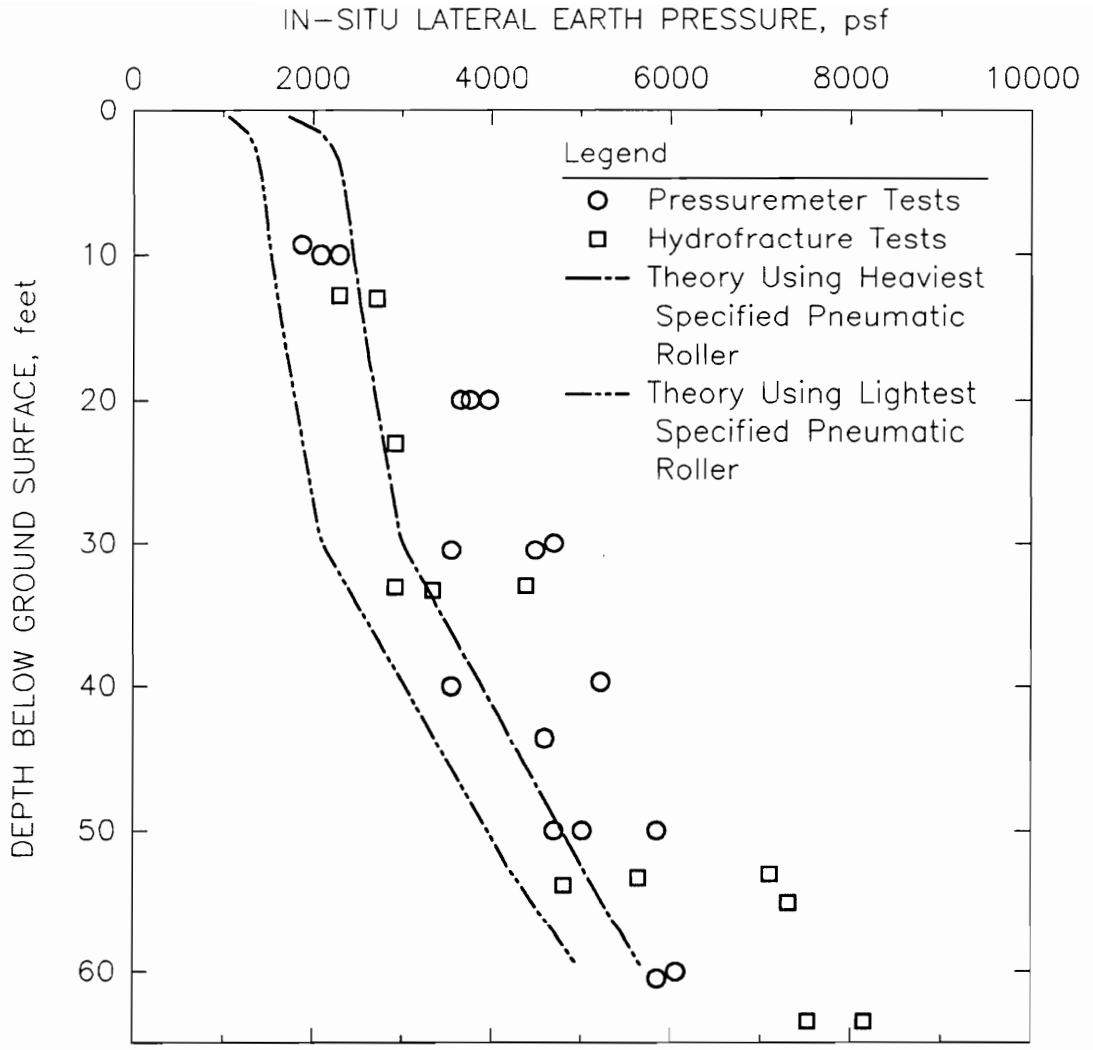

Figure 7.13: Calculated and Measured Lateral Earth Pressures at Snell Locks

test results might have produced measured pressures in even better agreement with the calculated pressures.

7.7 Summary

The measurements obtained from the Virginia Tech instrumented retaining wall facility are considered to be highly reliable because both load cells and pressure cells were used. The benefit of using both load cells and pressure cells is that the data are redundant, and therefore more reliable. The same technique was used by Carder et al. (1977) and Carder, et., al., (1980) in the TRRL model retaining wall. The measurements from the Virginia Tech instrumented retaining wall exhibit less scatter than those from the TRRL wall.

The test results showed that lateral pressures on the instrumented wall were higher when backfill was compacted with the rammer compactor than when it was compacted with the vibrating plate compactor. This is in agreement with calculations made using the compaction-induced earth pressure theory, because the peak contact force for the rammer compactor is higher than for the vibrating plate compactor. The results of tests performed using Light Castle sand as backfill are interesting because both compactors were equally effective in densifying the sand, yet the rammer compactor produced much higher horizontal pressures on the wall.

A study of the effects of various boundary conditions was performed to assess the influence of shear stresses between the backfill and the facility walls on the horizontal and vertical forces on the instrumented wall. Both experiments and analyses were performed to

evaluate the effects of changes in the boundary conditions. In the experiments, two polyethylene sheets with a layer of grease between them were used to reduce the shear stresses on the walls to very low levels. In the finite element analyses, the contacts between the backfill and the walls were modelled with interface elements whose properties were chosen to model either lubricated or non-lubricated wall conditions. The measured horizontal and vertical forces were in good agreement with the values from the finite element analyses. Both the experiments and the analyses showed very little influence of far wall lubrication on the measured forces. Both the experiments and the analyses showed an increase in horizontal force on the instrumented retaining wall when the instrumented wall was lubricated. From these studies, the estimated increase in horizontal force due to lubrication of the instrumented wall is 15 percent for Yatesville silty sand backfill compacted with the vibrating plate compactor. Smaller percentage increases are expected for backfill compacted with compactors that have higher contact forces.

Comparisons were made between the compaction-induced earth pressure theory developed in Chapter 6 and the measurements from three tests in which sand was used as backfill. These tests are the two instrumented retaining wall tests in which Light Castle sand was used, and the test of Carder et al. (1977), in which Bramshill sand was used. Good agreement between the theory and the measurements was obtained when the slope of the limiting pressure line, k_{lim}, was set equal to the reciprocal of the at-rest lateral pressure coefficient, $1/k_0$.

Theoretical predictions of compaction-induced lateral earth pressures are more difficult for silty and clayey soils that develop significant pore pressures during backfill placement and compaction. Three instrumented retaining wall tests performed with Yatesville silty sand backfill, and the test of Carder et al. (1980), which was performed with Iver silty clay backfill, were analyzed in the following ways using the theory developed in Chapter 6:

1) When the calculations were performed without consideration of pore pressure effects, the agreement between theory and measurements was fairly good for two tests in which the degree of saturation of the compacted backfill was about 65 percent. When analyzed this way, the agreement was less good for two tests in which the degree of saturation of the compacted backfill was about 85 percent. For the cases analyzed, the data show that increased degrees of saturation and increased pore pressure effects generally tend to result in increased lateral pressures.

2) Analyses were performed using the extended compaction-induced earth pressure theory developed in Chapter 6, with values of u_0 and B obtained from the results of unconsolidated-undrained triaxial compression tests performed using low confining pressures. The agreement between theory and measurements was generally poor. The extended compaction-induced earth pressure theory is based on the simplifying assumption that the pore pressure parameters A and B can be approximated as constants. The lack of agreement between this theory and the measurements indicates that the parameters A and B cannot be approximated as constants for the stress state range that includes the unloaded soil, the soil loaded by the compactor, and the soil loaded to failure in unconsolidated-undrained tests.

3) Analyses were also performed using the extended compaction-induced earth pressure theory developed in Chapter 6, with values of u_0 and B selected to provide a good fit between theory and measurements. The purpose of this exercise was to see if any constant values of the parameters A and B could be found to give agreement between theory and measurements. Values <u>were</u> found that gave good agreement between theory and measurements. This suggests that, if an appropriate means to evaluate the pore pressure parameters can be found, the extended compaction-induced earth pressure theory developed in Chapter 6 may be suitable for silty and clayey soils. Use of

k_0 oedometer tests in conjunction with concepts from the extended compaction-induced earth pressure theory may afford an effective means of addressing this problem. Further research would be necessary to evaluate this technique.

The cases of Eisenhower and Snell Locks, which are located on the Saint Lawrence Seaway, demonstrate the importance of compaction-induced lateral earth pressures on the performance of earth retaining structures. The lock walls are monolithic concrete gravity structures, 110 feet tall, with internal culverts. Backfill behind the walls is glacial till that was compacted with a heavy pneumatic roller. The compaction process induced high lateral earth pressures that caused the lock walls to crack. The cracked lock walls were subsequently repaired by installing post-tensioned anchors across the cracks.

As part of a study by the US Army Corps of Engineers to assess the integrity of the lock walls, pressuremeter and hydrofracture tests were made to measure the in-situ lateral pressure in the backfill. The availability of this data provided an opportunity to compare the measured lateral earth pressures with pressures calculated using the compaction-induced earth pressure theory. The theoretical pressures were calculated without considering pore pressure effects, and the results were found to agree well with the measured pressures.

CHAPTER 8 - VERTICAL SHEAR FORCES ON WALLS

8.1 Introduction

In conventional design of rigid retaining walls, it is assumed that there are no vertical shear stresses on the back side of the wall. Parameter studies performed by Ebeling et al. (1988), Ebeling et al. (1989), and Regalado et al. (1992), using the finite element method, have shown that there are vertical shear stresses on such walls. The shear stresses result from compression of the backfill under self-weight, which causes relative displacement at the wall-backfill interface and partial or full mobilization of the available shear strength at the contact. The resulting vertical force is beneficial. It tends to counteract the overturning moment from the lateral earth force.

In this chapter, a theory for calculating vertical shear forces on walls is developed, the parameter studies of Ebeling et al. (1988), Ebeling et al. (1989), and Regalado et al. (1992) are reviewed, and vertical shear force measurements from the instrumented retaining wall tests are presented and discussed.

8.2 Theory

Lateral earth pressures for design of retaining walls are ordinarily calculated using the conventional Rankine, Coulomb, or log-spiral theories for active or passive conditions, or Jaky's (1948)

empirical relationship for the at-rest condition. For cohesionless soils, the lateral earth pressure is given by

$$\sigma_h = k_h \gamma z \tag{8.1}$$

where σ_h = the lateral earth pressure on the wall at depth z, psf,

k_h = the lateral earth pressure coefficient,

γ = the soil unit weight, pcf, and

z = the depth below the ground surface, feet.

According to the conventional theories, the value of the lateral earth pressure coefficient is constant with depth for homogenous soil, so the pressure distribution is triangular. Integrating Eqn 8.1 to obtain the lateral force yields:

$$F_h = \frac{1}{2} k_h \gamma H^2 \tag{8.2}$$

where F_h = the applied horizontal force, lbs/ft, and

H = the wall height, feet.

As discussed in Chapters 6 and 7, if compaction-induced lateral earth pressures are considered, the variation of lateral pressure with depth is not linear, and, consequently, the value of the lateral earth pressure coefficient, k_h, is not constant. In such cases, there is utility in defining a lateral earth force coefficient, K_h, as follows:

$$F_h = \int_0^H \sigma_h \, dz \tag{8.3}$$

$$K_h = \frac{2F_h}{\gamma H^2} \tag{8.4}$$

The values of K_h from Eqn 8.4 will, in general, be a function of the wall height. The benefit of computing K_h in such cases is to provide a normalized indication of the effect of compaction-induced lateral stresses. If values of K_h can be estimated from theory or experience, then the lateral force can be calculated using K_h in the following equation, in the same manner that k_h was used in Eqn 8.2:

$$F_h = \frac{1}{2} K_h \gamma H^2 \tag{8.5}$$

The vertical shear force, F_v, applied by backfill to a wall is the integrated shear stress, τ, at the wall-backfill contact:

$$F_v = \int_0^H \tau \, dh \tag{8.6}$$

Rather than computing shear stress distributions for use in Eqn 8.6, it is customary to compute vertical shear forces for walls with cohesionless backfill by means of the following equation, which is analogous to Eqn 8.5:

$$F_v = \frac{1}{2} K_v \gamma H^2 \tag{8.7}$$

where F_v = the applied vertical shear force, lbs/ft,

K_v = the vertical shear <u>force</u> coefficient.

For active and passive conditions, the value of the vertical shear force coefficient, K_v, can be related to earth pressures calculated using conventional earth pressure theories based on limit equilibrium, e.g., the theories of Coulomb (1776) or Caquot and Kerisel (1948). In

these theories, the strength of a mass of soil behind the wall is assumed to be fully mobilized, and the interface strength at the contact between the wall and the backfill is also assumed to be mobilized. For cohesionless soils, the shear strength of the interface, τ_f, is proportional to the normal stress, σ_n:

$$\tau_f = \sigma_n \tan\delta \tag{8.8}$$

where $\tan\delta$ = the coefficient of interface friction, and

δ = the interface friction angle, degrees.

For vertical walls, the lateral earth pressure on the wall, σ_h, is the same as the normal stress at the interface, σ_n. When the interface strength is fully mobilized for a wall in the active or passive condition, Eqns 8.3 through 8.8 imply that the value of K_v is given by:

$$K_v = K_h \tan\delta \tag{8.9}$$

There is no simple theory for calculating values of K_v for the at-rest condition. Parameter studies using the finite element method have been performed by Ebeling et al. (1988), Ebeling et al. (1989), and Regalado et al. (1992) to evaluate the influence of several factors on K_v values. The results of these studies will be discussed subsequently. The remainder of this section is devoted to developing a theory for calculating values of K_v for the at-rest condition.

For conventional analyses of the active and passive wall conditions, the interface strength is fully mobilized and K_v is proportional to K_h, as indicated in Eqn 8.9. For the at-rest condition, on the other hand, the interface strength is not fully mobilized over

the full length of the backfill-wall contact, and K_v is not proportional to K_h. The reason for the difference is that relative movement between the backfill and the wall is necessary to mobilize shear stress at the interface.

For the at-rest case, the relative movement that occurs due to backfill compression does not mobilize the same percentage of the available interface strength for all wall heights. For high walls, the backfill compression and relative displacement at the interface are larger than for low walls, so a larger percentage of the available interface strength is mobilized. Thus, although Eqn 8.7 indicates that the shear force should be proportional to the square of the wall height, it seems likely that the shear force will vary in proportion to a higher power of the wall height than two. Consideration of the backfill compressibility and the degree of mobilization of the interface strength is the basis for the new vertical shear force theory described in the following paragraphs.

The 1-D backfill compressibility, m_v, is defined as

$$m_v = \frac{\partial \epsilon}{\partial p_v} \tag{8.10}$$

where ϵ = the vertical strain in 1-D compression, and

p_v = the vertical pressure, psf.

For many soils, the strain versus logarithm of pressure relationship is linear over a significant range of pressures. Linearity implies that the compressibility of an element of backfill soil is inversely proportional to its depth within the backfill:

$$m_v = \frac{C_\epsilon}{2.3\gamma z} \tag{8.11a}$$

where C_ϵ = the compression index, i.e., the slope of the strain versus logarithm of pressure plot.

The soil compressibility can also be expressed as a constant value for a given wall height using Eqn 8.11(a) evaluated at the average pressure during backfilling:

$$m_v = \frac{2C_\epsilon}{2.3\gamma H} \tag{8.11b}$$

The vertical shear force theory presented here was developed using both compressibility assumptions, as expressed in Eqns 8.11(a) and 8.11(b). The final vertical shear force is the same with either assumption, though some of the intermediate results, such as the deformation distribution and the shear stress distribution, are slightly different.

The geometry for developing the relationships is shown in the definition sketch in Figure 8.1, where the wall height and final backfill depth is H, the elevation at which the settlement and shear stresses are being calculated is h, the current elevation of the top of the backfill is y, and the depth below the current backfill surface is z. To begin, the rate at which strain develops in response to backfill placement is given by

$$\frac{\partial \epsilon}{\partial y} = \frac{\partial \epsilon}{\partial(\gamma y)}\gamma = \frac{\partial \epsilon}{\partial p}\gamma = m_v\gamma \tag{8.12}$$

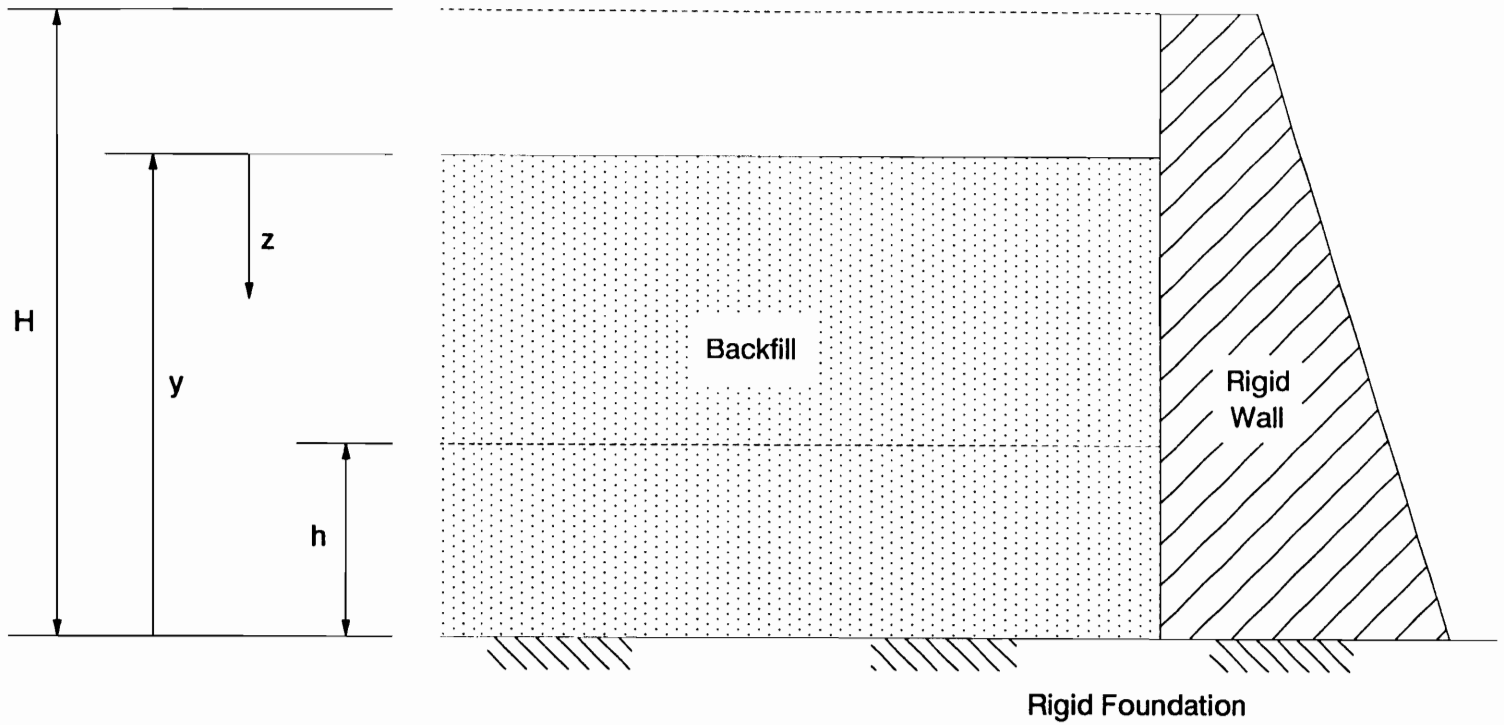

Figure 8.1: Definition Sketch for the Vertical Shear Force Theory

The rate at which the free-field settlement, S, occurs in response to backfill placement is obtained by integrating Eqn 8.12 over the depth from the level of interest to the bottom of the fill:

$$\frac{\partial S}{\partial y} = \int_{y-h}^{y} m_v \gamma \, dz \tag{8.13}$$

The relationship in Eqn 8.13 will be used to track the development of shear stresses at a particular elevation on the wall as filling proceeds. Eqn 8.13 can also be integrated to give the total free-field settlement at any elevation, h, within the backfill due to placement of the overlying backfill:

$$S = \int_{h}^{H} \frac{\partial S}{\partial y} \, dy \tag{8.14}$$

Evaluating Eqn 8.14 using the two expressions for compressibility in Eqns 8.11(a) and 8.11(b) yields the following corresponding expressions for the total free-field settlement at elevation h:

$$S = C_\epsilon [H \log_{10} H - h \log_{10} h - (H - h) \log_{10} (H - h)] \tag{8.15a}$$

$$S = \frac{C_\epsilon}{2.3H} h(H - h) \tag{8.15b}$$

According to both Eqns 8.15(a) and 8.15(b), the settlement is zero at the top and bottom of the fill, and the settlement is maximum at mid-height. Settlements computed using Eqn 8.15(a), in which compressibility is inversely proportional to pressure throughout the

backfill, are larger than those computed using Eqn 8.15(b), in which compressibility is assumed to be constant for a given wall height.

In addition to the backfill settlement distribution, the wall-backfill interface behavior is important in determining the magnitude of shear stresses on the wall. A simple model, which is shown in Figure 8.2, was used to approximate the interface behavior. The shear strength is assumed to be proportional to the normal stress, as indicated in Eqn 8.8. For interface shear stresses below the shear strength, the shear stress is assumed to be proportional to the relative displacement, Δ, between backfill and wall. When the shear stress equals the shear strength, the interface is assumed to be perfectly plastic. Accordingly, the initial interface shear stiffness, k_{ii}, is given by

$$k_{ii} = \frac{\partial \tau}{\partial \Delta} = \frac{\tau_f}{\Delta_{lim}} = \frac{\sigma_n \tan\delta}{\Delta_{lim}} \qquad (8.16)$$

where Δ_{lim} = the relative displacement at which failure occurs for an interface loaded in shear under constant normal stress, ft.

It is important to note that Δ_{lim} is used to define the shear stiffness, not the failure state of the interface. Failure is defined by the shear strength, τ_f, given by Eqn 8.8. The distinction is illustrated in Figure 8.3, which shows the effect of arriving at the same failure stress state by two different stress paths. In Figure 8.3(a), the normal stress is first increased along the path O to A without applying any shear stress, and then the interface is loaded to failure in shear along the path A to B without changing the normal stress. This stress path is similar to a conventional direct shear or

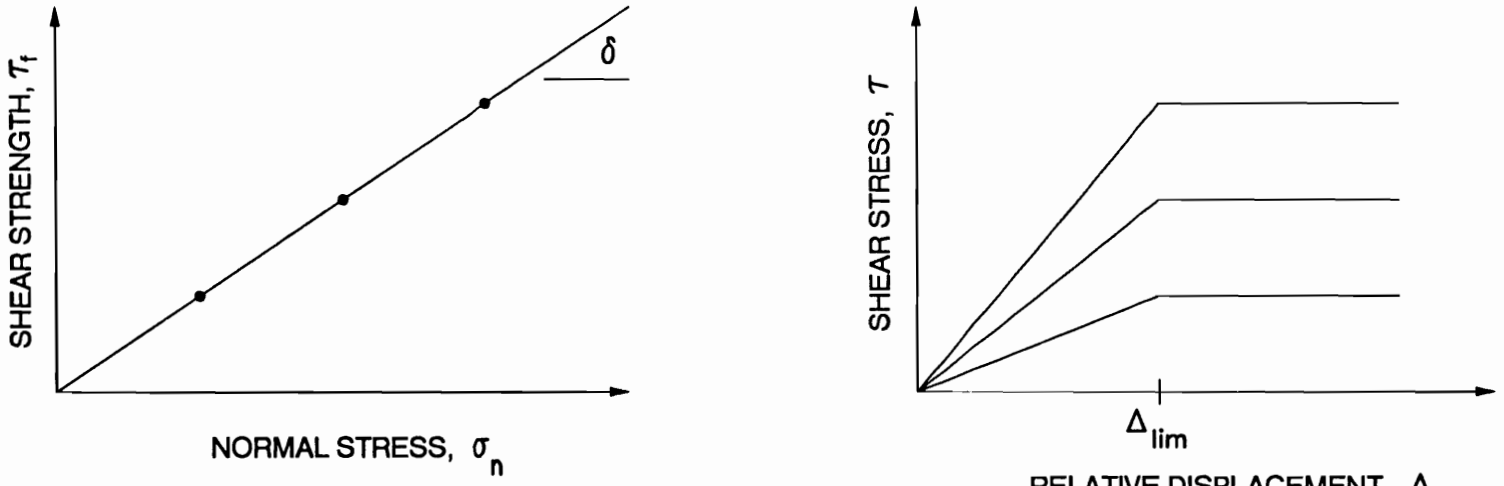

Figure 8.2: Interface Model for the Vertical Shear Force Theory

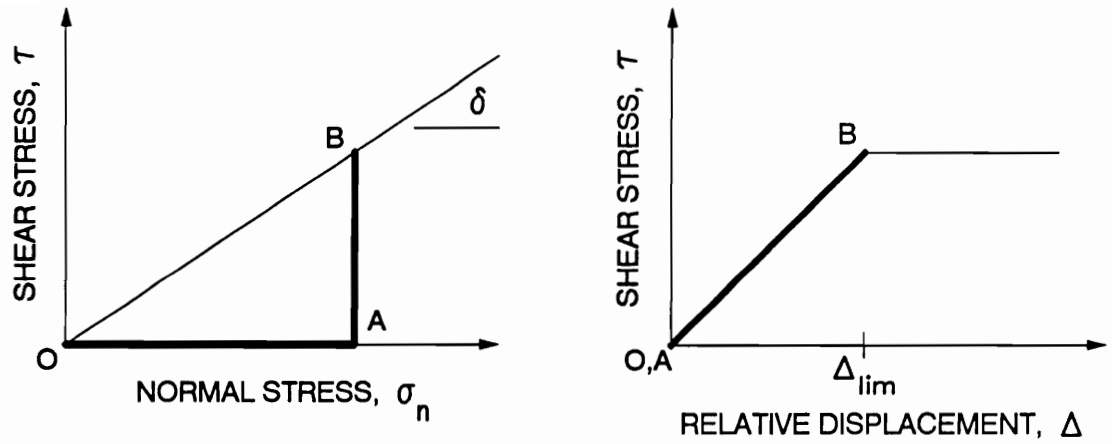

a) Effect of stress path O, A, B

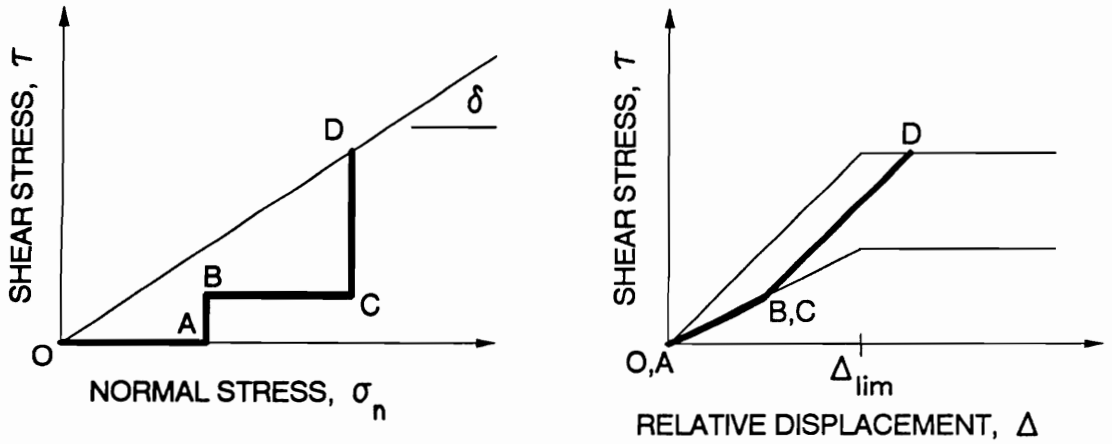

b) Effect of stress path O, A, B, C, D

Figure 8.3: Effect of Different Stress Paths on Interface Response

interface shear test. In this case, no shear displacement occurs during application of the normal load, and the displacement at failure is equal to Δ_{lim}. In Figure 8.3(b), the normal stress is first increased from 0 to A without applying any shear stress, and no shear displacement occurs. Next, the shear stress is increased from A to B while holding the normal stress constant, and shear displacement occurs according to the shear stiffness given by Eqn 8.16 for the current normal stress. Then the normal stress is increased again, this time from B to C while holding the shear stress constant. In the model, no shear displacement occurs during this increase in normal stress because there has been no change in shear stress. Finally, the shear stress is increased along the path from C to D while holding the normal stress constant. The shear displacement again occurs according to the shear stiffness for the current normal stress. As shown in Figure 8.3(b), the total displacement required to fully mobilize the shear strength at this normal stress level exceeds Δ_{lim}. This situation occurs because substantial displacement accumulated without mobilizing much shear stress while the normal stress was at a low level.

At all locations on the backfill-wall interface, both the interface normal stress and the interface shear stress increase monotonically as the backfill thickness increases. Consequently, there is no need to include unloading or reloading behavior in the interface model.

The interface behavior is related to displacements at the backfill-wall interface, but the settlement and settlement rate given by

Eqns 8.13 through 8.15 are for the free field. Settlements in the free field are larger than displacements at the wall. In this theory, it is assumed that the ratio between displacement at the wall and settlement in the free field is constant for a given soil and interface:

$$\frac{\Delta}{S} = r \tag{8.17}$$

where r = is the displacement ratio, with a value less than unity.

The value of r depends on the backfill stiffnesses and the interface strength and stiffness. The value of r also depends on the wall height since the extent of interface failure increases with increasing wall height and increases in the extent of interface failure tend to increase the value of r. Nevertheless, the value of r is assumed to be independent of the wall height in order to keep the theory reasonably simple. The approximation that r is constant may be most applicable before extensive interface failure occurs. Eqns 8.16 and 8.17 can be combined to yield the following equation for the rate at which the interface shear stress changes in response to free-field settlement:

$$\frac{\partial \tau}{\partial S} = \frac{\sigma_n r \tan\delta}{\Delta_{lim}} \tag{8.18}$$

Closed form expressions for the vertical shear stress distribution and the vertical shear force magnitude can be obtained from the preceding equations if the lateral earth pressure distribution is simple and if the wall height is below the critical height at which interface

failure begins to occur. In other situations, the equations can be evaluated numerically.

The vertical shear stress distribution is obtained by integration, using Eqns 8.13 and 8.18 as follows:

$$\tau = \int_{h}^{H} \frac{\partial \tau}{\partial y}\, dy = \int_{h}^{H} \frac{\partial \tau}{\partial S}\frac{\partial S}{\partial y}\, dy$$

$$= \int_{h}^{H} \frac{\sigma_n r \tan\delta}{\Delta_{lim}} \left[\int_{y-h}^{y} m_v \gamma \, dz \right] dy \qquad (8.19)$$

Eqn 8.19 can be evaluated using the two expressions for compressibility in Eqns 8.11(a) and 8.11(b). If the value of k_h is constant and the wall height is below the critical height, the following closed form expressions for the vertical shear stress corresponding to the compressibilities in Eqns 8.11(a) and 8.11(b) are obtained:

$$\tau = \frac{r\gamma k_h C_\epsilon \tan\delta}{\Delta_{lim}} \left[\frac{H^2}{2}\log_{10}H - hH\log_{10}H + \frac{hH}{2(2.3)} + \frac{h^2}{2}\log_{10}h \right.$$

$$\left. - \frac{h^2}{2(2.3)} - \frac{(H-h)^2}{2}\log_{10}(H-h) \right] \qquad (8.20a)$$

$$\tau = \frac{r\gamma k_h C_\epsilon \tan\delta}{2.3H\Delta_{lim}}(hH^2 - 2h^2H + h^3) \qquad (8.20b)$$

The shear stress from Eqn 8.20(a) is slightly larger than that from Eqn 8.20(b) above the mid-height of the backfill, and slightly

smaller below the mid-height. The critical wall height, H_{cr}, at which the strength of the interface first becomes fully mobilized at any location is obtained from Eqns 8.8 and 8.20. When Eqn 8.20(a) is used, the value of H_{cr} can be found numerically. When Eqn 8.20(b) is used, the following closed form expression for H_{cr} is obtained:

$$H_{cr} = \frac{4(2.3)\Delta_{lim}}{rC_{\epsilon}} \tag{8.21}$$

The total vertical shear force is obtained by integrating the shear stress from Eqn 8.19 over the wall height, as indicated in Eqn 8.6. The integration can be completed in closed form if k_h is constant and if the wall height is below the critical height. In this case, the same result is obtained, whether the compressibility is given by either Eqn 8.11(a) or Eqn 8.11(b):

$$F_v = \frac{r\gamma k_h C_{\epsilon} \tan\delta}{2.3\Delta_{lim}} \frac{H^3}{12} \tag{8.22}$$

Eqn 8.22 indicates that the vertical shear force is proportional to the wall height cubed, rather than squared as suggested by Eqn 8.7, for walls below the critical height when compaction-induced lateral pressures are not considered. Nevertheless, Eqn 8.7 can still be used to compute vertical shear forces in a manner consistent with Eqn 8.22 if it is considered that the value of the vertical shear force coefficient, K_v, is proportional to the wall height, as follows:

$$K_v = \frac{rk_h C_{\epsilon} \tan\delta}{6(2.3)\Delta_{lim}} H \tag{8.23}$$

For the general case, in which k_h is not constant and/or failure occurs along a portion of the wall-backfill interface, the shear stress, Eqn 8.19, and the shear force, Eqn 8.6, can be evaluated numerically.

To illustrate the type of results obtained using this theory, example calculations were performed using the compressibility formulation in Eqn 8.11(b) and the parameter values listed in Table 8.1. The values are hypothetical, but realistic, values for a compacted backfill soil. The values of γ, C_ϵ, and Δ_{lim} are typical of the measured values for the Yatesville silty sand, as described in Appendix A. The value of k_0 listed in Table 8.1 is obtained from Jaky's equation using a value of the effective stress internal friction angle, ϕ', of 40 degrees. The value of δ in Table 8.1 corresponds to a δ/ϕ' ratio of 0.75, which is in the range of values measured for the Yatesville silty sand. The value of r in Table 8.1 is estimated from the results of the finite element analysis described in Chapter 7.

Calculations were first performed using a constant value of k_h equal to the value of k_0 in Table 8.1, thus ignoring the effect of compaction-induced lateral earth pressures. The calculations were performed for wall heights of 5 and 12 feet. According to Eqn 8.21, the critical wall height is 9.2 feet for the parameter values listed in Table 8.1. Thus, interface failure does not develop for the 5-foot high wall, but interface failure does develop over a portion of the wall-backfill contact for the 12-foot high wall. The distributions of interface displacement, normal stress, and vertical shear stress on the two walls are shown in Figure 8.4. The displacement distributions from

TABLE 8.1: Parameter Values for Example Calculations of Vertical Shear Forces

Parameter	Value
Moist unit weight, γ	125 pcf
At-rest lateral earth pressure coefficient, k_0	0.36
Compression Index, C_ϵ	0.5%
Interface Friction Angle, δ	30 degrees
Interface displacement at shear failure under constant normal stress, Δ_{lim}	0.015 inches
Ratio between the interface displacement and the free-field backfill settlement at the same elevation, r	0.25

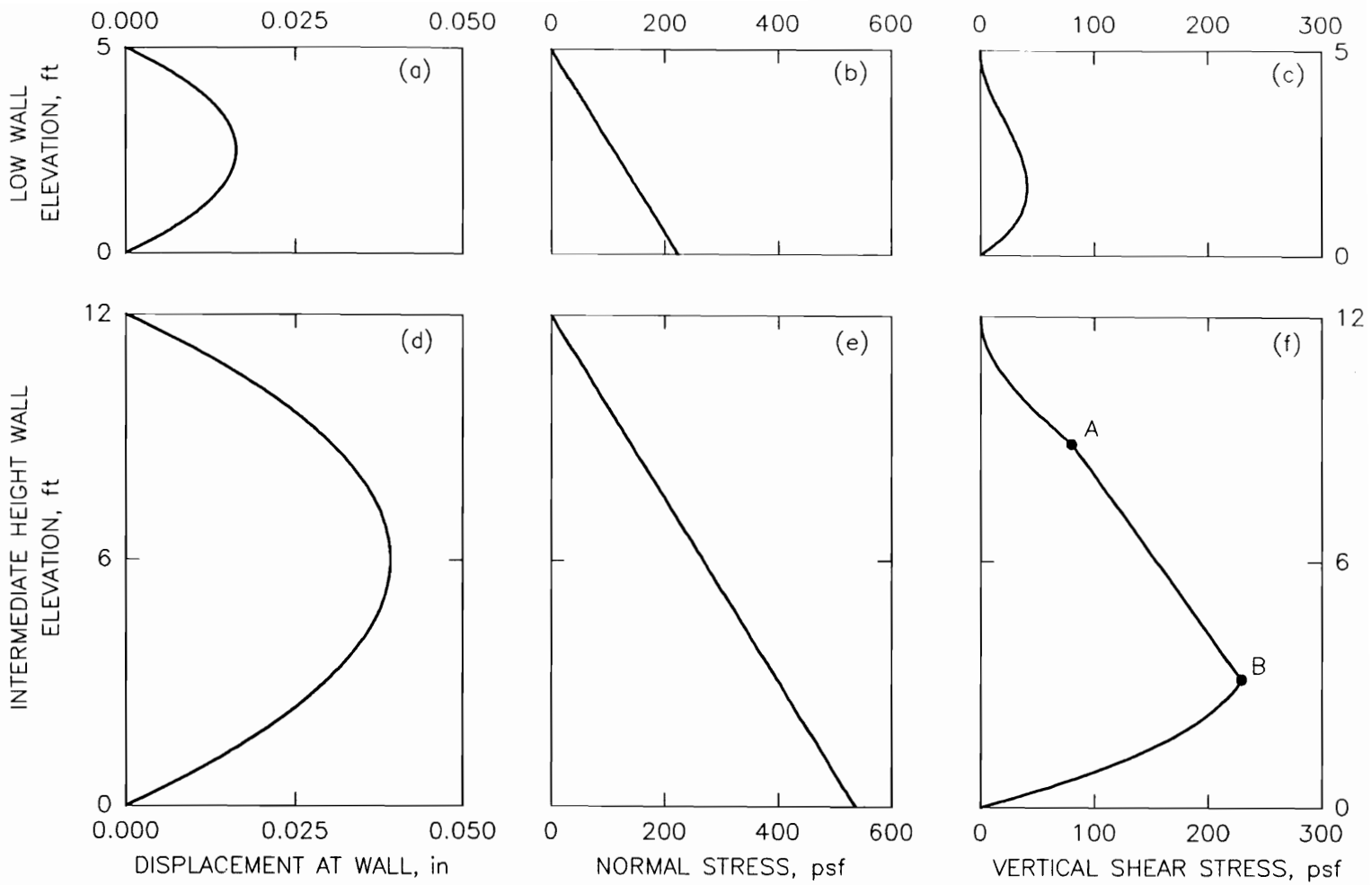

Figure 8.4: Theoretical Displacement, Normal Stress, and Shear Stress Distributions Without Compaction-Induced Stresses

Eqn 8.15(b) are parabolic, and the normal stress distributions are linear because compaction-induced lateral stresses are not included. For the 5-foot high wall, the shear stress distribution is cubic, as indicated in Eqn 8.20(b). For the 12-foot high wall, the portion of the interface between points A and B has failed, and the shear stress is proportional to the normal stress in this region. For very high walls, the shear stress distribution would be proportional to the normal stress over almost the entire wall height.

The total shear force is obtained by integrating the shear stress distributions over the height of the wall. For the 5-foot high wall in Figure 8.4, the total shear force is 120 pounds per foot. For the 12-foot high wall, the total shear force is 1430 pounds per foot.

One effect of backfill compaction behind a rigid wall is to increase lateral pressures above the at-rest pressures. The compaction-induced pressures, in turn, have an effect on the vertical shear stresses. The results of calculations performed with increased lateral pressures representative of those induced by compaction are shown in Figure 8.5. The parameter values listed in Table 8.1 were again used in the calculations. In this case, however, the higher lateral earth pressures shown in Figures 8.5(b) and 8.5(e) were used in the calculations. The vertical shear stress distributions shown were obtained by numerically integrating Eqn 8.19. In Figure 8.5(f), the interface has failed between points A and B, and the shear stress is proportional to the normal stress in this region. Because of the higher lateral stresses, the vertical shear stresses in Figure 8.5 are higher

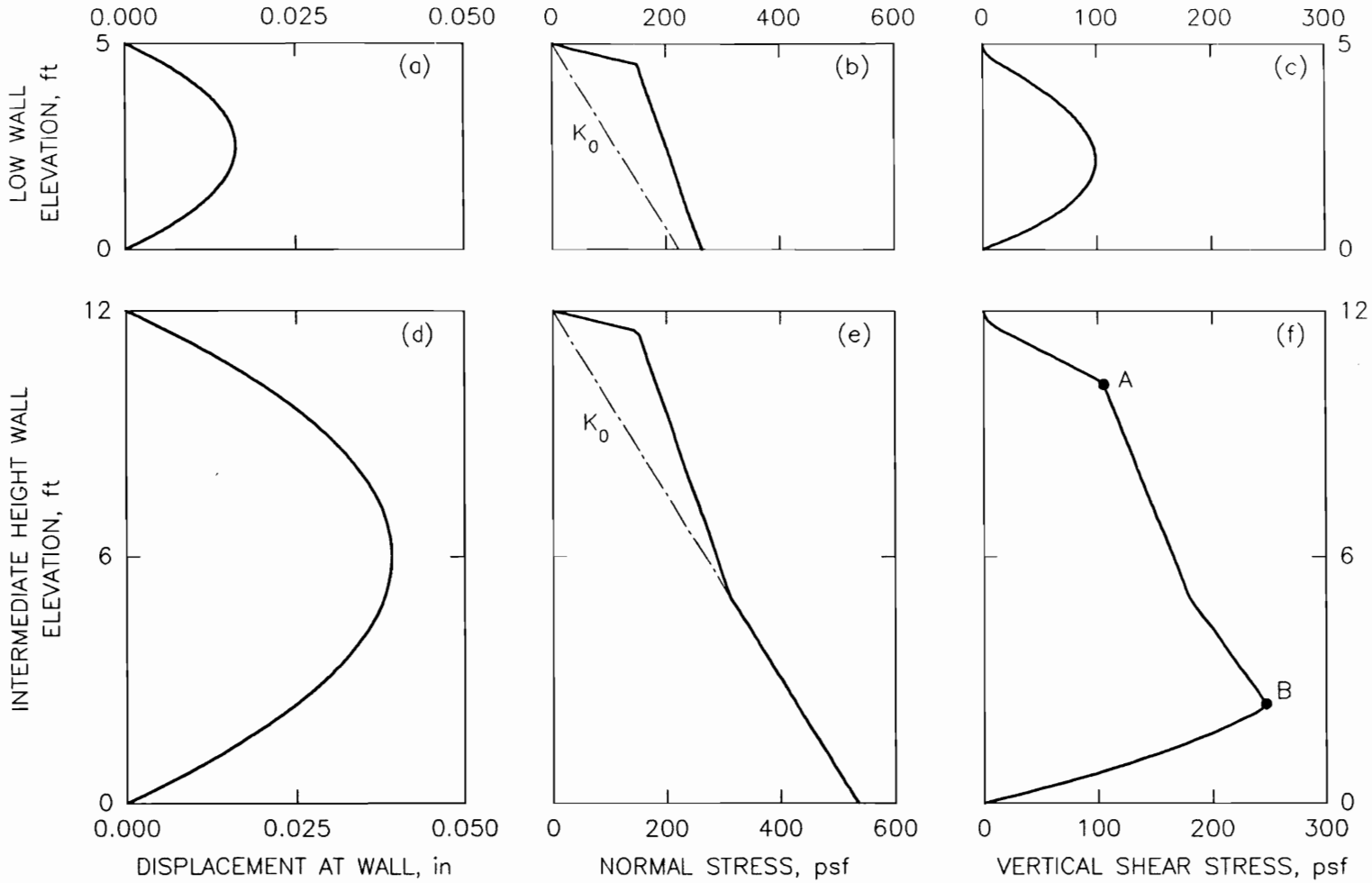

Figure 8.5: Theoretical Displacement, Normal Stress, and Shear Stress Distributions With Compaction-Induced Stresses

than those in Figure 8.4. For the 5-foot high wall in Figure 8.5, the total shear force is 330 pounds per foot. For the 12-foot high wall, the total shear force is 1740 pounds per foot.

Experience in applying the method and evaluating the parameters needs to be developed before this theory could be used in design applications. In particular, there is at present no simple method for evaluating the parameter, r. Nevertheless, the theory does provide a basis for understanding the influence of wall height, compaction-induced lateral pressures, backfill compressibility, and interface behavior on the vertical shear forces that backfills apply to rigid walls.

Conceptually, it is useful to group the factors that influence vertical shear forces into those that influence lateral pressures and those that influence the degree of interface shear strength mobilization. The contribution of the two groups can be expressed in dimensionless form using the earth force coefficients in Eqns 8.5 and 8.7. First, the mobilized interface strength can be characterized by the tangent of the mobilized angle of wall friction, $\tan\delta_{mob}$, which is equal to the ratio of F_v to F_h:

$$\tan\delta_{mob} = \frac{F_v}{F_h} \tag{8.24}$$

The value of $\tan\delta_{mob}$ cannot exceed the value of $\tan\delta$. From Eqns 8.5, 8.7, and 8.24,

$$K_v = K_h \tan\delta_{mob} \tag{8.25}$$

In Eqn 8.25, the value of K_h includes the effects of factors that influence lateral pressures, and the value of $\tan\delta_{mob}$ includes the effects of factors that influence the degree of interface strength mobilization. For instance, compaction increases the value of K_h, and increasing wall height and increasing backfill compressibility increase backfill settlement and, therefore, the value of $\tan\delta_{mob}$.

The effects of wall height and compaction on vertical shear forces are shown in Figure 8.6, in the terms of Eqn 8.25, for the conditions of the example calculations presented previously in this section. Without considering the effects of compaction, the value of K_h is constant and equal to the value of k_0 in Table 8.1; the value of $\tan\delta_{mob}$ increases with increasing wall height due to increasing backfill settlement; and the value of K_v is proportional to the value of $\tan\delta_{mob}$ as indicated by Eqn 8.25 when K_h is constant.

Figure 8.6(c) shows that, up to a wall height of 9.2 feet, the value of K_v is proportional to H, in accordance with Eqn 8.23. As the wall height continues to increase, the value of K_v asymptotically approaches the value of $k_0\tan\delta$, which in this case is 0.21, as more and more of the wall-backfill interface reaches a failure condition.

The situation when compaction-induced lateral pressures are considered is shown in Figures 8.6(d) through 8.6(f). In this case, the value of K_h is not constant but, instead, decreases with increasing wall height due to the limited depth of influence of the compaction-induced lateral earth pressures. The value of $\tan\delta_{mob}$ still increases with increasing wall height, but the value of K_v is almost constant, being

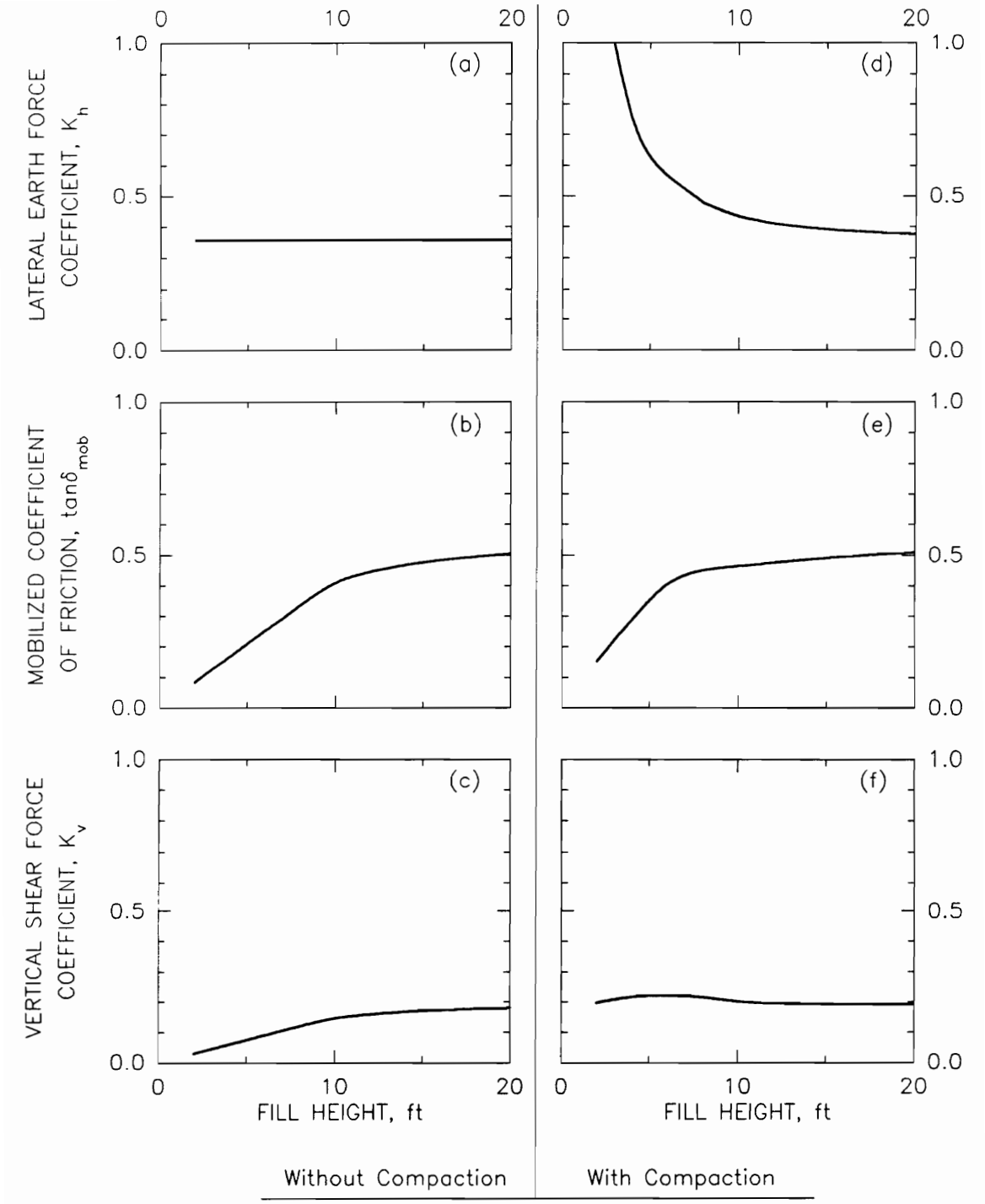

Figure 8.6: Theoretical Variation of Earth Force Coefficients

the product of a decreasing function, K_h, and an increasing function, $\tan\delta_{mob}$. Thus, compaction-induced lateral earth pressures can create a situation in which a constant value of K_v can be used in Eqn 8.7 to compute vertical shear force magnitudes over a wide range of wall heights.

The results presented in Figure 8.6 indicate that, for rigid walls with vertical back faces and cohesionless backfill, the value of K_v approaches the value of $k_0\tan\delta$ as the wall height increases. This follows from Eqn 8.25 because 1) the value of K_h approaches the value of k_0 as the wall height increases due to the limited depth of influence of compaction-induced lateral pressures and 2) the value of $\tan\delta_{mob}$ approaches the value of $\tan\delta$ as the wall height increases due to increasing backfill settlement. Thus, the ultimate value of K_v for high rigid walls founded on rock, $K_{v,ult}$, is $k_0\tan\delta$. $K_{v,ult}$ can be evaluated in terms of the effective stress internal friction angle, ϕ', using Jaky's expression for k_0 and assuming that the δ/ϕ' ratio is 0.75:

$$K_{v,ult} = (1 - \sin\phi')\tan(0.75\phi') \qquad (8.26)$$

Values of $K_{v,ult}$ determined using Eqn 8.26 are listed in Table 8.2 for a range of ϕ' values. The results indicate that, for cohesionless soils, the value of $K_{v,ult}$ is about 0.2. Accordingly, a reasonable value of K_v for use in Eqn 8.7 is 0.2 for all walls that: 1) are rigid (typically, concrete gravity walls founded on rock); 2) are high (the results in Figure 8.6 suggest that walls higher than about 20 feet would

TABLE 8.2: Values of $K_{v,ult}$

Effective Stress Angle of Internal Friction (degrees)	$K_{v,ult}$
25	0.20
30	0.21
35	0.21
40	0.21
45	0.20

satisfy this criterion); 3) are backfilled with cohesionless soil; and 4) have vertical back faces in contact with the backfill.

8.3 Factors That Influence Values of K_v

The analyses in the preceding section demonstrated that wall height, compaction-induced lateral pressures, backfill compressibility, and interface behavior all influence the value of the vertical shear force coefficient, K_v. Other factors that influence the value of K_v have been studied by Ebeling et al. (1988), Ebeling et al. (1989), and Regalado et al. (1992) using the finite element method. The purpose of these finite element studies was to evaluate the stresses applied to retaining walls, and compare the results with those of conventional analysis procedures, which rely on limit equilibrium methods. During the course of the work, the existence and importance of vertical shear forces on walls were identified, and values of K_v were calculated for a number of different wall configurations, foundation types, and backfill types.

8.3.1 Walls on Rock Foundations

Ebeling et al. (1988) and Ebeling et al. (1989) studied gravity walls on rock foundations. In the analyses, the backfill loads were applied in an incremental fashion to simulate the placement of backfill in lifts behind a real wall. The lateral loads applied by the backfill cause the wall to rotate, increasing contact pressures on the base of the wall at the toe and reducing them at the heel. For certain geometries and loads, the heel of the wall can separate from the rock

foundation. One challenge in modelling this process with finite elements is to accommodate tensile failure of interface elements between the wall and foundation without retaining excess stresses in the failed elements. Ebeling et al. (1988) developed the alpha method, in which the loads are applied in appropriately sized steps, to address this "overshoot" problem. The method was successful in achieving static equilibrium between interface element stresses and externally applied loads.

The wall configurations studied by Ebeling et al. (1988) and Ebeling et al. (1989) are shown in Figure 8.7. In every case, the wall is 40 feet high, 16 feet wide at the base, and is founded on a stiff rock foundation. The internal fiction angle of the backfill and the interface friction angle for the wall-backfill contact were both held constant at 39 and 31 degrees, respectively, for all the analyses. The constant parameter values are summarized in Table 8.3. The following parameter values were varied in the analyses: the value of Poisons ratio for the backfill, the backfill unit weight, the backfill stiffness, the interface stiffness, the presence or absence of a toe fill, the width of the wall at the top, whether the back of the wall was sloped or stepped, and water levels behind and in front of the wall. In addition, one analysis was performed with the wall completely restrained from movement. The parameter values were varied in a systematic way so that the independent influence of each parameter was disclosed. The values of the varied parameters for each analysis, and the resulting K_v values, are listed in Tables 8.4 (a) and (b).

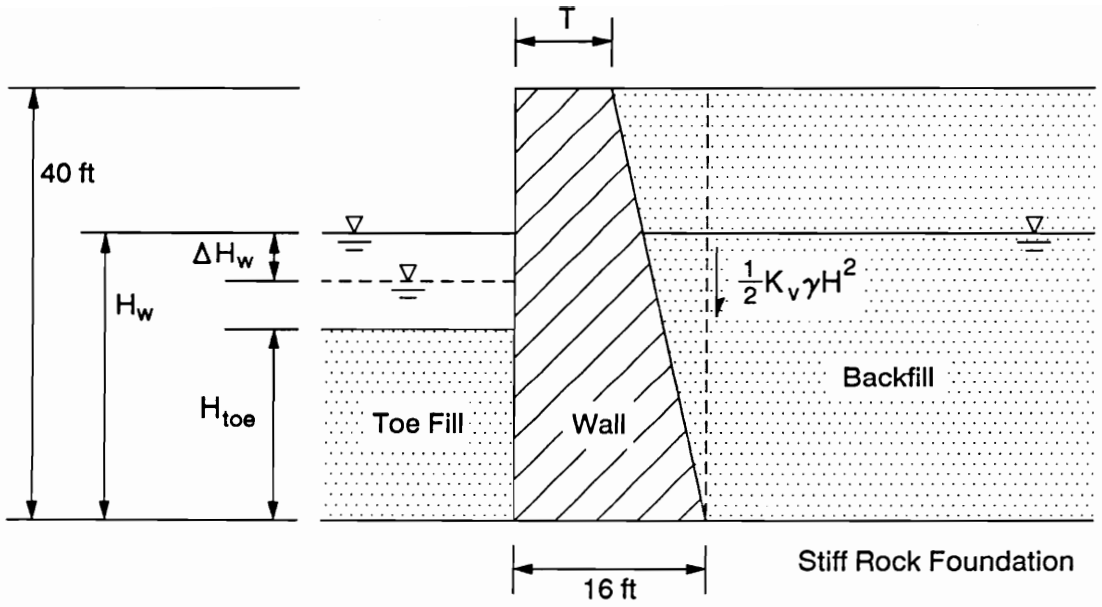

a) Sloped back

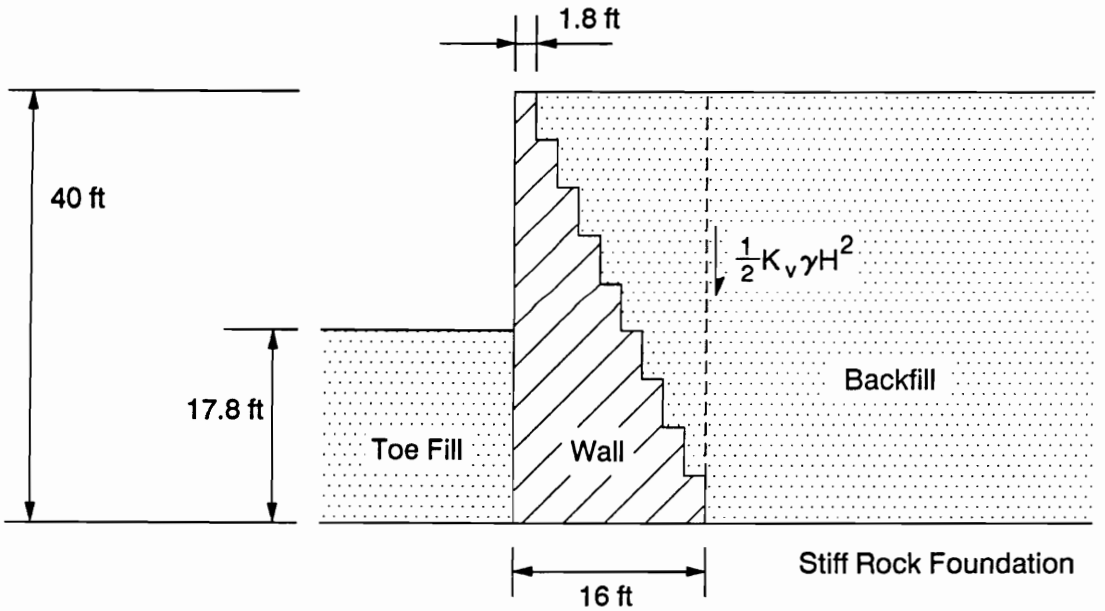

b) Stepped back

Figure 8.7: Wall Configurations Studied by Ebeling et al. (1988) and Ebeling et al. (1989)

TABLE 8.3: Constant Parameter Values for the Finite Element Analyses of Walls on Rock Foundations (after Ebeling et al. 1988, and Ebeling et al. 1989)

Parameter	Value
Internal friction angle of backfill, ϕ'	39 degrees
Young's modulus exponent of backfill, $n^{(1)}$	0.4
Failure ratio of backfill, $R_f^{(1)}$	0.7
Interface friction angle at wall-backfill contact, δ	31 degrees
Unit weight of concrete, γ_c	150 pcf
Modulus of elasticity of concrete, E_c	3×10^6 psi
Poisson's ratio of concrete, ν_c	0.2
Modulus of elasticity of rock, E_r	3×10^6 psi
Poisson's ratio of rock, ν_r	0.2

Note: 1) These parameters are used in the hyperbolic stress-strain formulation of Duncan and Chang (1970).

TABLE 8.4(a): Finite Element Analyses of Gravity Walls on Rock Foundations (after Ebeling et al. 1988, and Ebeling et al. 1989)

Run	Backfill Properties			Interface Shear Stiffness (pci)		Geometry			Wall Restrained	Water Levels		K_v
	Poisson's Ratio	Unit Weight (pcf)	K(1)	Wall-Rock	Wall-Soil(2)	H_{toe} (feet)	T (feet)	Stepped Back Face		H_w (feet)	ΔH_w (feet)	
13	0.15	135	450	10,000	20-300	0	8	N	N	0	0	0.14
14	0.30	135	450	10,000	20-300	0	8	N	N	0	0	0.13
15	0.38	135	450	10,000	20-300	0	8	N	N	0	0	0.13
16	0.15	120	450	10,000	20-300	0	8	N	N	0	0	0.14
17	0.15	135	450	10,000	20-300	17.8	8	N	N	0	0	0.14
18	0.15	135	450	10,000	20-300	17.8	8	N	Y	0	0	0.14
19	0.15	135	450	10	20-300	17.8	8	N	N	0	0	0.14
20	0.15	135	200	10,000	20-300	17.8	8	N	N	0	0	0.14
21	0.15	135	1200	10,000	20-300	17.8	8	N	N	0	0	0.12
22	0.15	135	2500	10,000	20-300	17.8	8	N	N	0	0	0.08

Notes: 1) K is the Young's modulus number in the hyperbolic stress-strain formulation of Duncan and Chang (1970).

2) The wall-soil interface shear stiffness varies with confining pressure.

TABLE 8.4(b): Finite Element Analyses of Gravity Walls on Rock Foundations (after Ebeling et al. 1988, and Ebeling et al. 1989)

Run	Backfill Properties			Interface Shear Stiffness (pci)		Geometry			Wall Restrained	Water Levels		K_v
	Poisson's Ratio	Unit Weight (pcf)	K(1)	Wall-Rock	Wall-Soil(2)	H_{toe} (feet)	T (feet)	Stepped Back Face		H_w (feet)	ΔH_w (feet)	
23	0.15	135	4000	10,000	20-300	17.8	8	N	N	0	0	0.06
24	0.15	135	6000	10,000	20-300	17.8	8	N	N	0	0	0.03
25	0.15	135	450	10,000	17-45	17.8	8	N	N	0	0	0.09
26	0.15	135	450	10,000	23-405	17.8	8	N	N	0	0	0.14
27	0.15	135	450	10,000	20-300	17.8	8	N	N	26.7	0	0.14
28	0.15	135	450	10,000	20-300	17.8	8	N	N	26.7	4.45	0.14
29	0.15	135	450	10,000	20-300	17.8	8	N	N	26.7	8.90	0.14
30	0.15	135	450	10,000	20-300	17.8	16	N	N	0	0	0.21
31	0.15	135	450	10,000	20-300	17.8	1.8	N	N	0	0	0.09
32	0.15	135	450	10,000	20-300	17.8	1.8	Y	N	0	0	0.12

Notes: 1) K is the Young's modulus number in the hyperbolic stress-strain formulation of Duncan and Chang (1970).

2) The wall-soil interface shear stiffness varies with confining pressure.

The K_v values are computed on a vertical plane above the wall heel. For all the analyses except run 30, the back sides of the walls are sloped or stepped, so that the vertical plane above the heel is within the backfill soil, not at the contact between the wall and the soil. For run 30, the back side of the wall is vertical and the K_v value therefore reflects the forces at the wall-backfill contact. This geometry is consistent with that considered in the simple theory described previously, and the K_v value of 0.21 for run 30 is the same as that derived earlier using the simple theory.

Comparing the results for runs 31, 17, and 30 demonstrates the influence of a wedge of flexible soil over the wall heel on the value of K_v. As the width of the wedge of flexible soil increases, the value of K_v decreases from 0.21, for no wedge of soil, to 0.09, for a large wedge of soil. The influence of the flexible wedge of soil is to reduce shear stresses on the vertical plane where K_v is calculated.

Another important factor influencing K_v values is the backfill stiffness, as indicated by the results of runs 20, 17, 21, 22, 23, and 24. As the backfill stiffness increases, the value of K_v for a wall with a sloped back side decreases from 0.14 to 0.03. The highest values of backfill stiffness used in these cases are higher than the stiffnesses of real backfill materials. Over a realistic range of stiffnesses, the value of K_v ranges from about 0.14 to 0.12, for the condition analyzed. The reason that increasing stiffness results in a decreasing K_v value is that the stiffer soil is less compressible and $\tan\delta_{mob}$ is smaller.

Increasing the value of Poisons ratio, which might be anticipated to have an effect similar to the effect of increasing the soil stiffness, in fact does not cause a significant change in K_v values, as indicated by the results of runs 13, 14, and 15. The reason for this outcome is that increasing Poisons ratio causes two compensating effects on vertical shear loads: 1) the compressibility decreases so that $\tan\delta_{mob}$ decreases, and 2) the lateral stresses increase so that K_h increases.

Comparing the results of runs 17 and 25 shows that a large decrease in the wall-backfill interface stiffness causes a decrease in the K_v value from 0.14 to 0.09, for the condition analyzed. In the limit, the K_v value for a wall with a completely lubricated, vertical back side would be zero.

The results in Table 8.4 show that another variable that has an appreciable effect on K_v values is whether the back of the wall is stepped or planar. The results of runs 31 and 32 show that the K_v value increases from 0.09 to 0.12 when the back of the wall has 9 steps. The reason for the difference is that the stepped back side provides more firm support for the wedge of soil between the wall and the vertical plane above the wall heel.

The other results in Table 8.4 show that K_v values are not significantly influence by the unit weight of the backfill, the wall-rock interface stiffness, the presence of a toe fill, water levels behind and in front of the wall, or compete restraint of the wall. It should be noted that the potential influence of some of these variables

on K_v values may be dampened due to the existence of the wedge of soil between the wall and the vertical plane above the wall heel in the base case.

8.3.2 Walls on Soil Foundations

Regalado et al. (1992) studied gravity walls and cantilevered walls on soil foundations. As part of this work, the alpha method developed by Ebeling et al. (1988) for interface elements was extended to include 2-D soil elements. The method was shown to yield good agreement with limit equilibrium calculations for walls in the full active condition.

The wall configurations studied by Regalado et al. (1992) are shown in Figure 8.8. In every case, the wall studied was 30 feet high and was founded on a 30-foot thick soil foundation. The base case, to which the other analyses can be compared, was a concrete gravity wall, 18 feet wide at the base, 9 feet wide at the top, and with a sloped back side. In the base case, the foundation and backfill soils were both dense sands, and there was no toe fill. The following parameter values were varied in the analyses: the shear stiffness of the interface between the wall and the foundation, the foundation soil type, the backfill soil type, the width of the base, the water level in the foundation, steps in the back side of gravity walls, and stem position in cantilevered walls. The constant parameter values, and values of the parameters that were varied, are listed in Tables 8.5 and 8.6. The K_v

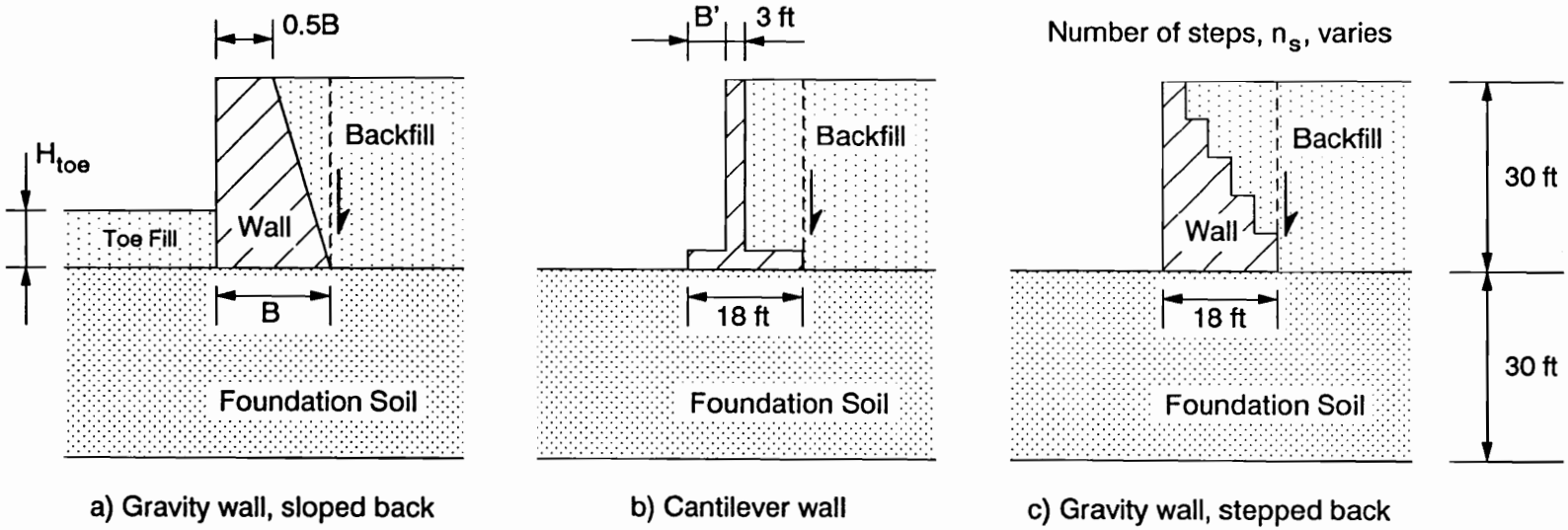

Figure 8.8: Wall Configurations Studied by Regalado et al. (1992)

TABLE 8.5: Parameter Values for Analysis of Gravity Walls on Soil Foundations (after Regalado et al. 1992)

Constant Parameters

Geometric

- $H = D_f = 30$ ft
- B_t/B = Ratio of width of top of wall to width of base of wall = 0.5

Material

- K_n = Normal stiffness of wall-base interface elements = 5.18×10^9 pcf
- γ_c = Unit weight of concrete = 150 pcf
- E_c = Modulus of elasticity of concrete = 4.3×10^8 pcf
- ν_c = Poisson's ratio of concrete = 0.20

Variable Parameters

Geometric

- B = Base width of wall
- h_t = Height of toe fill

Material

- K_s = Shear stiffness of wall-base interface elements elements
- D_r = Relative density for cohesionless backfill/ foundation soils
- RC, w% = Relative Compaction and Water content for cohesive backfill/foundation soils

Run No.	Base Int. El. K_s (pcf)	Fd'n D_r	Backfill D_r	Fd'n RC	Backfill RC	B (ft)	h_t (ft)	Comments
BFBC	1.64×10^5	75	75	-	-	18	0	Base Case
BF1A	(1.10×10^5)	75	75	-	-	18	0	Low K_s
BF1B	(2.20×10^5)	75	75	-	-	18	0	High K_s
BF2A	1.50×10^5	(50)	75	-	-	18	0	Medium Dense Sand Foundation
BF2B	1.80×10^5	(100)	75	-	-	18	0	Very Dense Sand Foundation
BF2C	1.64×10^5	75	75	-	-	18	0	Water Table at ground level
BF3A	1.64×10^5	75	(25)	-	-	18	0	Loose Sand Backfill
BF3B	1.64×10^5	75	(50)	-	-	18	0	Medium Dense Sand Backfill
BF3C	1.64×10^5	75	(100)	-	-	18	0	Very Dense Sand Backfill
BF3D	1.64×10^5	75	75	-	-	18	(9)	With Toe Fill
BF4A	1.64×10^5	75	75	-	-	(15)	0	B/H = 0.5
BF4B	1.64×10^5	75	75	-	-	(21)	0	B/H = 0.7
BF4C	1.64×10^5	75	75	-	-	(24)	0	B/H = 0.8
BF5A	1.42×10^5	-	75	(100)	-	18	0	SM-SC Foundation, 2% dry of opt.
BF5B	1.42×10^5	-	75	(95)	-	18	0	SM-SC Foundation, 2% wet of opt.
BF5C	1.54×10^5	-	75	(100)	-	18	0	CL Foundation, 2% dry of opt.
BF5D	1.30×10^5	-	75	(95)	-	18	0	CL Foundation, 1% wet of opt.
BF6A	1.64×10^5	75	-	-	(100)	18	0	SM-SC Backfill, 2% dry of opt.
BF6B	1.64×10^5	75	-	-	(95)	18	0	SM-SC Backfill, 2% wet of opt.
BF6C	1.64×10^5	75	-	-	(100)	18	0	CL Backfill, 2% dry of opt.
BF6D	1.64×10^5	75	-	-	(95)	18	0	CL Backfill, 1% wet of opt.

Note : Values in ( ) indicate a value other than the base case value

Hyperbolic parameters/properties used for soils

USC Class.	RC	w (%)	D_r (%)	K	n	K_b	m	ϕ	K_o	γ_s (pcf)	R_f
SW, SP	-	-	100	600	0.4	175	0.2	42°	0.33	145	0.70
SW, SP	-	-	75	450	0.4	125	0.2	39°	0.37	140	0.70
SW, SP	-	-	50	300	0.4	75	0.2	36°	0.41	135	0.70
SW, SP	-	-	25	200	0.4	50	0.2	33°	0.46	130	0.70
SM-SC	100	2% dry of opt	-	700	0.4	300	0.2	33°	.46	130	0.80
SM-SC	95	2% wet of opt	-	150	0.8	100	0.8	33°	.46	125	0.65
CL	106	2% dry of opt	-	700	0.1	350	0.0	30°	.50	115	0.70
CL	102	1% wet of opt	-	150	0.5	200	0.0	30°	.50	110	0.60

TABLE 8.6: Parameter Values for Analysis of Cantilevered and Stepped Back Walls on Soil Foundations (after Regalado et al. 1992)

Constant Parameters

Geometric

- H = Overall height of the wall = 30 feet
- B/H = Ratio of width of base of wall to the height of wall = 0.6
- t_b/H = Ratio of the thickness of the base slab to the height of the wall = 0.1 (cantilever walls only)
- t_w/H = Ratio of the thickness of the wall stem to the height of the wall = 0.1 (cantilever walls only)

Material

- K_n = Normal stiffness of wall-base interface elements = 5.18×10^9 pcf
- K_s = Shear stiffness of wall-base interface elements = 5.18×10^9 pcf
- γ_c = Unit weight of concrete = 150 pcf
- E_c = Modulus of elasticity of concrete = 4.3×10^8 pcf
- ν_c = Poisson's ratio of concrete = 0.20
- D_r = Relative density for cohesionless backfill/ foundation soils = 75 %

Variable Parameters

Geometric

- B' = Length of toe projection (Cantilever Walls only)
- n_s = Number of "steps" on wall face (Stepped-face walls only)

Run No.	B'(ft)	n_s	Comments
BF7A	0	-	Cantilever Wall; B'/B = 0.00
BF7B	3	-	Cantilever Wall; B'/B = 0.17
BF7C	6	-	Cantilever Wall; B'/B = 0.33
BF7D	9	-	Cantilever Wall; B'/B = 0.50
BF7E	12	-	Cantilever Wall; B'/B = 0.67
BF7F	15	-	Cantilever Wall; B'/B = 0.83
BF8A	-	2	Stepped-face Wall; n_s = 2
BF8B	-	5	Stepped-face Wall; n_s = 5
BF8C	-	10	Stepped-face Wall; n_s = 10

values from the analyses are listed in Table 8.7 for gravity walls and Table 8.8 for cantilevered walls.

The K_v value from the base case, run BFBC, in Table 8.7 was 0.07. The base case was similar in most respects to run 13 of Ebeling et al. (1988), except that the wall height was 30 feet and the foundation was soil in run BFBC, whereas the wall height was 40 feet and the foundation was rock in run 13. The K_v value from run 13 was 0.14. Based on the theoretical results in Figure 8.6, it is expected that the K_v value for a 30-foot high wall on rock would not be much less than the value for a 40-foot high wall. Thus, the effect of a soil foundation was to decrease the K_v value by about half for the case of a gravity wall with a sloped back side. The presence of a soil foundation permits significant settlement of the wall during backfilling. Wall settlement is related to differential movement between the backfill and the wall and, consequently, influences the development of shear stresses above the wall heel.

Comparisons within the group of analyses performed for walls on soil foundations indicate that the most important of the parameters studied are the backfill type and the number of steps in the back side of gravity walls. When the backfill was a relatively compressible silty or clayey soil, the K_v values range from 0.16 to 0.22, compared to the value of 0.07 obtained for the base case of a dense sand backfill. The higher compressibility of the backfill, with higher associated $\tan\delta_{mob}$ values was the main cause of the increased K_v values. However, for the wet clayey backfill soil, which produced the highest K_v value, 0.22, the

TABLE 8.7: Finite Element Analyses of Gravity Walls on Soil Foundations (after Regalado et al. 1992)

Run	Variation from Base Case	K_v
BFBC	None	0.07
BF1A	Low interface shear stiffness between wall and foundation	0.06
BF1B	High interface shear stiffness between wall and foundation	0.05
BF2A	Medium dense sand foundation	0.08
BF2B	Very dense sand foundation	0.08
BF2C	Ground water level at the ground surface	Unstable
BF3A	Loose sand backfill	0.05
BF3B	Medium dense sand backfill	0.07
BF3C	Very dense sand backfill	0.04
BF3D	With a dense sand toe fill, H_{toe} = 9 feet	0.10
BF4A	Narrow base, B = 15 feet	Unstable
BF4B	Wide base, B = 21 feet	0.07
BF4C	Very wide base, B = 24 feet	0.15
BF5A	SM-SC foundation soil, 2% dry of optimum	0.09
BF5B	SM-SC foundation soil, 2% wet of optimum	0.08
BF5C	CL foundation soil, 2% dry of optimum	0.09
BF5D	CL foundation soil, 1% wet of optimum	0.10
BF6A	SM-SC backfill soil, 2% dry of optimum	0.16
BF6B	SM-SC backfill soil, 2% wet of optimum	0.16
BF6C	CL backfill soil, 2% dry of optimum	0.18
BF6D	CL backfill soil, 1% wet of optimum	0.22
BF8A	Stepped back face, n_s = 2	0.20
BF8B	Stepped back face, n_s = 5	0.13
BF8C	Stepped back face, n_s = 10	0.10

TABLE 8.8: Finite Element Analyses of Cantilevered Walls on Soil Foundations (after Regalado et al. 1992)

Run	Variation from Base Case	K_v
BF7A	Cantilever Wall, B′ = 0 ft	0.06
BF7B	Cantilever Wall, B′ = 3 ft	0.10
BF7C	Cantilever Wall, B′ = 6 ft	0.09
BF7D	Cantilever Wall, B′ = 9 ft	0.10
BF7E	Cantilever Wall, B′ = 12 ft	0.11
BF7F	Cantilever Wall, B′ = 15 ft	Unstable

lateral earth force coefficient, K_h, was also significantly higher than for the dense sand backfill. These results should be taken with some caution since there is a question regarding the ability of the silty and clayey soils to maintain the shear stresses over time due to the effects of creep and stress relaxation. Also, experience shows clearly that walls backfilled with clayey soils often undergo large movements and suffer other problems.

The results of runs BF8A, BF8B, and BF8C indicate that the value of K_v increased progressively from 0.10 to 0.20 as the number of steps on the back side of the wall decreased from 10 to 2. The K_v value of 0.07 for the base case with the sloped back side was consistent with this progression. As mentioned previously for the analyses of walls on rock foundations, the reason for the increase was that the stepped back side provided more firm support for the wedge of soil between the wall and the vertical plane above the wall heel. It is interesting that the value of K_v approached the value of $K_{v,ult}$ as the number of steps decreased. If the number of steps was equal to one, the back side of the wall would be vertical. Thus, even though foundation flexibility did have an important influence on K_v values for walls with sloped back sides, it does not appear that foundation flexibility would cause a significant decrease in K_v values for gravity walls with vertical back sides. One possible reason for the difference is that the backfill compression which is most important for developing relative displacement between backfill and wall, and for developing the accompanying shear stresses, may occur close to the back of vertical walls. Additional

runs using gravity walls with vertical back sides should be made to confirm this.

The other results in Tables 8.7 and 8.8 show that the remaining factors that influence K_v values were less important than the backfill type and the number of steps in the back side of a gravity wall. Some of the results showed scatter that may be related to compensating effects as changes in material type were modelled. For example, the results from runs BF3A, BF3B, and BF3C indicate that the value of K_v increased and then decreased as the sand backfill density increased from a loose state through a medium dense state to a very dense state. In modelling increases in density, the unit weight increases, which tends to cause an increase in settlement. On the other hand, increasing density also causes an increase in stiffness, which tends to decrease settlements. Because these factors tend to counteract, reversals in the trends of the results can occur.

8.4 Shear Force Measurements

Vertical shear forces were measured during the instrumented retaining wall tests. The measured values are expressed in terms of the vertical shear force coefficient in Table 8.9, at the end of filling and approximately four days later. To facilitate understanding of the factors that influence the values of the measured vertical shear forces, the values of K_h and $\tan\delta_{mob}$ that yield the value of K_v according to Eqn 8.25 are also listed in the table.

TABLE 8.9: Earth Force Coefficient Measurements

Test Number	Soil Type(1)	Water Content (%)	Cmpctr Type(2)	No. of Lubed Walls(3)	At End of Filling			Four Days after Filling(4)		
					K_h	$\tan\delta_{mob}$	K_v	K_h	$\tan\delta_{mob}$	K_v
EP 5	YSS	9.3	Vib(5)	2	0.41	0.41	0.17	0.39	0.53	0.21
EP 6	YSS	9.7	Vib	2	0.31	0.58	0.18	0.25	0.83	0.21
EP 7	YSS	11.1	Vib	0	0.29	0.60	0.17	0.25	0.85	0.21
EP 8	YSS	12.1	Vib	2	0.27	0.74	0.20	0.23	1.02	0.23
EP 9	YSS	12.5	Vib	2	0.32	0.69	0.22	0.24	0.98	0.23
EP 10	YSS	11.8	Vib	3	0.37	0.03	0.01	0.31	0.08	0.03
EP 11	YSS	13.5	Vib	0	0.38	0.70	0.26	0.28	0.85	0.24
EP 12	YSS	12.3	Vib	2	0.33	0.69	0.23	0.27	0.87	0.23
EP 13	YSS	12.7	Ram	2	1.03	0.03	0.03	0.79	0.17	0.13
EP 14	YSS	10.1	Ram	2	0.84	0.15	0.13	0.74	0.19	0.14
EP 15	LCS	0.0	Ram	2	0.76	0.15	0.11	0.75	0.15	0.11
EP 16	LCS	0.0	Vib	2	0.45	0.27	0.12	0.46	0.26	0.12

Notes: 1) YSS indicates Yatesville silty sand. LCS indicates Light Castle sand.

2) Vib indicates the Wacker BPU2440A vibrating plate compactor. Ram indicates the Wacker BS60Y rammer compactor.

3) 2 indicates that the end wall and the wall opposite from the instrumented wall are lubricated. 3 indicates that the instrumented wall, the end wall, and the wall opposite from the instrumented wall are all lubricated.

4) The measurements for test EP 15 were taken 1.6 days after filling.

5) The Bobcat loader was operated on the backfill during backfill placement in test EP 5.

The K_v values for Yatesville silty sand compacted with the vibrating plate compactor are about 0.2, except for test EP 10 in which the instrumented wall was lubricated and the K_v value was consequently very low. With time after filling, the K_h values decreased slightly, probably due to relaxation of compaction induced stresses or to decrease in pore water pressures, and the $\tan\delta_{mob}$ values increased due to settlement of the backfill. The result is that the K_v values remained approximately constant, or increased slightly with time after filling.

The details of development of the K_v values during backfilling, and their change with time after filling, are shown in Figure 8.9 for tests EP 8 and 9. When the fill heights are low, the effects of compaction produce large K_h values, and small settlements produce small $\tan\delta_{mob}$ values. As the fill height increases, the value of K_h decreases and the value of $\tan\delta_{mob}$ increases, so that the value of K_v remains approximately constant. The situation during filling is very similar to the theoretical results shown in Figures 8.6(d) through 8.6(f). With time after filling, the K_h values decrease, the $\tan\delta_{mob}$ values increase, and the K_v values remain approximately unchanged.

When the rammer compactor was used on either the Yatesville silty sand or the Light Castle sand, the K_h values were very high, the $\tan\delta_{mob}$ values were very low, and the K_v values were low. Part of the reason that the $\tan\delta_{mob}$ values were low is that the rammer compactor produced dense, relatively incompressible backfill. However, another reason that the $\tan\delta_{mob}$ values were low is that the rammer compactor, with its very high contact force, tended to produce small bearing capacity failures in

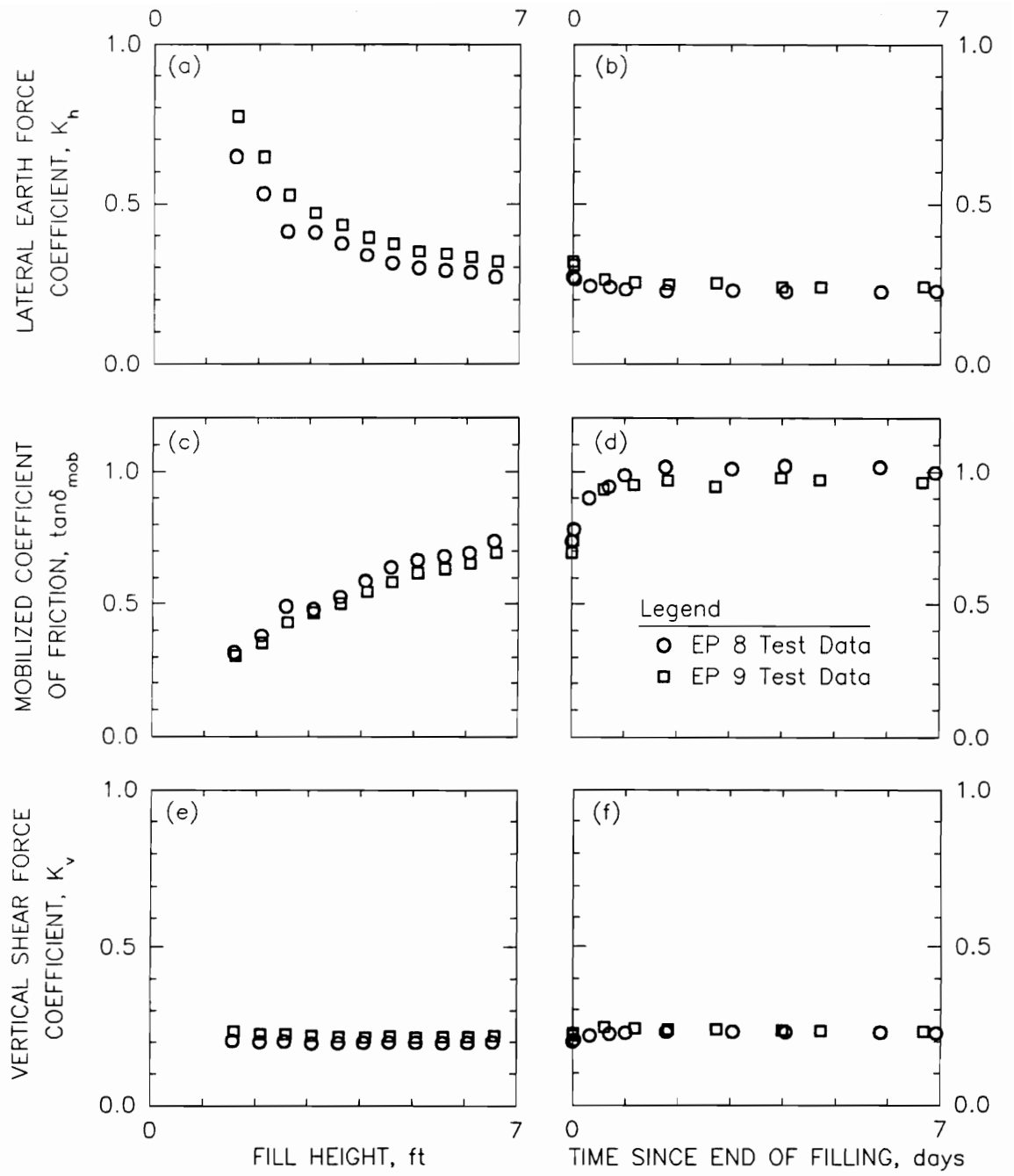

Figure 8.9: Earth Force Coefficients from Tests EP 8 and EP 9

the backfill, causing the soil to flow down beneath the rammer shoe and up in the passive zones beside the rammer shoe. In the pattern used to compact each lift of backfill, the last pass of the rammer was one shoe width away from the wall. This situation left a residual uplift stress on the wall in the uppermost few lifts of backfill. The development of the K_v value in test EP 14 during backfilling, and with time after backfilling, is shown in Figure 8.10. The negative values of $\tan\delta_{mob}$ and K_v shown for fill heights less than 3.5 feet reflect the uplift on the wall induced by the rammer compactor. As the fill height increased, backfill compression mobilized downward shear stresses on the wall and the $\tan\delta_{mob}$ and K_v values increased. The trend of the increase in K_v value with increasing fill height for test EP 14 suggests that a K_v value of 0.2 would have been developed with about 10 to 15 feet of backfill.

Operation of the vibrating plate compactor on the Light Castle sand backfill in test EP 16 also produced uplift on the wall and low K_v values. The dry, cohesionless Light Castle sand may have tended to flow up around the vibrating plate compactor base plate in a way that the moist Yatesville silty sand did not, thus producing a low K_v value at the end of filling in test EP 16.

The data in Table 8.9 show that the forces applied to the wall by the Light Castle were very stable with time. There was almost no relaxation of compaction induced stresses, and almost no creep settlements to increase $\tan\delta_{mob}$ values.

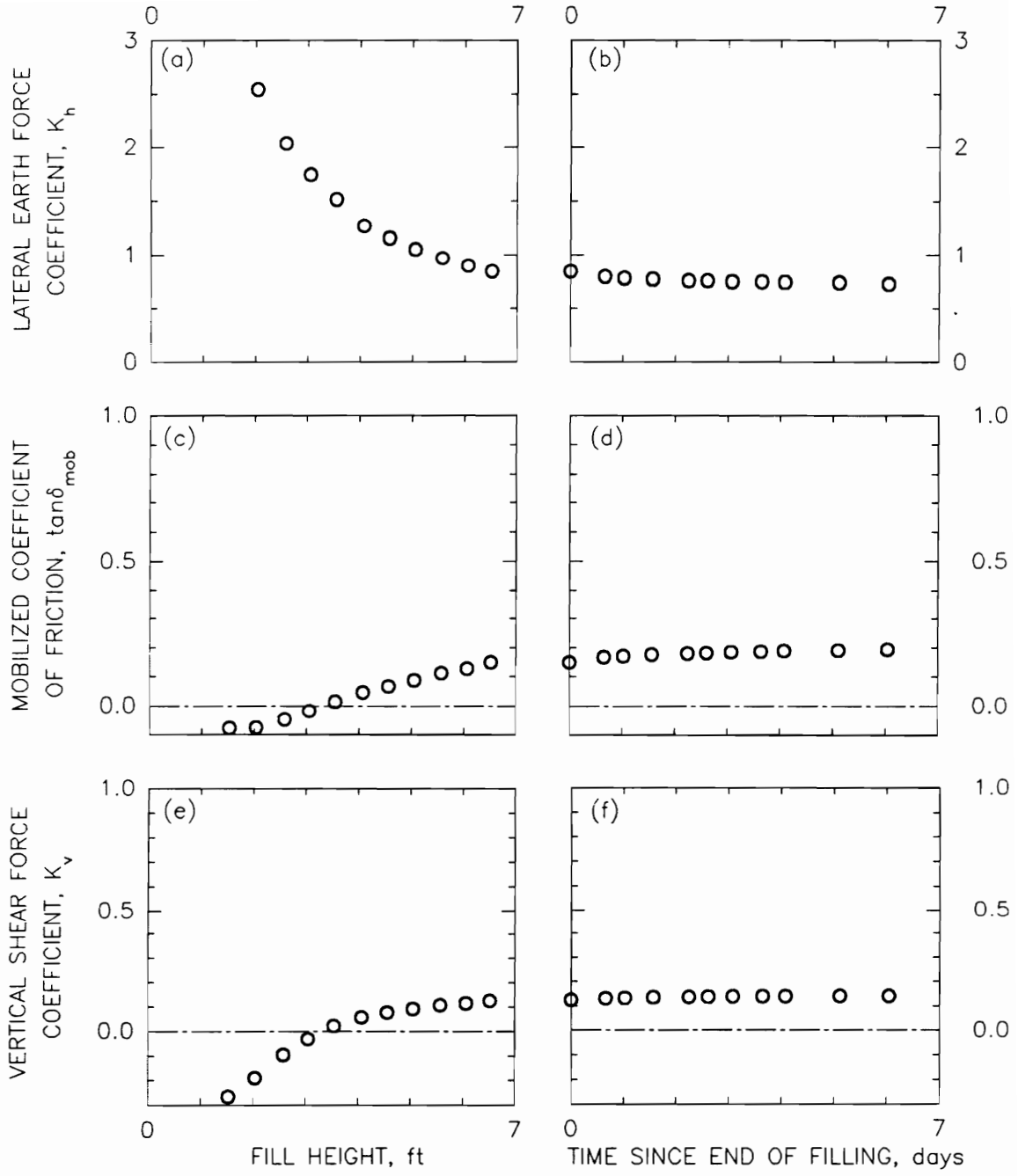

Figure 8.10: Earth Force Coefficients from Test EP 14

8.5 Summary

A theory was developed for calculating vertical shear forces applied by cohesionless backfill to rigid walls with vertical back sides. The theory is based on consideration of the backfill compression and the degree of mobilization of the interface strength between the wall and the backfill. Implications from the theory include the following:

1) The vertical shear force, F_v, increases with increasing backfill height, soil unit weight, lateral stress magnitude, soil compressibility, interface strength, and interface stiffness.

2) When compaction-induced lateral stresses are not considered in the analysis, the value of F_v is proportional to the wall height cubed for walls lower than a critical height. At the critical height, the interface strength becomes fully mobilized at some point along the wall-backfill contact. As the wall height continues to increase above the critical height, more of the interface reaches a failure condition, and the value of F_v approaches proportionality with the wall height squared.

3) When compaction-induced lateral stresses are considered, calculated values of the vertical shear force coefficient, K_v, increase because of the higher lateral earth pressures. Because the overall effect of compaction on lateral stresses decreases with increasing fill height, and because settlement increases with increasing fill height, K_v values can be almost constant over a significant range of wall heights in many cases.

Further studies and experience are needed to determine how the new theory can be used in design of earth retaining walls. In its present stage of development, the theory provides a useful basis for understanding the influence of various factors on the shear force magnitude. The theory suggests that the development of shear forces can be best understood in terms of the following relationship between the dimensionless earth force coefficients:

$$K_v = K_h \tan\delta_{mob} \quad (8.25)$$

In Eqn 8.25, the value of K_h includes the effects of factors that influence lateral pressures, and the value of $\tan\delta_{mob}$ includes the effects of factors that influence the degree of interface strength mobilization. For instance, compaction increases the value of K_h, and increasing wall height and increasing backfill compressibility increase the value of $\tan\delta_{mob}$. Eqn 8.25 also suggests that the ultimate value of K_v for high walls, $K_{v,ult}$, is about 0.2 for cohesionless backfill soil. Based on theoretical calculations, review of finite element parameter studies, and extrapolation of the instrumented retaining wall tests, this value of K_v will probably develop for walls over 20 feet high that: 1) are rigid, e.g., concrete gravity walls, 2) have vertical back sides, 3) are founded on rock, and 4) are backfilled with cohesionless soil.

The results of finite element parameter studies by Ebeling et al. (1988), Ebeling et al. (1989), and Regalado et al. (1992) were reviewed to assess the influence that several factors have on K_v values. In these studies, the value of K_v is computed on a vertical plane above the heel of the wall. Thus, K_v is evaluated at the wall-backfill contact for walls with vertical back sides, and K_v is evaluated on a plane within the backfill for walls with other configurations. The parametric studies disclosed that:

1) For a 40-foot high gravity wall with a vertical back side, founded on stiff rock, and backfilled with dense, cohesionless soil, the value of K_v is 0.21.

2) The value of K_v decreases for configurations in which the back side of the wall slopes away from the vertical plane above the heel of the wall. This configuration creates a wedge of

flexible soil between the back side of the wall and the vertical plane above the wall heel.

3) Increasing backfill stiffness, which is accompanied by decreasing backfill compressibility, results in decreasing values of K_v.

4) Decreasing interface stiffness results in decreasing values of K_v.

5) A stepped back side configuration results in higher K_v values than for a sloped back side because the steps provide more firm support for the wedge of soil between the wall and the vertical plane above the wall heel.

6) For walls with sloped back sides, a flexible foundation results in lower K_v values than a firm foundation. However, the analyses suggest that foundation flexibility may not cause a large reduction in the value of K_v for gravity walls with vertical back sides. Additional finite element studies could help to verify the latter conclusion.

Force measurements made during the instrumented retaining wall tests show that:

1) For Yatesville silty sand compacted with the vibrating plate compactor, the value of K_v is about 0.2, both during filling and over a four day period following filling. During filling, the value of K_h decreases and the value of $\tan\delta_{mob}$ increases as the backfill height increases, and these compensating effects resulted in an almost constant value of K_v. Similarly, after filling, the value of K_h decreased slightly and the value of $\tan\delta_{mob}$ increased with time, so that the value of K_v remained approximately unchanged.

2) For the rammer compactor operating on both the Yatesville silty sand and the Light Castle sand, and for the vibrating plate compactor operating on the Light Castle sand, operation of the compactors produced uplift stresses on the wall in the near surface lifts. This effect produced low K_v values. Nevertheless, the value of K_v increased with increasing fill height in these tests, and it appears that the value of K_v would approach 0.2 within backfill heights of 20 feet.

CHAPTER 9 - SUMMARY, CONCLUSIONS, AND RECOMMENDATIONS

Accurate estimation of the magnitudes of earth loads on walls is important for designing walls that are safe against instability, structural failure, and excessive deformation. Conventional approaches for calculating earth loads do not represent the important influences of soil-structure interaction effects, nor do they consider the influence of compaction equipment. Neglecting to consider these effects has led to excessively conservative design of walls in some cases, and to inadequate performance in others.

Seed and Duncan (1983), Ebeling et al. (1988), Ebeling et al. (1989), Sehn and Duncan (1990), and Regalado et al. (1992) have studied the influence that these factors have on loads applied by backfill to walls. The studies have shown that the loads depend on backfill behavior, wall characteristics, foundation characteristics, and the compaction equipment used. The research described herein continued the previous studies, focusing on rigid walls with vertical backs.

The purpose of the research was to measure the influences that compaction, soil type, and backfill height have on earth loads on walls, and to compare the measured loads with those expected from analyses.

This chapter presents a summary of the work accomplished, conclusions drawn from the work, and recommendations for further research.

9.1 Summary of the Work Accomplished

The following experimental work was completed:

1) A series of experiments were conducted to determine the cause of drift in pressure cell readings obtained using the instrumented retaining wall facility.

2) A vibrating plate compactor and a rammer compactor were instrumented so that the dynamic force and energy transfer during compaction could be measured. Measurements were made during operation of each compactor on moist Yatesville silty sand and on dry Light Castle sand.

3) Twelve tests were performed using the instrumented retaining wall facility: ten using moist Yatesville silty sand as backfill and two using dry Light Castle sand as backfill. Variables in the testing included the Yatesville silty sand water content, the number of lubricated walls in the test facility, and the compactor type. In all cases, the compacted lift thickness was 6 inches, and the total backfill height was 6.5 feet.

The following analytic work was completed:

1) Models based on Lysmer and Richart's (1966) analog for a dynamically loaded footing were developed for calculating dynamic compactor forces from compactor characteristics and soil properties. Calculated forces were compared to the measured forces.

2) The compaction-induced lateral earth pressure theory of Seed and Duncan (1983) was revised so that the model would be truly hysteretic. In the revised theory, the stress history of a soil element adjacent to the wall consists of a series of

nested stress path loops. The revised theory includes memory erasure when interior stress path loops are exceeded, and when the stress path moves down the passive failure line.

The revised compaction-induced theory was extended to include moist soils with significant fines content. The pore pressure response of partially saturated soil was modelled using Skempton's A and B pore pressure parameters.

Compaction-induced lateral earth pressures calculated using the revised and extended theory were compared to the measured pressures from the instrumented retaining wall tests.

The case histories of damage to Eisenhower and Snell Locks by compaction-induced lateral earth pressures were analyzed using the revised theory, and the calculated pressures were compared to lateral earth pressures measured in-situ.

3) A new theory for calculating vertical shear forces on rigid walls with vertical backs was developed. The theory is based on consideration of backfill compressibility and the degree of mobilization of the interface strength between the backfill and the wall.

Parameter studies performed by Ebeling et al. (1988), Ebeling et al. (1989), and Regalado et al. (1992), using the finite element method, were reviewed in light of the implications from the new vertical shear force theory.

The measured vertical shear forces from the instrumented retaining wall tests were evaluated in terms of the new theory and the results of the parameter studies.

9.2 Conclusions

The conclusions drawn from this research can be grouped into four subject areas: instrumentation behavior, compactor performance, compaction-induced lateral earth pressures, and vertical shear loads on walls. The conclusions concerning instrumentation behavior are:

1) The horizontal and vertical force measurements obtained with the instrumented retaining wall were free from scatter, presumably due to the relatively large contact area of 16 sq. ft. for each panel. The force measurements were also stable over time.

2) The pressure cell measurements obtained with the instrumented retaining wall exhibited both scatter and drift. The scatter was probably due to local variations in backfill conditions that influenced the pressure cell readings because of the small size of the cells. However, there are enough pressure cells in the wall that the pressure distribution on the wall could still be discerned. The pressure cell readings decreased with time after backfill placement. The pressure cell drift occurred because of moisture migration from the backfill to the concrete panels in which the cells are mounted. Significant drift began about one day after contact with moist soil.

3) During backfilling, the horizontal force obtained from the load cell readings agreed with the horizontal force obtained by integrating the pressure cell readings over the backfill height. With time after backfilling, the force from the pressure cell readings drifted below the force from the load cells.

The conclusions concerning compactor performance are:

1) The measured peak dynamic forces ranged from 1030 to 1680 pounds for the Wacker BPU2440A vibrating plate compactor used in this research. These forces are much less than the manufacturer's rating of 5400 pounds.

2) The measured peak dynamic forces ranged from 3520 to 8500 pounds for the Wacker BS60Y rammer compactor used in this research. These forces are generally much higher than the manufacturer's rating of 2775 pounds.

3) Measured energy transfer rates were about 400 ft-lbs/sec for the vibrating plate compactor and about 580 ft-lbs/sec for the rammer compactor.

4) The measured peak contact forces increased with increasing soil stiffness, but the measured transferred energy was approximately independent of soil stiffness.

5) Calculations using the models based on Lysmer and Richart's (1966) analog were in good agreement with the measured contact forces.

The conclusions concerning compaction-induced lateral earth pressures are:

1) The measured lateral earth pressures from compacted Light Castle sand on the instrumented wall were higher than the at-rest pressures calculated using Jaky's (1948) empirical relationship. Higher lateral pressures were measured when the rammer compactor was used to compact the backfill than when the vibrating plate compactor was used.

2) For the dry Light Castle sand, lateral earth pressures calculated using the revised compaction-induced earth pressure theory were in good agreement with the measured pressures.

3) For the moist Yatesville silty sand, the measured lateral earth pressures at the instrumented wall were higher when the rammer compactor was used to compact the backfill than when the vibrating plate compactor was used.

4) For the moist Yatesville silty sand, lateral earth pressures calculated using the revised compaction-induced lateral earth pressure theory without considering pore pressure effects were in fairly good agreement with the measured pressures for two tests in which the degree of saturation of the backfill was about 65 percent.

   For two tests in which the degree of saturation of the backfill was about 85 percent, better agreement could be obtained using the extended compaction-induced earth pressure theory. However, the values of the pore pressure parameters that gave the best agreement between theory and measurements were not the same as the values of the pore pressure parameters obtained from laboratory compression tests at low confining pressures.

5) Analyses of the case histories of Eisenhower and Snell Locks, for which the backfill was compacted glacial till, resulted in fairly good agreement between theory and measurements. Pore pressure effects were not considered in the theoretical calculations.

The conclusions concerning vertical shear forces on retaining walls are:

1) Vertical shear forces increase with increasing backfill height, soil unit weight, lateral stress magnitude, soil

compressibility, interface strength, and interface stiffness. Vertical shear forces on the vertical plane above the heel of a wall decrease as the slope of the back side of the wall becomes more inclined and the wedge of soil between the wall and the vertical plane above the heel becomes larger. When there is a substantial wedge of soil between the wall and the vertical plane above the wall heel, vertical shear forces on the plane above the wall heel decrease with increasing foundation flexibility. On the other hand, when the back side of the wall is vertical, it appears that foundation flexibility may not have a large influence on the magnitude of the vertical shear forces that develop.

2) Theory, finite element parameter studies, and experimental evidence combine to indicate that the value of the lateral earth force coefficient, K_v, is about 0.2 for walls over 20 feet high that: a) are rigid, e.g., concrete gravity walls, b) have vertical back sides, and c) are backfilled with cohesionless soil.

9.3 Recommendations for Further Research

The results of this research suggest that substantial additional benefits could be obtained by accomplishing the following research tasks:

1) Full size roller compactors should be instrumented to measure their dynamic contact force and transferred energy during compaction. This would provide a new and more valuable rating method for compactors that would a) permit calculation of lateral earth pressures on walls, b) permit estimating the in-situ stress state of compacted fills, and c) relate to the standard and modified Proctor test procedures currently used to determine acceptance of compacted fill.

2) Laboratory tests should be performed on specimens of moist soils at a variety of moisture and density conditions to measure the lateral stresses that result from vertical loading under laterally restrained conditions. The tests should be performed over a range of stresses that include the stress states before, during, and after compaction. The test results should be interpreted using the techniques developed in Chapter 6 to establish values of pore pressure parameters for use in the extended compaction-induced earth pressure theory.

3) Additional finite element analyses should be performed to complete the study of factors that influence vertical shear forces on walls. In particular, gravity walls and cantilevered walls of various heights on soil foundations should be analyzed. The gravity wall analyses should include walls with vertical back sides.

REFERENCES

Bishop, A. W. (1966). "The Strength of Soils as Engineering Materials," *Geotechnique*, 16(2), 91-130.

Bishop, I. W., Alpan, I., Blight, G. E., and Donald, I. B. (1960). "Factors controlling the strength of partly saturated cohesive soils," *Proc. ASCE Research Conf. on Shear Strength of Cohesive Soils*, 503-532.

Brandon, T. L., Clough, G. W., and Rahardjo, P. P. (1990). "Evaluation of Liquefaction Potential of Silty Sands Based on Cone Penetration Resistance," Geotechnical Engineering Report, The Charles E. Via, Jr., Department of Civil Engineering, Virginia Polytechnic Institute and State University, Blacksburg.

Broms, B. (1971). "Lateral Earth Pressures Due to Compaction of Cohesionless Soils," Proceedings of the Fourth Budapest Conference on Soil Mechanics and Foundation Engineering, Budapest, 373-384.

Campanella, R. G., and Vaid, Y. P. (1972). "A Simple K_0 Triaxial Cell," *Canadian Geotechnical Journal*, 9(3), 249-260.

Caquot, A., and Kerisel, J. (1948). *Tables for the calculation of passive pressure, active pressure and bearing capacity of foundations*. Transl. from the French by Maurice A. Bec., Paris, Gauthier-Villars, 120 p.

Carder, D. R., Pocock, R. G., and Murray, R. T. (1977). "Experimental Retaining Wall Facility - Lateral Stress Measurements with Sand Backfill," *Laboratory Report 766*, Transport and Road Research Laboratory, Crowthorne, Berkshire, UK.

Carder, D. R., and Krawczyk, J. V. (1975). "Performance of Cells Designed to Measure Soil Pressure on Earth Retaining Structures," *Laboratory Report 689*, Transport and Road Research Laboratory, Crowthorne, Berkshire, UK.

Christiansen, J. F. (1985). "Geotechnical Parameters, Glacial Till Backfill, Eisenhower and Snell Locks, Saint Lawrence Seaway, Massena, New York," Empire Soils Investigations, Inc.

Clough, G. W., and Duncan, J. M. (1969). "Finite Element Analyses of Port Allen Lock and Old River Locks," Report No. TE 69-3, College of Engineering, University of California, Berkeley, 264 p.

Corbett, D. A., Coyle, H. M., Bartoskewitz, R. E., and Milberger, L. J. (1971). "Evaluation of Pressure Cells Used for Field Measurements of Lateral Earth Pressures on Retaining Walls," *Research Report No. 169-1*, Texas Transportation Institute, Texas A&M University, College Station, Texas, September, 1971.

Cornforth, D. H. (1973). "Prediction of Drained Strength of Sands from Relative Density Measurements," ASTM Special Technical Publication 523, 281-303.

Coulomb, C. A. (1776). "An attempt to apply the rules of maxima and minima to several problems of stability related to architecture." *Mem. Acad. Roy. des Sciences*, Paris, 3, 38 p.

Coyle, H. M., and Bartoskewitz, R. E. (1976). "Earth Pressure on Precast Panel Retaining Wall," *Journal of the Geotechnical Engineering Division*, ASCE, 102(5), 441-456

D'Appolonia, D. J., Whitman, R. V. and D'Appolonia, E. (1969). "Sand Compaction with Vibratory Rollers," *Journal of the Soil Mechanics and Foundations Division*, ASCE, 95(1), 263-284.

Duncan, J. M. (1970). "Nonlinear Analysis of Stress and Strain in Soils," *Journal of the Soil Mechanics and Foundations Division*, ASCE, 96(5), 1629-1653.

Duncan, J. M., Williams, G. W., Sehn, A. L., and Seed, R. B. (1991). "Estimating Earth Pressures Due to Compaction," *Journal of the Geotechnical Engineering Division*, ASCE, 117(12), 1833-1847.

Duncan, J. M., and Seed, R. B. (1986). "Compaction-Induced Earth Pressures Under KO-Conditions," *Journal of the Geotechnical Engineering Division*, ASCE, 112(1), 1-22.

Dunnicliff, J. (1988). *Geotechnical Instrumentation for Monitoring Field Performance*, Wiley, New York, 577 p.

Ebeling, R. M., Clough, G. W., Duncan, J. M., and Brandon, T. L. (1988). "Methods of Evaluating the Stability and Safety of Gravity Earth Retaining Structures Founded on Rock, Volume I" The Charles E. Via, Jr., Department of Civil Engineering, Virginia Polytechnic Institute and State University, Blacksburg, 216 p.

Ebeling, R. M., Duncan, J. M., and Clough, G. W. (1989). "Methods of Evaluating the Stability and Safety of Gravity Earth Retaining Structures Founded on Rock, Volume II" The Charles E. Via, Jr., Department of Civil Engineering, Virginia Polytechnic Institute and State University, Blacksburg, 157 p.

Filz, G. M., Clough, G. W., and Duncan, J. M. (1990). "User's Manual for SOILSTRUCT," The Charles E. Via, Jr., Department of Civil Engineering, Virginia Polytechnic Institute and State University, Blacksburg.

Fredlund, D. G. (1979). "Appropriate concepts and technology for unsaturated soils," *Canadian Geotechnical Journal*, 16, 121-139.

Frocht, M. M. (1957). *Photoelasticity*, John Wiley and Sons, New York.

Goodman, R. E., Taylor, R. L., and Brekke, T. L. (1968). "A Model for Mechanics of Jointed Rocks," *Journal of the Soil Mechanics and Foundations Division*, ASCE, 94(3), 637-659.

Hilf, J. W. (1975). "Compacted Fill," in *Foundation Engineering Handbook*, Winterkorn, H. F., and Fang, H. Y., eds., Van Nostrand Reinhold, New York, 244-311.

Hondros, G. (1959). "The evaluation of Poisson's ratio and the modulus of materials of a low tensile resistance by the Brazilian (indirect tensile) test with particular reference to concrete," *Aust. J. Appl. Sci.* 10(3), 243-268.

Jaky, J. (1944). "The Coefficient of Earth Pressure at Rest," *Journal of the Society of Hungarian Architects and Engineers*, 7, 355-358.

Jones, C. J. F. P., and Sims, F. A. (1975). "Earth Pressures Against the Abutments and Wing Walls of Standard Motorway Bridges," *Geotechnique*, The Institution of Civil Engineers, London, 25(4), 731-742.

Krishnayya, A. V. G., and Eisenstein, Z. (1974). "Brazilian Tensile Test for Soil," *Canadian Geotechnical Journal*, 11(4), 632-642.

Krishnayya, A. V. G., Eisenstein, Z., and Morgenstern, N. R. (1974). "Behavior of Compacted Soil in Tension," *Journal of the Geotechnical Engineering Division*, ASCE, 100(9), 441-456.

Lee, I. K., and Ingles, O. G. (1968). "Strength and Deformation of Soils and Rocks," 251-294, in *Soil Mechanics, Selected Topics*, Lee, I. K., ed., Elsevier, New York.

Light Equipment Manufacturer's Bureau (1981a). "Uniform Method for Rating Vibratory Rammers, LEMB Standard No. 1," Construction Industry Manufacturer's Association, Milwaukee.

Light Equipment Manufacturer's Bureau (1981b). "Uniform Method for Rating Vibratory Plates, LEMB Standard No. 2," Construction Industry Manufacturer's Association, Milwaukee.

Lysmer, J., and Richart, F. E., Jr., (1966). "Dynamic Response of Footings to Vertical Loading," *Journal of the Soil Mechanics and Foundations Division*, ASCE, 92(1), 65-91.

Marachi, N. D., Chan, C. K., Seed, H. B., and Duncan, J. M. (1969). "Strength and deformation characteristics of rockfill materials," Report TE-69-5, College of Engineering, University of California, Berkeley.

Mitchell, J. K. (1986). "Practical Problems from Surprising Soil Behavior," *Journal of the Geotechnical Engineering Division*, ASCE, 112(3), 259-289.

Mosher, R. L., Bevins, T. L., and Neeley, B. D. (1991). "Structural Evaluation of Eisenhower and Snell Locks, Saint Lawrence Seaway, Massena, New York," Technical Report ITL-91-4, US Army Corps of Engineers, Waterways Experiment Station, Vicksburg.

Olsen, R. E. (1963). "Effective Stress Theory of Soil Compaction," *Journal of the Soil Mechanics and Foundations Division*, ASCE, 89(2), 27-45.

Peck, R. B. (1991) Personal communication to J. M. Duncan.

Rankine, W. J. M. (1857). "On the stability of loose earth," *Phil. Trans. Roy. Soc.*, London, 147, Part 1, 9-27.

Regalado, L. R., Duncan, J. M., and Clough, G. W. (1992). "Finite Element Analyses of the Safety and Stability of Gravity Earth Retaining Structures Founded on Soil," The Charles E. Via, Jr., Department of Civil Engineering, Virginia Polytechnic Institute and State University, Blacksburg, 294 p.

Roth, W. H., Lee, K. L., and Crandall, L. (1979). "Calculated and Measured Earth Pressures on a Deep Basement Wall," *Proceedings of the Third International Conference on Numerical Methods in Geomechanics*, 3, 1179-1191.

Schmertmann, J. H. (1991). "The Mechanical Aging of Soils," *Journal of the Geotechnical Engineering Division*, ASCE, 117(9), 1288-1330.

Schmertmann, J. H. (1986). "Horizontal Pressures on Eisenhower and Snell Lock Walls," Schmertmann and Crapps, Inc.

Schulze, L. W., Coyle, H. M., and Bartoskewitz, R. E. (1981). "Field Measurements of Earth Pressure on a Cantilever Retaining Wall," *Research Report No. 236-1*, Texas Transportation Institute, Texas A&M University, College Station, Texas, January, 1981.

Seed, R. B. and Duncan, J. M. (1986). "FE Analyses: Compaction-Induced Stresses and Deformations," *Journal of the Geotechnical Engineering Division*, ASCE, 112(1), 23-43.

Seed, R. B., and Duncan, J. M. (1983). "Soil-Structure Interaction Effects of Compaction-Induced Stresses and Deflection," Geotechnical Engineering Research Report No. UCB/GT/83-06, University of California, Berkeley.

Sehn, A. L. and Duncan, J. M. (1990). "Experimental Study of Earth Pressures on Retaining Structures," Geotechnical Engineering Division, Dept. of Civil Engineering, Virginia Polytechnic Institute and State University, Blacksburg.

Skempton, A. W. (1954). "The Pore Pressure Coefficients A and B," *Geotechnique*, 4(4), 143-147.

Smoltczyk, U., Vogt, N., and Hilmer, K. (1979). "Lateral Earth Pressure Due to Surcharge Loads," *Proceedings of the Seventh European Conference on Soil Mechanics and Foundation Engineering*, Brighton, England, 2, 131-139.

Spangler, M. G., and Mickle, J. L. (1956). "Lateral Pressures on Retaining Walls Due to Backfill Surface Loads," *Highway Research Board, Bulletin 141*, National Research Council, Washington, D. C., pp. 1-18.

Toombs, A. F. (1972). "The Performance of Bomag BW 75S and BW 200 Double Vibrating Rollers in the Compaction of Soil," Transport and Road Research Laboratory Report No. LR 480.

Vogt, N., Chara, G., Hilmer, K., Nowack, F., and Grimm, G. (1986). "Auswertung einer zehnjahrigen MeBreihe an der Schleuse Eiback," *Bautechnik*, Ernst and Sohn, Berlin, pp. 305-308.

Whiffen, A. C. (1954). "The Pressures Generated in Soil by Compaction Equipment," Symposium on Dynamic Testing of Soils, Special Technical Publication 156, ASTM, 186-210.

Wright, W. V. (1969). "A Study of Slope Stability and the Undrained Shear Strength of Clay Shales," Ph.D. Dissertation, Department of Civil Engineering, University of California, Berkeley.

Yoo, T-S., and Selig, E. T. (1979). "Dynamics of Vibratory-Roller Compaction," *Journal of the Geotechnical Engineering Division*, ASCE, 105(10), 1211-1231.

APPENDIX A - FIELD AND LABORATORY TESTS ON YATESVILLE SILTY SAND AND LIGHT CASTLE SAND

A.1 Yatesville Silty Sand

Yatesville silty sand is an alluvial soil from the foundation of Yatesville Lake Dam on Blaine Creek in Lawrence County, Kentucky. Prior to using the Yatesville silty sand as backfill in the instrumented retaining wall tests, the material was sieved through a wire mesh with 0.20-inch openings, and the oversize portion was discarded. The resulting soil contains about 40 to 50 percent non-plastic fines and classifies as a silty sand (SM) according to ASTM D-2487.

Some losses of material occurred during each instrumented retaining wall test. After test EP 12 it was necessary to add some soil to make up the necessary volume. The added soil, about 10 percent of the original volume, was obtained from a different batch of Yatesville silty sand that was being used in a concurrent testing program undertaken by Brandon et al. (1990). The added soil is from the same site and has approximately the same particle size distribution and specific gravity of solids as the original batch of Yatesville silty sand. The original batch is referred to as Yatesville silty sand No. 1 (YSS1), and the mixture used for tests EP 13 and 14 is referred to as Yatesville silty sand No. 2 (YSS2). As indicated in subsequent sections of this appendix, it is not possible to distinguish between YSS1 and YSS2 based on either index or strength properties. However, the

addition did influence the moisture-density characteristics, with the maximum dry density of the YSS2 being higher than that of the YSS1.

The following sections describe index property tests, strength tests, consolidation tests, and in-place unit weight measurements made for the Yatesville silty sand.

A.1.1 Particle Size Distribution and Specific Gravity of Solids

The particle size distribution of the Yatesville silty sand was determined in accordance with ASTM D-422 using mechanical sieve and hydrometer methods. The test results are presented in Figure A.1. As shown, there is no significant difference between the results for YSS1 and YSS2. The particle size distribution curves show that the soil is a silty fine sand with about 47 percent passing the No. 200 sieve.

The specific gravity of solids reported by Sehn and Duncan (1990) for YSS1 is 2.66. The specific gravity of solids reported by Brandon et al. (1990) for the added soil is 2.67. As part of this research, the specific gravity of solids was determined in accordance with ASTM D-854 for the YSS2 and found to be 2.67.

A.1.2 Moisture-Density Relations

Moisture-density relations were determined for the YSS1 using the standard Proctor (ASTM D-698) and modified Proctor (ASTM D-1557) compactive efforts. The results are presented in Figure A.2. For the standard Proctor effort, the maximum dry unit weight is 120 pcf and the optimum water content is 12.5 percent. For the modified Proctor effort,

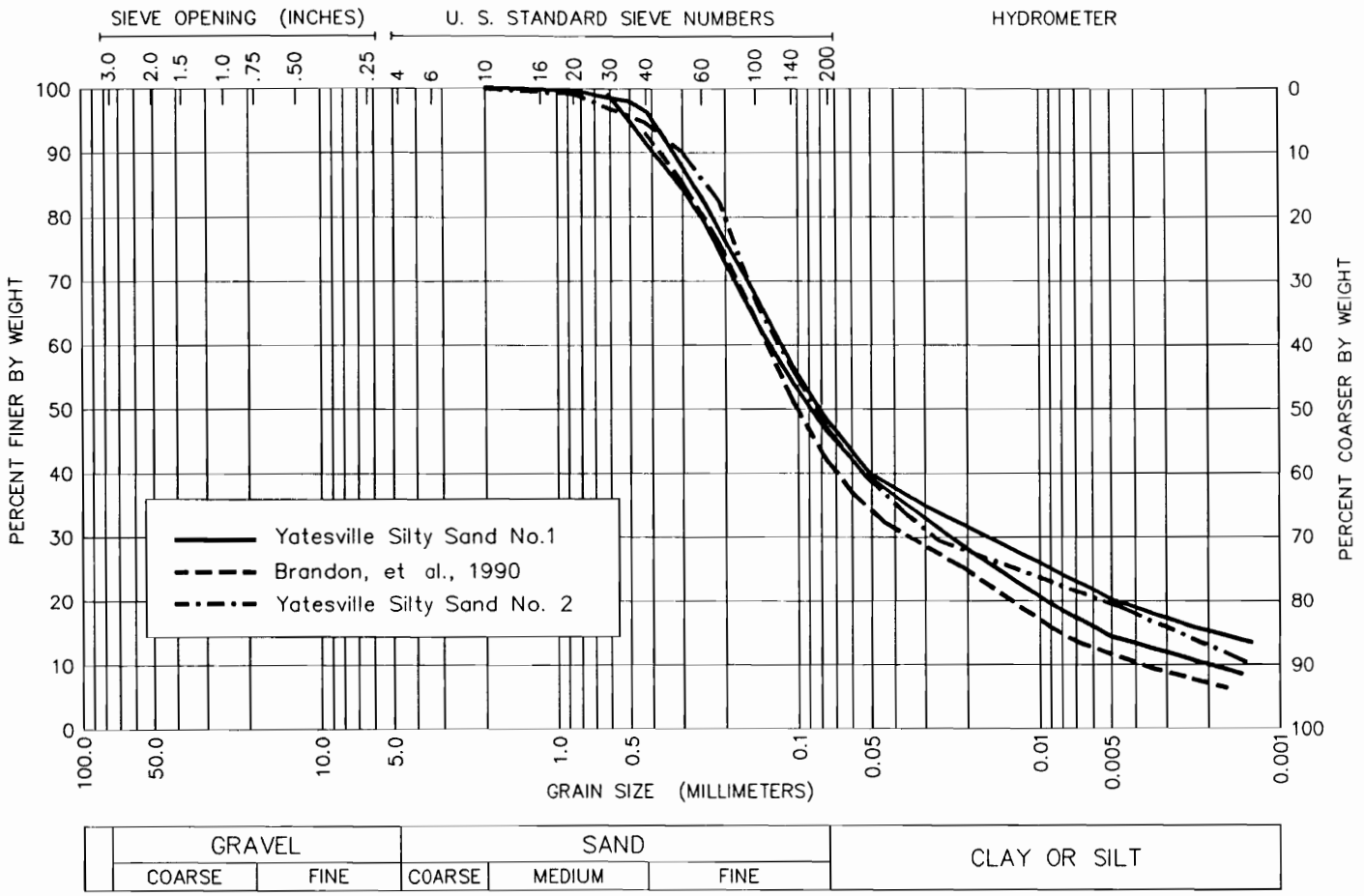

Figure A.1: Grain Size Distribution Curves for Yatesville Silty Sand

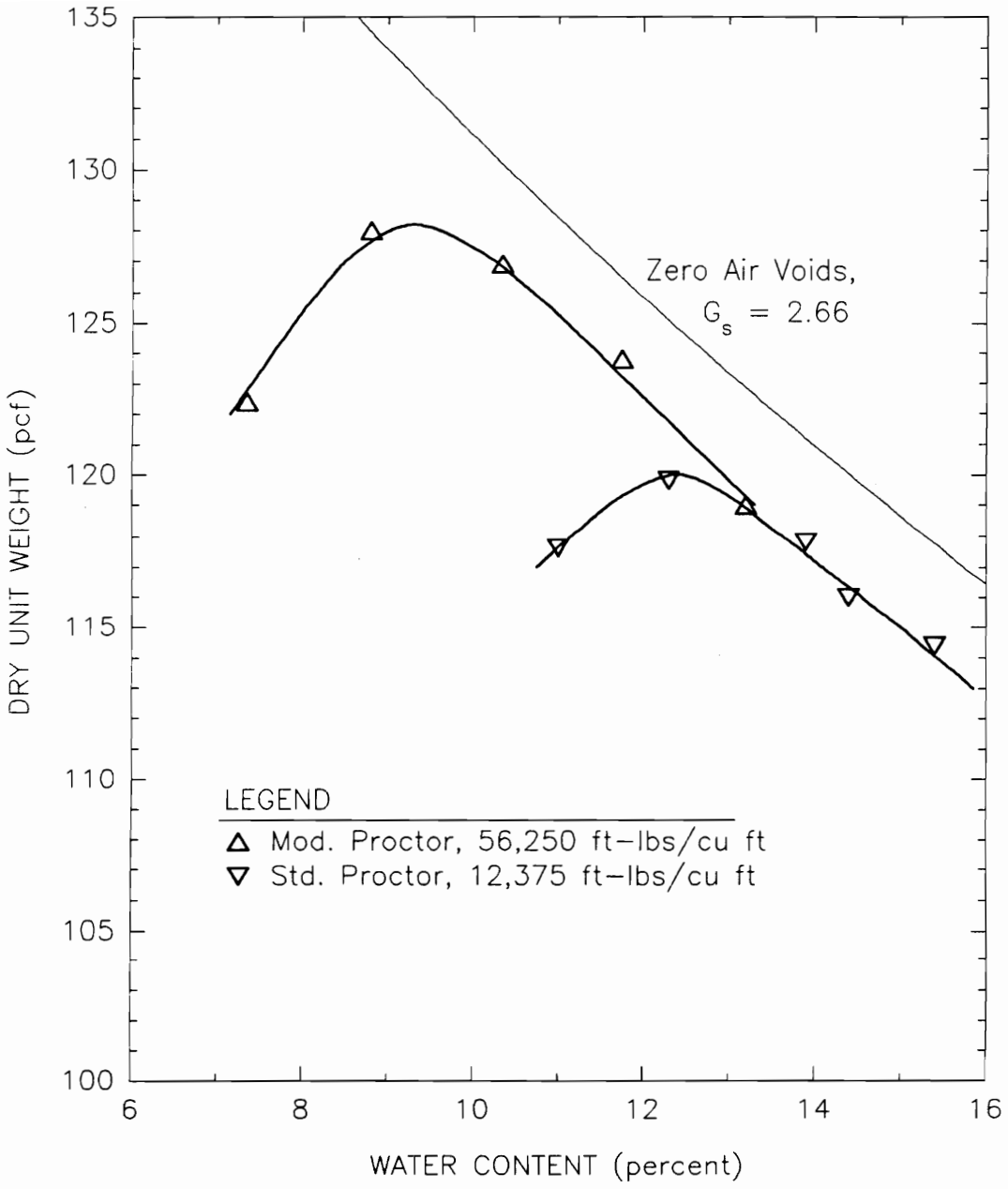

Figure A.2: Moisture-Density Relationships for Yatesville Silty Sand No. 1

the maximum dry unit weight is 128 pcf and the optimum water content is 9 percent.

Moisture-density relations determined for the YSS2 are presented in Figure A.3. As shown, the maximum dry unit weights for the YSS2 are about 4 to 5 pcf higher than for the YSS1 at the same compactive effort. The reason for the difference is unknown, since the materials seem virtually identical in every other respect. In addition to the standard and modified Proctor compactive efforts, two moisture-density curves at compactive efforts below the standard Proctor effort are also shown in Figure A.3. These low effort curves are used in the evaluation of compactor performance discussed in Chapter 5.

A.1.3 In-place Unit Weight Determinations

In-place unit weights of the compacted Yatesville silty sand were measured both by the sand cone method (ASTM D1556) and by weighing and measuring relatively undisturbed specimens obtained using 2.8-inch diameter, thin-wall Shelby tubes. Table A.1 lists the measured densities from instrumented retaining wall tests in which Yatesville silty sand was compacted in 6-inch-thick lifts, that is, tests EP 3 and EP 4 described by Sehn and Duncan (1990) and tests EP 5 through EP 14 described herein. For backfill compacted with the vibrating plate compactor, densities determined by the sand cone method are about 5 percent higher than those determined from Shelby tube specimens. The difference was smaller for backfill compacted with the rammer compactor. The differences in measured densities are probably due to two factors:

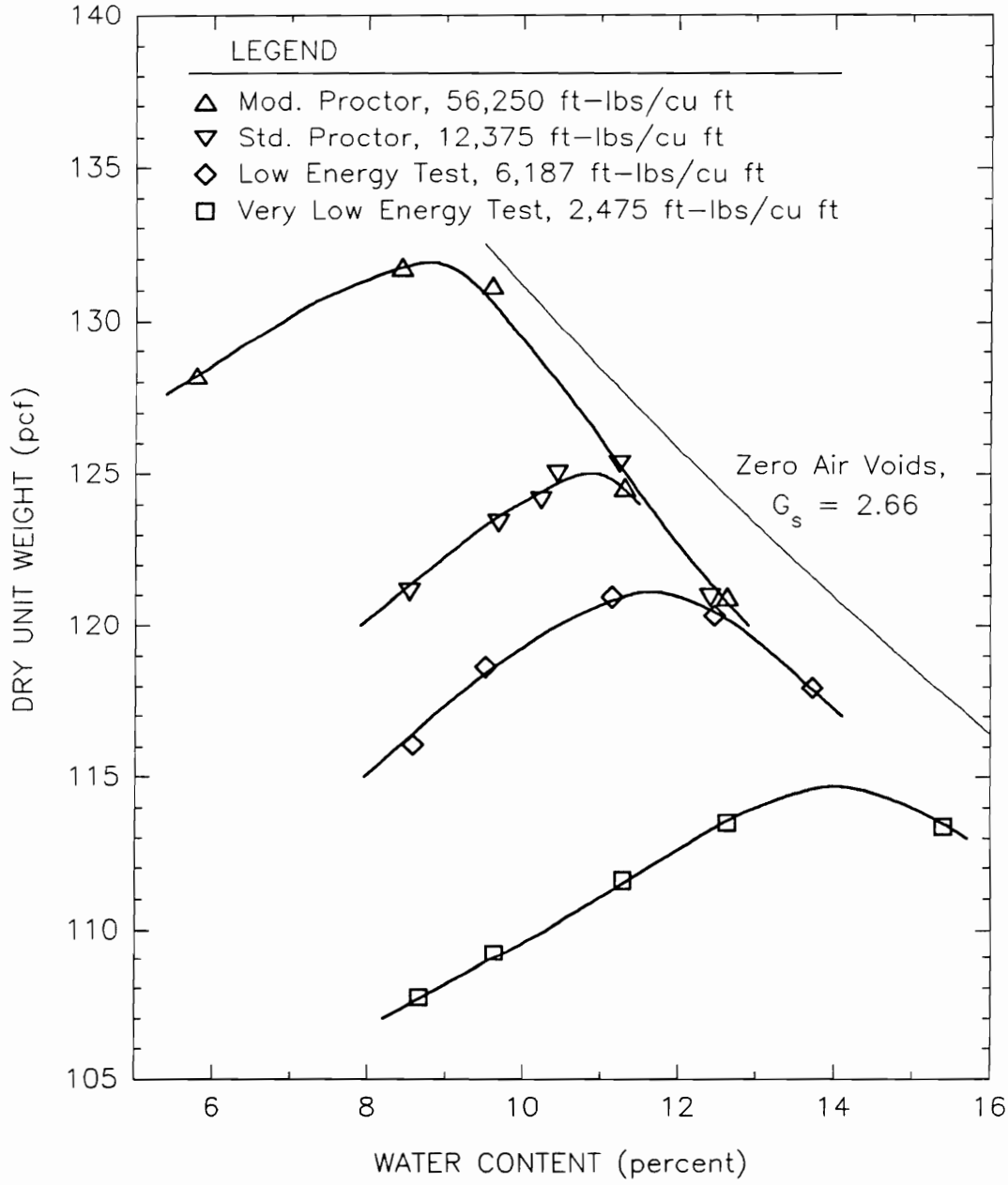

Figure A.3: Moisture-Density Relationships for Yatesville Silty Sand No. 2

TABLE A.1: In-Place Unit Weights, Yatesville Silty Sand

Instrumented Retaining Wall Test Number	Soil Type(1)	Water Content (percent)	Compactor	In-Place Dry Unit Weights (lbs. per cu. ft.)			
				Sand Cone	Corrected Sand Cone(2)	Shelby Tube(3)	Average(4)
EP 3	YSS1	13.7	Vib. Plate	120.0	117.7	110.7	114.2
EP 4	YSS1	10.1	Vib. Plate	106.0	104.0	101.1	102.5
EP 5	YSS1	9.3	Vib. Plate	105.3	103.3	101.7	102.5
EP 6	YSS1	9.7	Vib. Plate	105.3	103.3	100.4	101.9
EP 7	YSS1	11.1	Vib. Plate	111.2	109.1	106.0	107.6
EP 8	YSS1	12.1	Vib. Plate	113.4	111.3	108.6	109.9
EP 9	YSS1	12.5	Vib. Plate	116.9	114.7	110.6	112.7
EP 10	YSS1	11.8	Vib. Plate	114.6	112.5	107.2	109.8
EP 11	YSS1	13.5	Vib. Plate	114.3	112.2	108.4	110.3
EP 12	YSS1	12.3	Vib. Plate	114.3	112.2	108.4	110.3
EP 13	YSS2	12.7	Rammer & Vib. Plate	120.1	119.9	119.2	119.5
EP 14	YSS2	10.1	Rammer & Vib. Plate	120.5	119.7	117.6	118.6

Notes:

1) YSS1 indicates Yatesville silty sand No. 1. YSS2 indicates Yatesville silty sand No. 2.
2) The correction factors (obtained from the results in Table A.2) are 0.981 for tests EP 3 through EP 12, 0.998 for test EP 13, and 0.993 for test EP 14.
3) The values from Shelby tube specimens are the average unit weights from 2.8-inch diameter by 6-inch long specimens.
4) The average unit weight is the average of the corrected sand cone values and the Shelby tube values.

1) density gradients within the compacted lifts and 2) swelling resulting from disturbance and unloading during sampling.

The existence of density gradients in the compacted lifts was discovered during Brazilian tensile testing on 2.8-inch diameter by 1.5-inch high specimens. Specimens from the top of the lifts have higher unit weights than specimens from the middle or bottom of the lifts. The density gradient for test EP 9 is shown in Figure A.4. Density gradients influence unit weights determined by the sand cone method because the sand cone excavation is tapered. In this research, the sand cone excavations each extended through one lift of compacted backfill and were 6.5 inches in diameter at the top and about 1.5 inches in diameter at the bottom. Assuming that the shape of the sand cone excavation is a truncated paraboloid and that the density gradient within the lift is parabolic (as shown by the trend line in Figure A.4), the ratio between the average unit weight and the unit weight determined by the sand cone method can be calculated. Sufficient short specimen data exist to calculate this ratio for the five instrumented retaining wall tests listed in Table A.2. The ratios in Table A.2 are applied to the measured sand cone unit weights in Table A.1 to determine the corrected sand cone unit weights listed in Table A.1.

The corrected sand cone unit weights are about 3 percent greater than the unit weights from Shelby tube specimens. For Shelby tube specimens, swelling due to unloading during removal of the sample and disturbance during trimming tend to decrease unit weights. For example, strains and disturbance corresponding to an increase in diameter from

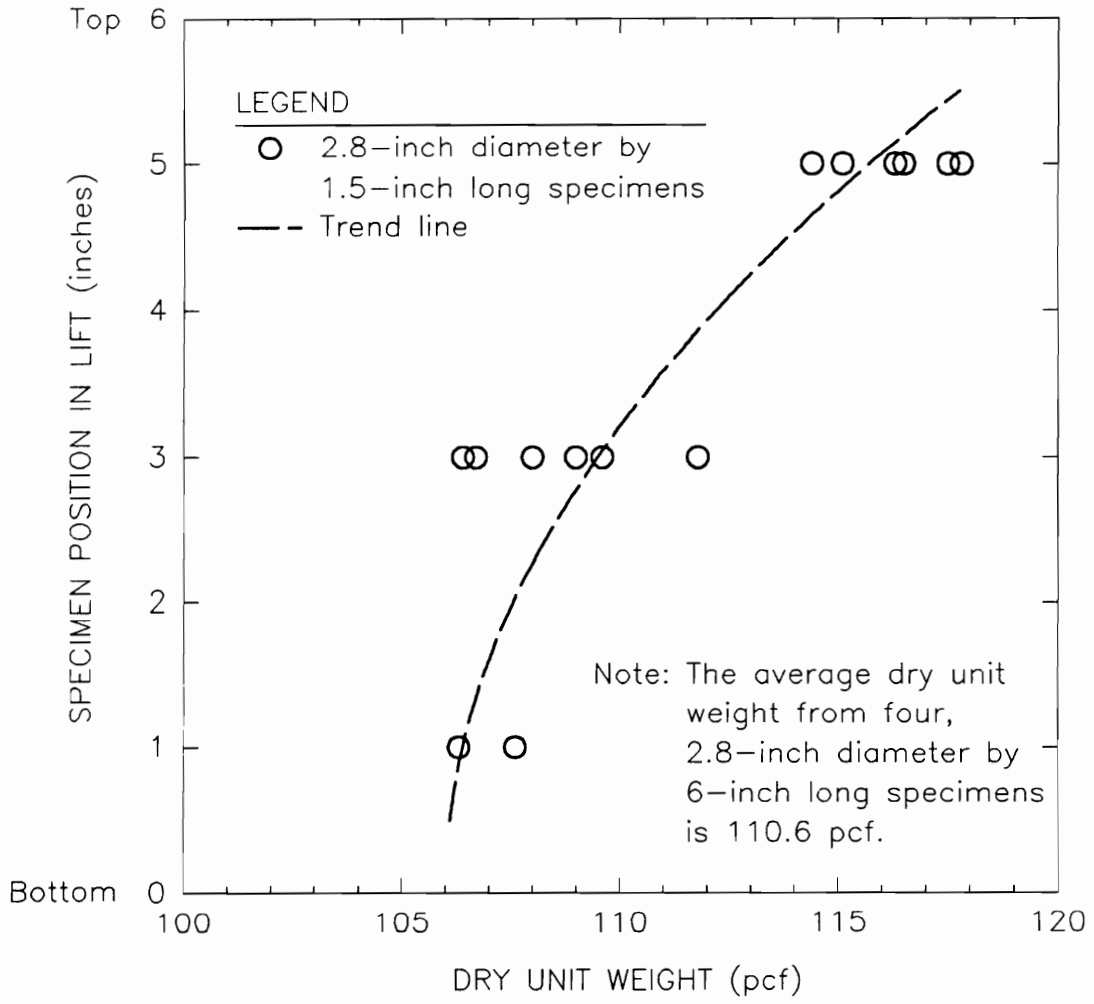

Figure A.4: Density Gradient Within the Compacted Lifts of Test EP 9

TABLE A.2: Correction Factors for Sand Cone Tests

Instrumented Retaining Wall Test Number	Compactor Type	Sand Cone Correction Factor
EP 5	Vib. Plate	0.977
EP 9	Vib. Plate	0.984
EP 12	Vib. Plate	0.984
EP 13	Rammer	0.998
EP 14	Rammer	0.993

Note: 1) The sand cone correction factor is the ratio between the average unit weight of a cylinder of soil to the average unit weight of a truncated paraboloid of soil, which represents the sand cone excavation. The ratio is less than unity when the density decreases with depth in a lift.

2.84 to 2.85 inches are accompanied by a 1 percent decrease in unit weight. For sand cone tests, on the other hand, swelling of the base soil into the excavation increases measured unit weights because the volume used for calculating the unit weight becomes smaller. Since these effects are in opposite directions for the two methods of determining unit weight, the best estimate is obtained by averaging the corrected sand cone unit weight with the value obtained from Shelby tube specimens. The resulting average unit weights are listed in Table A.1.

A.1.4 Unconsolidated-Undrained Triaxial Compression Tests

Unconsolidated-undrained triaxial compression tests were performed on specimens of the Yatesville silty sand obtained from Shelby tube samples taken from the compacted backfill of instrumented retaining wall tests EP 9, EP 13, and EP 14. Because a density gradient exists within the compacted lifts of the Yatesville silty sand, these compression tests were performed on short, 1.5-inch high by 2.8-inch diameter specimens. Bishop (1966) reports triaxial compression test results that show insignificant end restraint effects for specimens with height to diameter ratios as small as 0.5, provided that double lubricated membranes were used at both end platens. Adopting this approach, the end platens of the compression machine were lubricated using two layers of dental dam material. A thin coating of silicone grease was applied between the end platen and the first layer of dental dam, and another thin coating of silicone grease was applied between the two layers of dental dam. Each layer of dental dam was cut into eight pie shaped

wedges to reduce end restraint resulting from the tendency of lateral expansion of the sample to stretch the dental dam material. Because of the low confining pressures in the backfill during the instrumented retaining wall tests, the unconsolidated-undrained tests were performed with confining pressures of 0, 2, and 4 psi, which are the smallest confining pressures practical for the equipment used.

The test results are presented in Table A.3 and Figures A.5 and A.6. The specimens from test EP 9 and EP 13 were at about the same water content, 12.3 percent, so the results are shown together in Figure A.5. The specimens from test EP 14 have an average water content of 9.9 percent, and these results are shown separately in Figure A.6. There is considerable scatter in the data, but the following trends are nevertheless apparent: the strength increases with increasing confining pressure, with increasing unit weight, and with decreasing water content. These trends are as expected. Compressive strength trend lines for confining pressures of 0, 2, and 4 psi have been drawn in Figures A.5 and A.6. These trend lines are not always the very best fit through the data points, but they are consistent with the data and in accordance with expectations. The trend lines in Figures A.5 and A.6 were used to establish the total stress strength parameters shown in Figure A.7. For reference, the effective stress friction angles from Figure A.9, which is discussed in the next section of this Appendix, are also shown. The total stress fiction angles increase with increasing dry unit weight and with decreasing water content. The total stress friction angles are less than the effective stress friction angles. The

TABLE A.3: Unconsolidated-Undrained Compression Test Results for Yatesville Silty Sand[1]

Instrumented Retaining Wall Test Number	Specimen Position[2] (T/M/B)	Dry Unit Weight (pcf)	Water Content (percent)	Confining Pressure (psi)	Deviator Stress at Failure[3] (psi)	Initial Tangent Modulus (psi)
EP 9	M	106.7	12.1	0	11.9	145
	T	115.1	13.2	0	33.1	425
	T	116.5	12.1	0	29.7	460
	M	108.0	12.2	2	16.9	385
	M	109.0	12.4	2	19.0	256
	T	116.5	12.3	2	34.3	444
	M	106.4	12.3	4	16.4	396
	M	111.8	12.3	4	27.4	353
	T	114.4	12.4	4	32.4	294
					Average Modulus	350
EP 13	M	119.2	12.2	0	33.4	470
	T	121.4	11.8	0	39.2	390
	B	119.3	12.5	2	39.0	440
	T	120.0	12.2	2	42.4	485
	M	120.7	11.9	2	45.7	440
	M	118.6	12.7	4	42.2	480
	T	120.2	12.2	4	49.0	495
					Average Modulus	460
EP 14	B	114.5	10.1	0	33.3	800
	T	116.4	9.9	0	35.8	730

TABLE A.3 (Continued): Unconsolidated-Undrained Compression Test Results for Yatesville Silty Sand[1]

Instrumented Retaining Wall Test Number	Specimen Position[2] (T/M/B)	Dry Unit Weight (pcf)	Water Content (percent)	Confining Pressure (psi)	Deviator Stress at Failure[3] (psi)	Initial Tangent Modulus (psi)
EP 14	B	115.3	9.9	2	36.3	1200
	M	116.0	10.0	2	43.5	960
	M	118.0	9.6	2	41.2	850
	T	121.7	10.1	2	55.4	1030
	B	112.2	9.7	4	34.8	1050
	B	118.7	9.9	4	49.8	730
	T	120.6	9.6	4	57.9	870
					Average Modulus	910

Notes:
1) The tests were performed on short (1.5-inch high by 2.8-inch diameter) specimens using lubricated loading platens.

2) T, M, and B refer to the top, middle, and bottom positions within the compacted lifts.

3) Failure is defined at 15 percent axial strain unless the maximum deviator stress occurred prior to 15 percent strain. The 15 percent strain condition controlled for all specimens except the second specimen for test EP 9, for which the maximum stress occurred at an axial strain of 11.2 percent.

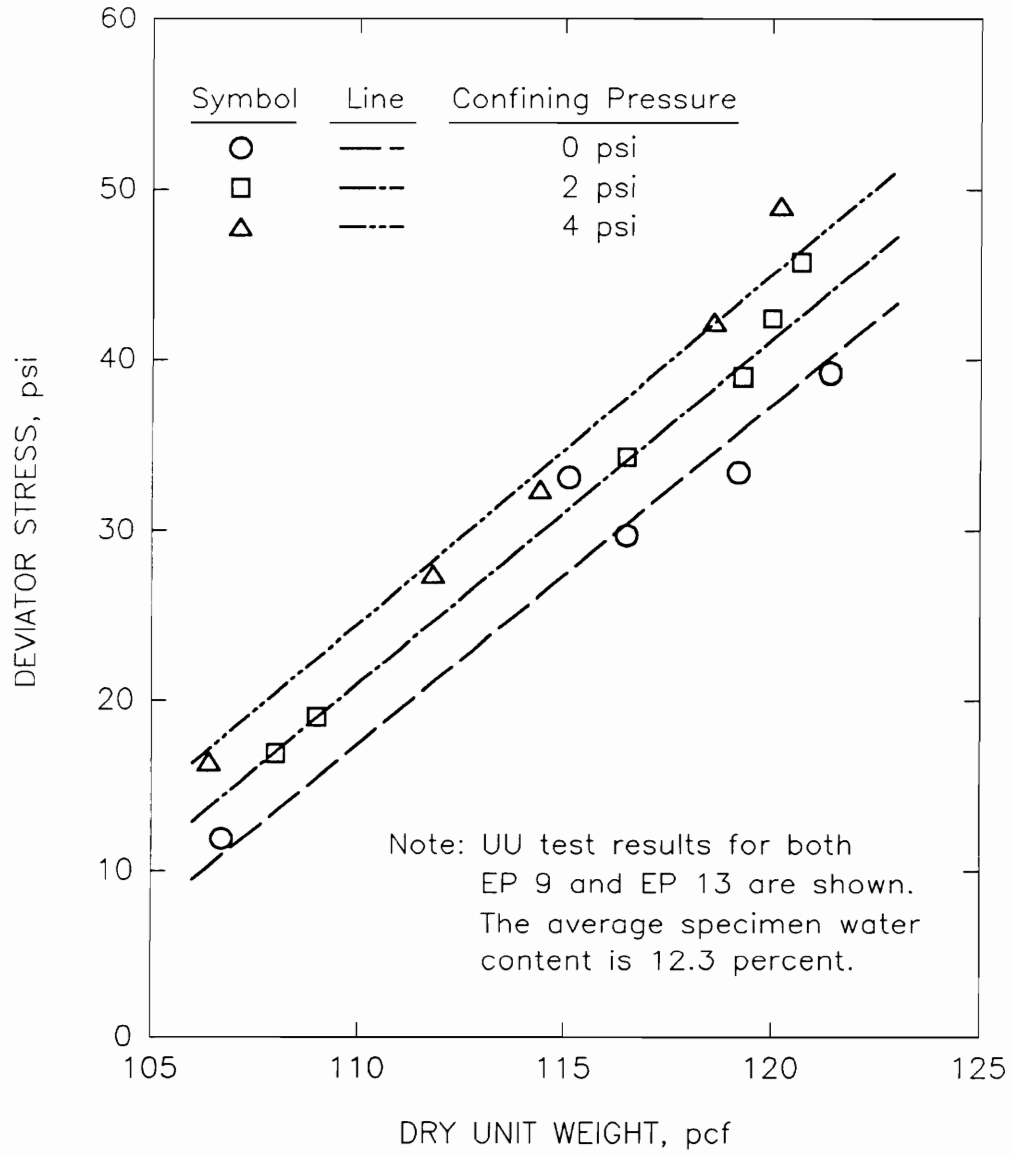

Figure A.5: Unconsolidated-Undrained Compression Test Results for Specimens from Tests EP 9 and EP 13

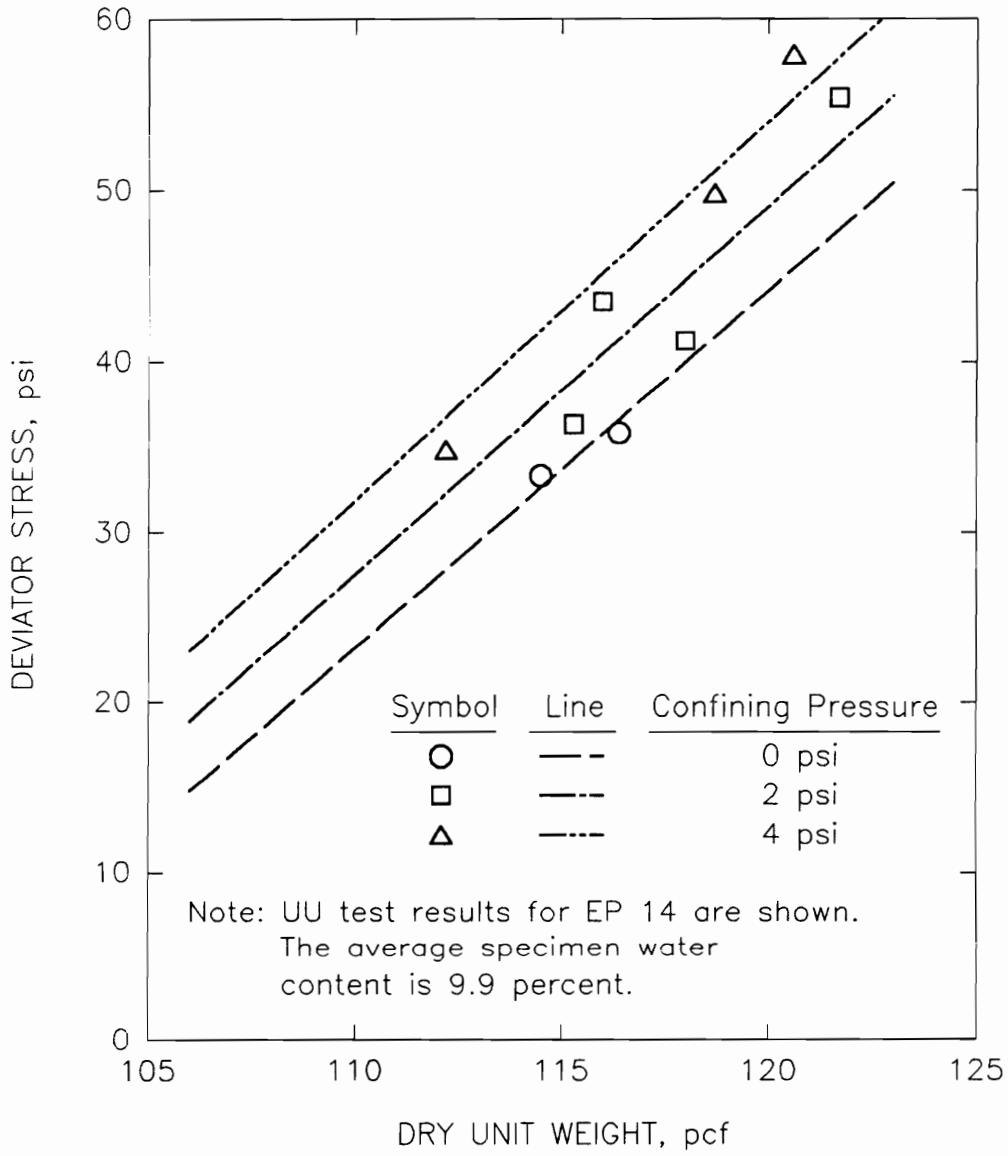

Figure A.6: Unconsolidated-Undrained Compression Test Results for Specimens from Test EP 14

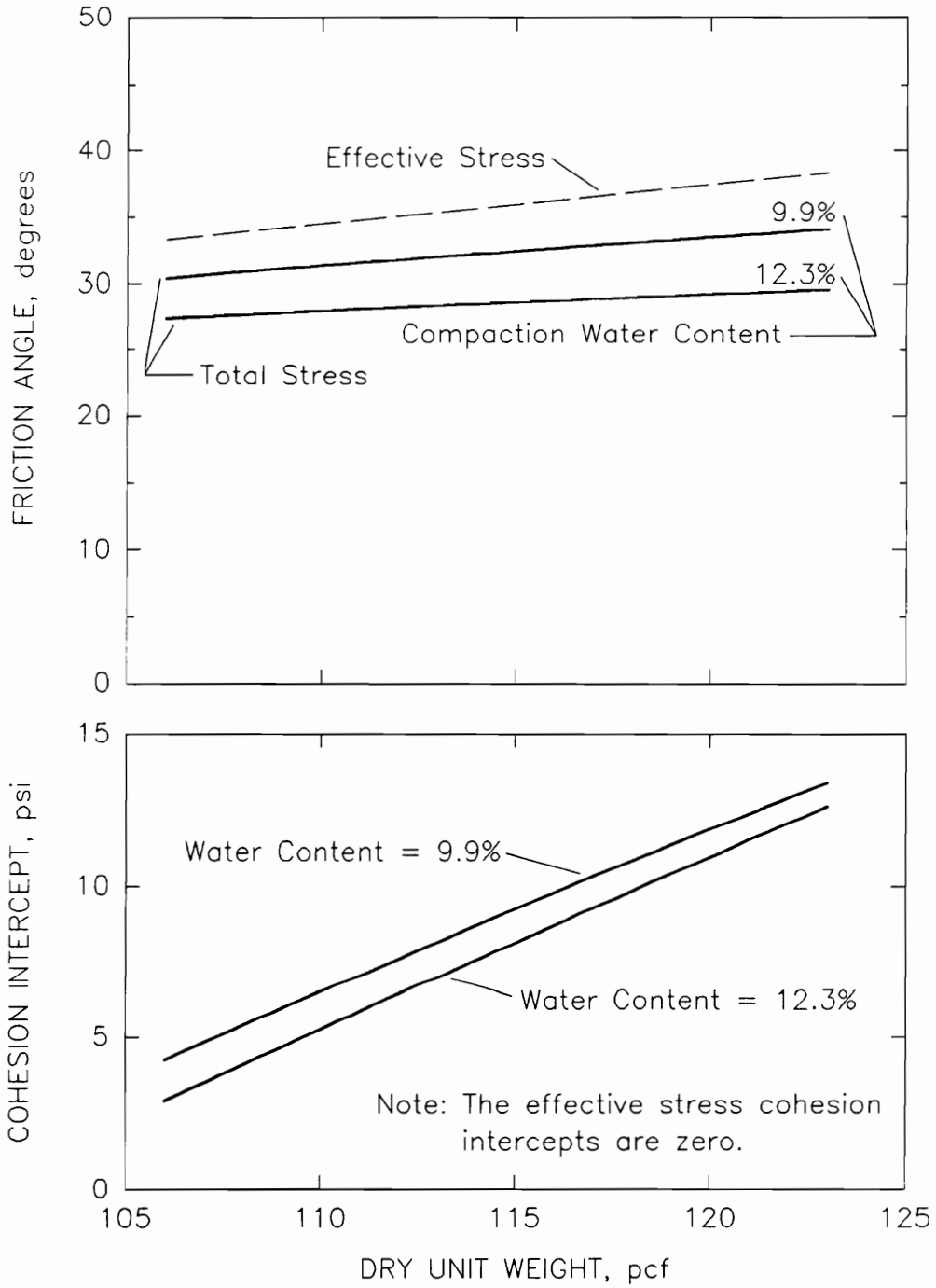

Figure A.7: Total Stress Strength Parameters from Unconsolidated-Undrained Tests for Yatesville Silty Sand

total stress cohesion intercepts increase with increasing dry unit weight and decreasing water content.

A typical deviator stress versus axial strain plot is shown in Figure A.8. The stress-strain curve is very nearly linear up to about 7 percent strain. Thus, the initial tangent modulus is applicable over a large strain range. The initial tangent moduli are listed in Table A.3. There is scatter in the data, and the moduli values do not seem to be strongly dependent on confining pressure. The scatter may be due to several factors, including: 1) variations in water content and density among the specimens from each instrumented retaining wall test, 2) varying degrees of disturbance during sampling and trimming, and 3) the effective stress from negative pore water pressures may make the effect of small changes in externally applied confining pressure relatively insignificant. The average values of initial tangent moduli for the specimens from instrumented retaining wall tests EP 9, EP 13, and EP 14 are listed in Table A.3.

A.1.5 Consolidated Undrained Triaxial Compression Tests

The results of back-pressure saturated, isotropically consolidated undrained triaxial compression tests with pore water pressure measurements performed on laboratory compacted specimens of Yatesville silty sand are reported by Brandon et al. (1990). The material used for these tests is the same material used to make up the lost volume of soil between instrumented retaining wall tests EP 12 and EP 13. As described previously, index property test results indicate that the

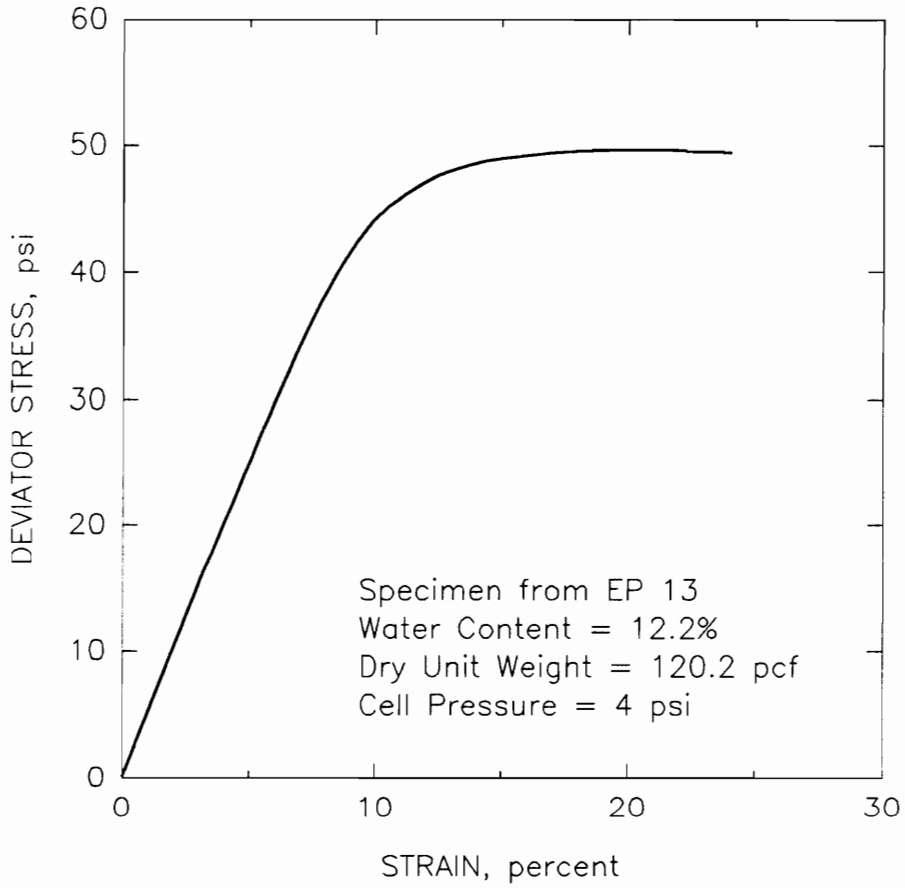

Figure A.8: Typical Stress-Strain Curve from the Unconsolidated-Undrained Tests on Yatesville Silty Sand

borrowed material is essentially the same as the material used for the instrumented retaining wall tests. The consolidated undrained test results disclose an effective stress cohesion intercept of zero and an effective stress friction angle whose value increases with increasing dry unit weight. The measured values of effective stress friction angle are presented in Figure A.9.

A.1.6 Brazilian Tensile Tests

Because of the interest in strength at low normal stresses in the instrumented retaining wall tests, several Brazilian tensile tests were performed on 1.5-inch high by 2.8-inch diameter specimens of Yatesville silty sand obtained from Shelby tube samples taken from the compacted backfill of instrumented retaining wall tests EP 1, 2, 3, 4, 12, 13, and 14. The tests were performed in general accordance with the procedures described in Krishnayya et al. (1974) and Krishnayya and Eisenstein (1974). In the Brazilian tensile test, a cylindrical specimen is loaded diametrically, and tensile stresses develop along the diametrical plane between the loading platens. Elastic solutions (Frocht, 1957, and Hondros, 1959) show that the tensile stress induced along the diametrical plane is approximately constant. The tensile strength at failure is computed from the elastic solution for the tensile stress, σ_t, at the center of the specimen according to:

$$\sigma_t = \frac{P}{\pi R t} \qquad (A.1)$$

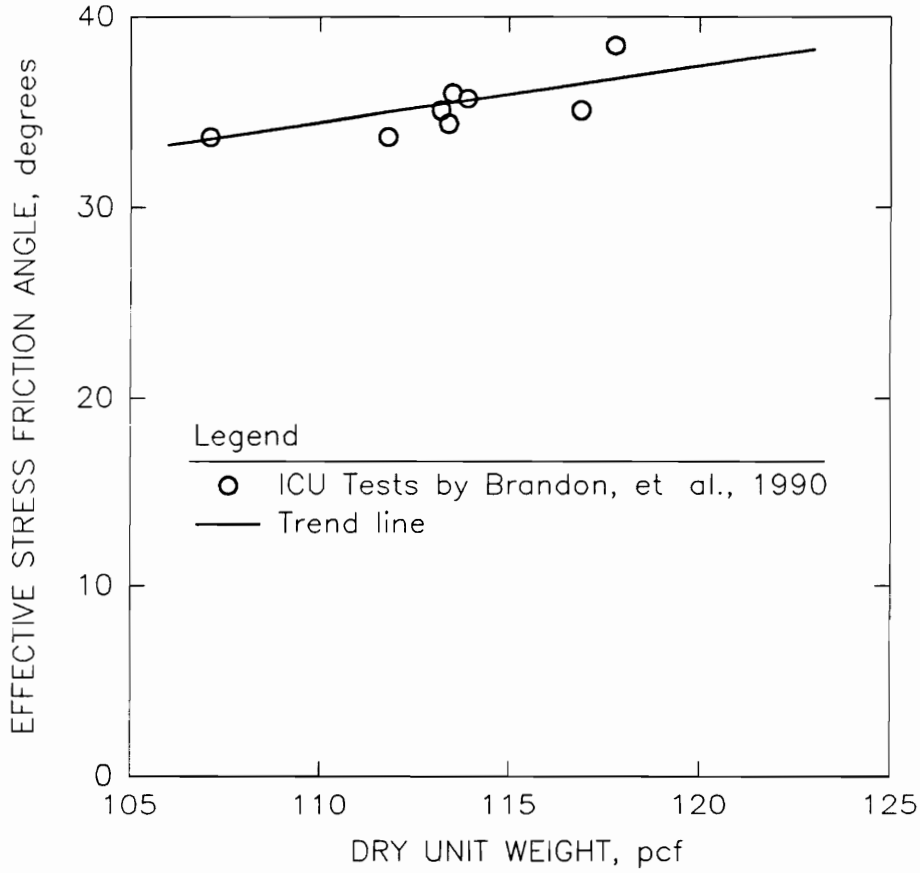

Figure A.9: Effective Stress Friction Angles for Yatesville Silty Sand

where P = the applied load, pounds,

R = the specimen radius, inches, and

t = the specimen thickness, inches.

The test results are presented in Table A.4 and Figure A.10. There is scatter in the data, but the figure shows that tensile strength tends to increase with increasing dry unit weight and decreasing water content. Contours of constant tensile strength have been drawn through the data points in Figure A.10.

A.1.7 Direct Shear Tests

Direct shear tests were performed on laboratory compacted specimens of Yatesville silty sand. The tests were performed in a 4 by 4-inch shear box machine in accordance with ASTM D-3080, except that the specimens were tested in their moist, as-compacted condition. The rate of shear displacement was determined based on a rate study in which the shear stress versus displacement curves were compared for three identical specimens sheared at different rates. The peak shear stresses from the rate study are listed in Table A.5. These results indicate that the peak shear stress is not strongly influenced by the displacement rate. A rate of 0.016 inches per minute was chosen for subsequent testing since this rate allowed adequate definition of the shear stress versus displacement curve, and because further reductions in displacement rate did not cause large changes in the measured peak shear stress.

TABLE A.4: Brazilian Tensile Test Results for Yatesville Silty Sand[1]

Instrumented Retaining Wall Test Number	Specimen Position[2] (T/M/B)	Dry Unit Weight (pcf)	Water Content (percent)	Tensile Strength (psi)
EP 1	-	118.6	14.1	3.05
	-	118.9	13.8	3.12
EP 2	-	114.6	13.3	2.59
	-	115.3	13.6	2.13
	-	112.3	13.8	1.56
	-	118.4	13.2	4.73
EP 3	-	117.0	12.7	3.98
	-	106.1	13.4	0.61
	-	116.4	12.9	3.98
	-	111.7	13.4	1.31
	-	106.0	13.7	0.48
EP 4	-	107.1	9.6	2.49
EP 12	M	107.9	12.8	1.04
	T	118.0	12.6	4.71
	M	111.1	12.4	1.80
	B	102.4	12.6	0.81
	T	120.5	12.3	4.35
	M	116.5	12.8	2.28
EP 13	T	118.3	12.3	4.10

TABLE A.4 (Continued): Brazilian Tensile Test Results for Yatesville Silty Sand[1]

Instrumented Retaining Wall Test Number	Specimen Position[2] (T/M/B)	Dry Unit Weight (pcf)	Water Content (percent)	Tensile Strength (psi)
EP 13	M	121.4	12.4	4.97
	B	120.7	11.6	3.37
EP 14	-	119.7	9.5	5.63
	B	114.9	10.0	2.02
	T	122.1	9.9	6.07
	M	118.1	9.9	3.83

Notes: 1) The tests were performed on 1.5-inch high by 2.8-inch diameter specimens.

2) T, M, and B refer to the top, middle, and bottom positions within the compacted lifts.

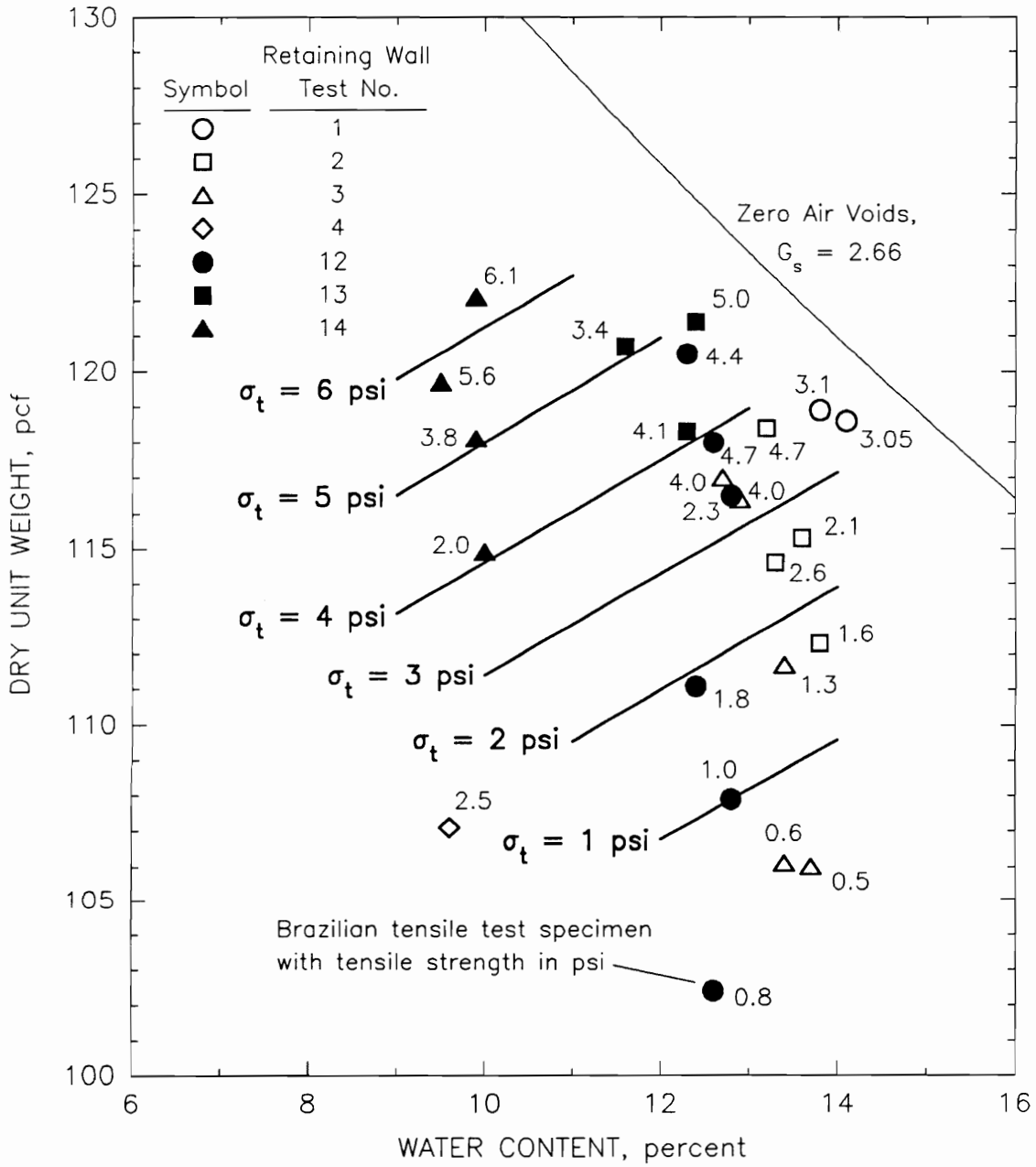

Figure A.10: Brazilian Tensile Test Results for Yatesville Silty Sand

TABLE A.5: Direct Shear Test Displacement Rate Study for Yatesville Silty Sand[1]

Direct Shear Test Number	Displacement Rate (in/min)	Dry Unit Weight (pcf)	Water Content (percent)	Stresses at Failure[2]	
				Normal Stress (psi)	Shear Stress (psi)
A	0.0360	117.9	12.1	2.91	4.95
B	0.0160	117.9	12.1	2.90	4.69
C	0.0048	118.0	12.0	2.90	4.56

Notes: 1) Test specimens were reconstituted in the 4-inch by 4-inch shear box.

2) Failure is defined at the point of maximum shear force. The normal load is kept constant throughout the test.

Three groups of direct shear tests were performed. The individual tests within each group were conducted using different normal stresses applied to specimens with approximately the same unit weight and water content so that an envelope could be defined at each moisture-density condition. The test results are listed in Table A.6 and shown in Figure A.11. The total stress friction angles are higher and the total stress cohesion intercepts are lower for the direct shear test results than for the unconsolidated undrained triaxial compression test results.

A.1.8 A Unified Undrained Strength Interpretation

The unconsolidated undrained compression tests, the Brazilian tensile tests, and the direct shear tests all provide measures of the undrained strength of the moist compacted Yatesville silty sand soil. In this section, the interpolated results at a single moisture density condition from the three methods are compared and discussed. For the comparison, the strengths were evaluated at a dry unit weight of 116 pcf and a water content of 11 percent, since this moisture density condition is in the range of the test conditions for all three methods.

From Figure A.7 for the unconsolidated undrained compression tests, the value of the total stress fiction angle is 30.8 degrees and the value of the total stress cohesion intercept is 9.3 psi for Yatesville silty sand with a dry unit weight of 116 pcf and a water content of 11 percent. This envelope is shown in Figure A.12. The Mohr's circles that would have generated the envelope with minor principal stresses of 0, 2, and 4 psi are also shown.

TABLE A.6: Direct Shear Test Results for Yatesville Silty Sand[1]

Direct Shear Test Group	Test Number	Dry Unit Weight (pcf)	Water Content (percent)	Stresses at Failure[2]	
				Normal Stress (psi)	Shear Stress (psi)
DS 1	S 1	118.0	12.1	1.05	2.97
	S 2	117.8	12.2	1.77	4.15
	S 3	117.9	12.1	2.91	4.95
	S 4	118.2	12.1	4.38	6.44
DS 2	S 5	110.7	12.1	1.05	2.20
	S 6	110.6	12.0	1.76	2.83
	S 7	110.1	12.2	3.09	4.21
	S 8	110.3	12.1	4.68	5.94
DS 3	S 9	110.9	8.2	1.04	3.13
	S 10	110.5	8.2	1.74	3.97
	S 11	110.6	8.2	2.87	5.37
	S 12	110.5	8.2	4.29	6.67

Notes: 1) Test specimens were reconstituted in the 4-inch by 4-inch shear box.

2) Failure is defined at the point of maximum shear force. The normal load is kept constant throughout the test.

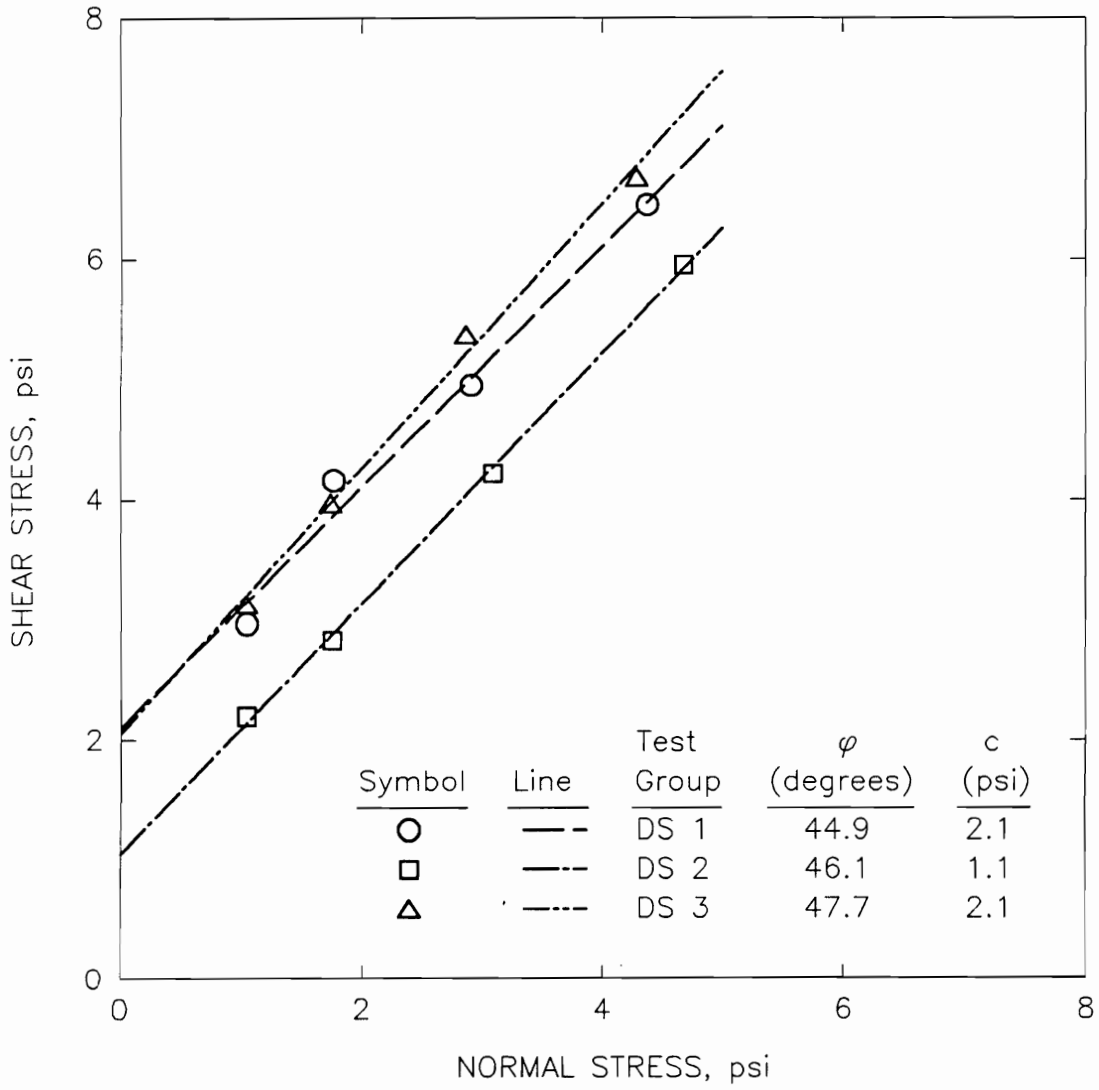

Figure A.11: Direct Shear Test Results for Yatesville Silty Sand

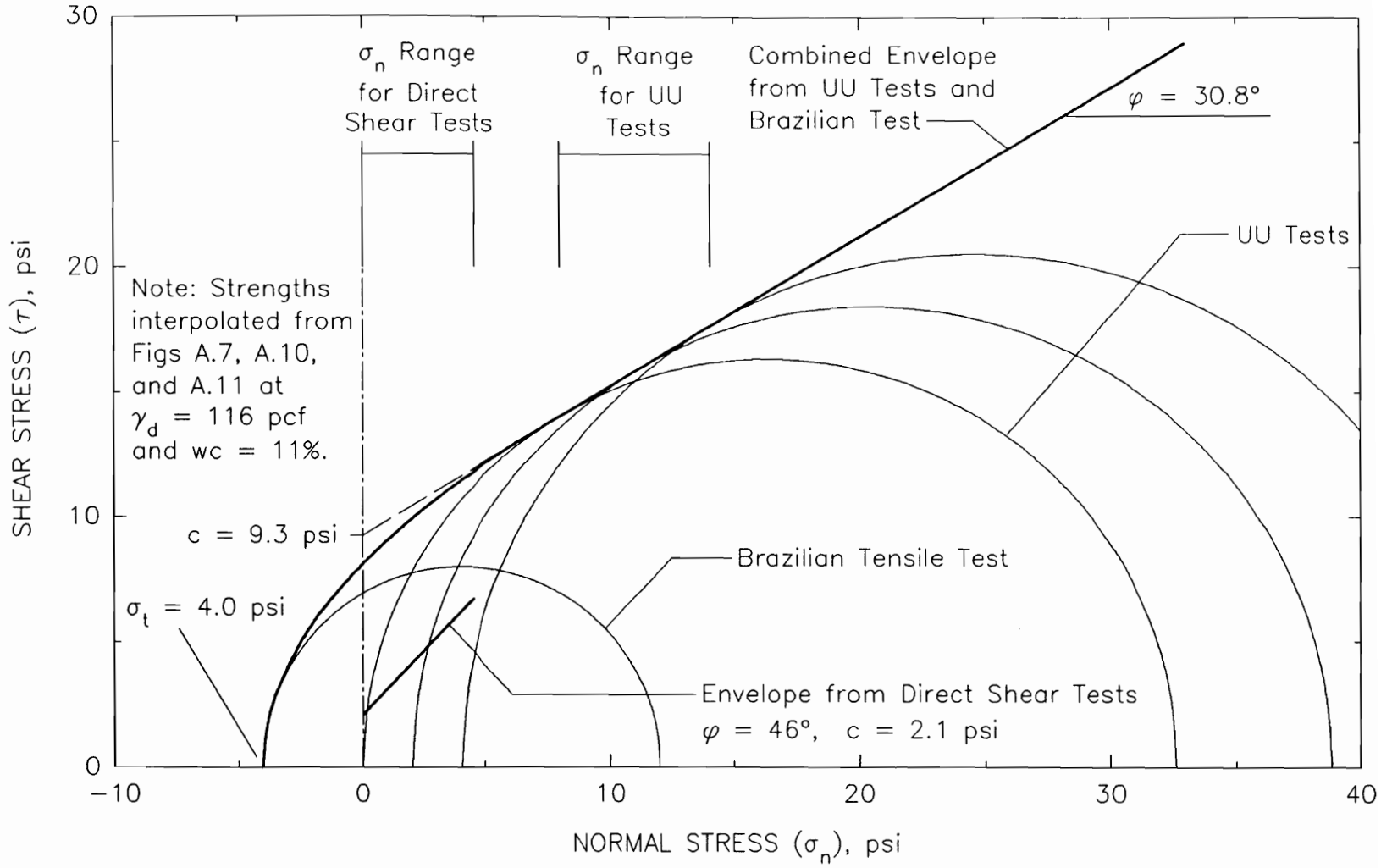

Figure A.12: A Unified Undrained Strength Interpretation for Yatesville Silty Sand

From Figure A.10 for the Brazilian tensile tests, the value of the tensile strength is 4.0 psi for Yatesville silty sand with a dry unit weight of 116 pcf and a water content of 11 percent. According to the elastic analysis from which Eqn A.1 is obtained, the corresponding compressive stress at the center of the Brazilian tensile test specimen is three times the tensile stress. Since these are principal stresses, the Mohr's circle for failure in the Brazilian tensile test may be drawn as shown in Figure A.12.

According to the Griffith-Brace tensile failure theory (Lee and Ingles, 1968), which is based on the existence of a large number of randomly oriented cracks in a material, the failure envelope is perpendicular to the normal stress axis at the tensile strength. The envelope is parabolic in the tensile stress region, and it intersects the shear stress axis at a value of shear stress equal to twice the tensile strength. Such an envelope is shown in Figure A.12, and it appears that the unconsolidated undrained compression test results are consistent with the Brazilian tensile test results when interpreted with the Griffith-Brace theory.

Interpolating from the results shown in Figure A.11 for the direct shear tests, the value of the total stress fiction angle is 46 degrees and the value of the total stress cohesion intercept is 2.1 psi for Yatesville silty sand with a dry unit weight of 116 pcf and a water content of 11 percent. This envelope is shown in Figure A.12. The value of the friction angle is larger for the direct shear tests than it is for the unconsolidated undrained compression tests, and the value of

the cohesion intercept is smaller. In the normal stress region where the direct shear tests were performed, the strengths from the direct shear tests are smaller than the strengths for the combined envelope derived from the unconsolidated undrained compression tests and the Brazilian tensile tests.

One possible reason for the difference is that the direct shear specimens were sheared within minutes after they were compacted, whereas the unconsolidated undrained specimens and the Brazilian tensile test specimens were tested months after they were compacted. Mitchell (1986) gives an example of strength gain in sand with time after disturbance by blasting. The strength gain was apparently not due to dissipation of excess pore pressures caused by the blasting since measurements indicated that the excess pore pressures completely dissipated within hours after the blast, whereas the increase in strength took weeks or months to develop. Mitchell indicated that the most probable cause of the strength gain was formation of silica acid gel films on particle surfaces or precipitation of silica as a cementing agent at the particle contacts. Schmertmann (1991) describes several examples of strength gain with time in sands. He believes that the strength gain occurs due to the effects of particle movement during secondary compression, including greater particle interlocking and internal arching to the stiffer and stronger parts of the soil structure. Effects such as those described by Mitchell (1986) and Schmertmann (1991) could account for the higher shear strengths measured in the unconsolidated undrained compression tests and the Brazilian tensile tests.

These results suggest that the total stress cohesion intercepts shown in Figure A.7 may not be applicable to conditions during backfilling. If, instead, the interpretation is based on the direct shear test results, the total stress cohesion intercepts vary with dry density and water content as shown in Figure A.13.

The higher friction angles measured in the direct shear tests are probably due to the following factors:

1) The normal stresses on the failure plane in the direct shear tests are lower than those on the failure plane in the unconsolidated undrained triaxial tests, as shown in Figure A.12. Higher friction angles are generally measured at lower normal stresses.
2) The direct shear test imposes stress and strain conditions similar to plane strain conditions. Generally, friction angles from plane strain tests, in which the intermediate principal stress is greater than the minor principal stress, are higher than friction angles from conventional triaxial tests, in which the intermediate principal stress equals the minor principal stress.
3) Aging effects, as described above, may have created an apparent preconsolidation in the unconsolidated undrained and Brazilian test specimens. Values of the friction angle for preconsolidated materials are generally lower than for normally consolidated materials.

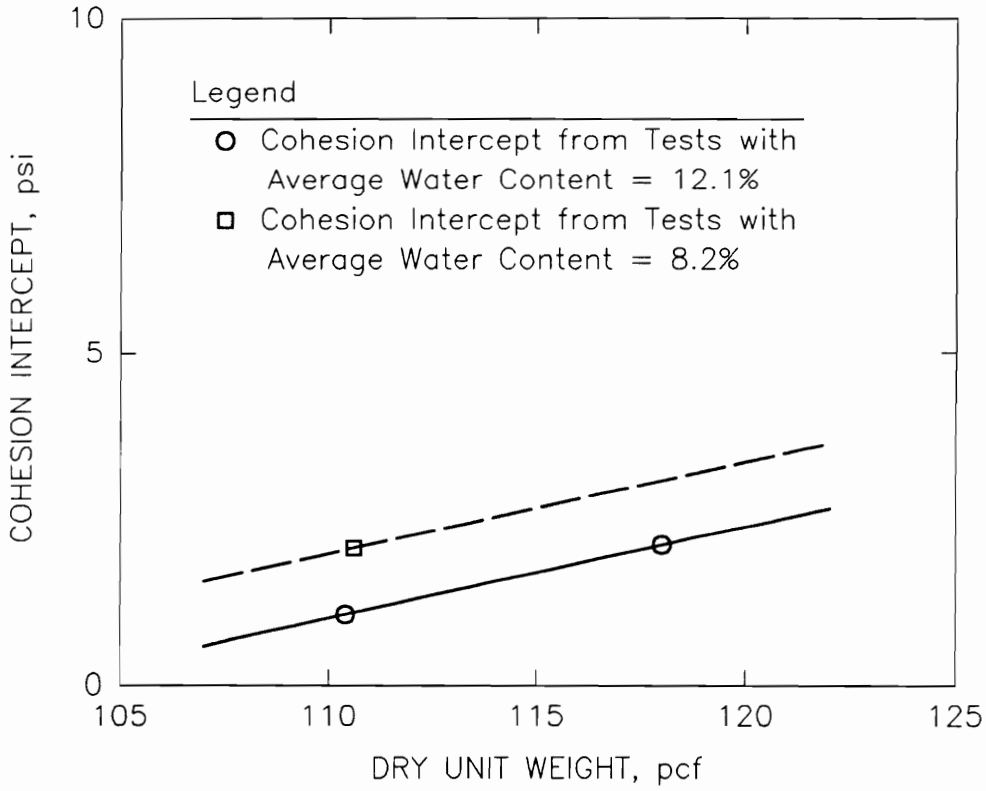

Figure A.13: Total Stress Cohesion Intercepts Interpreted from the Direct Shear Test Results from Yatesville Silty Sand

A.1.9 Interface Shear Tests

Direct shear type tests were performed to measure the shear strength at the interface between compacted Yatesville silty sand and a concrete surface similar to the instrumented retaining wall surface. These interface shear tests were performed with a small concrete block placed in the lower half of the shear box in the direct shear machine. The soil was compacted on top of the block in the upper half of the shear box. A displacement rate study verified that the 0.016 inch per minute rate used for the direct shear tests was also suitable for the interface tests.

Three groups of four interface shear tests were performed. The moisture-density condition for each interface test group was made to match approximately the moisture-density condition for the corresponding direct shear test group so that comparisons could be easily made. The test results are listed in Table A.7 and shown in Figure A.14. The interface friction angles are lower than the direct shear friction angles, and the interface adhesion intercepts are lower than the direct shear cohesion intercepts. The direct shear and interface test results are summarized in Table A.8, which indicates that the ratio between the interface friction coefficient and the soil friction coefficient ranges from 0.65 to 0.83.

A typical interface shear stress versus displacement curve is shown in Figure A.15. As shown, the shear stress rises rapidly to a peak that typically occurs before 0.02 inches displacement. The residual strength is typically not much less than the peak strength.

TABLE A.7: Interface Shear Test Results for Yatesville Silty Sand[1]

Interface Test Group	Test Number	Dry Unit Weight (pcf)	Water Content (percent)	Stresses at Failure[2]	
				Normal Stress (psi)	Shear Stress (psi)
IS 1	I 1	119.2	11.9	1.04	0.93
	I 2	118.9	11.8	1.74	1.42
	I 3	118.9	11.9	2.85	2.37
	I 4	118.3	12.0	4.25	3.57
IS 2	I 5	111.9	11.5	1.04	0.96
	I 6	112.0	11.4	1.75	1.40
	I 7	112.5	11.3	2.85	2.21
	I 8	111.7	11.1	4.63	3.52
IS 3	I 9	112.1	7.8	1.04	1.10
	I 10	110.4	7.6	1.73	1.56
	I 11	110.8	7.7	3.41	2.81
	I 12	110.9	7.7	4.25	3.36

Notes: 1) Test specimens were reconstituted in the 4-inch by 4-inch shear box.

2) Failure is defined at the point of maximum shear force. The normal load is kept constant throughout the test.

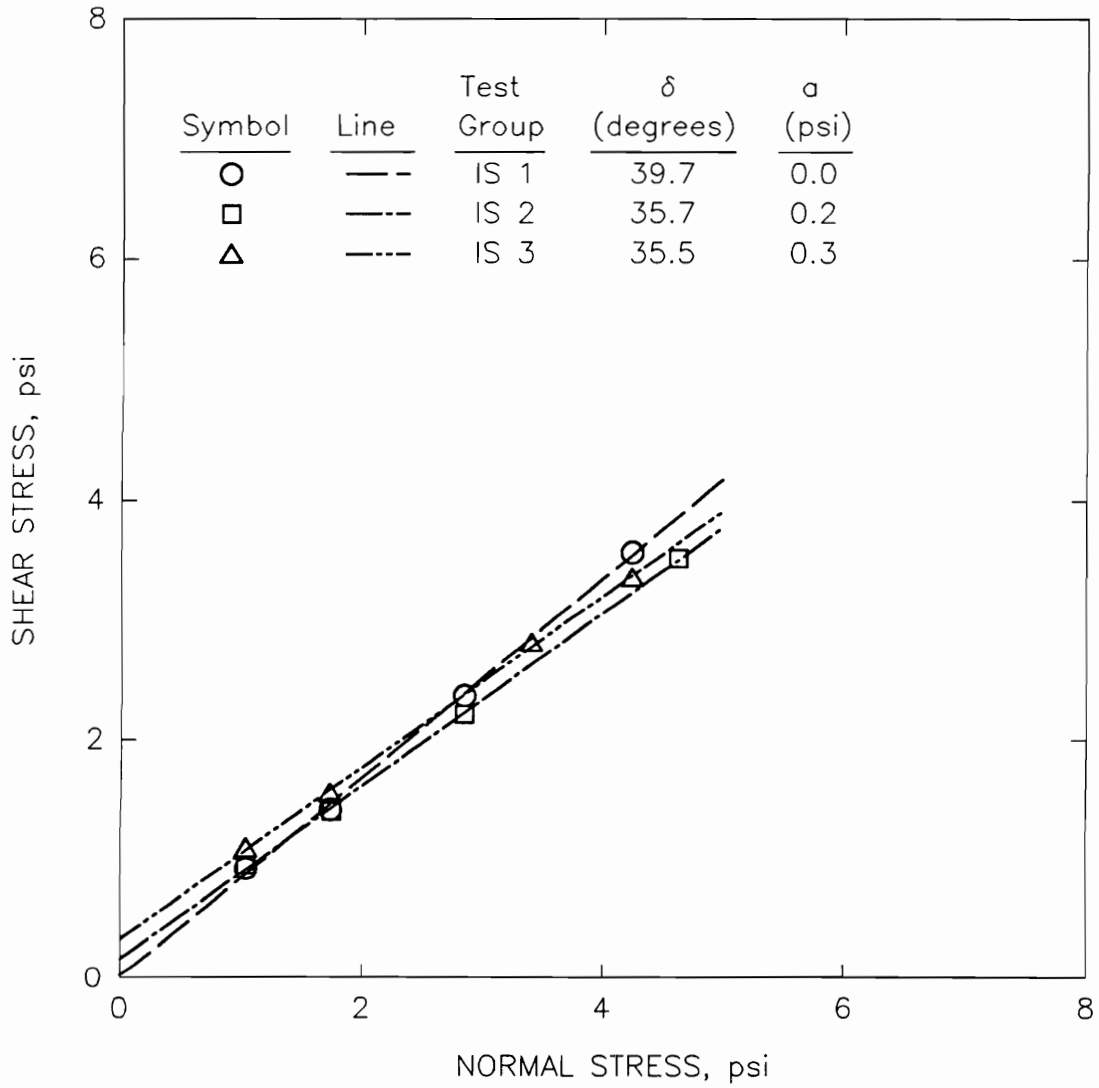

Figure A.14: Interface Shear Test Results for Yatesville Silty Sand

TABLE A.8: Summary of Direct Shear and Interface Shear Strength Parameters

Test Group[1]	Average Dry Unit Weight (pcf)	Average Water Content (percent)	Strength Parameters[2]		$\frac{\tan \delta}{\tan \phi}$
			ϕ or δ (degrees)	c or a (psi)	
DS 1	118.0	12.1	44.9	2.11	0.83
IS 1	118.8	11.9	39.7	0.02	
DS 2	110.4	12.1	46.1	1.06	0.69
IS 2	112.0	11.3	35.7	0.18	
DS 3	110.6	8.2	47.7	2.06	0.65
IS 3	111.1	7.7	35.5	0.35	

Notes: 1) DS indicates a direct shear test group. IS indicates an interface shear test group.

2) ϕ and c are, respectively, the internal friction angle and cohesion intercept from a direct shear test group. δ and a are, respectively, the interface friction angle and adhesion intercept from an interface shear test group.

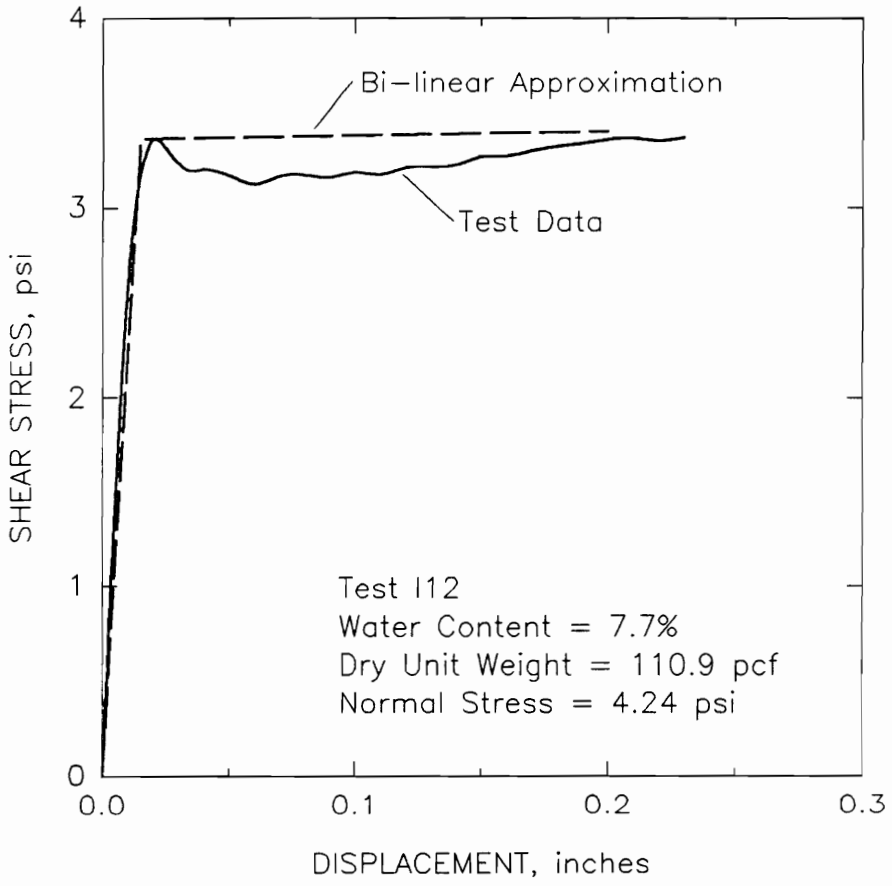

Figure A.15: Typical Stress-Displacement Curve from the Direct Shear Tests on Yatesville Silty Sand

For use in defining the shear stiffness of interface elements prior to failure in finite element analyses, the displacement at failure was taken to be 0.015 inches. The post-failure, tangent shear stiffness of interface elements is set at a low value. This type of bi-linear approximation is shown in Figure A.15.

A.1.10 Consolidation Tests

One dimensional consolidation tests were performed on specimens of Yatesville silty sand obtained from Shelby tube samples taken from the compacted backfill of instrumented retaining wall tests EP 10, EP 12, and EP 14. The tests were performed in general accordance with ASTM D-2435. In one set of tests, the specimens were inundated after applying the seating load. In the other set of tests, the specimens were tested in their moist, as-compacted conditions. Void ratio versus logarithm of applied pressure plots are presented for both sets of tests in Figures A.16 and A.17. Figure A.16, which presents the results for the inundated specimens, also includes the compression curve for a specimen consolidated from a slurry. The inundated specimens from the test wall backfill all approach the same void ratio at an applied pressure of 16 tsf. The specimen consolidated from a slurry has a slightly higher void ratio at the same pressure.

The compression curves for the moist specimens in Figure A.17 do not all approach a common point at high pressure. This reflects the effects of the different compactors and the different water contents during compaction for each test. For comparison, the test results for

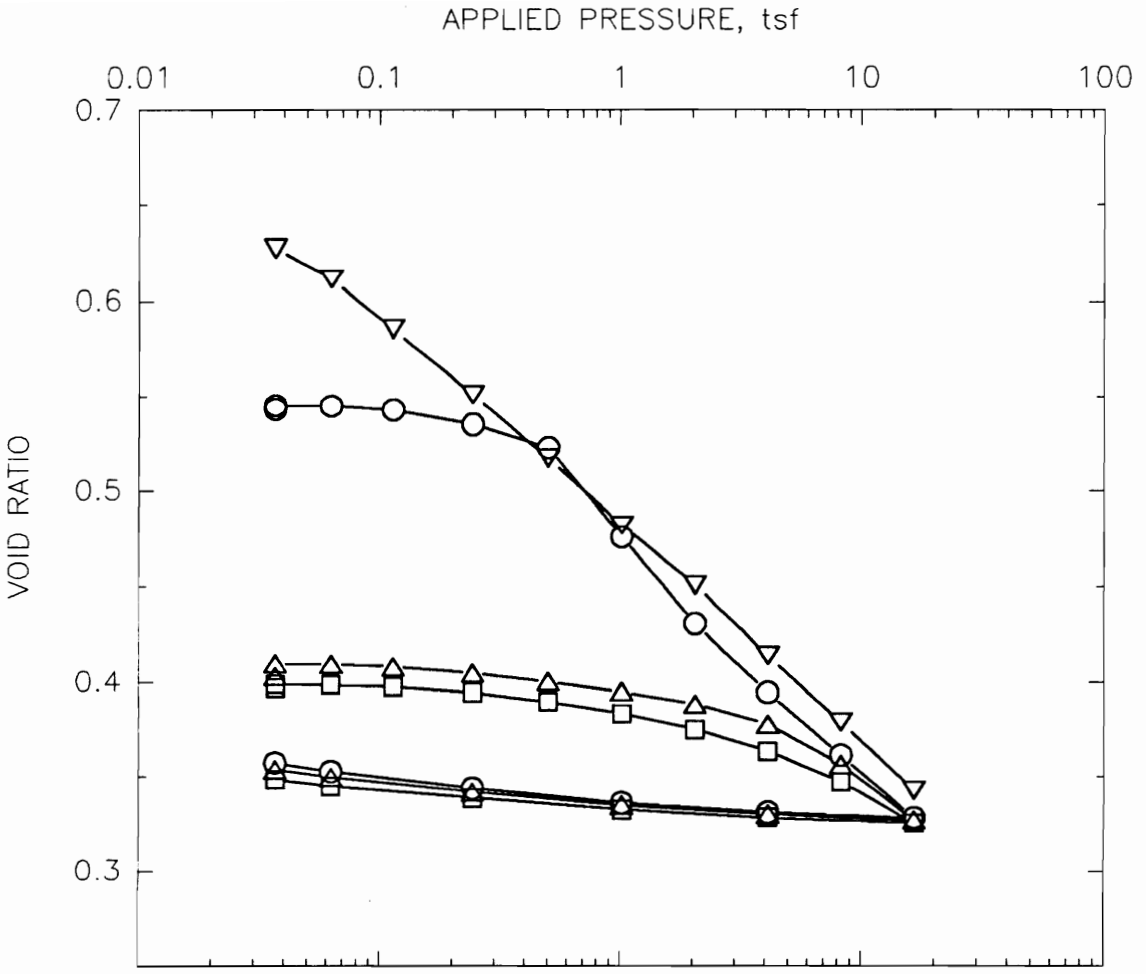

Symbol	Test	Initial Dry Unit Weight (pcf)	Initial Water Content (percent)	Final Water Content (percent)	Inundated (Y/N)
○	EP 10	107.6	12.3	13.4	Y
□	EP 12	118.8	12.0	12.6	Y
△	EP 14	118.3	9.6	12.3	Y
▽	Slurry	98.6	24.2	14.7	Y

Figure A.16: Consolidation Test Results for Inundated Yatesville Silty Sand

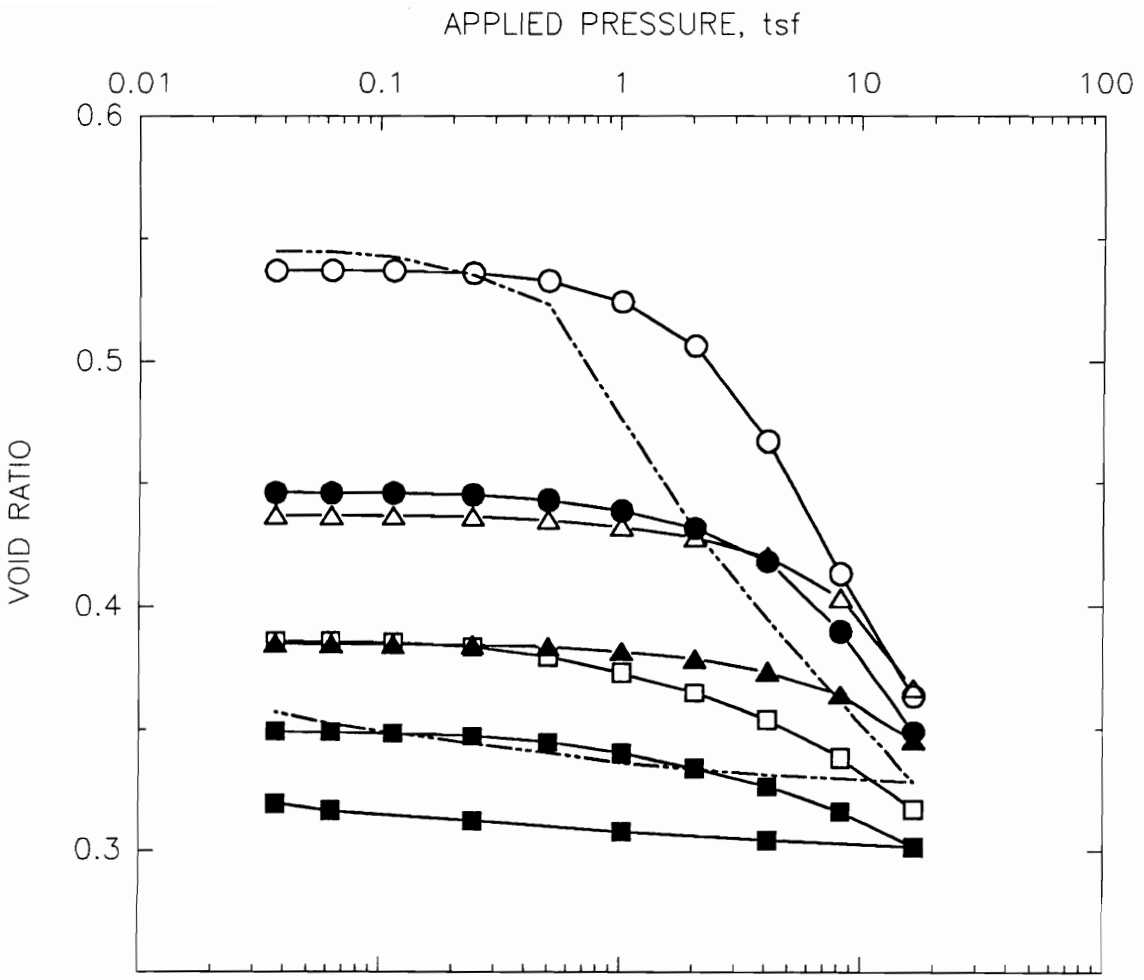

Symbol	Test	Initial Dry Unit Weight (pcf)	Initial Water Content (percent)	Final Water Content (percent)	Inundated (Y/N)
●	EP 10	114.8	11.6	11.8	N
○	EP 10	108.0	12.1	11.9	N
■	EP 12	123.0	11.7	11.7	N
□	EP 12	119.8	13.0	12.5	N
▲	EP 14	119.9	9.5	9.3	N
△	EP 14	115.5	9.7	9.4	N
—----	EP 10	107.6	12.3	13.4	Y

Figure A.17: Consolidation Test Results for Moist Yatesville Silty Sand

the inundated specimen from EP 10 are also shown on Figure A.17. This specimen had a high initial void ratio, and a significant part of the consolidation test loading is in the normally consolidated range. The consolidation curves from the moist specimens cross over the normally consolidated portion of the curve for the inundated specimen. This reflects the ability of the negative pore water pressures at the intergranular contact points of the moist soil to resist particle movement in response to applied load.

Strain versus arithmetic pressure plots in the low stress range are shown in Figure A.18. The plots are approximately linear in this stress range, and values of the constrained modulus are equal to the slopes of the curves. Constrained modulus values can be used to analyze compression of the backfill during filling. The constrained modulus values obtained from Figure A.18 are shown on the moisture density plot of Figure A.19, which also includes contours of constant constrained modulus drawn through the data.

A.2 Light Castle Sand

Light Castle sand is a clean, fine sand consisting predominantly of subangular grains of quartz. The sand was obtained from a quarry in Craig County, Virginia. The following sections describe index property tests, in-place unit weight measurements, and strength tests conducted on the Light Castle sand.

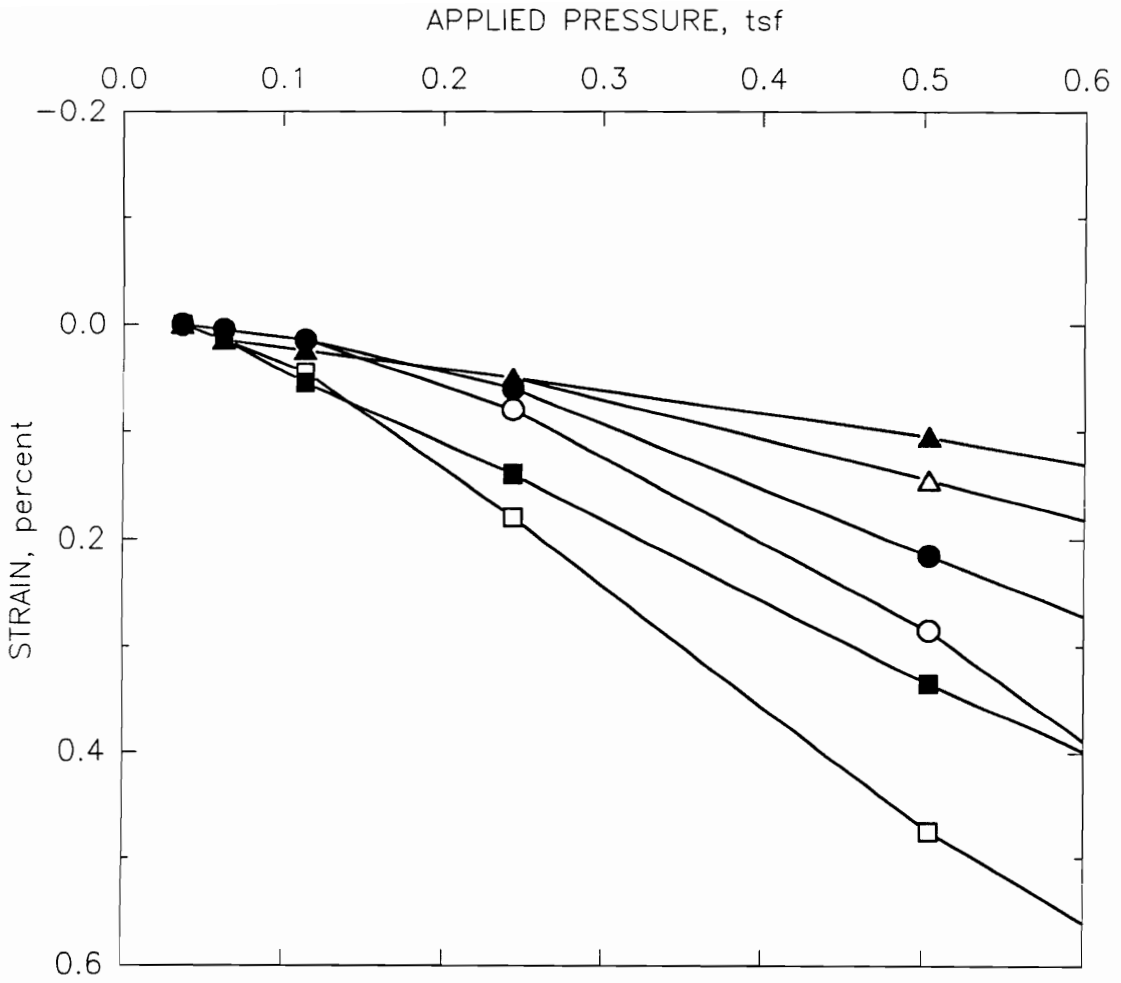

Symbol	Test	Initial Dry Unit Weight (pcf)	Initial Water Content (percent)	Final Water Content (percent)	Inundated (Y/N)
●	EP 10	114.8	11.6	11.8	N
○	EP 10	108.0	12.1	11.9	N
■	EP 12	123.0	11.7	11.7	N
□	EP 12	119.8	13.0	12.5	N
▲	EP 14	119.9	9.5	9.3	N
△	EP 14	115.5	9.7	9.4	N

Figure A.18: Consolidation Strain versus Arithmetic Pressure for Moist Yatesville Silty Sand

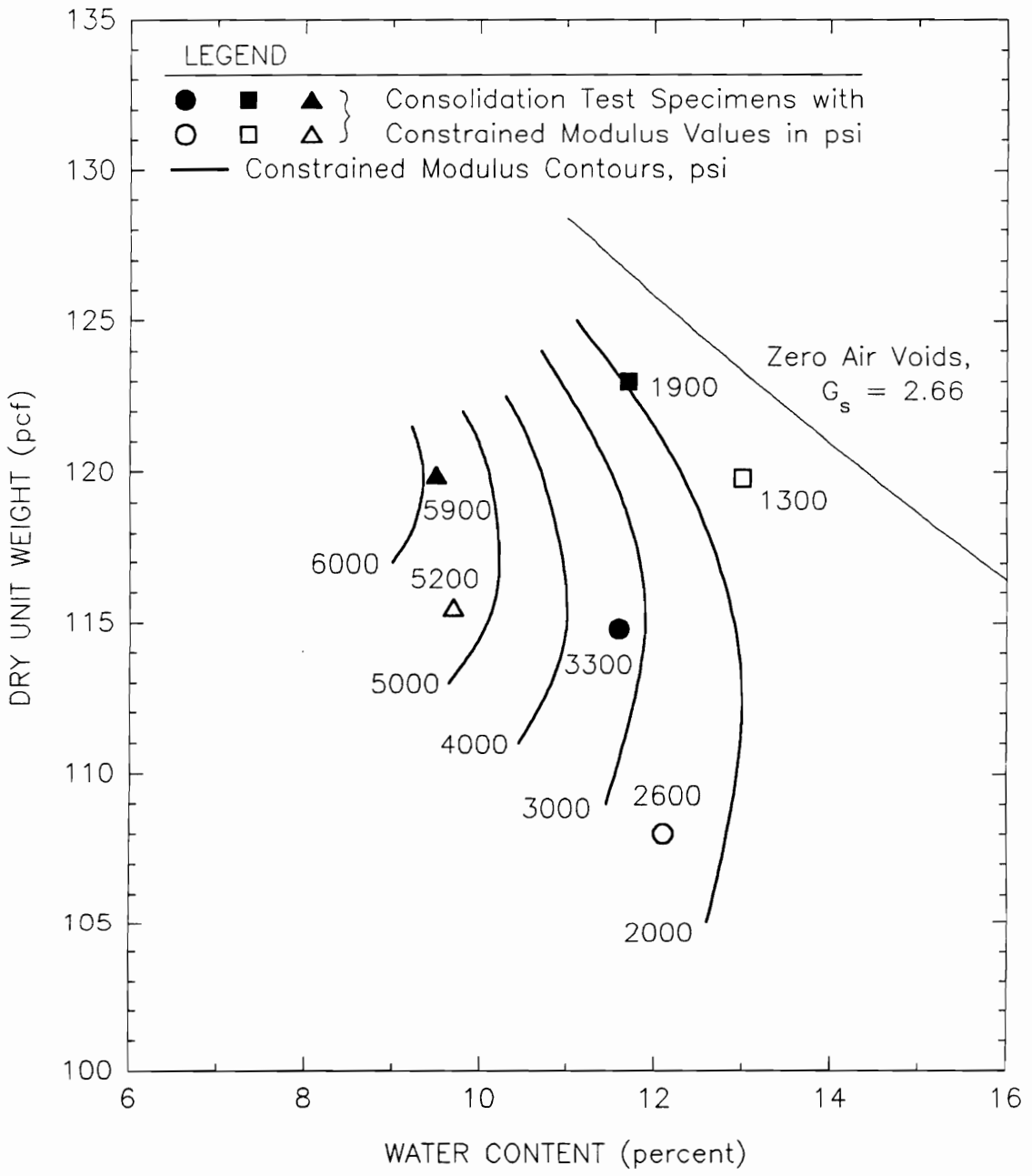

Figure A.19: Constrained Modulus Contours

A.2.1 Index Property Tests

A particle size distribution curve for the Light Castle sand is presented in Figure A.20. As shown, the soil is a clean, uniform, fine sand with less than 1 percent passing the No. 200 sieve.

The specific gravity of solids, determined in accordance with ASTM D-854, is 2.65.

The minimum index density of the Light Castle sand, determined in accordance with ASTM D-4254, Method A, is 88.5 pcf. The maximum index density of the Light Castle sand, determined in accordance with ASTM D-4253, Method 1, is 106 pcf.

A.2.2 In-place Unit Weight

In-place unit weights of the compacted Light Castle Sand were determined in two ways: 1) gross determinations were made for tests EP 15 and EP 16 using the entire mass of backfill, and 2) small sample determinations were made for test EP 15 using thin-wall Shelby tube samplers. The gross determinations were made by weighing the sand delivery hopper before and after each batch was placed in the backfill area. After all the sand was placed and compacted, the total volume of backfill was measured. From the total weight and total volume, the gross density was calculated. The Shelby tube determinations were made by pushing Shelby tubes into the sand, excavating adjacent to the tubes, pushing a shutter across the open bottom end of each tube, weighing the retained sand, and calculating the volume using the inside diameter of the Shelby tube's cutting edge and the distance pushed. Table A.9 lists the results for both types of determinations.

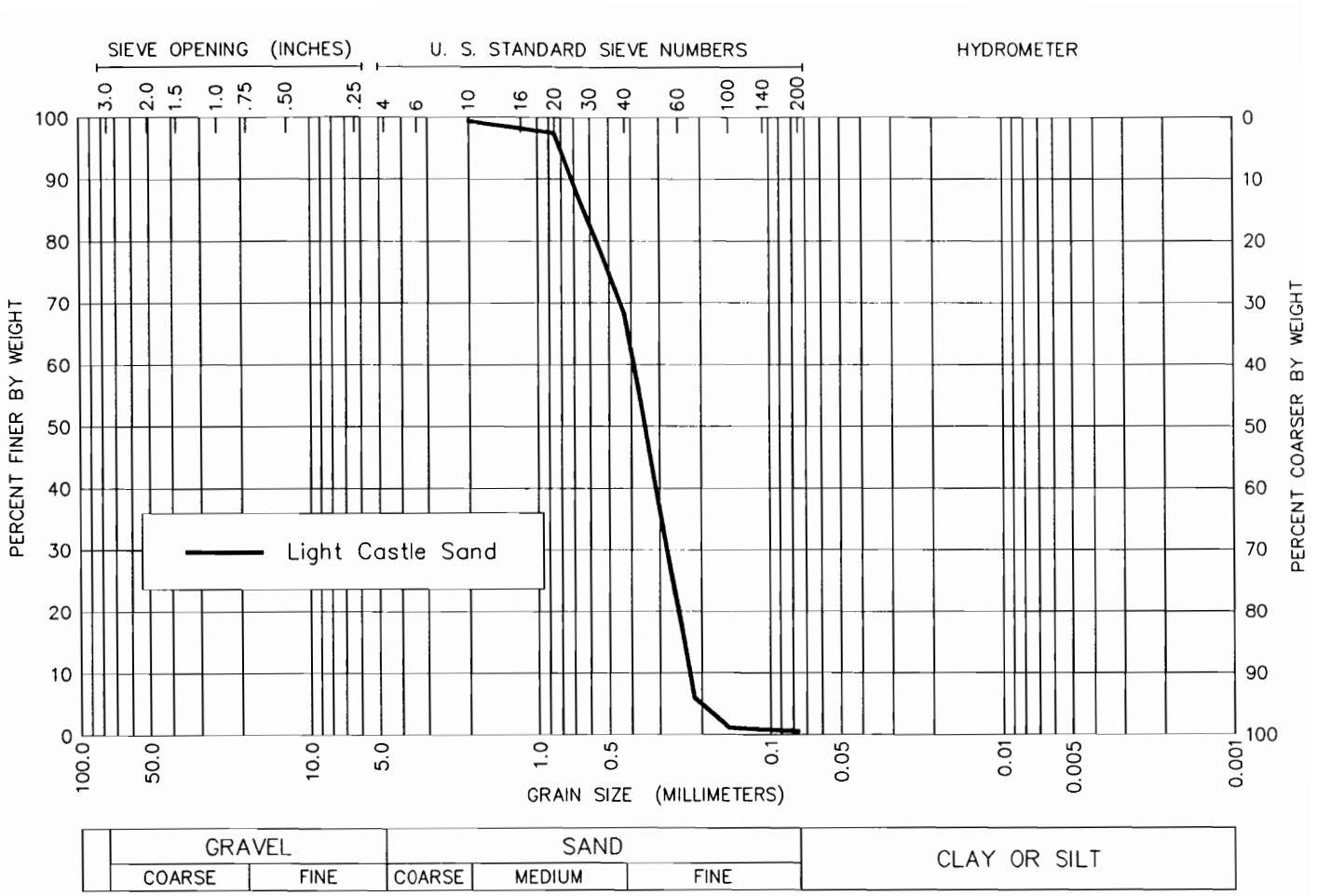

Figure A.20: Grain Size Distribution Curve for Light Castle Sand

TABLE A.9: In-Place Unit Weights, Light Castle Sand

Instrumented Retaining Wall Test Number	Compactor	In-Place Unit Weight (lbs. per cu. ft.)	
		Gross Determination	Small Sample Determination
EP 15	Rammer	106.2	105.7
EP 16	Vib. Plate	104.7	Not Made

The gross measurement agrees reasonably well with the small sample measurements for test EP 15, but the gross measurement does yield a slightly higher value of unit weight. For dense compacted sand, an effect of the Shelby tube's cutting edge may be to slightly loosen the sand as it enters the tube. Considering this effect, and the much larger sample size in the gross determination, the gross determination is taken as the best estimate of in-place unit weight for the Light Castle Sand.

The relative densities computed from the measurements in Table A.9 are 101 percent for test EP 15 and 94 percent for EP 16.

A.2.3 Strength Estimate

A strength estimate for the Light Castle sand was made using the results of consolidated undrained compression tests and direct shear tests, both at relative densities of about 75 percent, and extrapolating to higher relative densities using the method of Cornforth (1973). Stress paths from the consolidated undrained compression tests and strength values measured in the direct shear tests are shown in Figure A.21. The stress paths appear to define a failure line corresponding to ϕ' = 38.1 degrees, which is in close agreement with the ϕ' value of 38.6 degrees determined from the direct shear tests.

In Cornforth's method, the friction angle is described as a function of the "relative dry density", which is not the conventional relative density. Cornforth defines the relative dry density, RDD, as:

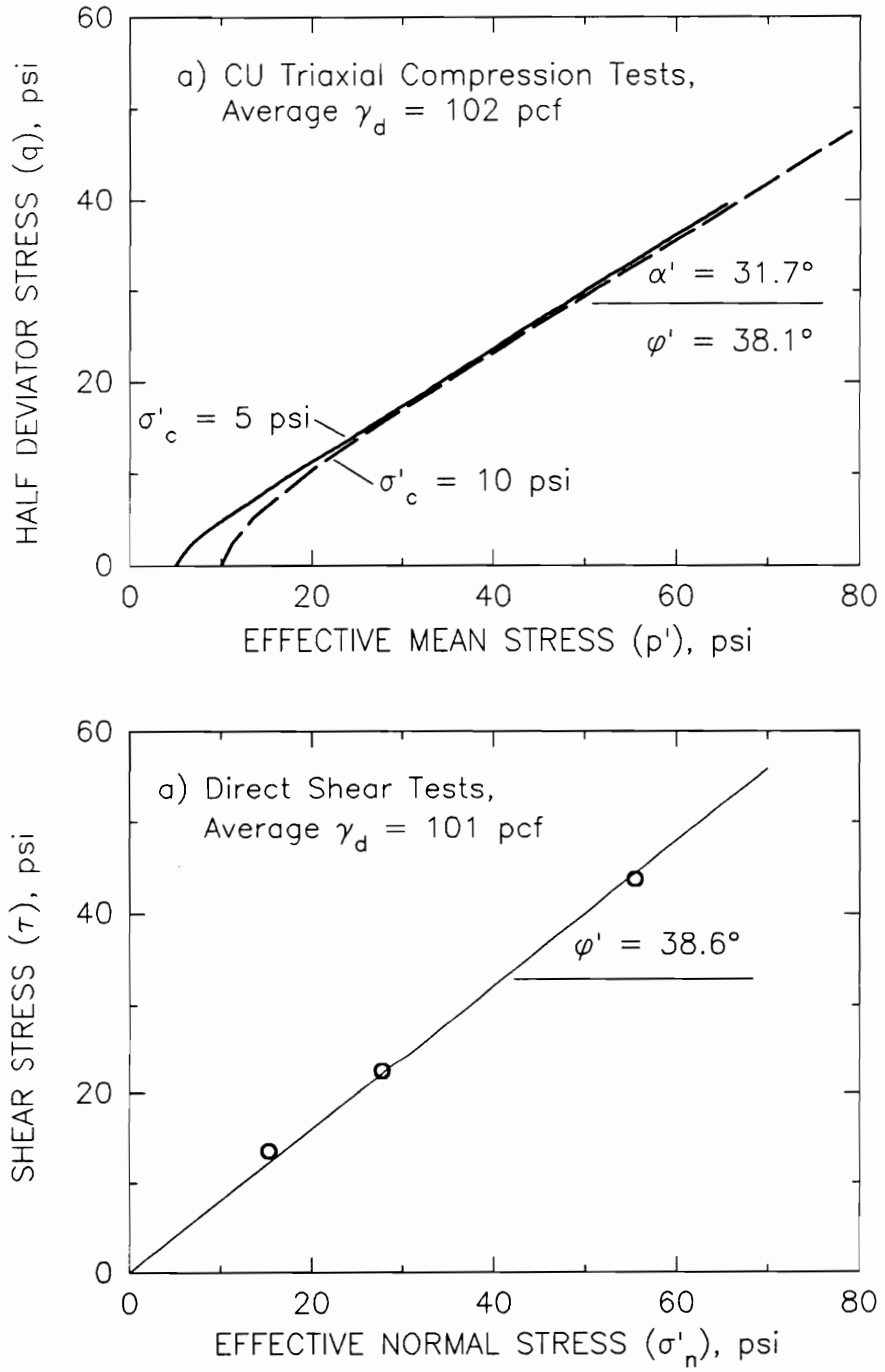

Figure A.21: Strength Test Results for Light Castle Sand

$$RDD = \frac{\gamma - \gamma_{min}}{\gamma_{max} - \gamma_{min}} \quad (A.2)$$

where γ = the in-place density, pcf,

γ_{min} = the minimum index density, pcf, and

γ_{max} = the maximum index density, pcf.

The effective stress friction angle, ϕ_d, is expressed as the sum of the ultimate friction angle, ϕ_{cv}, and the density component, ϕ_{dc}:

$$\phi_d = \phi_{cv} + \phi_{dc} \quad (A.3)$$

In Cornforth's method, the ultimate strength is determined from static angle of repose tests on loose specimens of dry sand. For the Light Castle sand, such tests resulted in an ultimate strength of 33.6 degrees. The density component of strength increases from 0 at the minimum index density to a value in the range from 9 to 12 degrees at the maximum index density for three sands in triaxial compression studied by Cornforth (1973). The relationships for Cornforth's Brasted sand, the Monterey sand of Marachi et al. (1969), and Light Castle sand are shown in Figure A.22. The values of ϕ_{dc} for Light Castle sand are more similar to those for Monterey sand than to those for Brasted sand.

Using the measured ϕ_{cv} value for Light Castle sand and the values of ϕ_{dc} from Figure A.22, the values of effective stress friction angle are 42 and 41 degrees for the relative densities of tests EP 15 and EP 16, respectively. A value of 42 degrees was used for both tests for the analyses described in Chapters 7 and 8.

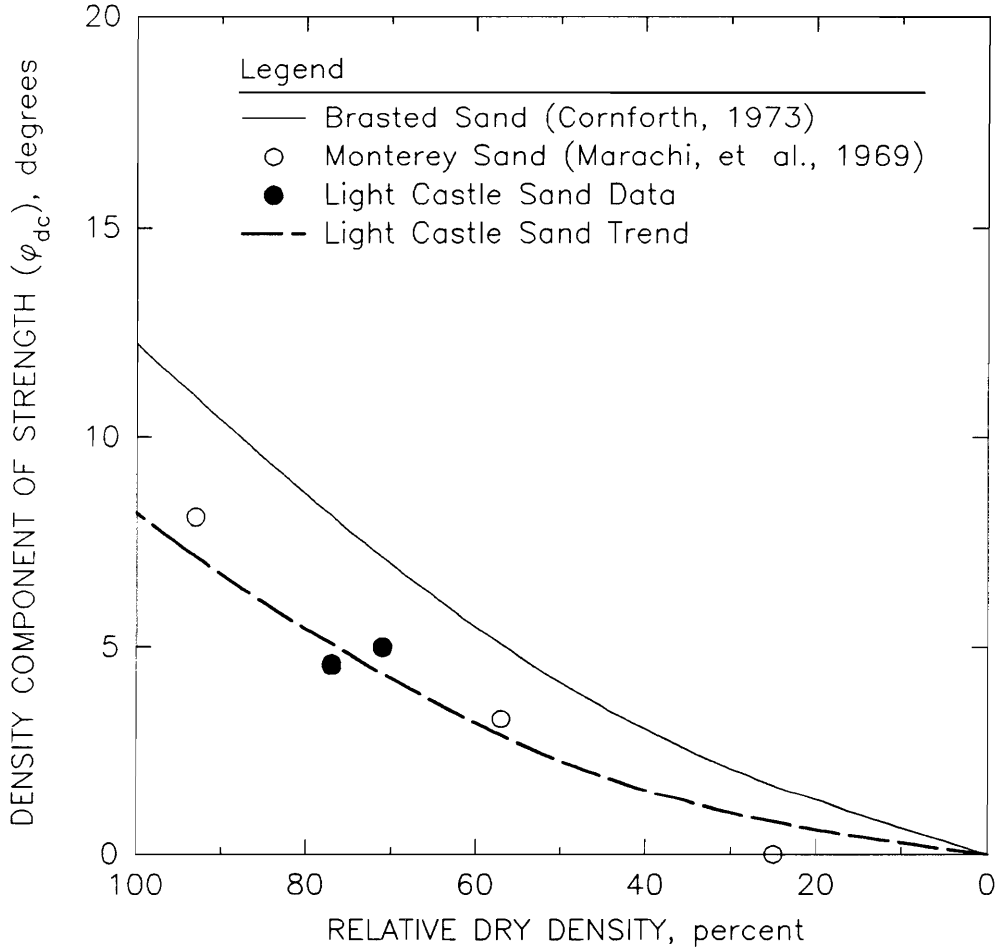

Figure A.22: Strength versus Density for Light Castle Sand

APPENDIX B - EPCOMPAC USER'S GUIDE AND PROGRAM LISTING

This appendix contains a user's guide for the program EPCOMPAC, which is described in Chapter 6. The program listing follows the user's guide.

Virginia Tech

The Charles E. Via, Jr.
Department of Civil Engineering

User's Guide for

EPCOMPAC

by

G. M. Filz,

J. M. Duncan,

and

R. B. Seed

April, 1992

Geotechnical Division

Department of Civil Engineering

Virginia Polytechnic Institute and State University

Blacksburg, VA 24061

BACKGROUND

The computer program NCOMP, written by R. B. Seed in 1983, calculated earth pressures due to compaction using the theory described by Duncan and Seed (1986). The program could be used interactively or in batch mode. A considerable amount of data was needed to describe the stresses induced by the compactor, the values of the soil properties, and the geometric parameters for the analyses.

In 1988 and 1989 the program was revised by J. M. Duncan, G. W. Williams, and R. B. Seed to reduce the amount of input required. Routines were added to calculate stresses for line loads (roller compactors) and plate loads (vibrating plate and rammer plate compactors). The program EPCOMP2 was developed to handle interactive input data file generation and to calculate stresses for plate compactors. EPCOMP2 called the program NCOMP3, which was a revised version of Seed's program NCOMP, to calculate the compaction-induced stresses.

In 1992, Filz and Duncan developed EPCOMPAC to replace both EPCOMP2 and NCOMP3. EPCOMPAC incorporates the revised and extended compaction-induced earth pressure theory developed by Filz (1992). Revisions were made to the theory described by Duncan and Seed (1986) to make the k_o model in the theory truly hysteretic. The theory was also extended to include the effects of pore pressure response in moist soil.

PROGRAM OPERATION

EPCOMPAC, which is written in Microsoft Quick Basic 4.5, runs on IBM PC and compatible microcomputers. The

program is interactive. It creates, edits, and stores data files. It also calculates elastic stresses for plate and roller compactors, computes compaction-induced lateral stresses, and writes output files.

With EPCOMPAC.EXE in the active drive, the user begins by running EPCOMPAC. The program first asks whether the user wants to edit, run, or create a data file.

Newly Created Data Files

If the user is creating a new data file, the program asks for a descriptive heading for the file, and then whether the compactor is a plate or a roller.

Plate Compactors. For plate compactors, the program prompts the user for these data:

- Plate width (B)
- Plate length (L)
- Distance to wall (a)
- Total load on plate (Q)
- Maximum depth for calculating stress (Z_{max})
- Lift thickness (d_z)
- Coefficient of earth pressure at rest (k_o)
- Effective stress friction angle (ϕ')
- Effective stress cohesion intercept (ϕ)
- Total stress friction angle (c')
- Total stress cohesion intercept (c)
- Skempton's pore pressure parameter A
- Total unit weight of soil (γ)

Roller Compactors. For roller compactors, the program prompts the user for these data:

- Roller width (B)

- Distance from roller to wall (L)
- Total load on roller (Q)
- Maximum depth for calculating stress (Z_{max})
- Lift thickness (d_z)
- Coefficient of earth pressure at rest (k_o)
- Effective stress friction angle (ϕ')
- Effective stress cohesion intercept (c')
- Total stress friction angle (ϕ)
- Total stress cohesion intercept (c)
- Skempton's pore pressure parameter A
- Total unit weight of soil (γ)

For effective stress analyses, the values of total stress friction angle and total stress cohesion intercept should be set equal to the corresponding effective stress values. In this case the value of Skempton's pore pressure parameter A may be set equal to zero since it does not influence the calculations.

For total stress analyses, the value of total stress friction angle must be less than or equal to the value of the effective stress friction angle. Enter a value of total stress cohesion intercept that satisfies the following expression:

$$c \geq c' \left(\frac{\tan\phi}{\tan\phi'} \right) \qquad (1)$$

where c = the total stress cohesion intercept
c' = the effective stress cohesion intercept
ϕ = the total stress friction angle
ϕ' = the effective stress friction angle

It is recommended that a value of A equal to 0.5 be used for total stress analyses. The program computes values of Skempton's pore pressure parameter B and the initial apparent pore water pressure, U_o, according to:

$$B = \frac{\sin\phi' - \sin\phi}{\left[1 + (2\ A - 1)\ \sin\phi\right] \sin\phi'} \qquad (2)$$

$$U_o = -\frac{\left[1 + (2\ A - 1)\ \sin\phi'\right] \cos\phi}{\left[1 + (2\ A - 1)\ \sin\phi\right] \sin\phi'}\ c + \frac{c'}{\tan\phi'} \qquad (3)$$

If, in total stress analyses, it is desired to use particular values of B and U_o, then the following values of ϕ and c should be entered:

$$\phi = \sin^{-1}\left[\frac{(1 - B)\ \sin\phi'}{1 + B\ (2\ A - 1)\ \sin\phi'}\right] \qquad (4)$$

$$c = \frac{\left[1 + (2\ A - 1)\ \sin\phi\right] \sin\phi'}{\left[1 + (2\ A - 1)\ \sin\phi'\right] \cos\phi}\left[\frac{c'}{\tan\phi'} - U_o\right] \qquad (5)$$

Changing Data Files After Input. After the user has input the last item, the program displays all the items in a numbered list, and asks if any of the input needs to be changed. The user responds by typing first the line number

and then the new value of the item to be changed. For no more changes, the user types zero + return, or return with no input.

Storing Data Files After Input. When there are no more changes to the file, the program displays a list of the files in the directory that have extensions ".DAT", and prompts the user for a name for the new data file. The file extension ".DAT" is automatically appended to the root file name provided by the user.

Analyses. EPCOMPAC calculates elastic stresses due to the compactor load and computes compaction-induced lateral stresses.

Output. When the analyses are completed, EPCOMPAC writes three output files: filename.OUT, filename.PVD, and filename.HYS. Filename.OUT contains the input data file name, the date and time of the run, the input data, and the calculated earth pressures due to compaction. Filename.PVD contains the calculated earth pressures versus depth in a comma delimited file suitable for use in plotting programs. Filename.HYS contains the calculated hysteretic stress path loops in a comma delimited file suitable for use in plotting programs.

Editing Data Files

To edit an existing data file, the user responds "E" (edit) to the first prompt by EPCOMPAC. The program then displays a list of the files in the active directory that have file extensions ".DAT", and prompts the user for the name of the file to edit.

When a valid data file name has been typed, the program displays the data as described earlier in the

section on changing data files after input. Subsequent operations are also the same as for newly created data files.

After the changes, if any, are completed, the program prompts for a filename. To use the same file name, and overwrite the preceding data, type return with no input. To avoid overwriting the preceding data file, enter a new file name.

Running a Data File Without Editing the Data

To run an existing data file without editing the data, the user responds "R" to the first prompt by EPCOMPAC. The program then displays a list of the files in the active directory that have file extensions ".DAT", and prompts the user for the name of the file to run.

When a valid data file name has been typed, the program calculates the compaction-induced stresses and writes output files without first displaying the input data.

ANALYSIS PROCEDURES

EPCOMPAC generates elastic stress profiles from compactor loads using the Boussinesq solution. Loads on plates are represented by 400 point loads distributed evenly over the area of the plate. Loads from roller compactors are represented as line loads, and the stresses are calculated from a closed form integration of the Boussinesq point load solution. Stresses are calculated at mid-depth in each lift.

EPCOMPAC analyses always use lift thicknesses that are uniform throughout the depth of the fill. The number of layers is equal to the depth of the fill divided by the lift thickness. This number should not be more than 100.

EPCOMPAC analyses always use values of the parameter α corresponding to the correlation between α and ϕ' recommended by Duncan and Seed (1986). These values are:

ϕ'	α
0	0.23
5	0,24
10	0.25
15	0.27
20	0.31
25	0.39
30	0.49
35	0.63
40	0.73
45	0.76
≤50	0.77

Intermediate values are determined by linear interpolation.

As recommended by Duncan and Seed (1986), the values of effective stress Poisson's ratio (ν') used in EPCOMPAC2 analyses are related to ϕ' by the equation:

$$\nu' = \frac{4 - 3 \sin\phi'}{8 - 4 \sin\phi'} \qquad (6)$$

Also as recommended by Duncan and Seed (1986), the value of β used in the analyses is always equal to 0.6.

The parameter k_{lim} is equal to the reciprocal of the effective stress, at-rest lateral earth pressure coefficient:

$$k_{lim} = \frac{1}{k_o} \tag{7}$$

EXAMPLES

Two examples are shown in the following pages. Example 1 is for a plate, and Example 2 is for a roller. The input and output files are given for each example.

REFERENCES

Duncan, J. M. and Seed, R. B. (1986) "Compaction - Induced Earth Pressures Under k_o Conditions," Journal of the Geotechnical Engineering Division, ASCE, Vol. 112, No. 1, January, 1986, pp. 1-22.

Filz, G. M. (1992) "An Experimental and Analytical Study of Earth Loads on Rigid Retaining Walls," Ph.D. Dissertation, Via Department of Civil Engineering, Virginia Polytechnic Institute and State University, Blacksburg, Virginia.

```
P
Plate compactor example
 1
 1
 .25
 4000
 10
 .5
 .38
 38
 0
 38
 0
 0
 120
```

Example 1 - Data file PLATE25.DAT for EPCOMPAC

```
Plate compactor example
Program EPCOMPAC, Version 2.0, February, 1992
Input data file used: PLATE25.DAT
Date of this run: 04-08-1992          Time of this run: 12:52:44

Compactor: Type = Plate
           Plate width =                        1.00 ft
           Plate length =                       1.00 ft
           Total load (static + dynamic) =  4,000.00 lbs
Geometry: Distance to wall =     0.25 ft     Total fill depth =  10.00 ft
          Lift thickness =       0.50 ft
Soil: Eff. coef. of E.P. at rest (K0) =  0.38       Klim =            2.63
      Eff. angle of int. fric. (phi') = 38.00 deg   Alpha =           0.69
      Eff. cohesion intercept (c') =     0.00 psf   Beta =            0.60
      Tot. angle of int. fric. (phi) =  38.00 deg   Eff. Poisson =    0.39
      Tot. cohesion intercept (c) =      0.00 psf   Skempton's B =    0.00
      Skempton's A parameter =           0.00       Total K0 =        0.38
      Moist unit weight =              120.00 pcf   Total Poisson =   0.39
```

Depth Below Surface (ft)	Total Stress Horizontal Pressures on the Wall (psf)			
	At Rest Component	Total Before Compaction	Peak During Compaction	Total After Compaction
0.25	11	11	1567	79
0.75	34	90	763	237
1.25	57	248	375	263
1.75	80	273	314	278
2.25	103	286	301	288
2.75	125	296	301	296
3.25	148	304	306	304
3.75	171	313	313	313
4.25	194	323	323	323
4.75	217	332	332	332
5.25	239	342	342	342
5.75	262	352	352	352
6.25	285	362	362	362
6.75	308	372	372	372
7.25	331	383	383	383
7.75	353	394	394	394
8.25	376	405	405	405
8.75	399	417	417	417
9.25	422	428	428	428
9.75	445	445	445	445

Example 1 - Output file PLATE25.OUT from EPCOMPAC

```
R
Roller compactor example
 7
 0
 1
 42000
 10
 .5
 .43
 35
 0
 35
 0
 0
 125
```

Example 2. - Data file ROLLER1.DAT for EPCOMPAC

```
Roller compactor example
Program EPCOMPAC, Version 2.0, February, 1992
Input data file used: ROLLER1.DAT
Date of this run: 04-08-1992          Time of this run: 12:51:03

Compactor: Type = Roller
           Roller width =                        7.00 ft
           Total load (static + dynamic) =  42,000.00 lbs
Geometry: Distance to wall =     1.00 ft     Total fill depth =  10.00 ft
          Lift thickness =       0.50 ft
Soil: Eff. coef. of E.P. at rest (K0) =  0.43       Klim =            2.33
      Eff. angle of int. fric. (phi') = 35.00 deg   Alpha =           0.63
      Eff. cohesion intercept (c') =     0.00 psf   Beta =            0.60
      Tot. angle of int. fric. (phi) =  35.00 deg   Eff. Poisson =    0.40
      Tot. cohesion intercept (c) =      0.00 psf   Skempton's B =    0.00
      Skempton's A parameter =           0.00       Total K0 =        0.43
      Moist unit weight =              125.00 pcf   Total Poisson =   0.40
```

Depth Below Surface (ft)	Total Stress Horizontal Pressures on the Wall (psf)			
	At Rest Component	Total Before Compaction	Peak During Compaction	Total After Compaction
0.25	13	13	379	73
0.75	40	88	1041	218
1.25	67	233	1015	363
1.75	94	378	861	407
2.25	121	421	736	438
2.75	148	451	689	463
3.25	175	475	658	483
3.75	202	495	637	501
4.25	228	513	624	517
4.75	255	528	616	531
5.25	282	542	612	544
5.75	309	554	611	556
6.25	336	566	612	568
6.75	363	577	615	578
7.25	390	588	619	589
7.75	417	598	624	600
8.25	443	609	631	611
8.75	470	620	639	622
9.25	497	630	647	633
9.75	524	641	656	644

Example 2 - Output file ROLLER1.OUT from EPCOMPAC

```
'--------------------------------------------------------------------------
'--------------------            EPCOMPAC              --------------------
'--------------------   Version 2.0  -  April, 1991    --------------------
'--------------------          Virginia Tech           --------------------
'--------------------------------------------------------------------------
DECLARE SUB findunloadpt (effsigv!)
DECLARE SUB editdata ()
DECLARE SUB parameters ()
DECLARE SUB hysteresis (delu!, totaldeltav!)
DECLARE FUNCTION boussinesq! (z!)
DECLARE SUB screendisplay ()
DECLARE SUB readdatafile ()
DECLARE SUB getfilename ()
DECLARE SUB openoutfiles ()
DECLARE SUB setuploops ()
DECLARE FUNCTION deltau! (sigv!, sigh!, lastsigv!, lastsigh!, effortotal$)
DECLARE SUB totalK0Model (totaldelsigv!)
DECLARE SUB K0caller1 (delu!, totaldelsigv!)
DECLARE SUB K0caller2 (effdelsigv!)
DECLARE SUB effK0Model (effdelsigv!)
CONST Max = 200
DIM SHARED head$, type$, hardbottom$        'from input data file
DIM SHARED B, L, a, Q, Zmax, dz             'from input data file
DIM SHARED effK0, effphi, effc, totalphi    'from input data file
DIM SHARED totalc, SkmptA, gam              'from input data file
DIM SHARED filename$                        'root of the filenames
DIM SHARED action$, scrntype$               'control flags
DIM SHARED fillonly$, firsttime$            'control flags
DIM SHARED effnu, totalK0, totalnu          'soil properties
DIM SHARED effphir, totalphir               'soil properties
DIM SHARED K1, alpha, beta, SkmptB          'soil properties
DIM SHARED effsigh0, effsigvftan            'soil properties
DIM SHARED effsigvmaxtan                    'soil properties
DIM SHARED peakv(Max), peakh(Max)           'soil state
DIM SHARED unloadh(Max), unloadv(Max)       'soil state
DIM SHARED beta(Max), numloops              'soil state
DIM SHARED u, totalsigh, totalsigv          'soil state
DIM SHARED liftsabove, numlifts             'fill geometry
DIM bous(Max), sighfillonly(Max)
hardbottom$ = "NO"
CALL screendisplay
DO
        LOCATE 8, 1
        DO
                INPUT "    Edit or Run an existing data file, or Create a new file (E/R/C) ",
                        action$
                action$ = UCASE$(action$)
        LOOP UNTIL action$ = "E" OR action$ = "R" OR action$ = "C"
        IF action$ = "E" OR action$ = "R" THEN CALL readdatafile
        IF action$ = "E" OR action$ = "C" THEN CALL editdata
        CALL parameters
```

```
CLS
LOCATE 5, 5
PRINT "Computing horizontal stresses due to the fill only."
LOCATE 6, 5
PRINT "Percent complete:   0 %"
fillonly$ = "yes"
CALL setuploops
FOR lift = 1 TO numlifts                'lifts numbered from top down.
        IF lift = 1 THEN
                deltagammaz = gam * dz / 2
        ELSE
                deltagammaz = gam * dz
        END IF
        CALL totalKOModel(deltagammaz)
        sighfillonly(lift) = totalsigh
        LOCATE 6, 23
        PRINT USING "###"; CINT(100 * lift / numlifts)
NEXT lift
fillonly$ = "no"
CALL openoutfiles
LOCATE 8, 5
PRINT "Computing Boussinesq stresses for the entire profile."
LOCATE 9, 5
PRINT "Percent complete:   0 %"
IF hardbottom$ = "NO" THEN
        range = numlifts
        start = numlifts
ELSE
        range = 2 * numlifts
        start = 1
END IF
FOR i = 1 TO range
        z = dz * (i - 1 / 2)
        bous(i - 1) = boussinesq(z)
        LOCATE 9, 23
        PRINT USING "###"; CINT(100 * i / range)
NEXT i
LOCATE 11, 5
PRINT "Computing compaction induced stresses and writing the results to files."
LOCATE 12, 5
PRINT "Percent complete:   0 %"
calcs = 0
totalcalcs = numlifts * (numlifts + 1) / 2 - start * (start - 1) / 2
firsttime$ = "yes"
FOR lift = start TO numlifts            'lifts numbered from top down.
        CALL setuploops
        FOR liftsabove = 0 TO lift - 1      'liftsabove = compactor position
                IF liftsabove = 0 THEN          '  in lifts above the lift
                        deltagammaz = gam * dz / 2   '  currently being analyzed.
                ELSE
                        deltagammaz = gam * dz
```

```
                        END IF
                        CALL totalKOModel(deltagammaz)
                        sighbefore = totalsigh
                        boussigh = bous(liftsabove)
                        IF hardbottom$ = "YES" THEN
                                currentnumlifts = numlifts - lift + 1 + liftsabove
                                image = 2 * currentnumlifts - liftsabove
                                boussigh = boussigh + bous(image)
                        END IF
                        CALL totalKOModel(boussigh / totalKO)
                        sighpeak = totalsigh
                        CALL totalKOModel(-boussigh / totalKO)
                        sighafter = totalsigh
                        calcs = calcs + 1
                        IF hardbottom$ = "NO" THEN
                                z = dz * (liftsabove + 1 / 2)
                                PRINT #2, USING "       ###.##      #####          #####"; z;
                                        sighfillonly(liftsabove + 1); sighbefore;
                                PRINT #2, USING "          #####          #####"; sighpeak;
                                        sighafter
                                WRITE #3, z, sighfillonly(liftsabove + 1), sighpeak, sighafter
                        END IF
                        LOCATE 12, 23
                        PRINT USING "###"; CINT(100 * calcs / totalcalcs)
                NEXT liftsabove
                IF hardbottom$ = "YES" THEN
                        z = dz * (lift - 1 / 2)
                        PRINT #2, USING "       ###.##      #####          #####"; z;
                                sighfillonly(lift); sighbefore;
                        PRINT #2, USING "          #####          #####"; sighpeak; sighafter
                        WRITE #3, z, sighfillonly(lift), sighpeak, sighafter
                END IF
        NEXT lift
        CLOSE
        DO
                CLS
                LOCATE 5, 5
                INPUT "Perform another analysis (y/n) ", repeat$
                repeat$ = UCASE$(repeat$)
        LOOP UNTIL repeat$ = "Y" OR repeat$ = "N"
        CLS
LOOP UNTIL repeat$ = "N"
Mono:    ' Monochrome screen error handling
        scrntype$ = "mono"
        RESUME NEXT
CLS
END

FUNCTION boussinesq (z)
'''''''''''''''''''''''''''''''''''''''''''''''''''''''''''''''''''''''''''''''''
'   Computes the Boussinesq horizontal stress at the wall due at
```

```
'   depth z due to the plate or roller compactor force at the surface.
'
'''''''''''''''''''''''''''''''''''''''''''''''''''''''''''''''''''''''''''''
a1 = 1 - totalnu
a2 = 1 - 2 * totalnu
IF type$ = "P" THEN  'a plate compactor
        dx = B / 20
        dy = L / 20
        boussh = 0
        FOR ix = 1 TO 20
                x = a + (ix - 1 / 2) * dx
                FOR iy = 1 TO 10
                        y = (iy - 1 / 2) * dy
                        R1 = SQR(x ^ 2 + y ^ 2 + z ^ 2)
                        P1 = (-Q / 400) / (8 * (3.1415926#) * a1)
                        P2 = (a2 * z) / (R1 ^ 3)
                        P3 = (3 * (x ^ 2) * z) / (R1 ^ 5)
                        P4 = (a2 * ((3 * z) - (4 * totalnu * z))) / (R1 ^ 3)
                        P5 = (3 * (3 - (4 * totalnu)) * (x ^ 2) * z) / (R1 ^ 5)
                        P6 = ((4 * a1 * a2) / (R1 * (R1 + z)))
                        P7 = (1 - ((x ^ 2) / (R1 * (R1 + z))) - ((x ^ 2) / (R1 ^ 2)))
                        dboussh = P1 * (P2 - P3 + P4 - P5 - P6 * P7)
                        boussh = boussh + 4 * dboussh  'doubled for x-axis sym and
                NEXT iy                              '  doubled again for rigid wall.
        NEXT ix
ELSE  'a roller compactor
        x1 = a
        x2 = a + B
        t1 = x2 ^ 3 / (x2 ^ 2 + z ^ 2) ^ 1.5
        t2 = x2 * a2 / ((x2 ^ 2 + z ^ 2) ^ .5 + z)
        t3 = x1 ^ 3 / (x1 ^ 2 + z ^ 2) ^ 1.5
        t4 = x1 * a2 / ((x1 ^ 2 + z ^ 2) ^ .5 + z)
        boussh = (Q / B) * (t1 - t2 - t3 + t4) / (z * 3.1415926#)
END IF
IF boussh < 0 THEN boussh = 0
boussinesq = boussh
END FUNCTION

FUNCTION deltau (sigv, sigh, lastsigv, lastsigh, effortotal$)
'''''''''''''''''''''''''''''''''''''''''''''''''''''''''''''''''''''''''''''
'   Calculates the incremental change in pore pressure that occurs
'   in response to  changes in total stress.
'
'''''''''''''''''''''''''''''''''''''''''''''''''''''''''''''''''''''''''''''
IF sigv > sigh THEN
        sig1 = sigv
        sig3 = sigh
ELSE
        sig1 = sigh
        sig3 = sigv
END IF
```

```
IF lastsigv > lastsigh THEN
        lastsig1 = lastsigv
        lastsig3 = lastsigh
ELSE
        lastsig1 = lastsigh
        lastsig3 = lastsigv
END IF
delsig1 = sig1 - lastsig1
delsig3 = sig3 - lastsig3
du = SkmptB * (delsig3 + SkmptA * (delsig1 - delsig3))
IF effortotal$ = "eff" THEN
        du = du / (1 - SkmptB)
END IF
deltau = du
END FUNCTION

SUB editdata
'.....................................................................
'   Edit an existing data file or create a new data file.
'   Saves the modified or new data file on disk under a user supplied name.
'
'.....................................................................
IF action$ = "C" THEN     ' Create a new input data set
        CLS
        PRINT "Type a heading for the problem"
        LINE INPUT head$
        DO
                INPUT "Compactor type: Plate or Roller (P/R) "; type$
                type$ = UCASE$(type$)
        LOOP UNTIL type$ = "P" OR type$ = "R"
        IF type$ = "P" THEN
                INPUT "Plate width,                              B = ", B
                INPUT "Plate length,                             L = ", L
                INPUT "Distance from edge of plate to wall,      A = ", a
                INPUT "Total load on plate,                      Q = ", Q
        ELSE
                INPUT "Roller width,                             B = ", B
                L = 0
                INPUT "Distance from edge of roller to wall,     A = ", a
                INPUT "Total load on roller,                     Q = ", Q
        END IF
        INPUT "Maximum depth for calculating stress, Zmax = ", Zmax
'    DO
'        INPUT "Hard base below fill (y/n)                  ", hardbottom$
'        hardbottom$ = UCASE$(hardbottom$)
'    LOOP UNTIL hardbottom$ = "Y" OR hardbottom$ = "N"
'    IF hardbottom$ = "Y" THEN
'        hardbottom$ = "YES"
'    ELSE
'        hardbottom$ = "NO"
'    END IF
```

```
        INPUT "Lift thickness,                          dz = ", dz
        INPUT "Eff. coeff. of earth pressure at rest,  K0 = ", effK0
        INPUT "Effective stress friction angle,      phi' = ", effphi
        IF effphi < 1 THEN
                effphi = 1
        ELSEIF effphi > 60 THEN
                effphi = 60
        END IF
        INPUT "Effective stress cohesion intercept,    c' = ", effc
        IF effc < 0 THEN
                effc = 0
        END IF
        INPUT "Total stress friction angle,          phi = ", totalphi
        IF totalphi < 1 THEN
                totalphi = 0
        ELSEIF totalphi > effphi THEN
                totalphi = effphi
        END IF
        INPUT "Total stress cohesion intercept,        c = ", totalc
        IF totalc < effc THEN
                totalc = effc
        END IF
        INPUT "Skempton's A pore pressure parameter       = ", SkmptA
        INPUT "Moist unit weight of soil,          gamma = ", gam
END IF
DO        ' Edit the input data set
        CLS
        LOCATE 2, 1: PRINT "Current values of the input variables:"
        PRINT
        PRINT " (1)  Heading = "; head$
        IF type$ = "P" THEN
                PRINT " (2)  Plate width,                          B = ", B
                PRINT " (3)  Plate length,                         L = ", L
                PRINT " (4)  Distance from edge of plate to wall,  A = ", a
                PRINT " (5)  Total load on plate,                  Q = ", Q
                PRINT " (6)  Maximum depth for calculating stress, Zmax = ", Zmax
'                PRINT " (7)  Hard base below fill,                    ", hardbottom$
                PRINT " (7)  Lift thickness,                      dz = ", dz
                PRINT " (8)  Eff. coeff. of earth pressure at rest, K0 = ", effK0
                PRINT " (9)  Effective stress friction angle,    phi' = ", effphi
                PRINT "(10)  Effective stress cohesion intercept,  c' = ", effc
                PRINT "(11)  Total stress friction angle,        phi = ", totalphi
                PRINT "(12)  Total stress cohesion intercept,      c = ", totalc
                PRINT "(13)  Skempton's A pore pressure parameter    = ", SkmptA
                PRINT "(14)  Moist unit weight of soil,        gamma = ", gam
        ELSE
                PRINT " (2)  Roller width,                         B = ", B
                PRINT " (3)  Distance from edge of roller to wall, A = ", a
                PRINT " (4)  Total load on roller,                 Q = ", Q
                PRINT " (5)  Maximum depth for calculating stress, Zmax = ", Zmax
'                PRINT " (6)  Hard base below fill,                    ", hardbottom$
```

```
            PRINT " (6)  Lift thickness,                              dz = ", dz
            PRINT " (7)  Eff. coeff. of earth pressure at rest,     K0 = ", effK0
            PRINT " (8)  Effective stress friction angle,         phi' = ", effphi
            PRINT " (9)  Effective stress cohesion intercept,       c' = ", effc
            PRINT "(10)  Total stress friction angle,              phi = ", totalphi
            PRINT "(11)  Total stress cohesion intercept,            c = ", totalc
            PRINT "(12)  Skempton's A pore pressure parameter          = ", SkmptA
            PRINT "(13)  Moist unit weight of soil,              gamma = ", gam
        END IF
        DO
            PRINT "  Enter the number corresponding to the variable to be changed."
            INPUT "  Enter zero (0) for no more changes.  ", numchange
            IF type$ = "R" AND numchange > 2 THEN numchange = numchange + 1
        LOOP UNTIL 0 <= numchange AND numchange <= 14
        CLS
        LOCATE 4, 5
        SELECT CASE numchange
            CASE 1
               LINE INPUT "Heading = ", head$
            CASE 2
               INPUT "Compactor width,                              B = ", B
            CASE 3
               INPUT "Plate length,                                 L = ", L
            CASE 4
               INPUT "Distance from edge of compactor to wall,      A = ", a
            CASE 5
               INPUT "Total load on compactor,                      Q = ", Q
            CASE 6
               INPUT "Maximum depth for calculating stress,     Zmax = ", Zmax
'       CASE 7
'           DO
'               INPUT "Hard base below fill (y/n) ", hardbottom$
'               hardbottom$ = UCASE$(hardbottom$)
'           LOOP UNTIL hardbottom$ = "Y" OR hardbottom$ = "N"
'           IF hardbottom$ = "Y" THEN
'               hardbottom$ = "YES"
'           ELSE
'               hardbottom$ = "NO"
'           END IF
               CASE 7
                  INPUT "Lift thickness,                              dz = ", dz
               CASE 8
                  INPUT "Eff. coeff. of earth pressure at rest,    K0 = ", effK0
               CASE 9
                  INPUT "Effective stress friction angle,        phi' = ", effphi
               CASE 10
                  INPUT "Effective stress cohesion intercept,      c' = ", effc
               CASE 11
                  INPUT "Total stress friction angle,             phi = ", totalphi
               CASE 12
                  INPUT "Total stress cohesion intercept,          c = ", totalc
```

```
                CASE 13
                        INPUT "Skempton's A pore pressure parameter      = ", SkmptA
                CASE 14
                   INPUT "Moist unit weight of soil,               gamma = ", gam
        END SELECT
        IF effphi < 1 THEN
                effphi = 1
        ELSEIF effphi > 60 THEN
                effphi = 60
        END IF
        IF effc < 0 THEN
                effc = 0
        END IF
        IF totalphi < 1 THEN
                totalphi = 0
        ELSEIF totalphi > effphi THEN
                totalphi = effphi
        END IF
        IF totalc < effc THEN
                totalc = effc
        END IF
LOOP UNTIL numchange = 0
' Store the input data on disk under a user specified file name
CALL getfilename
OPEN filename$ + ".dat" FOR OUTPUT AS #1
PRINT #1, type$
PRINT #1, head$
PRINT #1, B
PRINT #1, L
PRINT #1, a
PRINT #1, Q
PRINT #1, Zmax
'PRINT #1, hardbottom$
PRINT #1, dz
PRINT #1, effK0
PRINT #1, effphi
PRINT #1, effc
PRINT #1, totalphi
PRINT #1, totalc
PRINT #1, SkmptA
PRINT #1, gam
CLOSE #1
END SUB

SUB effK0Model (effdelsigv)
'''''''''''''''''''''''''''''''''''''''''''''''''''''''''''''''''''''''''''''
' Hysteretic effK0 model of soil loading and unloading.
' þ The model employs a series of nested loading and unloading loops.  Loop
'   zero is the outermost loop: peakh(0) & peakv(0) define the maximum
'   past loading point on the effK0 line and unloadh(0) & unloadv(0) define
'   the corresponding minimum unloading point on the K1 line.  The variable
```

```
'   numloops equals the current number of nested loops.  Thus,
'       peakv(0) => peakv(1) => peakv(1) => ... => peakv(numloops)
'       unloadv(0) <= unloadv(1) <= unloadv(2) <= ... <= unloadv(numloops)
' þ The value of numloops is adjusted if a load increment takes the stress
'   state outside the limits of interior hysteresis loops.
' þ A degenerate loop is constructed at the current stress state to
'   facilitate interpolation to calculate the stress state after the
'   next increment of load:
'   a) If a load increment is positive (effdelsigv > 0), and after finding the
'      the value of numloops necessary to make the loops nested properly,
'      numloops is increased by one (numloops = numloops +1) and a degenerate
'      loop is added at the current end of the loading path:
'        peakh(numloops) = peakh(numloops - 1) = effsigh
'        peakv(numloops) = peakv(numloops - 1) = effsigv
'        unloadh(numloops) =  effsigh
'        unloadv(numloops) =  effsigv
'   b) If a load increment is negative (effdelsigv < 0), the peak stress for the
'      innermost loop is set equal to the innermost unloading point:
'        peakh(numloops) = unloadh(numloops)
'        peakv(numloops) = unloadv(numloops)
' þ If unloading takes place from the effK0 line, an extra loop is inserted
'   in the nested set from the current unloading point to the target reloading
'   point on the effK0 line.
' þ Loading is always linear (either effK0 or beta-type) and unloading is either
'   linear (K1) or non-linear (alpha-type).
'
''''''''''''''''''''''''''''''''''''''''''''''''''''''''''''''''''''''''''''''''
IF effdelsigv = 0 THEN EXIT SUB
effsigv = peakv(numloops) + effdelsigv
IF effsigv <= 0 THEN
        effsigv = 0
        effsigh = 0
        numloops = 0
        unloadv(0) = 0
        unloadh(0) = 0
        peakv(0) = 0
        peakh(0) = 0
        EXIT SUB
END IF
IF effdelsigv > 0 THEN
        IF effsigv >= peakv(0) THEN   'a new maximum past loading point on effK0 line
                numloops = 0
                effsigh = effK0 * effsigv
                CALL findunloadpt(effsigv)
        ELSE   'find the (new) number of loops and calculate effsigh
                j = 0
                DO
                        j = j + 1
                LOOP UNTIL peakv(j) <= effsigv AND effsigv < peakv(j - 1)
                numloops = j
                slope = (peakh(j - 1) - peakh(j)) / (peakv(j - 1) - peakv(j))
```

```
                effsigh = peakh(j) + slope * (effsigv - peakv(j))
        END IF
        peakh(numloops) = effsigh
        peakv(numloops) = effsigv
        numloops = numloops + 1     'add the degenerate loop
        peakh(numloops) = effsigh
        peakv(numloops) = effsigv
        unloadh(numloops) = effsigh
        unloadv(numloops) = effsigv
ELSE    'effdelsigv < 0
        IF effsigv <= unloadv(0) THEN   'a new minimum unloading point
                numloops = 1
                IF effsigv > effsigvftan THEN
                        effsigh = K1 * effsigv + effsigh0
                        peakv(0) = effsigv * ((K1 + effsigh0 / effsigv) / effK0) ^ (1 / alpha)
                        peakh(0) = effK0 * peakv(0)
                        unloadv(0) = effsigv
                        unloadh(0) = effsigh
                ELSE
                        peakv(0) = effsigvmaxtan
                        peakh(0) = effK0 * peakv(0)
                        unloadv(0) = 0
                        unloadh(0) = 0
                        OCR = effsigvmaxtan / effsigv
                        effsigh = effK0 * OCR ^ alpha * effsigv
                END IF
        ELSE  'find the (new) number of loops and calculate effsigh
                j = 0
                DO
                        j = j + 1
                LOOP UNTIL unloadv(j - 1) < effsigv AND effsigv <= unloadv(j)
                numloops = j
                K2 = unloadh(j) / unloadv(j)
                IF unloadv(j - 1) > 0 THEN
                        K3 = unloadh(j - 1) / unloadv(j - 1)
                        alpha1 = LOG(K3 / K2) / LOG(unloadv(j) / unloadv(j - 1))
                ELSE
                        alpha1 = alpha
                END IF
                OCR1 = unloadv(j) / effsigv
                effsigh = K2 * (OCR1) ^ alpha1 * effsigv
        END IF
        unloadv(numloops) = effsigv
        unloadh(numloops) = effsigh
        IF ABS(peakh(numloops - 1) / peakv(numloops - 1) - effK0) < .0001 THEN
                IF numloops = 1 THEN
                        beta1 = beta
                ELSE
                        numer = peakh(numloops - 2) - unloadh(numloops - 1)
                        denom = peakh(numloops - 1) - unloadh(numloops - 1)
                        beta1 = beta(numloops - 1) * numer / denom
```

```
                END IF
                beta(numloops) = beta1
                peakh(numloops) = effsigh + beta1 * (peakh(numloops - 1) - effsigh)
                peakv(numloops) = peakh(numloops) / effK0
                numloops = numloops + 1
                beta(numloops) = 1
                unloadv(numloops) = effsigv
                unloadh(numloops) = effsigh
        END IF
        peakv(numloops) = effsigv
        peakh(numloops) = effsigh
END IF
END SUB

SUB findunloadpt (effsigv)
'''''''''''''''''''''''''''''''''''''''''''''''''''''''''''''''''''''''''''''''''''''
'   Uses Newton-Raphson iteration to find the unloading point
'   on the K1 line.
'
'''''''''''''''''''''''''''''''''''''''''''''''''''''''''''''''''''''''''''''''''''''
IF effsigv <= effsigvmaxtan THEN
        unloadv(0) = 0
        unloadh(0) = 0
ELSE
        effsigvf = effsigv            'a trial value to start
        count = 0
        DO
                count = count + 1
                IF count > 1000 THEN
                        PRINT "Iteration did not converge in SUB findunloadpt."
                        CLOSE
                        STOP
                END IF
                OCR = effsigv / effsigvf
                f = effsigh0 + K1 * effsigvf - effK0 * OCR ^ alpha * effsigvf
                fprime = K1 - (1 - alpha) * effK0 * OCR ^ alpha
                dsigv = -f / fprime
                effsigvf = effsigvf + dsigv
        LOOP UNTIL ABS(dsigv / effsigvf) < .00001
        unloadv(0) = effsigvf
        unloadh(0) = effsigh0 + K1 * effsigvf
END IF
END SUB

SUB getfilename
'''''''''''''''''''''''''''''''''''''''''''''''''''''''''''''''''''''''''''''''''''''
'   Gets the root of the file name from the user for identifying
'   username.DAT, username.OUT, username.PVD, and username.HYS files.
'
'''''''''''''''''''''''''''''''''''''''''''''''''''''''''''''''''''''''''''''''''''''
CLS
```

```
PRINT "The following data files are currently on your disk:"
SHELL "dir *.dat /w"
PRINT
PRINT "Type the root name of the data file you will use (8 character max.)"
PRINT "The file extensions will be added automatically:"
PRINT "  username.DAT for the input data file"
PRINT "  username.OUT for the tabular output data file"
PRINT "  username.PVD for the z vs sigma-h (after compaction) output file for plotting"
PRINT "  username.HYS for the sigma-h vs sigma-v output file for plotting"
PRINT
IF filename$ <> "" AND action$ = "E" THEN
        prompt$ = "<" + filename$ + ">"
        lastfilename$ = filename$
ELSE
        promt$ = ""
END IF
DO
        PRINT "File name "; prompt$;
        INPUT ; filename$
        IF filename$ = "" THEN
                filename$ = lastfilename$
        END IF
        IF INSTR(filename$, ".") <> 0 THEN
                rootlength = INSTR(filename$, ".") - 1
        ELSE
                rootlength = LEN(filename$)
        END IF
        IF rootlength > 8 THEN
                rootlength = 8
        END IF
        filename$ = LEFT$(filename$, rootlength)
LOOP UNTIL LEN(filename$) > 0
END SUB

SUB hysteresis (delu, totaldeltav)
'''''''''''''''''''''''''''''''''''''''''''''''''''''''''''''''''''''''''''''
'   Computes values of effdelsigv for the calls to SUB K0model.
'   The effdelsigv values are chosen from the effdeltav value to
'   provide a reasonably complete tracking of the hysteretic
'   loading path, which is written to the file username.HYS.
'
'''''''''''''''''''''''''''''''''''''''''''''''''''''''''''''''''''''''''''''
IF firsttime$ = "yes" THEN
        WRITE #4, 1, peakv(numloops), peakh(numloops), 0, 0
        firsttime$ = "no"
END IF
IF totalphi = 0 THEN
        CALL K0caller1(delu, totaldeltav)
        WRITE #4, liftsabove + 1, peakv(numloops), peakh(numloops), totalsigv, totalsigh
ELSE
        effdeltav = totaldeltav - delu
```

```
effsigvfinal = peakv(numloops) + effdeltav
IF effsigvfinal < 0 THEN
        effsigvfinal = 0
        effdeltav = -peakv(numloops)
END IF
DO UNTIL peakv(numloops) = effsigvfinal
        IF effdeltav > 0 THEN        'finds breaks in linear segments
                IF peakv(numloops) = peakv(0) THEN
                        effdelsigv = effsigvfinal - peakv(0)
                ELSE
                        IF peakv(numloops - 1) > peakv(numloops) THEN
                                loops = numloops - 1
                        ELSE
                                loops = numloops - 2
                        END IF
                        IF effsigvfinal > peakv(loops) THEN
                                effdelsigv = peakv(loops) - peakv(numloops)
                        ELSE
                                effdelsigv = effsigvfinal - peakv(numloops)
                        END IF
                        IF peakh(numloops) > peakv(numloops) AND peakv(loops) >
                                        peakh(loops) THEN
                                slope = (peakh(loops) - peakh(numloops)) / (peakv(loops) -
                                        peakv(numloops))
                                eqsigvh = (peakh(numloops) - slope * peakv(numloops)) / (1
                                        - slope)
                                IF effdelsigv + peakv(numloops) > 1.00001 * eqsigvh THEN
                                        effdelsigv = 1.00001 * eqsigvh - peakv(numloops)
                                END IF
                        END IF
                END IF
        ELSE      'effdeltav < 0
                IF unloadv(numloops) = unloadv(0) THEN
                        IF effsigvfinal > effsigvftan THEN
                                effdelsigv = effsigvfinal - unloadv(0)
                        ELSE
                                effdelsigv = effsigvftan - unloadv(0)
                        END IF
                ELSE
                        IF unloadv(numloops - 1) < unloadv(numloops) THEN
                                loops = numloops - 1
                        ELSE
                                loops = numloops - 2
                        END IF
                        IF effsigvfinal < unloadv(loops) THEN  'find unloading segment
                                        limits
                                endptsigv = unloadv(loops)
                        ELSE
                                endptsigv = effsigvfinal
                        END IF
```

```
                        IF unloadv(numloops) > unloadh(numloops) AND unloadh(loops) >
                                unloadv(loops) THEN
                                K2 = unloadh(numloops) / unloadv(numloops)
                                K3 = unloadh(loops) / unloadv(loops)
                                alpha1 = LOG(K3 / K2) / LOG(unloadv(numloops) /
                                unloadv(loops))
                                eqsigvh = unloadv(numloops) * K2 ^ (1 / alpha1)
                                IF endptsigv < .99999 * eqsigvh THEN
                                        endptsigv = .99999 * eqsigvh
                                END IF
                        END IF
                        effdelsigv = (endptsigv - unloadv(numloops)) / 2
                        FOR kprt1 = 1 TO 4   'subdivide non-linear unloading segments
                                effdelsigv = effdelsigv / 2
                                FOR kprt2 = 1 TO 2
                                        CALL KOcaller2(effdelsigv)
                                        WRITE #4, liftsabove + 1, peakv(numloops),
                                                peakh(numloops), totalsigv, totalsigh
                                NEXT kprt2
                        NEXT kprt1
                                CALL KOcaller2(effdelsigv)
                                WRITE #4, liftsabove + 1, peakv(numloops),
                                        peakh(numloops), totalsigv, totalsigh
                        effdelsigv = endptsigv - unloadv(numloops)
                END IF
        END IF
        CALL KOcaller2(effdelsigv)
        WRITE #4, liftsabove + 1, peakv(numloops), peakh(numloops), totalsigv, totalsigh
    LOOP
END IF
END SUB

SUB KOcaller1 (delu, totaldelsigv)
'''''''''''''''''''''''''''''''''''''''''''''''''''''''''''''''''''''''''''''''''
'   Computes effdelsigv, calls effKOModel, and recomputes delu.
'
'''''''''''''''''''''''''''''''''''''''''''''''''''''''''''''''''''''''''''''''''
effdelsigv = totaldelsigv - delu
lastotsigh = peakh(numloops) + u
lastotsigv = peakv(numloops) + u
CALL effKOModel(effdelsigv)
totsigh = peakh(numloops) + u + delu
totsigv = peakv(numloops) + u + delu
delu = deltau(totsigv, totsigh, lastotsigv, lastotsigh, "total")
u = u + delu
totalsigh = peakh(numloops) + u
totalsigv = peakv(numloops) + u
END SUB

SUB KOcaller2 (effdelsigv)
'''''''''''''''''''''''''''''''''''''''''''''''''''''''''''''''''''''''''''''''''
```

```
'   Calls effKOModel and computes delu.
'       Note: Call only if totalphi > 0.
'''''''''''''''''''''''''''''''''''''''''''''''''''''''''''''''''''''''''''''
lasteffsigh = peakh(numloops)
lasteffsigv = peakv(numloops)
CALL effKOModel(effdelsigv)
effsigh = peakh(numloops)
effsigv = peakv(numloops)
delu = deltau(effsigv, effsigh, lasteffsigv, lasteffsigh, "eff")
u = u + delu
totalsigh = peakh(numloops) + u
totalsigv = peakv(numloops) + u
END SUB

SUB openoutfiles
'''''''''''''''''''''''''''''''''''''''''''''''''''''''''''''''''''''''''''''
'   Opens the output files and writes the heading for filename$.OUT.
'
'''''''''''''''''''''''''''''''''''''''''''''''''''''''''''''''''''''''''''''
OPEN filename$ + ".out" FOR OUTPUT AS #2
OPEN filename$ + ".pvd" FOR OUTPUT AS #3
IF hardbottom$ = "NO" THEN OPEN filename$ + ".hys" FOR OUTPUT AS #4
PRINT #2, "    "; head$
PRINT #2, "    Program EPCOMPAC, Version 2.0, April, 1992"
PRINT #2, "    Input data file used: "; UCASE$(filename$) + ".DAT"
PRINT #2, "    Date of this run: "; DATE$; "          Time of this run: "; TIME$
PRINT #2,
IF type$ = "P" THEN
        PRINT #2, "    Compactor: Type = Plate"
        PRINT #2, USING "              Plate width =                        #.## ft"; B
        PRINT #2, USING "              Plate length =                       #.## ft"; L
ELSE
        PRINT #2, "    Compactor: Type = Roller"
        PRINT #2, USING "              Roller width =                      ##.## ft"; B
END IF
PRINT #2, USING "              Total load (static + dynamic) = ######,.## lbs"; Q
PRINT #2, USING "    Geometry: Distance to wall =     #.## ft     Total fill depth = ###.## ft"; a;
        Zmax
'PRINT #2, USING "              Lift thickness =      ##.## ft     Hard base below fill: \ \ "; dz;
        hardbottom$
PRINT #2, USING "             Lift thickness =      ##.## ft"; dz
PRINT #2, USING "    Soil: Eff. coef. of E.P. at rest (KO) =  #.##       Klim =           ##.##";
        effKO; K1
PRINT #2, USING "          Eff. angle of int. fric. (phi') = ##.## deg   Alpha =           #.##";
        effphi; alpha
PRINT #2, USING "          Eff. cohesion intercept (c') = ####,.## psf   Beta =            #.##";
        effc; beta
PRINT #2, USING "          Tot. angle of int. fric. (phi) =  ##.## deg   Eff. Poisson =    #.##";
        totalphi; effnu
PRINT #2, USING "          Tot. cohesion intercept (c) = #####,.## psf   Skempton's B =    #.##";
        totalc; SkmptB
```

```
PRINT #2, USING "          Skempton's A parameter =          #.##       Total K0 =        #.##";
        SkmptA; totalK0
PRINT #2, USING "          Moist unit weight =             ###.## pcf   Total Poisson =   #.##";
        gam; totalnu
PRINT #2,
PRINT #2, "       Depth       Total Stress Horizontal Pressures on the Wall (psf)"
PRINT #2, "       Below     ---------------------------------------------------"
PRINT #2, "      Surface     At Rest     Total Before    Peak During    Total After"
PRINT #2, "       (ft)      Component     Compaction     Compaction     Compaction"
PRINT #2, "      -------    ---------    ------------    -----------    -----------"
END SUB

SUB parameters
'''''''''''''''''''''''''''''''''''''''''''''''''''''''''''''''''''''''''''''''''''''
'   Computes parameters needed for the compaction induced earth
'   pressure analysis.
'
'''''''''''''''''''''''''''''''''''''''''''''''''''''''''''''''''''''''''''''''''''''
numlifts = CINT(Zmax / dz)
radperdegree = 3.1415926# / 180
'Effective stress parameters
        effphir = effphi * radperdegree
        effnuK0 = effK0 / (1 + effK0)
        effnu = (effnuK0 + .5) / 2
        K1 = 1 / effK0                                          'chose K1=1/K0
        'K1 = (TAN((45 * radperdegree) + (effphir / 2))) ^ 2     'or K1=Kp
        effsigh0 = effc * (K1 - 1) / TAN(effphir)
        IF effphi = 0 THEN alpha = .23
        IF effphi >= 0 AND effphi < 5 THEN alpha = (.23 + (.01 * (effphi) / 5))
        IF effphi >= 5 AND effphi < 10 THEN alpha = (.24 + (.01 * (effphi - 5) / 5))
        IF effphi >= 10 AND effphi < 15 THEN alpha = (.25 + (.02 * (effphi - 10) / 5))
        IF effphi >= 15 AND effphi < 20 THEN alpha = (.27 + (.04 * (effphi - 15) / 5))
        IF effphi >= 20 AND effphi < 25 THEN alpha = (.31 + (.08 * (effphi - 20) / 5))
        IF effphi >= 25 AND effphi < 30 THEN alpha = (.39 + (.1 * (effphi - 25) / 5))
        IF effphi >= 30 AND effphi < 35 THEN alpha = (.49 + (.14 * (effphi - 30) / 5))
        IF effphi >= 35 AND effphi < 40 THEN alpha = (.63 + (.1 * (effphi - 35) / 5))
        IF effphi >= 40 AND effphi < 45 THEN alpha = (.73 + (.03 * (effphi - 40) / 5))
        IF effphi >= 45 AND effphi < 50 THEN alpha = (.76 + (.01 * (effphi - 45) / 5))
        IF effphi >= 50 THEN alpha = .77
        effsigvftan = (1 - alpha) * effsigh0 / (alpha * K1)
        effsigvmaxtan = (K1 / ((1 - alpha) * effK0)) ^ (1 / alpha) * effsigvftan
        beta = .6
'Total stress parameters
        totalphir = totalphi * radperdegree
        num = SIN(effphir) - SIN(totalphir)
        denom = SIN(effphir) * (1 + (2 * SkmptA - 1) * SIN(totalphir))
        SkmptB = num / denom
        num = effK0 + SkmptB * SkmptA * (1 - effK0)
        denom = 1 - SkmptB * (1 - SkmptA) * (1 - effK0)
        totalK0 = num / denom
        totalnuK0 = totalK0 / (1 + totalK0)
```

```
        totalnu = (totalnuK0 + .5) / 2
END SUB

SUB readdatafile
'''''''''''''''''''''''''''''''''''''''''''''''''''''''''''''''''''''''''''''
'   Reads username.DAT file, if editting or running action was chosen.
'
'''''''''''''''''''''''''''''''''''''''''''''''''''''''''''''''''''''''''''''
filename$ = ""
CALL getfilename
OPEN filename$ + ".dat" FOR INPUT AS #1
INPUT #1, type$
LINE INPUT #1, head$
INPUT #1, B
INPUT #1, L
INPUT #1, a
INPUT #1, Q
INPUT #1, Zmax
'INPUT #1, hardbottom$
INPUT #1, dz
INPUT #1, effK0
INPUT #1, effphi
INPUT #1, effc
INPUT #1, totalphi
INPUT #1, totalc
INPUT #1, SkmptA
INPUT #1, gam
CLOSE #1
END SUB

SUB screendisplay
'''''''''''''''''''''''''''''''''''''''''''''''''''''''''''''''''''''''''''''
'   Displays a Virginia Tech logo and message on the screen.
'
'''''''''''''''''''''''''''''''''''''''''''''''''''''''''''''''''''''''''''''
        ON ERROR GOTO Mono
        SCREEN 1
        IF scrntype$ = "mono" THEN GOTO XNDRIVER
vt:
        COLOR 1, 3
        LINE (230, 4)-(250, 35)
        LINE -(265, 12)
        LINE (270, 4)-(260, 4)
        LINE -(250, 20)
        LINE -(240, 4)
        LINE -(230, 4)
        LINE (270, 4)-(310, 4)
        LINE -(305, 12)
        LINE -(290, 12)
        LINE -(275, 35)
        LINE -(265, 35)
```

```
        LINE -(280, 12)
        LINE -(265, 12)
        PAINT (280, 5), 2, 3
        DIM vt(718)
        GET (228, 2)-(312, 37), vt
        x = 228: y = 2
        xdelta = -2
start:
        xbound = -1
        WHILE xbound
                x = x + xdelta
                IF x < 1 THEN
                        GOTO ce
                END IF
                PUT (x, y), vt, PSET
        WEND
        GOTO start
ce:
        LOCATE 2, 14
        PRINT "Virginia Tech "
        PRESET (310, 190)
        LINE -(230, 190)
        LINE -(250, 159)
        LINE -(268, 159)
        LINE -(268, 167)
        LINE -(254, 167)
        LINE -(246, 182)
        LINE -(275, 182)
        LINE -(275, 159)
        LINE -(290, 159)
        LINE -(295, 167)
        LINE -(283, 167)
        LINE -(283, 171)
        LINE -(291, 171)
        LINE -(295, 178)
        LINE -(283, 178)
        LINE -(283, 182)
        LINE -(305, 182)
        LINE -(310, 190)
        PAINT (276, 185), 2, 3
        DIM ce(718)
        GET (228, 157)-(312, 192), ce
        x = 228: y = 157
        ydelta = -2
cestart:
        ybound = -1
        WHILE ybound
                y = y + ydelta
                IF y < 2 THEN
                        GOTO logo
                END IF
```

```
                PUT (x, y), ce, PSET
        WEND
        GOTO cestart
logo:
        LOCATE 4, 14
        PRINT "Department of "
        LOCATE 6, 12
        PRINT "Civil Engineering"
        start! = TIMER
        WHILE (TIMER - start!) < .5
        WEND
        LOCATE 8, 16
        PRINT "presents..."
        start! = TIMER
        WHILE (TIMER - start!) < .5
        WEND
        LOCATE 15, 17
        PRINT "EPCOMPAC"
        start! = TIMER
        WHILE (TIMER - start!) < 1
        WEND
        LOCATE 23, 14
        PRINT "  Version 2.0"
        start! = TIMER
        WHILE TIMER - start! < .5
        WEND
XNDRIVER:
        CLS
                ERASE vt, ce
                SCREEN 0
                WIDTH 80
        CLS
        SCREEN 0
        COLOR 14, 1
        CLS
        PRINT : PRINT : PRINT
        PRINT "    EPCOMPAC  Version 2  April, 1991"
        PRINT "    A computer program for calculating earth pressures on stiff,"
        PRINT "    unyielding walls due to compaction of the backfill."
        PRINT
END SUB

SUB setuploops
'.....................................................................
'   Zeros the variables which define the hysteresis loops.
'   If cohesion > zero, establishes a load history corresponding to
'   the minimum possible past loading consistent with a zero total stress.
'
'.....................................................................
ERASE peakv, peakh, unloadh, unloadv, beta
numloops = 0
```

```
IF totalc > effc THEN
        num = -COS(totalphir) * (1 + (2 * SkmptA - 1) * SIN(effphir)) * totalc
        denom = SIN(effphir) * (1 + (2 * SkmptA - 1) * SIN(totalphir))
        u = num / denom + effc / TAN(effphir)
        effdelsigv = -(1 / effKO) ^ (1 / alpha) * u
        CALL effKOModel(effdelsigv)
        effdelsigv = -effdelsigv - u
        CALL effKOModel(effdelsigv)
ELSE
        u = 0
END IF
END SUB

SUB totalKOModel (totaldelsigv)
'''''''''''''''''''''''''''''''''''''''''''''''''''''''''''''''''''''''''''''''''
'   Uses direct iteration to find the pore pressure response to
'   the applied vertical stress increment.  Then calls hysteresis()
'   or KOcaller1() to obtain the final value of effsigh.
'
'''''''''''''''''''''''''''''''''''''''''''''''''''''''''''''''''''''''''''''''''
DIM bakpeakv(Max), bakpeakh(Max), bakunloadv(Max), bakunloadh(Max)
baknumloops = numloops
baku = u
FOR i = 0 TO numloops
        bakpeakv(i) = peakv(i)
        bakpeakh(i) = peakh(i)
        bakunloadv(i) = unloadv(i)
        bakunloadh(i) = unloadh(i)
NEXT i
lastotsigv = peakv(numloops) + u
lastotsigh = peakh(numloops) + u
totsigv = lastotsigv + totaldelsigv
totsigh = lastotsigh + totaldelsigv / 2   'a starting trial value
delu = deltau(totsigv, totsigh, lastotsigv, lastotsigh, "total")
count = 0
DO
        count = count + 1
        IF count > 1000 THEN
                PRINT "Iteration did not converge in SUB totalKOModel"
                CLOSE
                STOP
        END IF
        lastdelu = delu
        CALL KOcaller1(delu, totaldelsigv)
        numloops = baknumloops
        u = baku
        FOR i = 0 TO numloops
                peakv(i) = bakpeakv(i)
                peakh(i) = bakpeakh(i)
                unloadv(i) = bakunloadv(i)
                unloadh(i) = bakunloadh(i)
```

```
        NEXT i
        criterion1 = ABS((delu - lastdelu) / totaldelsigv)
        divisor = (totalsigv + totalsigh) / 2
        IF divisor = 0 THEN
                divisor = 1
        END IF
        criterion2 = ABS((delu - lastdelu) / divisor)
LOOP UNTIL criterion1 < .00001 OR (criterion1 < .001 AND criterion2 < .00001)
IF hardbottom$ = "NO" AND fillonly$ = "no" THEN
        CALL hysteresis(delu, totaldelsigv)
ELSE
        CALL KOcaller1(delu, totaldelsigv)
END IF
END SUB
```

VITA

George Michael Filz was born in Ilwaco, Washington, on December 10, 1953. He received a Bachelor of Science degree in Mathematics from the University of Oregon in 1979, and a Bachelor of Science degree in Civil Engineering from Oregon State University in 1979. He received a Master of Science degree in Civil Engineering from Oregon State University in 1981. Mr. Filz obtained professional engineering experience working for L. R. Squier Associates, Inc., of Oregon during the period from 1981 to 1985, and for CH2M Hill, Inc., of Oregon during the period from 1985 to 1988. He has been a registered professional engineer since 1983.

Mr. Filz enrolled in the Civil Engineering Department at Virginia Polytechnic Institute and State University in 1988 to pursue a doctoral degree. He was employed by the university, initially as a research assistant and subsequently as an instructor.

Mr. Filz has accepted a position as an assistant professor of Civil Engineering at Virginia Polytechnic Institute and State University beginning in August, 1992.